

**The bathy phytochrome *PaBphP* of the  
human pathogen *Pseudomonas aeruginosa*:  
Introducing a novel perspective on  
light sensing in Proteobacteria**

vom Fachbereich Biologie

der Rheinland-Pfälzischen Technischen Universität Kaiserslautern-Landau

zur Verleihung des akademischen Grades Dr. rer. nat. genehmigte

**Dissertation**

von

**Christina Huber, M.Sc.**, geb. in Zweibrücken

**Mündliche Prüfung:** 12.01.2024

Dekan:

Promotionskommissionsvorsitzender:

**Berichterstattende:**

Prof. Dr. Stefan Kins

Prof. Dr. Stefan Kins

Prof. Dr. Nicole Frankenberg-Dinkel

Prof. Dr. Matthias Hahn

»Man sieht nur mit dem Herzen gut. Das Wesentliche ist für die Augen unsichtbar.«

»On ne voit bien qu'avec le cœur. L'essentiel est invisible pour les yeux.«

~ Antoine de Saint-Exupéry aus Der Kleine Prinz – Le Petit Prince ~

Für meine Familie.

# **Table of Contents**

<b>Table of Contents .....</b>	<b>I</b>
<b>Abbreviations .....</b>	<b>VI</b>
<b>1 Introduction.....</b>	<b>1</b>
1.1 Light is an essential environmental factor on earth .....	1
1.2 Phytochrome discovery opened up a new chapter in the fascinating field of photoreception .....	1
1.3 The boundound chromophore is able to photoconvert .....	4
1.4 Prototypical and bathy phytochromes are widely distributed in different classes of bacteria.....	5
1.5 Bacteria use two-component systems to sense and respond to ever-changing environmental conditions.....	8
1.6 <i>Pseudomonas aeruginosa</i> is an opportunistic pathogen.....	9
1.6.1 <i>P. aeruginosa</i> exhibits a wide variety of motility forms.....	11
1.6.2 The phytochrome of <i>P. aeruginosa</i> is organized in an operon with its heme oxygenase.....	12
1.6.3 <i>P. aeruginosa</i> utilizes two heme oxygenases to build various isomers of its chromophore .....	13
1.7 Objectives of this work.....	14
<b>2 Material and Methods .....</b>	<b>15</b>
<b>2.1 Materials and chemicals.....</b>	<b>15</b>
2.1.1 Equipment .....	15
2.1.2 Special material, chemicals, enzymes, kits, and antibodies .....	16
<b>2.2 Bacterial strains, plasmids, and oligonucleotides .....</b>	<b>18</b>
2.2.1 Bacterial strains.....	18
2.2.2 Plasmids .....	20
2.2.3 Oligonucleotides .....	22

---

<b>2.3 Microbial methods .....</b>	<b>23</b>
2.3.1 Sterilization .....	23
2.3.2 Culture media and supplements .....	23
2.3.3 Storage of <i>E. coli</i> and <i>P. aeruginosa</i> cells .....	24
2.3.4 Cultivation of <i>E. coli</i> or <i>P. aeruginosa</i> cells .....	25
2.3.5 Determination of cell density .....	25
2.3.6 Analysis of aerobic growth of <i>P. aeruginosa</i> .....	25
2.3.7 Preparation of chemically competent <i>E. coli</i> cells .....	26
2.3.8 Transformation of chemically competent <i>E. coli</i> cells.....	26
2.3.9 Conjugation of <i>P. aeruginosa</i> via biparental mating .....	27
<b>2.4 Phenotypic analysis of <i>Pseudomonas aeruginosa</i> .....</b>	<b>27</b>
2.4.1 Swimming Motility .....	27
2.4.2 Investigation of secreted pyocyanin amounts .....	28
2.4.3 Statistical evaluation of phenotypic assays .....	28
<b>2.5 Molecular biological methods .....</b>	<b>29</b>
2.5.1 Preparation of genomic DNA from <i>P. aeruginosa</i> .....	29
2.5.2 Preparation of plasmid DNA from <i>E. coli</i> .....	29
2.5.3 Agarose gel electrophoresis .....	29
2.5.4 Restriction digestion of DNA .....	30
2.5.5 Polymerase chain reaction (PCR) .....	30
2.5.6 Purification of PCR products .....	31
2.5.7 Extraction of DNA fragments from agarose gels.....	31
2.5.8 Determination of nucleic acid concentrations.....	31
2.5.9 Ligation of DNA fragments .....	32
2.5.10 Splicing-by-overlap extension (SOE) PCR.....	32
2.5.11 Generation of <i>P. aeruginosa</i> mutants via two-step allelic exchange .....	33
2.5.12 Site-directed mutagenesis.....	34
2.5.13 Colony PCR .....	35
2.5.14 Analysis of DNA sequences.....	35
<b>2.6 Protein biochemical and biophysical methods .....</b>	<b>36</b>
2.6.1 Test expression of recombinant genes and their encoding proteins.....	36
2.6.2 Heterologous production of recombinant proteins in <i>E. coli</i> .....	36
2.6.3 Homologous production of recombinant proteins in <i>P. aeruginosa</i> .....	37

---

2.6.4 Cell disruption of <i>E. coli</i> and <i>P. aeruginosa</i> cells.....	38
2.6.5 Purification of recombinant proteins.....	38
2.6.6 Determination of protein and biliverdin IX $\alpha$ concentration.....	39
2.6.7 SDS-polyacrylamide gel electrophoresis .....	40
2.6.8 Western blot transfer of proteins .....	42
2.6.9 Immuno-detection of fusion proteins .....	42
2.6.10 Ultraviolet-visible spectroscopy.....	43
2.6.11 Calculation of Pr- and Pfr-fraction in (photo-)stationary phytochrome samples from absorption spectra.....	44
2.6.12 <i>In vitro</i> protein kinase assays .....	44
<b>3 Results .....</b>	<b>46</b>
<b>Part 1 – The bacterial phytochrome <i>PaBphP</i> of the human opportunistic pathogen <i>Pseudomonas aeruginosa</i> .....</b>	<b>46</b>
3.1 Homologous expression and purification of the <i>P. aeruginosa</i> bacterial phytochrome was successful.....	46
3.2 The conformation of the chromophore - stabilized by two amino acid residues - influences autophosphorylation behavior of <i>PaBphP</i> .....	49
3.3 <i>PaBphP</i> is a bathy phytochrome and is inactive in its dark-adapted Pfr-ground state...	52
3.4 The chromophore biliverdin IX $\alpha$ and its covalent bond is not absolutely required for kinase activity of <i>PaBphP</i> .....	55
3.5 <i>PaBphP</i> is the histidine kinase required for activation of the response regulator <i>PaAlgB</i> .....	58
3.6 <i>PaKinB</i> is the phosphatase required for dephosphorylation of the response regulator <i>PaAlgB</i> .....	60
3.7 The deletion of <i>bphP</i> , <i>bphOP</i> and <i>kinB</i> in <i>P. aeruginosa</i> PA14 do not affect the bacterial growth .....	62
3.8 Phosphorylation state of the kinase <i>PaBphP</i> and of the corresponding response regulator <i>PaAlgB</i> regulates swimming motility .....	64
3.9 Phosphorylation state of the kinase <i>PaBphP</i> and of the corresponding response regulator <i>PaAlgB</i> regulate pyocyanin secretion.....	65

<b>Part 2 – Bathy and prototypical phytochromes in different non-photosynthetic human and plant pathogens .....</b>	<b>67</b>
3.10 Heterologous expression and purification of the <i>A. tumefaciens</i> and <i>P. syringae</i> prototypical phytochromes was successful.....	67
3.11 Heterologous expression and purification of various bacterial bathy phytochromes was successful.....	68
3.12 An HWE type HKD was identified in AvBphP2.....	72
3.13 Spectral absorption properties identify <i>AtBphP1</i> as a conventional and <i>PstBphP1</i> as an unconventional prototypical phytochrome .....	74
3.14 The spectral absorption properties of <i>PaBphP</i> are widespread among the bathy type phytochromes.....	75
3.15 The autokinase activity of bathy and prototypical BphPs differs – but still shares similarities.....	79
3.16 Dark reversion rates of various bathy and prototypical BphPs differ .....	82
<b>4 Discussion .....</b>	<b>84</b>
<b>Part 1 – Understanding the function of the phytochrome in the heterotrophic bacterium <i>Pseudomonas aeruginosa</i> .....</b>	<b>84</b>
4.1 The bacterial phytochrome <i>PaBphP</i> – An unorthodox far-red/red light sensor or the reevaluation of a traditional pattern? .....	84
4.2 The reaction of the far-red/red light sensor <i>PaBphP</i> to blue light – A special feature or biophysically explainable?.....	86
4.3 The phytochrome has the ability to form a photoconvertible holo-protein with different BV isomers – <i>PaBphP</i> a promiscuous light receptor?.....	87
4.4 The BphP/AlgB/KinB regulation system of <i>P. aeruginosa</i> – Part of a complex network? .....	88
<b>Part 2 – Comprehensive systematic analysis of various BphPs provides new insights into light-triggered signaling processes.....</b>	<b>95</b>
4.5 The presence of HWE type histidine kinases - Extending the diversity within the histidine kinase subfamilies? .....	95
4.6 The paradox of bathy and prototypical phytochromes – Do they end up sharing more similarities or more differences? .....	97
4.7 Bathy phytochromes in different Proteobacteria – Model systems for a new classification of their light sensing function? .....	105

<b>5 Summary.....</b>	<b>111</b>
<b>6 Zusammenfassung .....</b>	<b>113</b>
<b>References.....</b>	<b>115</b>
<b>Appendix.....</b>	<b>134</b>
<b>Curriculum Vitae.....</b>	<b>IX</b>
<b>Erklärung.....</b>	<b>XI</b>
<b>Darlegung des Eigenanteil.....</b>	<b>XII</b>
<b>Darlegung aller benutzten Hilfestellungen und Hilfsmitteln.....</b>	<b>XIV</b>
<b>Danksagung .....</b>	<b>XV</b>

## Abbreviations

Abbreviations of the International System of Units (SI) are not listed separately. For amino acids (IUPAC) the three-letter code is used in the text, while the one-letter code is used to designate the protein variants.

$\alpha$	Pfr-fraction in a phytochrome population ( $\alpha = [P_{fr}]/([P_{fr}]+[P_r])$ )
$\epsilon$	Molar absorption coefficient
5-Me-PCA	5-methyl-phenazine-1-carboxylic acid
AHT	Anhydrotetracycline
Amp	Ampicillin
APS	Ammonium persulfate
Arnt	Aryl hydrocarbon receptor nuclear translocator protein
ATP	Adenosine triphosphate
<i>A. tumefaciens</i>	<i>Agrobacterium tumefaciens</i> (synonyms <i>Agrobacterium fabrum</i> , <i>Rhizobium radiobacter</i> )
<i>A. vitis</i>	<i>Allorhizobium vitis</i> (synonym <i>Agrobacterium vitis</i> )
BCIP	5-Bromo-4-chloro-3-indolyl phosphate
BLUF domain	Blue-light sensing using FAD domain
BphP	bacterial Phytochrome / Bacteriophytochrome
BSA	Bovine serum albumin
BV	Biliverdin
CA domain	Catalytic and ATP-binding domain
c-di-GMP	bis-(3'-5')-cyclic dimeric guanosine monophosphate
CF	Cystic fibrosis
CO	Carbon monoxide
Cph	cyanobacterial Phytochrome
CRC cycle	Cyst-rod-cyst cycle
CV	Column volume
Da	Dalton
dATP	Deoxyadenosine triphosphate
dCTP	Deoxycytidine triphosphate
dGTP	Deoxyguanosine triphosphate
DHp domain	Dimerization and histidine phosphotransfer domain
DMSO	Dimethyl sulfoxide
DNA	Deoxyribonucleic acid
dNTP	Deoxynucleoside triphosphate
DR	Dark reversion
<i>D. radiodurans</i>	<i>Deinococcus radiodurans</i>
DTT	Dithiothreitol
dTTP	Deoxythymidine triphosphate
EDTA	Ethylenediaminetetraacetic acid
e.g.	for example (latin <i>exempli gratia</i> )



EPS	Extracellular polymeric substances
EtOH	Ethanol
EV	Empty vector
<i>F. diplosiphon</i>	<i>Fremyella diplosiphon</i>
Fig.	Figure
Fph	fungal Phytochrome
fwd	forward
GAF domain	cGMP-specific phosphodiesterase/adenylyl cyclase/FhlA domain
gDNA	genomic DNA
Gene KO	Gene knockout
Gm	Gentamicin
HAMP domain	Histidine kinases, adenylyl cyclases, methyl-accepting chemotaxis proteins, phosphatases domain
HF	High-fidelity
HK	Histidine kinase
HKD	Histidine kinase domain
HO	Heme oxygenase
HWE kinases	HK family with conserved HWE motif
IPTG	Isopropyl $\beta$ -D-1-thiogalactopyranoside
Kan	Kanamycin
LB	Lysogeny broth
LED	Light-emitting diode
LOV domain	Light-oxygen-voltage-sensing domain
MeOH	Methanol
MWCO	Molecular weight cut-off
NBT	Nitro blue tetrazolium chloride
n.d.	not determined
n.s.	not significant
OD	Optical density
OD <sub>Xnm</sub>	OD at X nm
ORF	Open reading frame
OUT domain	Output domain
P $\Phi$ B	Phytochromobilin
<i>P. aeruginosa</i>	<i>Pseudomonas aeruginosa</i>
PAS domain	Per-Arnt-Sim domain
PCA	Phenazine-1-carboxylic acid
PCB	Phycocyanobilin
PCN	Phenazine-1-carboxamide
PCR	Polymerase chain reaction
Per	Periodic circadian clock protein
Pfr	far-red light absorbing form of phytochrome
pH	Potential of hydrogen (latin <i>potentia hydrogenii</i> )
PHY domain	Phytochrome-specific domain

Pr	red light absorption form of phytochrome
<i>P. syringae</i>	<i>Pseudomonas syringae</i>
PVDF	Polyvinylidene fluoride
PYO	Pyocyanin
QS	Quorum sensing
RBS	Ribosome binding site
REC domain	Receiver domain
<i>R. palustris</i>	<i>Rhodopseudomonas palustris</i>
rpm	revolutions per minute
RR	Response regulator
RT	Room temperature
<i>R. tataouinensis</i>	<i>Ramlibacter tataouinensis</i>
ROS	Reactive oxygen species
rev	reverse
SDS	Sodium dodecyl sulfate
SDS-PAGE	SDS-polyacrylamide gel electrophoresis
SEC	Size exclusion chromatography
Sim	Single-minded protein
SOE PCR	Splicing-by-overlap extension PCR
T4P	Type IV pili
T4SS	Type IV secretion system
Tab.	Table
TCS	Two-component systems
TEMED	Tetramethylethylenediamine
Tet	Tetracycline
Ti plasmid	Tumor-inducing plasmid
UV/Vis	Ultraviolet-visible
Übers. d. Verf.	Translation by the author (german <i>Übersetzung des Verfassers</i> )
v/v	volume per volume
Vfr	Virulence factor regulator
w/v	weight per volume
WT	Wild type
<i>X. campestris</i>	<i>Xanthomonas campestris</i>
<i>X. oryzae</i>	<i>Xanthomonas oryzae</i>
Z/E	<i>Zusammen/Entgegen</i> notation of the C15=C16 double bond stereochemistry of a tetrapyrrole chromophore
<i>ZZEssa, ZZZssa</i>	<i>Zusammen/Entgegen</i> and <i>syn/anti</i> stereochemical notation of methine bridges of a tetrapyrrole chromophore

# 1 Introduction

## 1.1 Light is an essential environmental factor on earth

What is light? Why do we need light? And most importantly, how do we use the available light? On the one hand, these are probably very philosophical questions, but on the other hand, they can be answered biologically, biochemically, and biophysically. The perception of light signals is of great importance to many organisms and is a common characteristic of all living beings. In addition to its function as a source of energy, actinic light can also be a source of information in all domains of life (Kottke *et al.*, 2018). The existence of receptors that absorb light from a wide range of spectral regions has enhanced the ability of organisms to adapt their behavior and physiology to ever-changing environmental conditions over the course of evolution (Montgomery and Lagarias, 2002). When discussing photoreceptors in general, rhodopsin is the most obvious example. It is a visual receptor molecule found in the retina of vertebrates, in the facet eyes of insects, or in other invertebrates (Pepe, 1999). Besides rhodopsin, photoreceptors are classified into different families based on the specific wavelength at which they are activated and the embedded chromophore: phytochromes, xanthopsins, cryptochromes, LOV (light-oxygen-voltage-sensing) domain containing phototropins, and BLUF (blue-light sensing using FAD) domain proteins (Möglich, 2019; van der Horst and Hellingwerf, 2004). These photoreceptors are blue light sensors with the only exception of phytochromes, which specifically detect red light at wavelengths of around 630-750 nm (Montgomery and Lagarias, 2002). Common to all photoreceptors is the use of light stimuli as the driving force for isomerization, electron-, or proton-transfer of or within an attached chromophore. These chemophysical conversions cause conformational changes in photoreceptor proteins, altering their properties and inducing a cellular signal. Due to this, downstream components of the photoreceptor signaling cascade are activated to ensure a biological response (Hellingwerf, 2000).

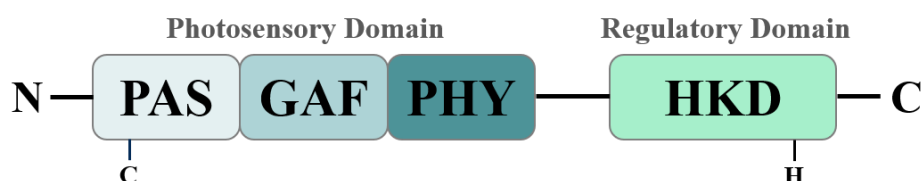
## 1.2 Phytochrome discovery opened up a new chapter in the fascinating field of photoreception

Phytochromes are a class of far-red and red light sensing photoreceptor proteins (Montgomery and Lagarias, 2002). Originally, they were discovered in plants over sixty years ago and believed to be exclusive for this kingdom (Borthwick *et al.*, 1952a; Borthwick *et al.*, 1952b). Plant phytochromes aid the sessile organisms in adapting their photosynthesis, seed

germination, and flowering time to changing light conditions (Butler *et al.*, 1959; Mathews, 2006). The model organism for phytochrome studies in plants is *Arabidopsis thaliana* with its five different phytochromes PhyA-PhyE (Furuya, 1993; Sharrock and Quail, 1989). Around thirty years after their initial discovery, phytochromes were also found in lower plants, including bryophytes, ferns, and algae (Kolukisaoglu *et al.*, 1995; Lagarias *et al.*, 1995). Further years of extensive research have revealed the presence of red light photoreceptors in various other organisms, including fungi (Fphs), cyanobacteria (Cphs), and non-photosynthetic, heterotrophic bacteria (BphPs) (Montgomery and Lagarias, 2002). These phytochromes are distinguished by their ability to sense and respond to different quality red light, despite inhabiting entirely different environments and lifestyles. Notably, some of the earliest discovered and well-studied BphPs belong to *Deinococcus radiodurans* (*DrBphP*) and *Pseudomonas aeruginosa* (*PaBphP*) (Bhoo *et al.*, 2001; Davis *et al.*, 1999). Thus, years of research have demonstrated the existence of phytochromes beyond the plant kingdom, and concurrently, the resemblance between bacterial and fungal phytochromes. *Aspergillus nidulans* serves as an exemplary organism for investigating photoreceptor functionality in fungi (Blumenstein *et al.*, 2005; Mooney and Yager, 1990; Röhrig *et al.*, 2013), but fungal phytochromes are also found in *Botrytis cinerea* (Schumacher, 2017), *Aspergillus fumigatus* (Fuller *et al.*, 2013; Idnurm, 2013) or *Ustilago maydis* (Sánchez-Arreguin *et al.*, 2020). The phytochrome signal is crucial for determining the vegetative or generative phase of development in these organisms. Additionally, light perception is linked to the repression or promotion of conidiation (Schumacher, 2017). Cphs affect growth, acclimation of photosynthesis, and phototaxis in different cyanobacteria, including *Synechocystis*, *Anabaena* and *Nostoc* (Fiedler *et al.*, 2005; Fiedler *et al.*, 2004; García-Domínguez *et al.*, 2000). The phytochromes found in cyanobacteria can be roughly divided into three categories: the Cph1-family, which resembles plant phytochromes; the Cph2-family, which exhibits strong similarity to bacterial phytochromes; and cyanobacteriochromes, with special GAF domain features (Ikeuchi and Ishizuka, 2008; Montgomery and Lagarias, 2002; Rockwell and Lagarias, 2010; Takala *et al.*, 2020). The role of bacterial phytochromes is still enigmatic, however evidence indicates their primary function resides in regulating virulence (Mukherjee *et al.*, 2019; Otero *et al.*, 2016). Furthermore, the structure of bacterial phytochromes is largely conserved (Fig. 1.1). A holo-phytochrome consists of an apo-protein and a bound chromophore, displaying a dimeric quaternary structure. The composition of the apo-phytochrome is characterized by two major domains: a N-terminal photosensory core module and a C-terminal regulatory histidine kinase domain (HKD) with a conserved histidine residue (Montgomery and Lagarias, 2002).

This carboxy-terminal HKD functions as an output module activating physiological responses by transferring signals to downstream components of the phytochrome signaling cascade. The amino-terminal photosensory domain is composed of the Per-Arnt-Sim (PAS), succeeded by the cGMP-specific phosphodiesterase/adenylyl cyclase/FhlA (GAF) and the phytochrome-specific (PHY) domains (Montgomery and Lagarias, 2002). The PAS domain derives from the “periodic circadian clock” protein (PER) in *Drosophila melanogaster*, the vertebrate “aryl hydrocarbon receptor nuclear translocator” protein (ARNT), and the “single-minded” protein (SIM) from *D. melanogaster*, where they were originally described. Today, these domains are important cytosolic signaling domains ubiquitously found in Bacteria, Eukarya, and Archaea in a number of proteins. PAS domains are capable of sensing light, oxygen, and redox state by binding small molecules such as heme or other tetrapyrroles, flavins, and aromatic compounds as cofactors (Taylor and Zhulin, 1999). In multidomain proteins, PAS and GAF domains frequently co-occur, and GAF domains are also able to attach small prosthetic groups (Ho *et al.*, 2000). GAF domains were initially described in cGMP-specific phosphodiesterases from vertebrates, as well as in cyanobacterial adenylyl cyclases, and in the bacterial formate hydrogenlyase transcriptional activator FhlA (Aravind and Ponting, 1997).

### Apo-Phytochrome



### Holo-Phytochrome

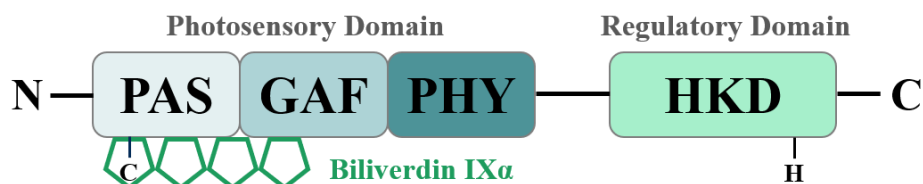


**Fig. 1.1: Domain organization of bacterial phytochromes in their apo- and holo-form.**

Bacterial phytochromes consist of a photosensory domain (turquoise shades) and a regulatory domain (green). The photosensory domain of BphPs is composed of three subdomains: PAS (Per-Arnt-Sim), GAF (cGMP-specific phosphodiesterase/adenylyl cyclase/FhlA), and PHY (phytochrome-specific). In absence of the chromophore the protein exists as an apo-phytochrome. In the holo-phytochrome, the conserved cysteine residue (represented by “C”) in the PAS domain facilitates autocatalytic biliverdin IX $\alpha$  (BV IX $\alpha$ ; green pentagons) binding. Despite binding in the PAS domain, the chromophore is also located in the GAF domain (chromophore-binding pocket). The regulatory domain is usually a typical bacterial HKD with a conserved histidine residue (represented by “H”) for autophosphorylation.

The PAS and GAF domain combine to form the chromophore-binding pocket, which facilitates the assembly of the chromophore by an autocatalytic reaction (Lagarias and Lagarias, 1989). Generally, the chromophore is responsible for light reception and varies across the phytochrome subfamilies. It is an open-chain tetrapyrrole (bilin) derived from the heme degradation pathway. Heme is cleaved by regiospecific heme oxygenases (HO), leading to one or more biliverdin isomer products (Frankenberg-Dinkel, 2004). For bacterial and fungal phytochromes, biliverdin IX $\alpha$  (BV IX $\alpha$ ) serves as chromophore, requiring no additional synthesis steps (Bhoo *et al.*, 2001), whereas plants and cyanobacteria incorporate further reduced chromophores. They employ phytochromobilin (P $\Phi$ B) or phycocyanobilin (PCB), respectively, derived from regiospecific reductions of BV IX $\alpha$  by bilin reductases (Frankenberg *et al.*, 2001). In addition to the type of tetrapyrrole, different among the families, phytochromes can also be classified based on the region where the chromophore binds. Usually, the chromophore is covalently linked to a conserved cysteine residue via a thioether bond. The chromophore binding site for P $\Phi$ B or PCB on plant and cyanobacterial phytochromes is located in the GAF domain, while BV IX $\alpha$  is attached to the PAS domain of Fphs and BphPs (Montgomery and Lagarias, 2002). Although it binds to the PAS domain, the chromophore is actually located in the chromophore-binding pocket, which extends beyond the GAF domain (Yang *et al.*, 2008).

### **1.3 The covalently bound chromophore is able to photoconvert**

The photochromism exhibited by phytochromes is supported by the bound chromophore. Upon light absorption, the chromophore BV IX $\alpha$  undergoes a conformational change, altering its interaction within the protein. This reversible photoisomerization (Fig. 1.2), known as a “flip-and-rotate” process, enables the organisms to convert quality and quantity of light into biochemical signals by triggering additional steps of the photosignaling cascade (Hellingwerf, 2000). The photoswitch is reflected in the alternation of two relatively stable parental states of the phytochrome: the red light-absorbing Pr-form (*ZZZssa*) and the far-red light-absorbing Pfr-form (*ZZEssa*) (Braslavsky *et al.*, 1997; Siegelman and Firer, 1964). These two spectrally distinct forms are dependent on the exposure to red or far-red light and caused by a (*Z*)/(*E*) isomerization of the C15-C16 double bond in the conjugated chromophore system between pyrrole ring C and D (Li and Lagarias, 1992). The configuration of *ZZZssa* and *ZZEssa* describes the *Zusammen*(opposite)/*Entgegen*(together) and *syn/anti* stereochemical notation of the methine bridges of the chromophore BV IX $\alpha$ . The absorption maximum of the Pr-form in bacterial phytochromes is around 700 nm, whereas that of the Pfr-form is around 750 nm. The

different bilin derivatives employed within the phytochrome families of fungi, plants, heterotrophic bacteria, and cyanobacteria lead to varying absorption maxima. While BV IX $\alpha$  (BphPs and Fphs) possesses a more pronounced  $\pi$ -electron system and absorbs light of longer wavelength, PCB present in cyanobacterial phytochromes and P $\Phi$ B found in plant phytochromes absorb light of shorter wavelengths (Lagarias and Lagarias, 1989).

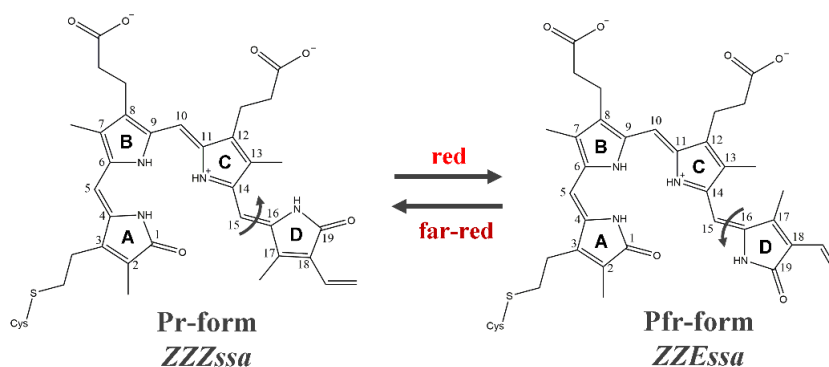


**Fig. 1.2: Isomerization of the chromophore biliverdin IX $\alpha$  of bacterial and fungal phytochromes.**

The double bond between ring C and D of the open-chain tetrapyrrole biliverdin IX $\alpha$  undergoes a (Z)/(E) isomerization when exposed to red or far-red light. The chromophore conversion in the protein results in the formation of the Pr-form (ZZZssa) upon far-red light irradiation or the Pfr-form (ZZEssa) upon red light irradiation in bacterial (BphPs) and fungal (Fphs) phytochromes. Figure modified from Chernov *et al.*, 2017.

The thermal stability of the Pr- and Pfr-form is inconsistent within the group of biliverdin-binding phytochromes. The relaxation to the thermodynamically favorable ground state is a process called dark reversion (DR) (Borthwick *et al.*, 1952b; Taylor, 1968). Depending on the pattern of this thermally driven transformation, bacterial phytochromes can be categorized into two groups: prototypical, also called canonical, and bathy phytochromes. In prototypical phytochromes, the red light-absorbing Pr-form ( $\lambda_{\max}$  700 nm, Z isomer) dominates in the absence of light and is the thermodynamically stable ground state (Chen *et al.*, 2004). In contrast, the DR route of bathy phytochromes proceeds from Pr to Pfr ( $\lambda_{\max}$  750 nm, E isomer) (Giraud and Verméglio, 2008; Rottwinkel *et al.*, 2010). Bathy phytochromes exhibit a bathochromic shift, resulting in a longer wavelength spectral absorption compared to the ground state absorption of prototypical BphPs (Kamlet and Taft, 1976; Rottwinkel *et al.*, 2010).

#### 1.4 Prototypical and bathy phytochromes are widely distributed in different classes of bacteria

Known representatives with BphPs of both types – prototypical and bathy – are mostly found in the phylum of Proteobacteria (synonym Pseudomonadota) (Tab. 1.1). Bacterial species possessing a BV-binding phytochrome are widely distributed in the class of Alphaproteo-

bacteria, specifically in the order of Hyphomicrobiales (synonym Rhizobiales) (Rottwinkel *et al.*, 2010). The best-known member of this bacterial order is *Agrobacterium tumefaciens* (synonyms *Agrobacterium fabrum* and *Rhizobium radiobacter*), which possesses the prototypical *AtBphP1* and the bathy *AtBphP2* (Karniol and Vierstra, 2003). The list can be extended, for instance, mentioning the BphPs of *Allorhizobium vitis* (synonym *Agrobacterium vitis*) (Rottwinkel *et al.*, 2010), *Rhodopseudomonas palustris* (Auldrige and Forest, 2011), or *Bradyrhizobium* (Giraud *et al.*, 2002). However, phytochromes also exist in the plant pathogens *Ramlibacter tataouinensis* (De Luca *et al.*, 2019), *Pseudomonas syringae* (Bhoo *et al.*, 2001), *Xanthomonas campestris* (Otero *et al.*, 2016), in the human pathogen *Pseudomonas aeruginosa* (Davis *et al.*, 1999) or in *Deinococcus radiodurans* (Bhoo *et al.*, 2001), indicating that the presence is not limited to Alphaproteobacteria or rhizobial soil bacteria.

**Tab. 1.1: Summary of prototypical and bathy phytochromes from various organisms of the Proteobacteria phylum (Alpha-, Beta- and Gammaproteobacteria) as well as of Deinococcota (Deinococci). Phytochromes containing an HKD are designated with (✓) while BphPs lacking an HKD are designated with (-).**

Organism	BphP	type	HKD	Ref.
<b>Alphaproteobacteria</b>				
<i>Agrobacterium tumefaciens</i>	<i>AtBphP1</i>	prototypical	✓	1, 2
	<i>AtBphP2</i>	bathy	✓	1, 2
<i>Allorhizobium vitis</i>	<i>AvBphP1</i>	prototypical	✓	2
	<i>AvBphP2</i>	bathy	✓	2
<i>Rhodopseudomonas palustris</i> CEA001	<i>RpBphP1</i>	bathy	-	2-5
<i>Rhodopseudomonas palustris</i> CGA009	<i>RpBphP2</i>	prototypical	✓	4, 6
	<i>RpBphP3</i>	prototypical	✓	4, 6
	<i>RpBphP5</i>	bathy	✓	2, 4
	<i>RpBphP6</i>	bathy	✓	2, 4
<i>Bradyrhizobium</i> ORS278	<i>BrBphP1</i>	bathy	-	3
<b>Betaproteobacteria</b>				
<i>Ramlibacter tataouinensis</i>	<i>RtBphP1</i>	prototypical	✓	7
	<i>RtBphP2</i>	bathy	✓	7
<b>Gammaproteobacteria</b>				
<i>Pseudomonas aeruginosa</i>	<i>PaBphP</i>	bathy	✓	8-10
<i>Pseudomonas syringae</i>	<i>PstBphP1</i>	prototypical	✓	10, 11
	<i>PstBphP2</i>	prototypical	✓	10, 11
<i>Xanthomonas campestris</i>	<i>XccBphP</i>	bathy	-	12
<b>Deinococci</b>				
<i>Deinococcus radiodurans</i>	<i>DrBphP</i>	prototypical	✓	10

(1) Karniol and Vierstra, 2003; (2) Rottwinkel *et al.*, 2010; (3) Giraud *et al.*, 2002; (4) Auldrige and Forest, 2011; (5) Papiz *et al.*, 2019; (6) Giraud *et al.*, 2005; (7) De Luca *et al.*, 2019; (8) Davis *et al.*, 1999; (9) Tasler *et al.*, 2005; (10) Bhoo *et al.*, 2001; (11) Shah *et al.*, 2012; (12) Otero *et al.*, 2016



Although the photosensory domain, comprised of the PAS, GAF, and PHY subdomains, is conserved among all bacterial phytochromes, there are distinct differences in the regulatory domains. The output domains may comprise of a classical HKD, an HWE-type histidine kinase domain with a linked response regulator (RR), a combination of both kinase types or even a PAS9 domain for protein-protein interaction (Fig. 1.3).

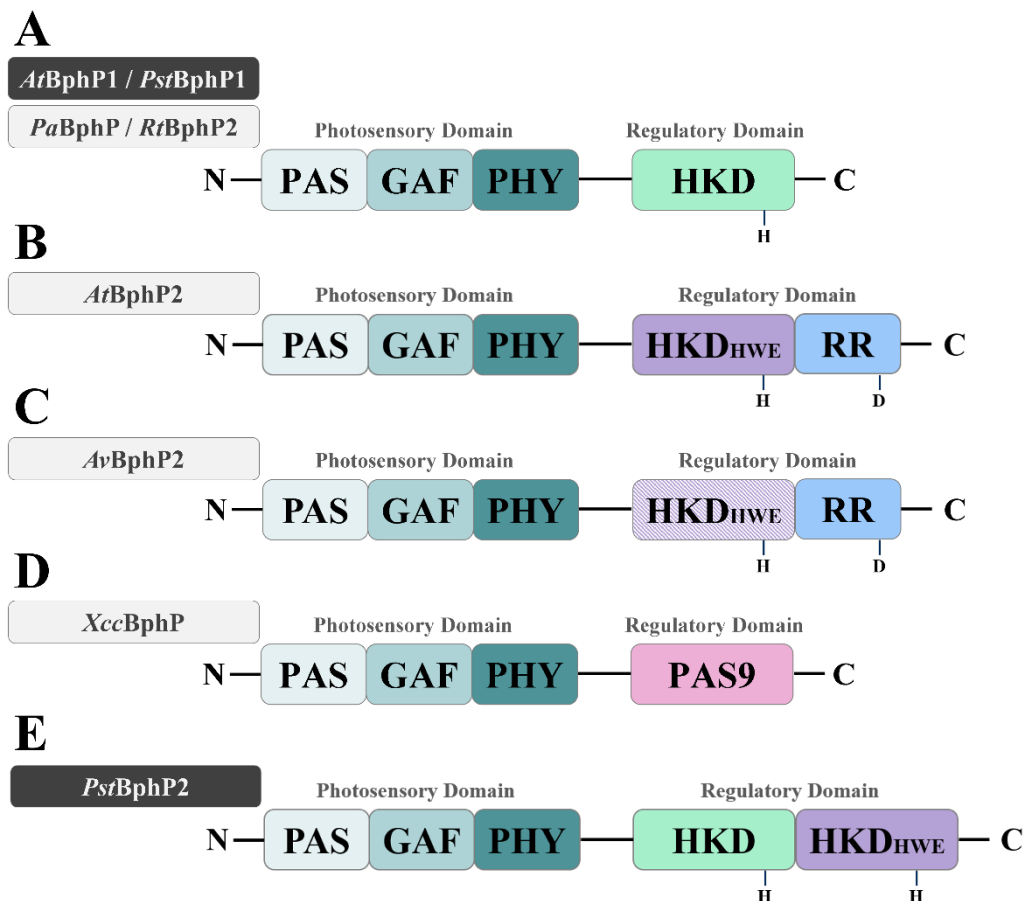


**Fig. 1.3: Domain arrangements of prototypical and bathy phytochromes from different organisms.**

The photosensory domain (turquoise shades) of the shown phytochromes are composed of a PAS, GAF, and PHY domain. Depending on the organism (*A. tumefaciens*, *AtBphP1* [A] and *AtBphP2* [B], *P. syringae*, *PstBphP1* [A] and *PstBphP2* [E], *P. aeruginosa*, *PaBphP* [A]; *R. tataouinensis*, *RtBphP2* [A]; *A. vitis*, *AvBphP2* [C]; *X. campestris*, *XccBphP* [D]) the regulatory domain is composed of a histidine kinase domain (HKD; green), an HWE-like histidine kinase domain (HKD<sub>HWE</sub>; purple) with an attached response regulator (RR; blue), or a PAS9 domain (pink). *AvBphP2* has an unclear type of HKD, indicated by the faintly dashed box. The conserved histidine residues in the respective HKD or in the HKD<sub>HWE</sub> are labeled as “H”, while the conserved aspartate residues in the respective RR are indicated with “D”. Prototypical phytochromes are highlighted with dark gray boxes and bathy phytochromes are highlighted with light gray boxes.

## 1.5 Bacteria use two-component systems to sense and respond to ever-changing environmental conditions

The C-terminal histidine kinase output domain in numerous BphPs exhibits a structure and characteristics identical to that of typical sensor kinases of bacterial two-component systems (TCS) (Bhoo *et al.*, 2001). Different organisms utilize this signaling pathway strategy to sense and respond to extra- as well as intracellular signals and stimuli (Gao and Stock, 2009; Parkinson, 1993; Stock *et al.*, 2000). In bacteria, the regulation involves a histidine-aspartate phosphotransfer system that facilitates adaptation to various environmental conditions and the modification of behavior. Basic cellular processes like metabolism, motility, development, antibiotic resistance, and virulent activity are regulated within the cells (Gao and Stock, 2009; Jacob-Dubuisson *et al.*, 2018). TCSs involve two signaling modules: a regulatory homodimeric sensor kinase and a corresponding cytoplasmic localized RR (Fig. 1.4). The kinase is composed of an N-terminal stimulus-detecting sensor domain and a C-terminal cytosolic HKD. The sensory domain can be located either in the cytosol (those containing a PAS and/or GAF domain), in the cell membrane, or extracellularly. This domain has a modular and diverse architecture and is linked to the highly conserved catalytic core HKD. If required, they are connected via a membrane-spanning linker (HAMP domain) (Jacob-Dubuisson *et al.*, 2018; Mascher *et al.*, 2006; Parkinson, 2010; Perry *et al.*, 2011; Stock *et al.*, 2000). Moreover, the HKD comprises an N-terminal dimerization and histidine phosphotransfer (DHp) domain as well as a C-terminal catalytic and ATP-binding (CA) domain. The DHp domain includes the H-box with the conserved His residue, allowing phosphorylation, and mediating the dimerization of the sensor kinase. The CA domain is responsible for ATP-binding, -hydrolysis, and the transfer of the  $\gamma$ -phosphoryl group to the His residue. Additionally, this domain is characterized by the N-box, F-box, and G-rich boxes (cf. Fig. 3.16) (Stewart, 2010; Stock *et al.*, 2000). When a specific stimulus is recognized by the sensory domain, it triggers a conformational change allowing autophosphorylation of the HKD (Burgie *et al.*, 2016; Takala *et al.*, 2014). Hydrolysis of ATP, an energy source available in the bacterial cells and bound to the CA domain, results in the release of the  $\gamma$ -phosphoryl group that binds to the conserved His residue of the DHp domain. Consequently, the phosphorylated kinase becomes a phosphodonor. The high-energy phosphoryl group is subsequently transferred to the conserved Asp residue of the N-terminal receiver (REC) domain of the corresponding stand-alone or attached RR (Gao and Stock, 2009; Möglich, 2019; Stock *et al.*, 2000). The resulting activation of the C-terminal output (OUT) domain of the response regulator ultimately initiates a specific cellular response (Stock *et al.*, 2000). This domain is characterized either by a DNA-binding

motif or catalytic enzyme activity, but it can also interact with RNA, ligands, or other proteins to modify the cellular physiology indirectly (Galperin, 2010; Gao and Stock, 2009; Perry *et al.*, 2011). However, direct DNA-binding by helix-turn-helix motifs is most common in output modules of RRs, enabling them to function as transcriptional regulators by either up- or downregulating target gene transcription. DNA-binding RRs can be categorized into OmpR-like, NarL-like, or NtrC-like subfamilies based on the comparison of their sequence and structure with those that have been previously classified (Galperin, 2006; Gao and Stock, 2009). Dephosphorylation of the RR is achieved directly via intrinsic phosphatase activity in case of a multifunctional sensor kinase or by a phosphatase, acting as another component and antagonist of the kinase (Gao and Stock, 2009; Russo and Silhavy, 1993).

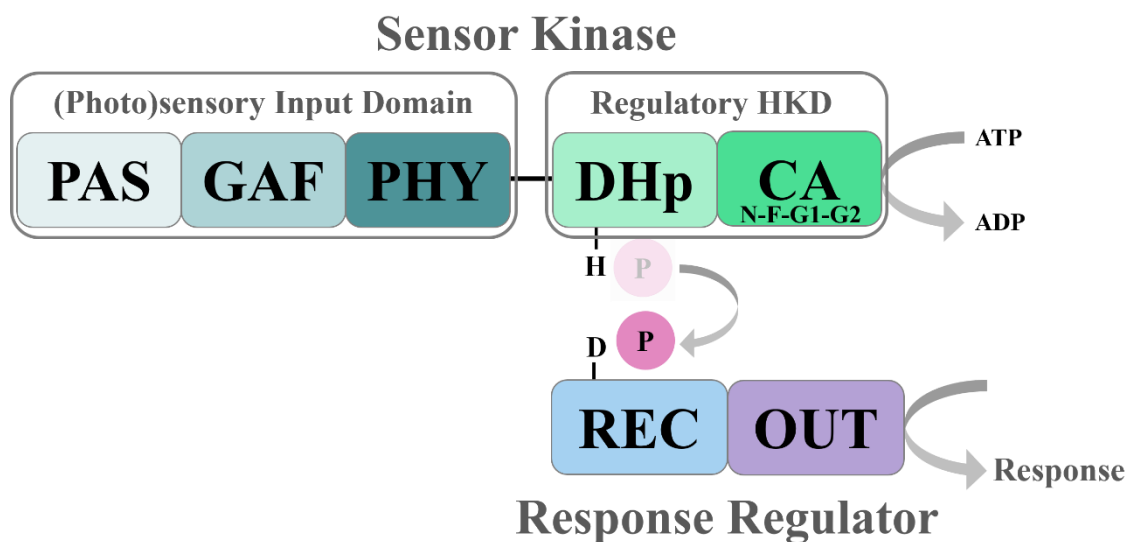


**Fig. 1.4: Schematic representation of two-component signaling system and mechanism of signal transduction using a bacterial phytochrome as an example.**

The (photo)sensory domain of a sensor histidine kinase detects intra- or extracellular stimuli. This perception triggers autophosphorylation of the HKD. ATP is hydrolyzed at the catalytic and ATP-binding (CA) domain and the  $\gamma$ -phosphoryl group binds to the conserved histidine (H) residue in the H-box of the dimerization and histidine phosphotransfer (DHp) domain. Subsequently, the phosphoryl group is transferred to the conserved phosphor-accepting aspartate (D) residue of the receiver (REC) domain of the corresponding RR. The transfer leads to a conformational change of the RR and a cellular response, mediated by the output (OUT) domain of the RR. The CA domain contains an N-box, F-box, G1-box, and G2-box, which are characterized by a conserved Asn, Phe, or some Gly residues, respectively.

## 1.6 *Pseudomonas aeruginosa* is an opportunistic pathogen

Notwithstanding the fact that a wide range of bathy BphPs have been discovered in recent time, *P. aeruginosa* was one of the first heterotrophic bacteria in which a bathy phytochrome has been identified over 20 years ago (Bhoo *et al.*, 2001; Davis *et al.*, 1999). *P. aeruginosa* is a Gram-negative, rod-shaped, monotrichous Gammaproteobacterium that is ubiquitous in our environment. Within its genus, *P. aeruginosa* is a true pioneer, because it is the best

characterized member, and its genome is one of the largest bacterial genomes. The most commonly used laboratory strains are PAO1 and PA14 whose genomes have been fully sequenced with 6.26 Mbp and 6.54 Mbp, respectively (He *et al.*, 2004; Klockgether *et al.*, 2011; Stover *et al.*, 2000). The bacteria possess a high number of TCS and about 10 % of all identified genes encode either elements of these signal pathway cascades or transcriptional regulators (Stover *et al.*, 2000). Therefore, as further suggested by its universal occurrence, *P. aeruginosa* has a significant ability to adapt to a wide range of environmental conditions. It is distributed across a variety of habitats and ecosystems, including water and soil, but can also be found in human, animal, or plant tissues (Diggle and Whiteley, 2020; Rahme *et al.*, 1995; Spiers *et al.*, 2000). Additionally, *P. aeruginosa* is an opportunistic pathogen with high rates of multidrug resistance and natural antibiotic tolerance, justifying its clinical relevance (Botelho *et al.*, 2019; Hancock and Speert, 2000). It is the prevalent nosocomial pathogen and causes several acute as well as chronic infections, especially in immunocompromised patients (Goodman *et al.*, 2004; Lyczak *et al.*, 2000). The bacterium is responsible for a broad range of infections, particularly affecting the blood, the urinary tract, soft tissues or the skin, ears, and eyes of human hosts. Furthermore, *Pseudomonas* is able to infect the lungs of cystic fibrosis (CF) patients, and its persistence is the leading cause of death in this disease pattern (Courtney *et al.*, 2007; FitzSimmons, 1993; Govan and Deretic, 1996; Murray *et al.*, 2007). Virulence factors, including the blue-green phenazine pyocyanin (PYO), are responsible for all these infections. PYO has a high redox-active potential, enabling *Pseudomonas* to produce reactive oxygen species (ROS), leading to an antibiotic and antifungal activity against most other bacteria and fungi. Furthermore, it induces cell death in eukaryotic cells infected by CF. This inhibitory effect promotes the formation of infections and concomitantly confers a selective advantage to *P. aeruginosa* for its growth and development in certain environments (Baron and Rowe, 1981; Lau *et al.*, 2004). Along with secretion of virulence factors, the ability of the bacteria to form biofilms is crucial for the establishment of infections. During chronic infections, *P. aeruginosa* attaches to surfaces, creating a biofilm matrix mainly composed of extracellular polymeric substances (EPS). These surface-attached bacterial communities are more resistant to antimicrobial agents and protected against various environmental influences (O'Toole and Kolter, 1998; Overhage *et al.*, 2008). These bacterial aggregations can not only be found in wounds' biofilms, but also on implants and catheters used in the medical field (Khoury *et al.*, 1992) or in drinking water distribution systems (Liu *et al.*, 2016). The bacterium plays a crucial role as a model organism in microbiology, earning the description of a "lab rat" by Diggle and

Whiteley, due to its significant and pervasive relevance in both medical and industrial sectors (Diggle and Whiteley, 2020).

### 1.6.1 *P. aeruginosa* exhibits a wide variety of motility forms

The survival and adaptation of a bacterium in its environment are often decided by its growth and movement (Zegadło *et al.*, 2023). An outstanding trait of *P. aeruginosa*, compared to many other bacteria, is the ability to utilize different forms of active motility (Fig. 1.5). The opportunistic pathogen is capable of swimming, swarming and twitching motility due to its type IV pili (T4P) and its polar flagellum (Diggle and Whiteley, 2020). Swimming motility is the basic form of movement and is typical for flagellated bacteria (Fig. 1.5A). When found in aqueous environments, these organisms are capable to rotate their polar flagellum (Corral *et al.*, 2020; Miyata *et al.*, 2020; Taylor and Koshland, 1974). Using a “run-reverse-turn” motility mechanism they can move through liquid habitats (Qian *et al.*, 2013).

On semisolid surfaces, some Gram-negative bacteria, including *P. aeruginosa*, exhibit swarming motility mediated by their flagella and T4P (Fig. 1.5B) (Harshey, 1994; Köhler *et al.*, 2000). This form of motility is a multicellular behavior and is used for the initial surface contact during infections (Fraser and Hughes, 1999; Hahn, 1997). In addition to the flagellum and T4P, rhamnolipids, which are secreted by the bacterium and lower the surface tension, are also playing a critical role in swarming motility (Fauvart *et al.*, 2012; Köhler *et al.*, 2000).

On biotic and abiotic solid surfaces, *P. aeruginosa* employs its T4P exclusively for twitching. The process involves the extension of the T4P, the adhesion of the tip to a surface, and both the forward motion and the subsequent retraction (Fig. 1.5C) (Bradley, 1980; Talà *et al.*, 2019). Twitching motility is also essential for the maturation of biofilms.

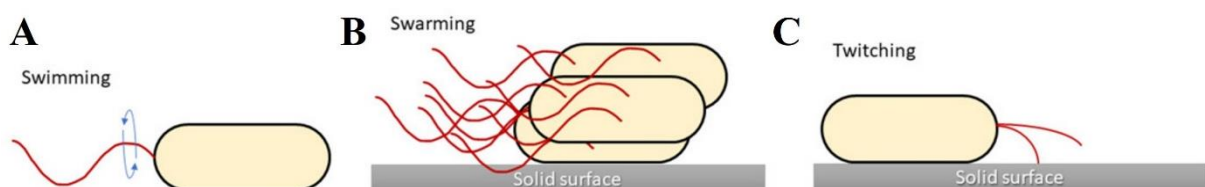


**Fig. 1.5: Schematic representation of the different movement types of *P. aeruginosa*.**

(A) Swimming, (B) swarming and, (C) twitching motility with the corresponding structures (pili or flagella) responsible for the movement (highlighted in red). Figure modified from Zegadło *et al.*, 2023 and Wadhwa and Berg, 2022.

### 1.6.2 The phytochrome of *P. aeruginosa* is organized in an operon with its heme oxygenase

The bacterial phytochrome BphP of *P. aeruginosa* acts as a sensor histidine kinase within a described TCS. The *bphP* and *bphO* genes, required for holo-phytochrome assembly, are arranged in a bicistronic operon (Fig. 1.6) (Barkovits *et al.*, 2008). The downstream located *bphP* gene encodes the apo-phytochrome, whereas the upstream located *bphO* gene encodes a HO. This enzyme is necessary for producing the linear tetrapyrrole BV IX $\alpha$  from heme (Wegele *et al.*, 2004). BV IX $\alpha$  can autocatalytically bind to a conserved cysteine residue in the PAS domain of the phytochrome via a thioether bond. The expression of the operon is regulated by the alternative sigma factor RpoS and is cell density dependent (Barkovits *et al.*, 2008; Barkovits *et al.*, 2011). Furthermore, *bphP* expression is regulated via the transcriptional activator LasR, facilitated by a LasR binding site located between *bphO* and *bphP* (Barkovits *et al.*, 2011). No putative RR (*bphR*) is encoded downstream of *bphP* in *P. aeruginosa*, in contrast to other phytochrome systems like in *P. putida* or *D. radiodurans* (Bhoo *et al.*, 2001).

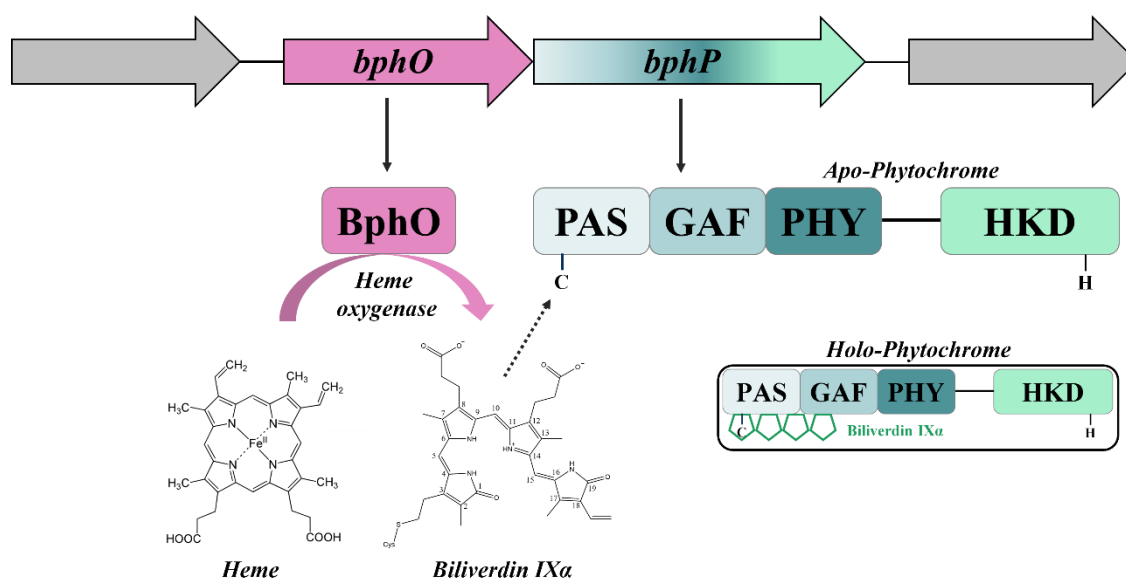


**Fig. 1.6: Genetic organization of the bacterial phytochrome operon in *Pseudomonas aeruginosa*.**

The genes *bphP* and *bphO* encode the two required components for assembling a holo-phytochrome. BphO is a HO, cleaving heme to produce the chromophore BV IX $\alpha$ . BphP is the apo-phytochrome, containing the conserved cysteine residue in its PAS domain, which autocatalytically binds BV IX $\alpha$ .

### 1.6.3 *P. aeruginosa* utilizes two heme oxygenases to build various isomers of its chromophore

Phylogenetic analysis identified different classes of bacterial HOs: the cyanobacterial HO-1 and HO-2 family, the Isd, HmuO, PigA/HemO as well as BphO family (Frankenberg-Dinkel, 2004; Wilks, 2002). In addition to *bphO*, the gene encoding for a HO organized in the phytochrome operon, *P. aeruginosa* encodes a second HO (HemO; synonym PigA). BphO and HemO, both share the same function as all HO, catalyzing the cleavage of heme to BV (Fig. 1.7). The reaction requires three molecules of oxygen as well as seven electrons for each heme and additionally yields iron ( $\text{Fe}^{2+}$ ) and carbon monoxide (CO) (Frankenberg-Dinkel, 2004; Wegele *et al.*, 2004). Many HOs from pathogenic organisms are only induced under conditions of iron limitation in order to utilize the released  $\text{Fe}^{2+}$  and recover a lack of iron (Wilks and Schmitt, 1998). The two HOs from *P. aeruginosa* exhibit different regio-specificity towards heme, resulting in the formation of distinct chromophore isomers. While BphO is a classical HO that oxidizes the  $\alpha$ -carbon bridge in the heme precursor resulting in the formation of BV IX $\alpha$ , HemO produces the atypical isomers BV IX $\beta$  and BV IX $\delta$  (Caignan *et al.*, 2002; Wegele *et al.*, 2004). This difference in regio-specificity results from a 100° heme rotation in HemO compared to  $\alpha$ -hydroxylating HOs, such as BphO (Caignan *et al.*, 2002).

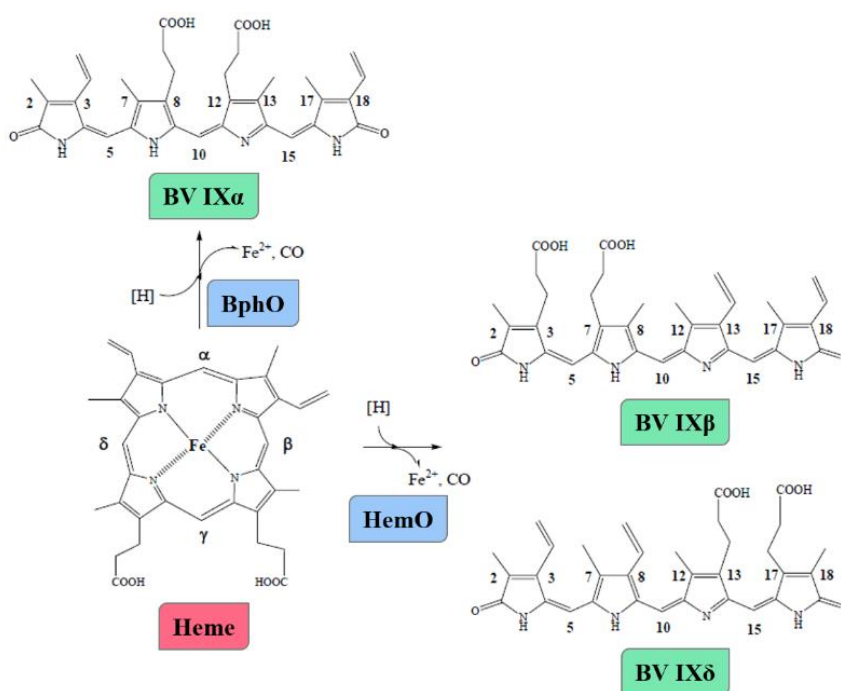


**Fig. 1.7: Heme cleavage catalyzed by *P. aeruginosa* heme oxygenases BphO and HemO.**

The two HOs show different regio-specificity towards heme. BphO cleaves heme at the  $\alpha$ -carbon bond, yielding BV IX $\alpha$ , while HemO cleaves heme at the  $\beta$ - or  $\delta$ -carbon bond, resulting in BV IX $\beta$  or BV IX $\delta$ . The reaction additionally produces CO and  $\text{Fe}^{2+}$ . Figure modified from Frankenberg-Dinkel, 2004 and Wegele *et al.*, 2004.

## 1.7 Objectives of this work

The discovery of phytochromes beyond the plant kingdom has paved the way for a novel area of research. The ever-advancing technology of genome sequencing has enabled the description of phytochromes in heterotrophic organisms, including bacteria and fungi. Most of these BphPs are described and shown to be sensor histidine kinases within TCSs, generating light-dependent physiological responses in the cells. Although the photobiology, and three-dimensional structure of most of the bacterial phytochromes have been extensively studied, the correlation between phytochrome photostate and autokinase output remains poorly understood. Therefore, the biological function in bacteria is still unclear. This is especially true for the bathy BphP of the human opportunistic pathogen *P. aeruginosa*. Despite its discovery over 20 years ago, little progress has been accomplished in understanding its physiological role. Meanwhile, it is evident that *PaBphP* is controlling light-dependent virulence-mediated behavior. The present study aimed to comprehensively investigate the phytochrome of *P. aeruginosa*, focusing on the chromophore/protein conformation and its connection to the autokinase activity. To elucidate the detailed function of *PaBphP*, it was necessary to determine its active parental state – Pr or Pfr – and identify the conditions that strongly inhibit or block the activity of the kinase. Additionally, the phytochrome had to be studied within the context of its TCS, and phenotypical assays, including mutant and overexpression strain analysis, had to be performed.

While there is a fairly good understanding for prototypical phytochromes that the highest kinase activity is observed in the Pr-form under dark conditions, the reports of the autokinase activity of bathy phytochromes are only limited. For this reason, a systematic analysis of *PaBphP*, four others bathy BphPs, and two additional prototypical BphPs had to be conducted to achieve a comprehensive and general statement of the photostate/autokinase output correlation. In addition, one of the main objectives of this work was to develop a method for calculating the Pr/Pfr-fractions for each phytochrome, allowing the direct correlation of these well-defined stationary values with the autophosphorylation output.



## 2 Material and Methods

### 2.1 Materials and chemicals

#### 2.1.1 Equipment

**Table 2.1: Instruments used in this study.**

Type of instrument	Name	Manufacturer
Agarose gel electro. chamber	Maxi-VG	VWR International
Autoclave	VX 150	Systec
Blotting system	Semidry Blot Trans-Blot®SD	Bio-Rad
Centrifuges and rotors	5415 D (Rotor: F45-24-11) 5810 R (Rotor: A-4-62) Z32HK (Rotor: 221.17 V20) Sorvall LYNX 6000 (Rotor: T29-8x50 and F9-6x1000)	Eppendorf Eppendorf Hermle Thermo Fisher Scientific
Clean bench	Anthos Antares 48	Biohit HealthCare
Gel documentation system	Gel iX20 Imager	Intas
High pressure homogenizer	LM 10 Microfluidizer	Microfluidics
Illumination equipment	Iso lab construction 66182 Quartz Tungsten Halogen Lamp Housing 71445 Electronic Safety Shutter	Biophysics RPTU LOT-Oriel LOT-Oriel
Incubator	kelvitron®t	Heraeus Instruments
Incubator shaker	Innova™ 2300 Platform Shaker Innova® 44 Incubator Shaker Series	New Brunswick Scientific New Brunswick Scientific
Interference filter Fig. S1	Dark Blue 435 nm #2458312 Red 690 nm Wratten Nr. 87 (750 nm)	Baader Planetarium LOT-Oriel Kodak
LEDs / laser diodes Fig. S1	426 nm blue (DLE-038-046) 667/791 nm red/far-red (LNCT28PS01WW)	Everlight Electronics Panasonic
Magnetic stirrer	MR 3001 MR Hei-Standard	Heidolph Instruments Heidolph Instruments
Multimeter	True RMS 3410 DMM	PeakTech®
Optical multichannel analyzer	Ocean Optics USB2000+UV/Vis	Ocean Optics / Ocean Insight
pH meter	pH 50+ DHS	Dostmann Electronic
Phosphoimager	Typhoon FLA 7000	GE Healthcare
Pipettes	Research® Research® Plus	Eppendorf Eppendorf

---

Power supply	PowerPac™ HC PowerPac™ Basic Power Source 300V EPS301 EPS601 Power Solution HCPS 1500 Konstanter SLP 240-40	Bio-Rad Bio-Rad VWR Amersham Biosciences GE Healthcare HyCell LOT-Oriel
Scales	R 300 S Atilon ATL-623 RS-232 4000/AR	Sartorius Acculab Sartorius Group KERN & SOHN GmbH Europe
SDS-PAGE chamber	Mini-PROTEAN® Tetra system Mini-PROTEAN®	Bio-Rad Bio-Rad
Spectrometer	8453 UV visible system NanoDrop™ Lite Ultrospec 500 pro	Agilent Technologies Thermo Fisher Scientific Amersham Biosciences
Thermo block	Thermocell CHB-202 Thermomixer compact	Bioer Eppendorf
Thermal cycler	peqstar 2 TGradient	Peqlab Biometra
Ultra-pure water system	MilliQ® Integral Water Purification System	Merck Millipore
Ultrasonic homogenizer	Sonoplus GM2200, UW 2200 with tip KE 76	Bandelin
Vacuum pump	Laboport®	KNF Neuberger
Vortexer	REAX 2000	Heidolph Instruments

---

### 2.1.2 Special material, chemicals, enzymes, kits, and antibodies

All chemicals used in this study were of ACS grade or higher and were purchased from AppliChem GmbH (Darmstadt, Germany), Bio-Rad (Hercules, CA), Becton Dickinson (Franklin Lakes, NJ), Carl Roth GmbH + Co. KG (Karlsruhe, Germany), Merck KGaA (Darmstadt), Serva Electrophoresis GmbH (Heidelberg, Germany), Sigma-Aldrich (St. Louis, MO) and Thermo Fisher Scientific (Waltham, MA) unless stated otherwise.

Table 2.2: Special material, chemicals, enzymes, kits, and antibodies used in this study.

Type of product/material	Name of product/material	Manufacturer
<b>Special material and chemicals</b>		
ATP solution	ATP $\geq 99\%$ , 100 mM solution	Carl Roth
Bradford reagent	ROTI <sup>®</sup> Quant (5x)	Carl Roth
Centrifugal filter units	Amicon <sup>®</sup> Ultra-4, MWCO 10,000 Microspin <sup>™</sup> G-50 Columns	Merck Millipore cytiva
Chromophore	Biliverdin-hydrochlorid	Sigma-Aldrich
Column material for affinity chromatography	Strep-Tactin <sup>®</sup> Sepharose <sup>®</sup> TALON <sup>®</sup> Superflow <sup>™</sup>	Iba cytiva
Cuvettes	Semi-micro cuvettes, 1.6 ml, 10 mm	ratiolab <sup>®</sup>
Dialysis tubing	Servapore <sup>®</sup> dialysis tubing, MWCO 12,000-14,000, diameter 16 mm	Serva
DNA loading dye	Gel Loading Dye, Purple (6x)	New England Biolabs
DNA size standard	GeneRuler <sup>™</sup> 1 kb Plus DNA Ladder	Thermo Fisher Scientific
Imaging plate	BAS-IP MS 2040	Fujifilm
Protein size standard	Blue Prestained Protein Standard, Broad Range	New England Biolabs
	Color Prestained Protein Standard, Broad Range	New England Biolabs
	PageRuler <sup>™</sup> Prestained Protein Ladder	Thermo Fisher Scientific
	Prestained protein marker	proteintech
	Unstained Protein Standard, Broad Range	New England Biolabs
Radioactive ATP	[ $\gamma$ - <sup>32</sup> P]-ATP (SRP-301), 500 $\mu$ Ci	Hartmann Analytic
Sterile filter	0.22 $\mu$ m Syringe Filter, PVDF (Sterile), Blue, 33 mm	Starlab International
	0.45 $\mu$ m Syringe Filter, PVDF (Sterile), Yellow, 33 mm	Starlab International
Transfer membrane	Transfer membrane ROTI <sup>®</sup> PVDF 0.45 $\mu$ m	Carl Roth
<b>Enzymes and kits</b>		
DNaseI	DNaseI	AppliChem
DNA ligase	T4 DNA ligase	New England Biolabs
DNA polymerase	<i>Phusion</i> DNA polymerase	AG Frankenberg-Dinkel
	<i>Pfu</i> DNA polymerase	AG Frankenberg-Dinkel
DNA polymerase buffer	5x <i>Phusion</i> <sup>®</sup> HF Reaction Buffer	New England Biolabs
	10x <i>Pfu</i> Reaction Buffer	AG Frankenberg-Dinkel
dNTPs	dNTP-Mix (dATP, dCTP, dGTP, dTTP)	Axon Labortechnik
Genomic DNA isolation	NucleoSpin <sup>®</sup> Microbial DNA kit	Macherey-Nagel

Gibson assembly	<i>Phusion</i> <sup>®</sup> high-fidelity DNA polymerase T5 exonuclease <i>Taq</i> DNA ligase	New England Biolabs New England Biolabs New England Biolabs
Lysozyme	Lysozyme, lyophilized	Carl Roth
PCR clean-up	NucleoSpin <sup>®</sup> Gel and PCR Clean-up kit	Macherey-Nagel
Plasmid DNA miniprep	NucleoSpin <sup>®</sup> Plasmid EasyPure kit E.Z.N.A. <sup>®</sup> Plasmid DNA Mini Kit I	Macherey-Nagel Omega Bio-Tek Inc
Restriction endonucleases	Restriction endonucleases High-fidelity (HF <sup>®</sup> ) restriction endonucleases	New England Biolabs New England Biolabs
<b>Antigen</b>	<b>Antibody</b>	<b>Manufacturer</b>
Polyhistidine-tag	6x-His tag monoclonal antibody (1:3,000)	Invitrogen
Mouse IgG	Goat anti-mouse IgG (whole molecule)-alkaline phosphatase antibody (1:10,000)	Sigma-Aldrich
Strep-tag II	Strep-Tactin <sup>®</sup> AP conjugate (1:4,000)	Iba
<i>Pa</i> BphP	Rabbit $\alpha$ BphP-Serum #SA3585 (1:5,000)	Eurogentec
Rabbit IgG	Goat anti-rabbit IgG (whole molecule)-alkaline phosphatase antibody (1:30,000)	Sigma-Aldrich

## 2.2 Bacterial strains, plasmids, and oligonucleotides

### 2.2.1 Bacterial strains

Table 2.3: Bacterial strains used in this study.

Bacterial Strain	Characteristics	Reference
<i>Escherichia coli</i> strains		
DH5 $\alpha$	F <sup>-</sup> <i>endA1 glnV44 thi-1 recA1 relA1 gyrA96 deoR nupG purB20</i> $\phi$ 80 <i>dlacZ</i> $\Delta$ M15 $\Delta$ ( <i>lacZYA-argF</i> )U169, <i>hsdR17</i> (r <sub>K</sub> <sup>-</sup> m <sub>K</sub> <sup>+</sup> ), $\lambda$ <sup>-</sup>	(1)
S17-I	Tp <sup>r</sup> Sm <sup>r</sup> <i>recA thi pro hsdR</i> -M <sup>+</sup> RP4:2-Tc::Mu-Km::Tn7/ $\lambda$ pir	(2)
S17-I pEXG2_ $\Delta$ <i>bphP</i>	S17-I with pEXG2_ $\Delta$ <i>bphP</i> , Gm <sup>R</sup>	This study
S17-I pEXG2_ $\Delta$ <i>bphOP</i>	S17-I with pEXG2_ $\Delta$ <i>bphOP</i> , Gm <sup>R</sup>	This study
S17-I pEXG2_ $\Delta$ <i>kinB</i>	S17-I with pEXG2_ $\Delta$ <i>kinB</i> , Gm <sup>R</sup>	This study
Top10	F <sup>-</sup> <i>mcrA</i> $\Delta$ ( <i>mrr-hsdRMS-mcrBC</i> ) $\phi$ 80 <i>lacZ</i> $\Delta$ M15 $\Delta$ <i>lacX74 nupG recA1 araD139<math>\Delta</math>(<i>ara-leu</i>)7697 <i>galE15 galK16 rpsL</i>(Str<sup>R</sup>) <i>endA1</i> <math>\lambda</math><sup>-</sup></i>	Invitrogen
Top10 pBAD/HisB_ <i>Rt</i> BphP2HmuO	Top10 with pBAD/HisB_ <i>Rt</i> BphP2HmuO; Amp <sup>R</sup>	(3)

BL21(DE3)	<i>F ompT gal dcm lon hsdS<sub>B</sub>(r<sub>B</sub>m<sub>B</sub><sup>-</sup>) λ(DE3 [lacI lacUV5-T7p07 ind1 sam7 nin5]) [malB<sup>+</sup>]<sub>K-12</sub>(λ<sup>S</sup>)</i>	(4)
BL21(DE3) pASK_ <i>Pa</i> AlgB	BL21(DE3) with pASK- <i>Pa</i> AlgB; Amp <sup>R</sup>	This study
BL21(DE3) pASK_ <i>Pa</i> KinBCD	BL21(DE3) with pASK- <i>Pa</i> KinBCD; Amp <sup>R</sup>	This study
BL21(DE3) pASK_ <i>Pa</i> KinBCD_P390S	BL21(DE3) with pASK- <i>Pa</i> KinBCD_P390S; Amp <sup>R</sup>	This study
BL21(DE3) pASK_ <i>At</i> BphP1	BL21(DE3) with pASK- <i>At</i> BphP1; Amp <sup>R</sup>	This study
BL21(DE3) pET21b_ <i>At</i> BphP2	BL21(DE3) with pET21b- <i>At</i> BphP2; Amp <sup>R</sup>	This study
BL21(DE3) pET21b_ <i>At</i> BphP2_D783N	BL21(DE3) with pET21b- <i>At</i> BphP2_D783N; Amp <sup>R</sup>	This study
BL21(DE3) pET21b_ <i>Av</i> BphP2	BL21(DE3) with pET21b- <i>Av</i> BphP2; Amp <sup>R</sup>	(3)
BL21(DE3) pET21b_ <i>Av</i> BphP2_D793A	BL21(DE3) with pET21b- <i>Av</i> BphP2_D793A; Amp <sup>R</sup>	(3)
BL21(DE3) pET52_ <i>Pst</i> BphO_BphP1	BL21(DE3) with pET52- <i>Pst</i> BphO_BphP1; Amp <sup>R</sup>	This study
BL21(DE3) pASK_ <i>Pst</i> BphP2	BL21(DE3) with pASK- <i>Pst</i> BphP2; Amp <sup>R</sup>	This study
BL21(DE3) pET24a_ <i>Xcc</i> BphP	BL21(DE3) with pET24a- <i>Xcc</i> BphP; Kan <sup>R</sup>	(3)
BL21(DE3) pET24a_ <i>Xcc</i> BphPΔPAS9	BL21(DE3) with pET24a- <i>Xcc</i> BphPΔPAS9; Kan <sup>R</sup>	(3)
<b><i>Pseudomonas aeruginosa</i> strains</b>		
PA14	<i>P. aeruginosa</i> wild type UCBPP-14	(5)
PA14Δ <i>bphP</i> / PA14Δ <i>bphP</i> *	2.0-kb in-frame deletion of <i>bphP</i> in PA14 background	This study Pielage 2017*
PA14Δ <i>bphP</i> pHERD26T	<i>bphP</i> deletion mutant with pHERD26T; Tet <sup>R</sup>	This study
PA14Δ <i>bphP</i> pHERD26T_ <i>Pa</i> BphP	<i>bphP</i> deletion mutant with pHERD26T_ <i>Pa</i> BphP; Tet <sup>R</sup>	This study
PA14Δ <i>bphP</i> pHERD26T_ <i>Pa</i> BphP_H513A	<i>bphP</i> deletion mutant with pHERD26T_ <i>Pa</i> BphP_H513A; Tet <sup>R</sup>	This study
PA14Δ <i>bphP</i> * pHERD26T_ <i>Pa</i> BphP_D194H	<i>bphP</i> deletion mutant with pHERD26T_ <i>Pa</i> BphP_D194H; Tet <sup>R</sup>	(6)
PA14Δ <i>bphP</i> * pHERD26T_ <i>Pa</i> BphP_S261A	<i>bphP</i> deletion mutant with pHERD26T_ <i>Pa</i> BphP_S261A; Tet <sup>R</sup>	(6)
PA14Δ <i>bphP</i> * pHERD26T_ <i>Pa</i> BphP_C12A	<i>bphP</i> deletion mutant with pHERD26T_ <i>Pa</i> BphP_C12A; Tet <sup>R</sup>	(7)

PA14 $\Delta$ <i>kinB</i>	1.7-kb in-frame deletion of <i>kinB</i> in PA14 background	This study
PA14 $\Delta$ <i>bphOP</i>	2.7-kb in-frame deletion of <i>bphOP</i> in PA14 background	This study
PA14 $\Delta$ <i>bphOP</i> pHERD26T_ <i>PaBphP</i>	<i>bphOP</i> deletion mutant with pHERD26T_ <i>PaBphP</i> ; Tet <sup>R</sup>	This study

\* The plasmids pHERD26T\_*PaBphP*\_D194H, pHERD26T\_*PaBphP*\_S261A, and pHERD26T\_*PaBphP*\_C12A were used in an incorrect *bphP* deletion mutant (gene is correctly deleted, but strain is Gm<sup>R</sup>) from J. Pielage, 2017.

(1) Hanahan, 1983; (2) de Lorenzo and Timmis, 1994; (3) Schultheiß, 2023; (4) Studier and Moffatt, 1986; (5) Rahme *et al.*, 1995; (6) Bilici, 2020; (7) Denig, 2020

## 2.2.2 Plasmids

Table 2.4: Plasmids used in this study.

Plasmid	Characteristic	Reference
Plasmids used in <i>Escherichia coli</i>		
pASK-IBA3	Expression vector, heterologous overexpression in <i>E. coli</i> , Strep-tag II, <i>tet</i> promoter, Amp <sup>R</sup>	IBA Lifesciences
pASK_ <i>PaBphP</i>	pASK-IBA3 derivative, coding region of <i>bphP</i> from <i>P. aeruginosa</i> (PAO1_4117) at <i>XbaI/XhoI</i> site with C-terminal Strep-tag II, <i>tet</i> promoter, Amp <sup>R</sup>	(1)
pASK_ <i>PaAlgB</i>	pASK-IBA3 derivative, coding region of <i>algB</i> from <i>P. aeruginosa</i> (PA14_72380) at <i>XbaI/XhoI</i> site with C-terminal Strep-tag II, <i>tet</i> promoter, Amp <sup>R</sup>	RPTU Microbiology (Pielage 2021)
pASK_ <i>PaKinBCD</i>	pASK-IBA3 derivative, coding region of cytosolic domain of <i>kinB</i> from <i>P. aeruginosa</i> (PA14_72390; Gly198-Val595) at <i>BamHI</i> site with C-terminal Strep-tag II, <i>tet</i> promoter, Amp <sup>R</sup>	(2)
pASK_ <i>PaKinBCD</i> _P390S	pASK_ <i>PaKinBCD</i> with encoded amino acid exchange → Pro (390) by Ser	This study
pASK_ <i>AtBphP1</i>	pASK-IBA3 derivative, coding region of <i>bphP1</i> from <i>A. tumefaciens</i> at <i>XbaI/HindIII</i> site with C-terminal Strep-tag II, <i>tet</i> promoter, Amp <sup>R</sup>	RPTU Microbiology
pET21b_ <i>AtBphP2</i>	pET21b derivative, coding region of <i>bphP2</i> from <i>A. tumefaciens</i> at <i>BamHI/NdeI</i> site with C-terminal His-tag, T7 promoter, Amp <sup>R</sup>	(3)
pET21b_ <i>AtBphP2</i> _D783N	pET21b_ <i>AtBphP2</i> with encoded amino acid exchange → Asp (783) by Asn	This study

pET21b_AvBphP2	pET21b derivative, coding region of <i>bphP2</i> from <i>A. vitis</i> at <i>NdeI/XhoI</i> site with C-terminal His-tag, T7 promoter, Amp <sup>R</sup>	(4)
pET21b_AvBphP2_D793A	pET21b_AvBphP2 with encoded amino acid exchange → Asp (783) by Ala	(5)
pET52_PstBphO_BphP1	pET52 3C/LIC derivative, coding region of <i>bphO</i> from <i>P. syringae</i> (PSPTO_1901) with N-terminal Strep-tag II and <i>bphP1</i> from <i>P. syringae</i> (PSPTO_1902) with C-terminal His-tag, T7 promoter, Amp <sup>R</sup>	(6)
pASK_PstBphP2	pASK-IBA3 derivative, coding region of <i>bphP2</i> from <i>P. syringae</i> (PSPTO_2652) at <i>XbaI/KpnI</i> site with C-terminal Strep-tag II, <i>tet</i> promoter, Amp <sup>R</sup>	RPTU Microbiology (Halscheidt 2010)
pBAD/HisB_RtBphP2HmuO	pBAD/HisB derivative, coding region of <i>bphP2</i> from <i>R. tatouinensis</i> (Rta_28950) at <i>BglII/EcoRI</i> site with N-terminal His-tag and <i>hmuO</i> from <i>Bradyrhizobium</i> sp. ORS278 at <i>EcoRI/HindIII</i> site, P <sub>BAD</sub> , Amp <sup>R</sup>	(7)
pET24a_XccBphP	pET24a derivative, coding region of <i>bphP</i> from <i>X. campestris</i> pv. <i>campestris</i> strain 8004 residue 1-634 (XC_4241) at <i>NdeI/BamHI</i> site with N-terminal His-tag, T7 promoter, Kan <sup>R</sup>	(8)
pET24a_XccBphPΔPAS9	pET24a derivative, coding region of <i>bphP</i> from <i>X. campestris</i> pv. <i>campestris</i> strain 8004 residue 1-511 (XC_4241) at <i>NdeI/BamHI</i> site with N-terminal His-tag, T7 promoter, Kan <sup>R</sup>	(8)

#### Plasmids used in *Pseudomonas aeruginosa*

pHERD26T	<i>E. coli</i> / <i>P. aeruginosa</i> shuttle vector, homologous overexpression in <i>P. aeruginosa</i> , P <sub>BAD</sub> , Tet <sup>R</sup>	(9)
pHERD26T_PaBphP	pHERD26T derivative, coding region of <i>bphP</i> from <i>P. aeruginosa</i> (PAO1_4117) at <i>XbaI/KpnI</i> site with C-terminal Strep-tag II, P <sub>BAD</sub> , Tet <sup>R</sup>	(10)
pHERD26T_PaBphP_H513A	pHERD26T_PaBphP with encoded amino acid exchange → His (513) by Ala	(11)
pHERD26T_PaBphP_D194H	pHERD26T_PaBphP with encoded amino acid exchange → Asp (194) by His	(12)
pHERD26T_PaBphP_S261A	pHERD26T_PaBphP with encoded amino acid exchange → Ser (261) by Ala	(12)
pHERD26T_PaBphP_C12A	pHERD26T_PaBphP with encoded amino acid exchange → Cys (12) by Ala	(11)

pEXG2	Allelic exchange vector for construction of markerless deletion mutants or single-nucleotide substitutions in <i>P. aeruginosa</i> , Gm <sup>R</sup>	(13)
pEXG2_Δ <i>bphP</i>	pEXG2 derivative, truncated version of <i>bphP</i> from <i>P. aeruginosa</i> (PAO1_4117; 147 bp) with 621 bp upstream and 818 bp downstream at <i>HindIII/EcoRI</i> site, Gm <sup>R</sup>	RPTU Microbiology (Pielage 2017)
pEXG2_Δ <i>bphOP</i>	pEXG2 derivative, truncated version of <i>bphOP</i> from <i>P. aeruginosa</i> (PA14_10700/10710; 123 bp) with 513 bp upstream and 451 bp downstream at <i>EcoRI/BamHI</i> site, Gm <sup>R</sup>	This study
pEXG2_Δ <i>kinB</i>	pEXG2 derivative, truncated version of <i>kinB</i> from <i>P. aeruginosa</i> (PA14_72390; 54 bp) with 437 bp upstream and 469 bp downstream at <i>HindIII/BamHI</i> site, Gm <sup>R</sup>	This study

(1) Tasler *et al.*, 2005; (2) Schneckmann, 2021; (3) Lamparter and Michael, 2005; (4) Rottwinkel *et al.*, 2010; (5) Schultheiß, 2023; (6) Shah *et al.*, 2012; (7) De Luca *et al.*, 2019; (8) Otero *et al.*, 2016; (9) Qiu *et al.*, 2008; (10) Heine, 2014; (11) Denig, 2020; (12) Bilici, 2020; (13) Rietsch *et al.*, 2005

### 2.2.3 Oligonucleotides

Table 2.5: Oligonucleotides used in this study.

Primer	Sequence (5' – 3')
Primer for construction of plasmids for homologous recombination	
pEXG2Δ <i>bphOP</i> _upF	GCGAATTCGGGCCTGAAGGAAGTGAAGCAGT
pEXG2Δ <i>bphOP</i> _upR	CGCAGGCAGAAGGTGATTTCTGCGTGCAGGTCACGGG
pEXG2Δ <i>bphOP</i> _downF	ATCACCTTCTGCCTGCGCCT
pEXG2Δ <i>bphOP</i> _downR	GCGGATCCGCGTACGGTCTTGCGCTTGC
→ Construction of pEXG2_Δ <i>bphOP</i>	
pEXG2Δ <i>kinB</i> _upF	TTAGCTAAGCTTCTCAACGTGATGGTGCTC
pEXG2Δ <i>kinB</i> _upR	TCACACCGGGAGGAACAACCGGGTCCGGA
pEXG2Δ <i>kinB</i> _downF	TTGTTCTCCCGGTGTGACCGGGGCCGCT
pEXG2Δ <i>kinB</i> _downR	AATCTAGGATCCGTCTGGTATCCGTTACG
→ Construction of pEXG2_Δ <i>kinB</i>	
Primer for construction of overexpression plasmids for <i>Escherichia coli</i>	
pASK- <i>PaAlgB</i> _fwd	CGTCTAGATAACGAGGGCAAAAAACCA
pASK- <i>PaAlgB</i> _rev	CCCTCGAGTAGGCCGTACTGCTTGCG
→ Construction of pASK- <i>PaAlgB</i>	
pASK- <i>PaKinBCD</i> _fwd	ATTCGAGCTCGGTACCCGGGATGGGCGCAC



pASK-*Pa*KinBCD\_rev CCTGCAGGTCGACCTCGAGGGACACCGGCA

### → Construction of pASK-*Pa*KinBCD

Primer for site-directed mutagenesis on overexpression plasmids for *Escherichia coli*

pASK-*Pa*KinBCDP390S  
\_fwd CCTGCGCGCCTCCCACGAGCTCCGCACGTCGGTGACCGG

pASK-*Pa*KinBCDP390S  
\_rev CCGGTCACCGACGTGCGGAGCTCGTGGGAGGCGCGCAGG

### → Construction of pASK-*Pa*KinBCD\_P390S

pET21b-*At*BphP2D783N  
\_fwd GACGTCGCCATTCTCAACATCAATCTTGGATCCGACACC

pET21b-*At*BphP2D783N  
\_rev GGTGTCGGATCCAAGATTGATGTTGAGAATGGCGACGTC

### → Construction of pET21b-*At*BphP2\_D783N

Primer for sequencing

pEXG2\_seqF CGACCTCATTCTATTAGACTCTCGTTTGGATTGC

pEXG2\_seqR GTTCGCTCGCGTATCGGTGATTTCATTCTG

$\Delta$ *bphOP*\_seqF GGGGATATCCATTTTCGCGGAAG

$\Delta$ *bphOP*\_seqR GCTCCATGAATTTCGTCGGGG

$\Delta$ *kinB*\_seqF GCGCTTCATCCAGGACAAGG

$\Delta$ *kinB*\_seqR CGCCTGGTGGATGAGAACCG

pET\_seqF GCTAGTTATTGCTCAGCGG

pET\_seqR TAATACGACTCACTATAGGG

## 2.3 Microbial methods

### 2.3.1 Sterilization

All media and supplements used for cultivation of microbial cultures were sterilized before utilization. Heat-stable solutions and plastic reaction tubes were autoclaved for 20 min at 120 °C and 1 bar, while heat-sensitive solutions were sterilized by filtration. Therefore, 0.2 µm pore size filters were used, and the solutions were added to the heat-sterilized media. In contrast, glassware was sterilized by dry heat at 180 °C for 3 h.

### 2.3.2 Culture media and supplements

Autoclaved lysogeny broth (LB-Lennox) medium with appropriate antibiotics and/or supplements was used for aerobic cultivation of liquid *E. coli* or *P. aeruginosa* cultures. Solid medium was prepared by adding 1.5 % (w/v) agar-agar prior to autoclaving. Solid cultivation

for *P. aeruginosa* phenotypic swimming assays was performed using LB and technical Difco™-agar from Becton Dickinson (BD).

**Table 2.6: Culture media, antibiotics, and supplements used in this study.**

Culture media, antibiotics, and supplements			
<b>LB-medium; Lennox (pH = 7.0)</b>		<b>BD™ Swimming-agar (pH = 7.0)</b>	
Tryptone	10 g/l	LB Lennox (BD)	20 g/l
Yeast extract	5 g/l	Difco™-agar (BD)	0.3 % (w/v)
NaCl	5 g/l		
<b>BD™ Pseudomonas Isolation-agar (pH = 7.0 ± 0.2)</b>			
Bacto Peptone	20 g/l	Mg Chloride	1.4 g/l
Potassium Sulfate	10 g/l	Irgasan®	0.025 g/l
Agar	13.6 g/l	Glycerol	20 ml/l
<b>Antibiotic</b>	<b>Stock conc.</b>	<b>conc. <i>E. coli</i></b>	<b>conc. <i>P. aeruginosa</i></b>
Ampicillin (Amp) in H <sub>2</sub> O	100 mg/ml	100 µg/ml	-
Gentamicin (Gm) in H <sub>2</sub> O	10 or 300 mg/ml	10 µg/ml	300 µg/ml
Kanamycin (Kan) in H <sub>2</sub> O	50 mg/ml	50 µg/ml	-
Tetracycline (Tet) in 70 % (v/v) EtOH	5 or 50 mg/ml	5 µg/ml	100 µg/ml
<b>Supplement</b>	<b>Solvent</b>	<b>Stock concentration</b>	<b>Final concentration</b>
Anhydrotetracycline	Dimethylformamide	2 mg/ml	200 ng/ml
IPTG	H <sub>2</sub> O	1 M	0.5 mM
L(+)-Arabinose	H <sub>2</sub> O	10 % (w/v)	0.1 % (w/v)
D(+)-Sucrose	H <sub>2</sub> O	50 % (w/v)	15 % (w/v)

### 2.3.3 Storage of *E. coli* and *P. aeruginosa* cells

For short-term storage of *E. coli*, cells were streaked out on LB-agar plates with the appropriate antibiotic, if necessary, and stored at 4 °C. For short-term storage of *P. aeruginosa*, LB-agar plates were stored at room temperature. For long term-storage, both *E. coli* and *P. aeruginosa* strains were stored at -80 °C. Overnight cultures of *E. coli* were diluted in media containing 20 % (v/v) glycerol, and *P. aeruginosa* overnight cultures were diluted in media containing 7.5 % (v/v) DMSO.

### **2.3.4 Cultivation of *E. coli* or *P. aeruginosa* cells**

For initially grow *E. coli* or *P. aeruginosa* on solid medium, bacteria were taken from a glycerol or DMSO stock (chapter 2.3.3) using a sterile inoculation loop and spread out on an LB-agar plate. Additives, such as antibiotics (Tab. 2.6), were added to the solid medium for selection conditions. Plates were incubated overnight at 37 °C or for 48 h at room temperature and served as stock plates for liquid cultures. To prepare overnight cultures, LB medium was inoculated into a test tube or in an Erlenmeyer flask with a single colony from the previously grown LB-agar plate or from a freshly transformed *E. coli* culture. The volume was chosen individually depending on the amount needed for subsequent experiments. If necessary, an appropriate amount of respective antibiotic was added to the medium before inoculation. Cultures were incubated overnight at 37 °C with constant shaking (160 rpm, Innova™ 2300 Platform Shaker). The following day, the main cultures, whose medium was also supplemented with additives as necessary, were then inoculated 1:100 with the *E. coli* overnight culture for subsequent experiments. For *P. aeruginosa*, the volume of the overnight culture used for inoculation was calculated so that the main culture had an OD<sub>600nm</sub> of 0.1 or 0.2 at time point zero.

### **2.3.5 Determination of cell density**

The optical density (OD) of liquid bacterial cultures was determined photometrically at a wavelength of 600 nm. LB or the respective used medium served as the reference for the measurement. An OD<sub>600nm</sub> of 1 corresponds to approximately  $1 \times 10^9$  *E. coli* cells/ml culture.

### **2.3.6 Analysis of aerobic growth of *P. aeruginosa***

For the analysis of growth phases and behavior, *P. aeruginosa* strains were cultured at 37 °C in a total volume of 200 ml LB medium under aerobic conditions (160 rpm, Innova™ 2300 Platform Shaker). LB overnight cultures were diluted as described in chapter 2.3.4. Incubation was performed for a maximum of 26 h. At various time points (at least every hour), culture samples (1 ml) were taken to monitor the OD<sub>600nm</sub>. The measured cell densities were plotted logarithmically against the time. In addition, another culture sample (1 ml) was taken simultaneously and centrifuged (RT, 11,000 rpm, 3 min, Eppendorf 5415 D, rotor: F45-24-1). Proteins in the resulting cell pellets were separated by SDS-PAGE and analyzed by Western blot, as well as an immunological detection procedure using a polyclonal serum against PaBphP.

### **2.3.7 Preparation of chemically competent *E. coli* cells**

*E. coli* cells are not naturally competent and do not possess the ability to take up foreign DNA molecules from their environment. However, this competence can be induced by chemical treatment. For this, 100 ml LB medium was inoculated 1:100 with an overnight culture of the respective *E. coli* strain. This culture was incubated under constant shaking (160 rpm, Innova™ 2300 Platform Shaker) at 37 °C to an OD<sub>600nm</sub> of 0.5-0.6. After reaching this optical density, the culture was divided into two batches of 50 ml and centrifuged (4 °C, 4,000 rpm, 10 min, Eppendorf 5810 R, rotor: A-4-62). After removal of the supernatant, the pellets were each carefully resuspended in 25 ml ice-cooled CaCl<sub>2</sub> solution (50 mM) and the suspensions were incubated on ice for one hour. The incubation was followed by another identical centrifugation step. After discarding the supernatant, the pellets were each carefully resuspended in 5 ml ice-cooled CaCl<sub>2</sub> solution (50 mM) mixed with 15 % (v/v) glycerol. The chemically competent *E. coli* cells were stored in 200 µl aliquots at -80 °C after freezing them in liquid nitrogen.

### **2.3.8 Transformation of chemically competent *E. coli* cells**

For transformation, thawed chemically competent *E. coli* cells (200 µl) were gently mixed with 50-100 ng plasmid DNA, 10-20 µl of a ligation or 15 µl of a Gibson assembly reaction and incubated on ice for 30 min. Subsequently, the cells were subjected to heat shock at 42 °C for 2 min. After 2 min on ice, 700 µl LB medium was added to the batch and the bacteria were incubated at 37 °C for 1 h under constant shaking (160 rpm, Innova™ 2300 Platform Shaker). After the incubation period, 100 µl of the culture was spread on a selective LB-agar plate, with the appropriate antibiotic. In case of difficult transformations, the samples were centrifuged (RT, 11,000 rpm, 3 min, Eppendorf 5415 D, rotor: F45-24-11) and part of the supernatant was discarded. The cell pellet was resuspended in 100 µl of the remaining medium and plated to obtain a higher cell density. An equal volume of sterile water was mixed with chemically competent cells and treated identically, as a control experiment. The LB-agar plates were incubated overnight at 37 °C or at room temperature for 48 h. The next day, the Petri dishes were sealed with parafilm and stored at 4 °C or used directly for overnight cultures and protein production experiments.

### **2.3.9 Conjugation of *P. aeruginosa* via biparental mating**

Conjugation of *P. aeruginosa* via biparental mating was performed using *E. coli* S17-I as the donor strain. Overnight cultures of the respective *P. aeruginosa* strain and transformed *E. coli* S17-I cells, carrying the desired plasmid, were prepared in 10 ml LB medium supplemented with antibiotics if necessary. For the biparental mating, the grown overnight cultures were mixed in a ratio of 9:1 (donor:recipient) in a total volume of 2 ml and incubated at room temperature for 30 min. Afterwards, the cells were sedimented by centrifugation (RT, 4,000 rpm, 1 min, Eppendorf 5415 D, rotor: F45-24-11) and carefully resuspended in 100  $\mu$ l fresh LB medium. The entire suspension was spotted onto an LB-agar plate and incubated upright at 37 °C for 24 h. The following day, the cell material was harvested with a sterile inoculation loop and resuspended in 0.9 % NaCl (w/v). A serial dilution in 0.9 % (w/v) NaCl solution was performed afterwards. 100  $\mu$ l of each dilution step ( $10^{-1}$  to  $10^{-4}$ ) was plated on Pseudomonas Isolation-agar (Tab. 2.6) with the addition of the selection antibiotic and incubated overnight at 37 °C. Enrichment of the conjugated bacteria was followed by one re-plating step on Pseudomonas Isolation-agar and two re-plating steps on LB-agar containing the appropriate antibiotic.

## **2.4 Phenotypic analysis of *Pseudomonas aeruginosa***

### **2.4.1 Swimming Motility**

To study the swimming motility of *P. aeruginosa* cells, overnight cultures of *P. aeruginosa* harboring pHERD26T derivatives were diluted in 15 ml LB medium ( $OD_{600nm} = 0.1$  at time point zero) supplemented with tetracycline. They were grown at 37 °C under constant shaking (160 rpm, Innova™ 2300 Platform Shaker) and ambient light conditions (Fig. S1C) until  $OD_{600nm}$  was approximately 0.7. After induction of the gene expression with 0.1 % (w/v) L(+)-arabinose and further incubation for 3 h at 37 °C with constant shaking (160 rpm; ambient light), the cell density of each 2 ml of the cultures was adjusted to an  $OD_{600nm} = 1.5$  in LB medium. Subsequently, 1  $\mu$ l of the culture was spotted on swimming-agar (Tab. 2.6) with four different strains per plate and incubated upright for 24 h at 30 °C. The swimming agar plates (square plates, 120x120 mm, 60 ml medium per petri dish, dried 20 min with lid closed and 10 min with lid open) were supplemented with 0.1 % (w/v) L(+)-arabinose and tetracycline. Evaluation was performed by measuring the diameter of the swimming zone the next day.

### 2.4.2 Investigation of secreted pyocyanin amounts

After incubation for 3 h and removal of a portion of the cultures for the swimming assay, the flasks were incubated for a further 2 h at 37 °C with constant shaking (160 rpm, Innova™ 2300 Platform Shaker; ambient light). After this step, the OD<sub>600nm</sub> was determined and 1.5 ml of each culture was pelleted by centrifugation (RT, 11,000 rpm, 3 min, Eppendorf 5415 D, rotor: F45-24-11). The absorption at 695 nm ( $\lambda_{\text{pyocyanin}} = 695 \text{ nm}$ ) was measured from 1 ml of each culture supernatant. The measured OD<sub>695nm</sub> was divided by the OD<sub>600nm</sub> to determine the amount of pyocyanin secreted by different cultures with comparable cell densities.

### 2.4.3 Statistical evaluation of phenotypic assays

Following the experimental procedure, the results were statistically evaluated. The first step was to calculate the mean value and standard deviation using Microsoft Excel (part of descriptive statistics). Next, all data sets, were tested for their normal or Gaussian distribution (“Statistics; Descriptive Statistics; Normality Test; Shapiro-Wilk (stricter) or Kolmogorov-Smirnov with a significance level of 0.05” in Origin, Version 2022. OriginLab Corporation, Northampton, MA, USA.). Only if a normal distribution cannot be rejected, the data set can be used for the Student’s *t*-test and the *F*-test. The *F*-test determines whether a data set is hetero- or homoscedastic and which type of *t*-test to use for the subsequent significance check. In Microsoft Excel, the *F*-test can be integrated with the *t*-test. The *t*-test calculates the *p*-value. If the *p*-value is less than 0.05, the difference is statistically significant with a 95 % confidence (n.s.:  $p \geq 0.05$ ; \*:  $0.01 \leq p < 0.05$ ; \*\*:  $0.001 \leq p < 0.01$ ; \*\*\*:  $p < 0.001$ ). When a data set was compared to more than one other, a Bonferroni’s multiple comparison test was performed. The Bonferroni correction corrects the *p*-value depending on the number of comparisons: new *p*-value = old *p*-value / number of comparisons (e.g. two comparisons: n.s.:  $p \geq 0.025$ ; \*:  $0.005 \leq p < 0.025$ ; \*\*:  $0.0005 \leq p < 0.005$ ; \*\*\*:  $p < 0.0005$ ). With three or more comparisons, the *p*-value decreases further.

Student’s *t*-test with *F*-test for Microsoft Excel (german version):

(=T.Test(Matrix1;Matrix2;2;Wenn(F.Test(Matrix1;Matrix2)<0.05;3;2))

## **2.5 Molecular biological methods**

### **2.5.1 Preparation of genomic DNA from *P. aeruginosa***

For isolation of genomic/chromosomal DNA, LB medium was inoculated with the appropriate *P. aeruginosa* strain and incubated overnight at 37 °C under constant shaking (160 rpm, Innova™ 2300 Platform Shaker). The next day, the NucleoSpin® Microbial DNA kit (Macherey-Nagel) was used for preparation according to the manufacturer's protocol.

### **2.5.2 Preparation of plasmid DNA from *E. coli***

To isolate plasmid DNA, a single colony of *E. coli* DH5α harboring the desired plasmid was inoculated into LB medium containing the appropriate antibiotic and incubated overnight at 37 °C under constant shaking (160 rpm, Innova™ 2300 Platform Shaker). The next day, 2 ml of the culture was centrifuged (RT, 11,000 rpm, 3 min, Eppendorf 5415 D, rotor: F45-24-11) and the plasmid was purified using the NucleoSpin® Plasmid EasyPure kit (Macherey-Nagel) or the E.Z.N.A.® Plasmid DNA Mini Kit I (Omega Bio-Tec Inc) according to the instructions of the manufacturer.

### **2.5.3 Agarose gel electrophoresis**

Agarose gel electrophoresis is used to separate nucleic acids using an agarose matrix in a horizontal electrophoresis chamber. The separation depends on the length and conformation (linearized, double-stranded, supercoiled, etc.) of the DNA fragments (Aaij and Borst, 1972). The negatively charged DNA moves from the cathode to the anode in the electric field, with small fragments passing through the gel matrix faster than large ones. A concentration of 0.8-1 % (w/v) agarose was dissolved in 1x TAE buffer (Tris-acetate pH 8.0, 2 M; EDTA, 50 mM; 50x) and melted. The gel was allowed to polymerize at room temperature in a pre-prepared gel chamber. Gel loading dye (purple, 6x, NEB) was added to the DNA samples prior to application. Furthermore, the GeneRuler™ 1 kb Plus DNA Ladder (Thermo Fisher Scientific) served as the reference to determine the size and amount of DNA in the fragments. Electrophoresis was performed at a constant voltage of 90-120 V in 1x TAE buffer until the fragments were completely separated (approximately 40-60 min). After running, the gel was incubated in a photosensitive ethidium bromide solution for 20 min before visualization of nucleic acids by irradiation with UV light (312 nm) in the documentation system (Intas).

## 2.5.4 Restriction digestion of DNA

Restriction digestion of plasmids or PCR products was performed using restriction endonucleases or high-fidelity (HF<sup>®</sup>) restriction endonucleases (NEB) according to the manufacturer's instructions using the appropriate buffers provided by NEB. The digested DNA was incubated for one hour (restriction endonucleases) or 20-30 min (HF<sup>®</sup> restriction endonucleases) at 37 °C. Test restrictions were performed in a total volume of 10 µl with 1 µl 10x CutSmart<sup>®</sup> or 10x rCutSmart<sup>™</sup>, 1 µl of the respective enzyme and 100-300 ng plasmid DNA. Preparative DNA digestions were performed using larger amounts of the substrates. Subsequently, the restriction enzymes were heat-inactivated, if possible (depending on the enzyme; see neb-online.de). For double digestion, the reaction was performed sequentially with thermal inactivation of the first enzyme before adding the second one. Successful restriction of linearized plasmid DNA of known size was verified by agarose gel electrophoresis (chapter 2.5.3).

## 2.5.5 Polymerase chain reaction (PCR)

Polymerase chain reaction (PCR) was used to amplify specific DNA fragments (Mullis and Faloona, 1987). The laboratory's own purified *Pfu* DNA polymerase or *Phusion* HF-DNA polymerase were used for the PCR reactions (Tab. 2.7). The elongation time was adjusted according to the capacity of the polymerase and the size of the DNA fragment to be amplified (Tab. 2.8). For the *Phusion* HF-DNA polymerase, the 5x HF buffer provided by NEB was used and for the *Pfu* DNA polymerase, a laboratory's own 10x buffer was used. The annealing temperature for primer annealing was individual for each employed primer (approx.  $T_m - 5$  °C).

**Tab. 2.7: Standard PCR reaction with *Phusion* HF-DNA polymerase or *Pfu* DNA polymerase and composition of *Phusion* HF-DNA polymerase mix as well as 10x *Pfu* Reaction buffer.**

Component	Final concentration / volume
<i>Phusion</i> HF (5x) or <i>Pfu</i> Reaction buffer (10x)	1x
dNTPs	200 µM each
DMSO	5 % (v/v)
Primer fwd	0.5 µM
Primer rev	0.5 µM
Template DNA	10-100 ng
<i>Phusion</i> HF or <i>Pfu</i> DNA polymerase	0.5 / 1 µl or 1 / 2 µl
H <sub>2</sub> O	@ 25 / 50 µl



<i>Phusion</i> <sup>®</sup> HF-DNA polymerase		<i>Pfu</i> Reaction buffer (10x)	
purified polymerase	2 $\mu$ l	Tris-HCl (pH = 8.2)	200 mM
1 M DTT	8 $\mu$ l (= 2 mM)	KCl	100 mM
Phusion storage buffer	390 $\mu$ l	(NH <sub>4</sub> ) <sub>2</sub> SO <sub>4</sub>	100 mM
Tris-HCl (pH = 8)	100 mM	MgSO <sub>4</sub>	20 mM
EDTA	0.2 mM	Triton X-100	1 % (v/v)
NP-40	0.2 % (v/v)	BSA (nuclease-free)	1 mg/ml
Tween-20	0.2 % (v/v)		
DTT	2 mM		

**Tab. 2.8: Standard PCR thermocycler program for *Phusion* HF-DNA polymerase with 30 s/kb or *Pfu* DNA polymerase with 60 s/kb elongation time.**

Reaction step	Temperature	Time	
Initial denaturation	98 °C	1-5 min	
Denaturation	98 °C	30 s	
Annealing	primer-specific	30 s	30-35x
Elongation	72 °C	30 s/kb or 60 s/kb	
Final elongation	72 °C	10 min	
Cooling	8 °C	$\infty$	

### 2.5.6 Purification of PCR products

The NucleoSpin<sup>®</sup> Gel and PCR Clean-up kit (Macherey-Nagel) was used according to manufacturer's instructions to purify PCR products.

### 2.5.7 Extraction of DNA fragments from agarose gels

In the case of an impure PCR product, the desired amplified fragment was cut out of an agarose gel. Therefore, low melting point agarose was used and dissolved in 1x TAE buffer (1.2 % (w/v)). Gel electrophoresis using a gel with wider pockets was performed and the gel was stained as described in chapter 2.5.3. The desired DNA fragment was cut out with a clean scalpel under UV irradiation (312 nm) using the NucleoSpin<sup>®</sup> Gel and PCR Clean-up kit (Macherey-Nagel) according to the instructions of the manufacturer.

### 2.5.8 Determination of nucleic acid concentrations

The concentration of the genomic or plasmid DNA in aqueous solutions was determined by measuring the absorption at 260 nm using a NanoDrop<sup>™</sup> Lite photometer (Thermo Fisher Scientific). For the concentration measurement, 1  $\mu$ l of DNA was used after a reference

determination with H<sub>2</sub>O or elution buffer. An absorption of 1 corresponds to a double-stranded DNA concentration of 50 ng/μl. The ratio of the absorption at 260 nm and 280 nm indicates contamination of the samples and represents the purity. An absorption ratio of  $A_{260\text{nm}}/A_{280\text{nm}}$  around 1.8 was considered enough for sufficiently pure double-stranded DNA solutions. Alternatively, the concentration of an unknown DNA sample could be determined using an agarose-gel (chapter 2.5.3) and a DNA standard for comparison.

### **2.5.9 Ligation of DNA fragments**

To ligate a digested vector (50-100 ng) and a DNA fragment, both were incubated together in a 1:3 molar ratio with T4 DNA ligase (NEB) in 10x T4 DNA ligase buffer (NEB) at 17 °C overnight. The next day, the enzyme was heat-inactivated at 65 °C for 10 min and the ligation product (total volume 20 μl) was transformed into chemically competent *E. coli* DH5α cells and plated on selective LB agar (chapter 2.3.8).

### **2.5.10 Splicing-by-overlap extension (SOE) PCR**

In the course of this work, the two-step allelic exchange method was used for *P. aeruginosa* genome engineering (Hmelo *et al.*, 2015). In particular, the use of this method allowed the generation of marker-less in-frame chromosomal deletions in *P. aeruginosa* PA14. The constructs specifically required for the generation of gene knockout strains were generated using splicing-by-overlap extension (SOE) PCR. In two separate PCR reactions, the flanking up- and downstream regions of the gene of interest (PA14\_10700 and/or PA14\_10710 or PA14\_72390) were amplified from PA14 gDNA with specific primer pairs (Up-F and Up-R or Down-F and Down-R; Tab. 2.5). The primers were designed so that the fragments flanking the gene of interest contained the start- and stop-codon of the target gene and an additional number (multiple of 3) of nucleotides from the open reading frame (ORF). The end of the primer Up-R was homologous to the primer Down-F and both the primers Up-F and Down-R contained restriction sites for the multiple cloning site of the target vector pEXG2. Upon successful completion, amplification was verified by agarose-gel electrophoresis (chapter 2.5.3) and the fragments were purified using the NucleoSpin® Gel and PCR Clean-up kit (Macherey-Nagel). Both fragments were used in equal amounts as templates in the subsequent PCR reaction. In this step, only the Up-F and Down-R primer pair was supplied to align the homologous regions between the upstream and downstream fragments and to amplify the fused fragment (Fig. 2.1).

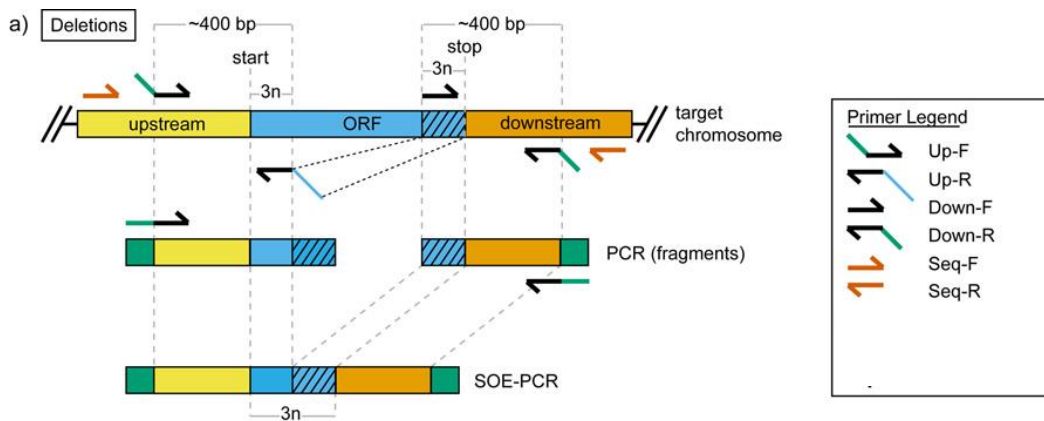


**Fig. 2.1: Principle of the splicing-by-overlap extension PCR.**

In two separate reactions, first the anchoring upstream (yellow) and downstream (orange) regions of the open reading frame (ORF) of the target gene (blue) were amplified. In the next PCR reaction step, these fragments were used as templates to generate a fusion DNA-fragment with a short version of the target gene. Primers are designed with specific modifications: restriction sites (green), homologous region to the downstream fragment (blue) or sequencing primers (orange) that bind within the *P. aeruginosa* genome up- and downstream of the modified genomic region (see primer legend). Figure modified from Hmelo *et al.*, 2015.

### 2.5.11 Generation of *P. aeruginosa* mutants via two-step allelic exchange

The fragment originated from the SOE PCR (chapter 2.5.10) and flanking the gene of interest, was ligated into the suicide vector pEXG2 to generate pEXG2\_Δ*bphP*, pEXG2\_Δ*bphOP* and pEXG2\_Δ*kinB*. These plasmids were used to transform *E. coli* S17-I (chapter 2.3.8) and mobilized by conjugation into the recipient PA14-WT or PA14Δ*kinB* strains via biparental mating (chapter 2.3.9). Single-crossover recombinants with the site-specifically integrated plasmid were screened on Pseudomonas Isolation-agar containing gentamicin. Ten single colonies were selected from these plates, incubated overnight at 37 °C on LB-agar and then streaked out twice on LB-agar containing 15 % (w/v) sucrose. Incubation of the merodiploid exconjugants forces a second homologous recombination event and the removal of the vector DNA containing the negative selection marker *sacB*. Since this gene encodes a levansucrase, an enzyme that uses sucrose as a substrate for the synthesis of toxic products, this counter-selection step recovered the double-crossover mutants (Fig. 2.2). Mutants considered for further screening therefore had to be both, sucrose-resistant as well as gentamicin sensitive and were additionally verified by colony PCR (chapter 2.5.13) and Sanger sequencing (chapter 2.5.14).

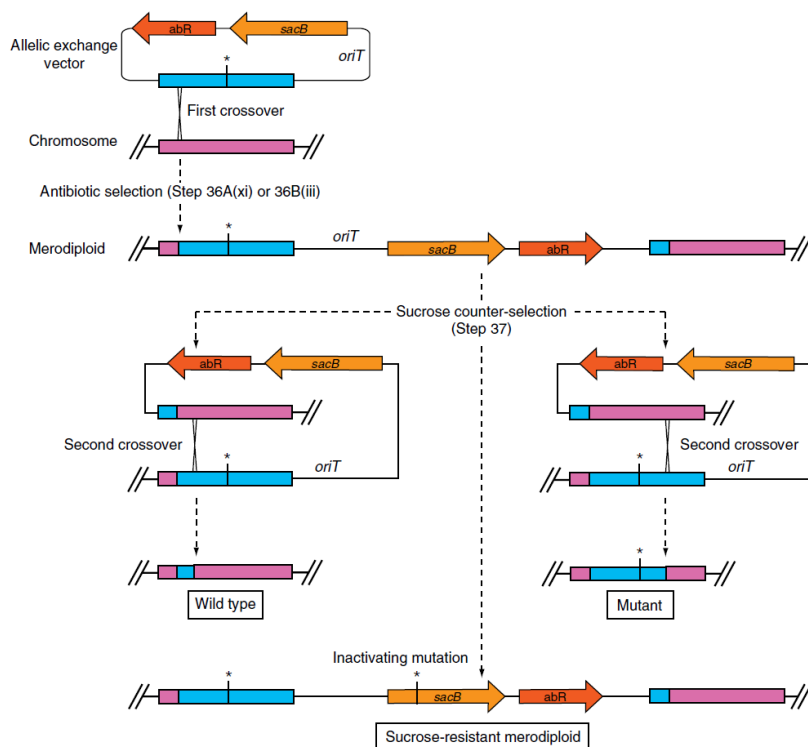


**Fig. 2.2: Generation of *P. aeruginosa* mutants via two-step allelic exchange.**

Two-step allelic exchange using the pEXG2 vector, which harbors the *sacB* gene and an antibiotic resistance (gentamicin) gene. During the first homologous recombination event, the complete suicide vector is integrated into the *P. aeruginosa* genome, producing gentamicin-resistant bacteria. During the second recombination event, forced by sucrose counter-selection, the vector backbone is removed from the genome. The result of this second crossover is a population of sucrose-resistant and gentamicin sensitive bacteria. Colony PCR and Sanger sequencing were employed to genetically verify the bacterial genomes. (figure taken from Hmelo *et al.*, 2015)

### 2.5.12 Site-directed mutagenesis

Site-directed mutagenesis is used to introduce specific mutations into a DNA sequence and study the resulting effect on the structure and activity of the encoded protein. Specific oligonucleotides (Tab. 2.5) have been designed to generate nucleobase substitutions within the gene. Site-directed mutagenesis of *PakinBCD* (P390S) and *AtbphP2* (D783N) was accomplished using pASK\_*PaKinBCD* and pET21b\_*AtBphP2* (Tab. 2.9). Methylation of the parental plasmid allowed its elimination from the reaction mix by restriction digestion (chapter 2.5.4) with *DpnI*. Afterwards, the digest was available for transformation in chemically competent *E. coli* DH5 $\alpha$  cells (chapter 2.3.8) and the plasmids were verified after preparation by “silent site restriction digest” as well as Sanger sequencing (chapter 2.5.14). Silent sites are silent mutations bearing a restriction site that can be incorporated into the gene using oligonucleotides. Therefore, successful nucleobase exchange can be verified by restriction digestion (*PakinBCD*, *SacI*; *AtbphP2*, *BamHI*).

**Tab. 2.9: PCR reaction and thermocycler program for site-directed mutagenesis of *PaKinBCD* and *AtbphP2* to generate the resulting protein variants *PaKinBCD\_P390S* and *AtBphP2\_D783N*.**

Component	Volume	
<i>Phusion</i> buffer (5x) <b>or</b> <i>Phusion</i> GC buffer (5x)	10 $\mu$ l	
dNTPs	1.0 $\mu$ l	
DMSO	2.5 $\mu$ l	
pASK- <i>PaKinBCDP390S_fwd</i> <b>or</b> pET21b- <i>AtBphP2P783N_fwd</i>	1.0 $\mu$ l	
pASK- <i>PaKinBCDP390S_rev</i> <b>or</b> pET21b- <i>AtBphP2P390S_rev</i>	1.0 $\mu$ l	
pASK- <i>PaKinBCD</i> (10 ng/ $\mu$ l) <b>or</b> pET21b- <i>AtBphP2</i> (12 ng/ $\mu$ l)	2.0 $\mu$ l	
<i>Phusion</i> HF	2.0 $\mu$ l	
H <sub>2</sub> O	30.5 $\mu$ l	

Reaction step	Temperature	Time	
Initial denaturation	98 °C	1 min	
Denaturation	98 °C	30 s	
Annealing	68 °C	1 min	18 x
Elongation	72 °C	2.5 min	
Final elongation	72 °C	10 min	
Cooling	8 °C	$\infty$	

### 2.5.13 Colony PCR

Verification of successful generation of new plasmids as well as screening for the genomic integration of mutant alleles in *P. aeruginosa* was conducted via colony PCR. In order to check a plasmid, single colonies of transformed *E. coli* DH5 $\alpha$  were picked, streaked onto a fresh selective LB-agar plate, and resuspended in 10  $\mu$ l H<sub>2</sub>O. 1  $\mu$ l of this suspension served directly as the PCR template. To check *P. aeruginosa* deletion mutants, bacterial colonies were similarly preserved, but resuspended in 100  $\mu$ l H<sub>2</sub>O and also used directly as the PCR template (1  $\mu$ l). The PCR reactions were performed by extending the initial denaturation step to 10 min and were set up as described in chapter 2.5.5 using *Phusion* HF or the *Pfu* DNA polymerase (25  $\mu$ l final volume).

### 2.5.14 Analysis of DNA sequences

Sequencing for the validation of modified plasmids or DNA fragments amplified by PCR was performed using Sanger sequencing (Sanger *et al.*, 1977a; Sanger *et al.*, 1977b) by the company Eurofins Genomics. The required mixture of DNA, oligonucleotide and H<sub>2</sub>O was prepared according to the manufacturer's instructions. Analysis of the sequencing data was performed using Clustal Omega "Multiple Sequence Alignment" (<https://www.ebi.ac.uk/Tools/msa/clustalo/>) and SnapGene<sup>®</sup>.

## 2.6 Protein biochemical and biophysical methods

### 2.6.1 Test expression of recombinant genes and their encoding proteins

The optimal temperature and time conditions for protein production in *E. coli* or *P. aeruginosa* were determined in test expression/production experiments. For this, a main culture with a final volume of 100-250 ml and the appropriate antibiotic was inoculated 1:100 (*E. coli*) or  $OD_{600nm} = 0.1$  at time point zero (*P. aeruginosa*) with an overnight culture. This culture was incubated at 37 °C under constant shaking (160 rpm, Innova™ 2300 Platform Shaker) until an  $OD_{600nm} = 0.5-0.6$  (*E. coli*) or 0.7 (*P. aeruginosa*) was reached. Then, a “before induction” (bI) sample (1 ml) was collected and pelleted by centrifugation (RT, 11,000 rpm, 3 min, Eppendorf 5415 D, rotor: F45-24-11) and the gene expression was induced with L(+)-arabinose, AHT or IPTG. The yield and solubility of the corresponding protein was tested under different conditions (37 °C and 30 °C for 3-5 h, 17 °C oN or 10 °C for 5 d). After each incubation period, an “after induction” (aI) sample (1 ml) was collected and treated as the “bI” sample. The cell pellets were resuspended in different amounts of SDS sample buffer (all adjusted to an identical  $OD_{600nm}$ ), heat-denatured (5 min, 95 °C), separated by SDS-PAGE (chapter 2.6.7) and analyzed by an immunological detection (chapter 2.6.8 and 2.6.9). The optimal conditions for protein production were determined by comparing the samples.

### 2.6.2 Heterologous production of recombinant proteins in *E. coli*

Based on the results of the test expressions, the production of recombinant phytochrome proteins and proteins from our studied TCS in *P. aeruginosa* was performed under various conditions (Tab. 2.10). Freshly transformed *E. coli* cells harboring the different plasmids were grown in 15 ml LB media supplemented with the respective antibiotic overnight at 37 °C under constant shaking conditions (100 rpm, Innova® 44 Incubator Shaker). For protein production the cells were used to inoculate 1 l LB-ampicillin or LB-kanamycin (1:100). Gene expression was induced by the addition of 0.5 mM IPTG, 200 ng/ml AHT or 0.1 % L(+)-arabinose when  $OD_{600nm} = 0.5-0.6$  was reached. After a defined incubation time and temperature (Tab. 2.10), the cells were harvested (chapter 2.6.4) and used directly for protein purification or stored at -20 °C.

**Tab. 2.10: Used plasmids, protein tags (C = C-terminal, N = N-terminal), *E. coli* strains, inducers (Indu.), antibiotics (AB), incubation temperatures (Temp.) and time for production of phytochrome proteins from different organisms as well as proteins from the TCS in *P. aeruginosa* and their variants.**

Protein	Plasmid	tag	<i>E. coli</i>	Indu.	AB	Temp.	Time
<b>AtBphP2*</b>	pET21b_AtBphP2 pET21b_AtBphP2 <sub>D783N</sub>	His (C)	BL21(DE3)	IPTG	Amp	17 °C	oN
<b>AvBphP2*</b>	pET21b_AvBphP2 pET21b_AvBphP2 <sub>D793A</sub>	His (C)	BL21(DE3)	IPTG	Amp	10 °C	5 d
<b>RtBphP2</b>	pBAD/HisB-RtBphP2-HmuO	His (N)	Top10	Ara	Amp	30 °C	4 h
<b>XccBphP*</b>	pET24a_XccBphP pET24a_XccBphP $\Delta$ PAS9	His (C)	BL21(DE3)	IPTG	Kan	17 °C	oN
<b>AtBphP1</b>	pASK_AtBphP1	Strep (C)	BL21(DE3)	AHT	Amp	17 °C	oN
<b>PstBphP1</b>	pET52_PstBphO-BphP1	His (C)	BL21(DE3)	IPTG	Amp	17 °C	oN
<b>PaAlgB</b>	pASK_PaAlgB	Strep (C)	BL21(DE3)	AHT	Amp	17 °C	oN
<b>PaKinBCD*</b>	pASK_PaKinBCD pASK_PaKinBCD <sub>P390S</sub>	Strep (C)	BL21(DE3)	AHT	Amp	17 °C	oN

\* Same procedure also for the variants AtBphP2\_D783N, AvBphP2\_D793A, XccBphP $\Delta$ PAS9 and KinBCD\_P390S.

His = polyhistidine-tag; Strep = Strep-tag II; IPTG = isopropyl  $\beta$ -D-1-thiogalactopyranoside; Ara = L(+)-arabinose; AHT = anhydrotetracycline; Amp = ampicillin; Kan = kanamycin; oN = overnight

### 2.6.3 Homologous production of recombinant proteins in *P. aeruginosa*

Homologous production of PaBphP and variants was based on pHERD26T derivatives, bearing the phytochrome gene with a C-terminal Strep-tag II under the control of a p<sub>BAD</sub> promoter. *P. aeruginosa* PA14 $\Delta$ bphP cells harboring pHERD26T\_PaBphP or constructs containing histidine-513-to-alanine (H513A), aspartate-194-to-histidine (D194H), serine-261-to-alanine (S261A), and cysteine-12-to-alanine (C12A) mutation (Tab. 2.11) were grown in 50 ml LB media supplemented with tetracycline overnight at 37 °C under constant shaking conditions (100 rpm, Innova<sup>®</sup> 44 Incubator Shaker). For protein production, the overnight cultures were used to inoculate 1 l LB-tetracycline media (OD<sub>600nm</sub> = 0.1 at time point zero) and gene expression was induced by the addition of 0.1 % L(+)-arabinose at OD<sub>600nm</sub> = 0.7. For apo-phytochrome production, pHERD26T\_PaBphP was mobilized by conjugation into PA14 $\Delta$ bphOP, and the above-mentioned procedure was followed. After further incubation at 17 °C overnight, the cells were harvested (chapter 2.6.4) and used directly for protein purification or stored at -20 °C.

**Tab. 2.11: Used plasmids and *P. aeruginosa* strains for production of the phytochrome protein *PaBphP* and its protein variants.**

Protein	Plasmid	<i>P. aeruginosa</i> strain
<i>PaBphP</i>	pHERD26T_ <i>PaBphP</i>	PA14Δ <i>bphP</i> ; PA14Δ <i>bphOP</i>
<i>PaBphP_H513A</i>	pHERD26T_ <i>PaBphP</i> <sub>H513A</sub>	PA14Δ <i>bphP</i>
<i>PaBphP_D194H</i>	pHERD26T_ <i>PaBphP</i> <sub>D194H</sub>	PA14Δ <i>bphP</i>
<i>PaBphP_S261A</i>	pHERD26T_ <i>PaBphP</i> <sub>S261A</sub>	PA14Δ <i>bphP</i>
<i>PaBphP_C12A</i>	pHERD26T_ <i>PaBphP</i> <sub>C12A</sub>	PA14Δ <i>bphP</i>

#### 2.6.4 Cell disruption of *E. coli* and *P. aeruginosa* cells

Cell harvesting was performed by centrifugation for 15 min (4 °C, 9,000 rpm, Sorvall LYNX 6000, rotor: F9-6x1,000) and dissolved in ice-cold lysis buffer (2 ml buffer per g of cells) supplemented with lysozyme and DNase I. After 30 min incubation on ice, the cells were lysed using the cell fluidizer (Microfluidics™) technology, which converts process pressures into shear rates and provides high digestion rates (2-3 rounds at 15,000 psi). Lysed cells were centrifuged for 1 h (4 °C, 19,000 rpm, Sorvall LYNX 6000, rotor: T29-8x50) and the crude extract containing the soluble proteins was filtered through a PVDF syringe filter (0.45 μm pore diameter). All protein solutions (expected *RtBphP2*, *PaAlgB*, *PaKinBCD*, *PaKinBCD\_P390S* and apo-*PaBphP*) were incubated with excess BV IXα (200 mM, 4 °C, 1 h) in the dark to achieve almost complete saturation with the chromophore prior to affinity chromatography.

#### Lysis buffer / buffer W (1x)

Tris-HCl pH 8.0	100 mM
NaCl	300 mM
Triton X-100*	1 % (v/v)

\* for *RtBphP2*, *XccBphP*, *XccBphPΔPAS9*

#### 2.6.5 Purification of recombinant proteins

Affinity chromatography allows the isolation of the desired protein fused to a tag (Strep-tag II or polyhistidine-tag) from the total cell lysate. Cell lysates of *PaBphP* as well as variants, *AtBphP1*, *PaAlgB*, *PaKinBCD* and *PaKinBCD\_P390S* overproduction were loaded onto a Strep-Tactin® Sepharose® resin (Iba) and treated according to the instructions of the manufacturer. *AtBphP2*, *AvBphP2* or the protein variants as well as *XccBphP*, *XccBphPΔPAS9*, *RtBphP2* and *PstBphP1* were purified using TALON® Superflow™ (cytiva) and also used



according to protocol of the manufacturer. After the lysates were applied to the respective resin (flow-through), the columns were washed with 10 CV buffer W (washing fraction). Subsequently, the proteins were eluted with either 25 mM d-Desthiobiotin (Strep) or 75 mM imidazole (His) in buffer W. Elution is enabled by the displacement of the tags by the competitive compounds d-Desthiobiotin and imidazole. Fractions were stored on ice until further use and samples were taken from the cell lysate, the flow-through, the washing fraction as well as the elution and prepared for SDS-PAGE analysis. The resins were regenerated according to the instruction of the company and stored at 4 °C until further use. After elution, the purified proteins were dialyzed in kinase buffer overnight at 4 °C with continuous stirring. This has the advantage of increasing the protein stability by using a buffer with a lower salt concentration and removing the d-Desthiobiotin as well as the imidazole from the solution. For this, a buffer volume of 100x the elution fraction was used. The proteins were concentrated using a centrifugal concentrator (Amicon) by centrifugation (4 °C, 4,000 rpm, 5 min, Eppendorf 5810 R, rotor: A-4-62) for several times. The concentrator was previously rinsed with H<sub>2</sub>O and equilibrated with kinase buffer. After dialysis, the proteins were analyzed again by SDS-PAGE to assess purity and quantity.

<b>Kinase buffer (1x)</b>	
Tris-HCl pH 8.0	50 mM
NaCl	100 mM
MgCl <sub>2</sub>	5 mM
Glycerol	10 % (v/v)

### 2.6.6 Determination of protein and biliverdin IX $\alpha$ concentration

The concentration of the purified proteins was determined based on the absorption at 280 nm according to the Beer-Lambert law. Molar extinction coefficients (Tab 2.12) were calculated based on the amino acid sequence with the corresponding tag as described by Gill and von Hippel (Gill and von Hippel, 1989) or Protein Calculator v3.4 (<http://protcalc.sourceforge.net/>).

$$c [\mu\text{M}] = \frac{A_{280 \text{ nm}} \times \text{DF}}{\epsilon_{280 \text{ nm}} \times d}$$

$$c [\text{mg/ml}] = \frac{M_r \times A_{280 \text{ nm}} \times \text{DF}}{\epsilon_{280 \text{ nm}} \times d}$$

c = protein concentration  
 $A_{280\text{nm}}$  = absorption at 280 nm

( $\mu\text{M}$  or mg/ml)

DF	= dilution factor	
$\epsilon_{280\text{nm}}$	= molar absorption coefficient	( $\text{M}^{-1}\text{cm}^{-1}$ )
d	= optical path length	(cm)
$M_r$	= molecular mass / weight	(Da = g/mol)

**Tab. 2.12: Molecular mass and molar absorption coefficients ( $\epsilon_{280\text{ nm}}$ ) used for the calculation of protein concentrations.**

Fusion protein	Molecular Mass	Molar absorption coefficient $\epsilon_{280\text{ nm}}$
<i>Pa</i> BphP*-Strep	83 kDa	72,410 $\text{M}^{-1}\text{cm}^{-1}$
<i>Pa</i> AlgB-Strep	52 kDa	34,520 $\text{M}^{-1}\text{cm}^{-1}$
<i>Pa</i> KinBCD*-Strep	47 kDa	16,620 $\text{M}^{-1}\text{cm}^{-1}$
<i>Pst</i> BphP1-His	83 kDa	72,170 $\text{M}^{-1}\text{cm}^{-1}$
<i>Pst</i> BphP2-Strep	109 kDa	99,460 $\text{M}^{-1}\text{cm}^{-1}$
<i>At</i> BphP1-Strep	85 kDa	104,100 $\text{M}^{-1}\text{cm}^{-1}$
<i>At</i> BphP2*-His	95 kDa	78,570 $\text{M}^{-1}\text{cm}^{-1}$
<i>Av</i> BphP2*-His	95 kDa	81,820 $\text{M}^{-1}\text{cm}^{-1}$
His- <i>Rt</i> BphP2	83 kDa	71,220 $\text{M}^{-1}\text{cm}^{-1}$
<i>Xcc</i> BphP-His	71 kDa	74,370 $\text{M}^{-1}\text{cm}^{-1}$
<i>Xcc</i> BphP $\Delta$ PAS9-His	59 kDa	64,400 $\text{M}^{-1}\text{cm}^{-1}$

\* For the respective protein variants, the same values are valid.

BV IX $\alpha$  (Sigma-Aldrich), was dissolved in ~ 6-8 ml DMSO. Its absorption was calculated by recording the absorption at 698 nm after dilution in 2.5 % HCl in MeOH. The concentration of the chromophore was determined using a molar absorption coefficient of 32.6  $\text{mM}^{-1}\text{cm}^{-1}$  ( $\epsilon_{698\text{nm}}$ ; Heirwegh *et al.*, 1991) within the Beer-Lambert law.

### 2.6.7 SDS-polyacrylamide gel electrophoresis

Denaturing and discontinuous SDS-PAGE (sodium dodecyl sulfate-polyacrylamide gel electrophoresis) can be used to separate proteins according to their difference in size and to analyze their molecular mass (Laemmli, 1970). The detergent sodium dodecyl sulfate (SDS) attaches to the proteins, giving them a negative charge proportional to their size and masking their native charge. Due to the charge, the individual proteins are separated in the electric field along the polyacrylamide matrix according to their molecular mass – larger proteins migrate slower through the acrylamide matrix than smaller proteins. Polyacrylamide gels consisting of a stacking (5.25 % (w/v) acrylamide concentration; pH 6.8), a resolving (10 % (w/v) acrylamide concentration; pH 8.8) and a stopping gel (Tab. 2.13; 2.14). Samples were mixed with sample

buffer, incubated at 95 °C for 5 min and centrifuged (RT, 13,000 rpm, 5 min, Eppendorf 5415 D, rotor: F45-24-11) prior to application to the gel. Each gel pocket was loaded with 15-20  $\mu$ l of sample and 5  $\mu$ l of a protein size standard (Tab. 2.2) was used. Electrophoresis was performed by applying a constant voltage of 180 V for 50-60 min in 1x SDS running buffer. Staining of the polyacrylamide gel in Coomassie staining solution for 10 min and subsequent decolorizing in a EtOH/acetic acid solution or water under shaking conditions allowed visualization of the proteins in the gel. Protein staining is based on the attachment of Coomassie brilliant blue (G250) to amino acids with aromatic or basic side chains.

**Tab. 2.13: Buffers and solutions used for SDS-PAGE and staining of the gel.**

Stacking gel buffer (4x)		Resolving gel buffer (4x)	
Tris-HCl pH 6.8	0.5 M	Tris-HCl pH 8.8	1.5 M
SDS	4 % (w/v)	SDS	0.4 % (w/v)
SDS sample buffer (4x)		SDS running buffer (10x)	
Tris-HCl pH 6.8	0.1 M	Tris-HCl pH 8.8	0.25 M
SDS	8 % (w/v)	Glycine	1.92 M
Glycerol	40 % (v/v)	SDS	1 % (w/v)
$\beta$ -Mercaptoethanol	10 % (v/v)		
Bromphenol blue	1 % (w/v)		
Staining solution		Destaining solution	
Acetic acid	10 % (v/v)	Acetic acid	10 % (v/v)
Ethanol	30 % (v/v)	Ethanol	30 % (v/v)
Coomassie brilliant blue	0.25 % (w/v)		

**Tab. 2.14: Composition of stacking (5.25 %), resolving (10 %), and stopping gel for SDS-PAGE.**

	Stacking gel	Resolving gel	Stopping gel
H <sub>2</sub> O	4.60 ml	6.70 ml	315 $\mu$ l
4x Stacking gel buffer	2.00 ml	-	-
4x Resolving gel buffer	-	4.00 ml	250 $\mu$ l
Acrylamide*	1.40 ml	5.30 ml	420 $\mu$ l
10 % (w/v) APS	30 $\mu$ l	100 $\mu$ l	13 $\mu$ l
TEMED	20 $\mu$ l	10 $\mu$ l	2 $\mu$ l

\* Rotiphorese®Gel 30 (37.5:1, acrylamide:bisacrylamide)

## 2.6.8 Western blot transfer of proteins

To detect tagged proteins with specific antibodies, the proteins have to be irreversibly immobilized on a PVDF membrane. This immobilization is performed by western blotting, in which proteins previously separated by SDS-PAGE (chapter 2.6.7) are transferred to the membrane by electron transfer. Prior to the blotting, the PVDF membrane was first activated in 100 % methanol for 5 min and equilibrated together with Whatman® papers and the SDS-PAGE gel in Towbin buffer (10 min). Electro transfer was performed for 18 min at a constant voltage of 15 V using the semidry blot method. The sandwich consisting of the SDS-PAGE gel and the PVDF membrane between Whatman® papers, was placed between the anode and cathode of the blotting machine.

## 2.6.9 Immuno-detection of fusion proteins

After the transfer, the PVDF membrane was incubated with 10 ml BSA solution (3 % (w/v) in TBS-T) for 1 h at RT or overnight at 4 °C to saturate non-specific binding sites. Further steps for immuno-detection of *PaBphP*, Strep-tag II or polyhistidine-tag fusion proteins are summarized in Tab. 2.15. Alkaline phosphatase coupled to the secondary antibody or to the Strep-Tactin® AP conjugate catalyzes the NBT/BCIP (0.33 % (v/v)/0.66 % (v/v)) color reaction in AP buffer. The chromogenic reaction results in a purple coloration, which is visible as an insoluble product on the membrane. The colorimetric reaction was stopped by washing the membrane with H<sub>2</sub>O.

**Tab. 2.15: Steps of immune-detection of *PaBphP* or Strep-tag II as well as polyhistidine-tag fusion proteins after transfer to PVDF membrane and incubation with blocking solution.**

	<i>PaBphP</i>	Strep-tag II	polyhistidine-tag
<b>3x 5 min</b>	TBS-T buffer	TBS-T buffer	TBS-T buffer
<b>15 min</b>	-	Avidin (2 µg/ml in TBS-T)	-
<b>1 h</b>	Rabbit α BphP-Serum 1:5,000	Strep-Tactin® AP conjugate 1:4,000	6x-His tag monoclonal AB 1:3,000
<b>3x 5 min</b>	TBS-T buffer	-	TBS-T buffer
<b>1 h</b>	Anti-Rabbit IgG-AP 1:30,000	-	Anti-Mouse IgG-AP 1:10,000
<b>2x 5 min</b>	TBS-T buffer	TBS-T buffer	TBS-T buffer
<b>2x 5 min</b>	TBS buffer	TBS buffer	TBS buffer
<b>Detection</b>	NBT/BCIP	NBT/BCIP	NBT/BCIP

\* NBT (10 % (w/v) in 70 % (v/v) DMF); BCIP (5 % (w/v) in 100 % DMF)

**Tab. 2.16: Buffers used for immuno-detection.**

<b>TBS-T buffer (1x)</b>		<b>AP buffer (1x)</b>	
Tris-HCl pH 7.4	50 mM	Tris-HCl pH 9.5	100 mM
NaCl	140 mM	NaCl	100 mM
Tween 20	0.1 % (v/v)	MgCl <sub>2</sub>	5 mM
<b>TBS buffer (1x)</b>		<b>Towbin buffer* (1x)</b>	
Tris-HCl pH 7.4	50 mM	Tris-base	25 mM
NaCl	140 mM	Glycin	192 mM

\* pH not adjusted, should be between 8.1 and 8.5 (depending on quality of Tris and Glycin)

### 2.6.10 Ultraviolet-visible spectroscopy

UV/Vis measurements were performed on an Agilent 8453 UV/Visible spectroscopy system at room temperature using a Hellma precision quartz cuvette (100  $\mu$ l sample volume, 10 mm optical path). The purified proteins were diluted in 1x kinase buffer – this buffer also served as the blank. Photostationary states of phytochromes (excepted *PaBphP\_D194H* and *PaBphP\_S261A*) were obtained by exposing the samples in the spectrometer chamber sufficiently long to darkness, far-red (791 $\pm$ 2 nm, Panasonic, laser diode), red (667 $\pm$ 2 nm; Panasonic, laser diode) or blue (426 $\pm$ 70 nm, Everlight, LED) light irradiation (Fig. S1A). *PaBphP\_D194H* and *PaBphP\_S261A* were irradiated with white light passed through interference filters (red 690 $\pm$ 10 nm; far-red 750 $\pm$ 5 nm; Fig. S1B). In order to compare the dark reversion rates, all bathy phytochromes were first irradiated with far-red light to generate pure Pr-forms and all prototypical phytochromes were irradiated with red light to generate pure Pfr-forms. The following dark adaptation was tracked by absorption spectroscopy for 2 h (*PaBphP*), 24 h (*PaBphP*, *AtBphP2*, *AtBphP2\_D783N*, *AvBphP2*, *RtBphP2*, *AtBphP1* and *PstBphP1*) or for 96 h (*XccBphP* and *XccBphP $\Delta$ PAS9*). For measurements, the window of the cuvette was completely covered with the protein solution. Difference spectra were manually obtained by subtracting the blue light irradiated, the red light irradiated or the dark incubated form from the far-red light irradiated Pr-form. The time of irradiation with the different light sources and the time of dark incubation are reported in the corresponding figure legend. OD<sub>280nm</sub> was set to “1” for all spectra (excepted Fig. 3.17B; Fig. 3.18) and the linear approximation of the scattering background (550-850 nm) was subtracted from each spectrum.

### 2.6.11 Calculation of Pr- and Pfr-fraction in (photo-)stationary phytochrome samples from absorption spectra

The calculation of the Pr- and Pfr-fractions as well as the application in “MATLAB (R2022a, academic use), Natick, Massachusetts: The MathWorks Inc.” was done in collaboration with AG Diller Biophysics, RPTU. To determine the fraction  $\alpha = [P_{fr}]/([P_{fr}]+[P_r])$  of Pfr in a given (photo-)stationary phytochrome sample, the Q-band region in the respective UV/Vis spectrum was analyzed. To this end, the characteristic photocycle of the respective phytochrome was reduced to a simple binary kinetic model, comprising the two-limiting species Pfr and Pr, two photochemical rates  $k_{Pfr \rightarrow Pr}$  as well as  $k_{Pr \rightarrow Pfr}$ , and the rate for dark-reversion  $k_{DR}$ . Based on this model,  $\alpha$  for any given (photo-) stationary phytochrome sample can be obtained by simulating the experimental Q-band spectrum  $A(\tilde{\nu})$  via the fitting function  $A(\tilde{\nu}) = c \cdot [\alpha \cdot P_{fr}^0(\tilde{\nu}) + (1 - \alpha) \cdot P_r^0(\tilde{\nu})]$  with  $P_{fr}^0(\tilde{\nu})$  and  $P_r^0(\tilde{\nu})$  the pure spectra of Pfr and Pr, respectively, taken at the same concentration to achieve the quantitative relation between their extinction coefficients, and  $c$  an overall scaling constant.  $P_{fr}^0(\tilde{\nu})$  was obtained by complete dark reversion for bathy phytochromes, whereas for prototypical phytochromes the sample was illuminated with red light before and during the absorption measurement.  $P_r^0(\tilde{\nu})$  was obtained by illuminating the sample far-red before and during the absorption measurement in both phytochrome types. The illumination during the measurement process inhibits dark reversion and thus ensure complete enrichment of the respective pure form. To account for scattering contributions, a linear background was subtracted from the Q-band region (550 – 850 nm). For fitting procedure,  $P_{fr}^0(\tilde{\nu})$  and  $P_r^0(\tilde{\nu})$  were modelled as superpositions of multiple Gaussian functions. (paragraph adapted from Merle Strack, Biophysics, RPTU)

### 2.6.12 *In vitro* protein kinase assays

Autophosphorylation assays were performed in kinase buffer with purified phytochromes (5–10  $\mu$ M) and were initiated by the addition of 2.5  $\mu$ Ci [ $\gamma$ - $^{32}$ P]-ATP (Hartmann Analytic) in a final volume of 12.5  $\mu$ l. Reactions of *Pa*BphP, the locked variants (D194H and S261A), *Pa*BphP\_C12A, *Pa*BphP\_H513A and apo-*Pa*BphP were incubated under ambient light conditions for various time frames. *Pa*BphP\_H513A served as a negative control for these assays. In another approach *Pa*BphP was irradiated with far-red light ( $t = 0$ ) for 5 min in a newly designed illumination set-up (Fig. S2) and incubated under dark conditions for different periods. To analyze the autophosphorylation activity of *Pa*BphP, *At*BphP2, *At*BphP2\_D783N, *Av*BphP2, *Av*BphP2\_D793A, *Rt*BphP2, *At*BphP1 and *Pst*BphP1 under different light conditions, the proteins were irradiated with far-red (791 $\pm$ 2 nm), red (690 $\pm$ 10 nm), blue

(426±70 nm) light for 5 min in the illumination set-up or incubated overnight in the dark before the addition of radiolabeled ATP (Fig. S1A). The start of the reaction with [ $\gamma$ - $^{32}$ P]-ATP was followed by another 5 min (excepted *PstBphP1*, 10min) incubation under the respective light condition or in darkness before termination. To stop the autophosphorylation reactions, 2.5  $\mu$ l of 4x SDS sample buffer and 1.5  $\mu$ l of 0.5 M EDTA were added. For *AvBphP2* and *AvBphP2\_D793A*, excess of radiolabeled ATP was removed prior to electrophoresis using Microspin™ G-50 columns (cytiva) according to manufacturer's instruction.

Transphosphorylation assays were performed to investigate the transfer of phosphoryl group between a sensor kinase and its corresponding regulator. For this, the response regulator *PaAlgB* and the autophosphorylated kinase *PaBphP* or variants were incubated in equimolar amounts (5-10  $\mu$ M) under ambient light conditions and the reaction was stopped at different time points. *PaAlgB* incubated alone with radiolabeled ATP served as a negative control. To analyze the transphosphorylation activity of *PaBphP* under different light conditions, the protein was irradiated for 10 min as in the autophosphorylation assay. The start of the reaction with [ $\gamma$ - $^{32}$ P]-ATP was followed by 10 min incubation under the respective light condition or in the dark prior to the addition of *PaAlgB*. The *PaBphP/PaAlgB* mixture was incubated for another 10 min under the appropriate light condition or in darkness before termination.

For dephosphorylation assays, the regulator *PaAlgB* and autophosphorylated *PaBphP* were incubated in equimolar amounts (5-10  $\mu$ M) under ambient light conditions for different time frames. To get rid of excess radiolabeled ATP, Microspin™ G-50 columns were used according to the instructions of the manufacturer. After the addition of *PaKinB* (or *PaKinB\_P390S* as a control), the dephosphorylation reactions were terminated at different time points.

Irradiation intensity as well as time, and corresponding definition of  $\alpha$ -values were determined by previous UV-Vis spectroscopy (chapter 2.6.10). Light exposure for kinase assays used the same laser diodes and LED utilized for the spectroscopy experiments (Tab. 2.1). The samples were separated on a 10 % SDS-PAGE gel (chapter 2.6.7). The gel was transferred to an imaging plate (Fujifilm) and visualized using a Typhoon™ FLA 7000 (GE Healthcare) phosphoimager.

#### ATP mix (5x)

[ $\gamma$ - $^{32}$ P]-ATP (10 $\mu$ Ci/ $\mu$ l)	2.5 $\mu$ Ci (= 0.25 $\mu$ l)
ATP solution (100 mM)	10 mM (= 0.25 $\mu$ l)
H <sub>2</sub> O	2 $\mu$ l

### 3 Results

Phytochromes are an important class of photoreceptors, whose photobiology and three-dimensional structure have been well studied. The human opportunistic pathogen *Pseudomonas aeruginosa* possesses a bathy phytochrome, employed for light sensing. These bathy type phytochromes are found in a minority of bacteria and their physiological role in these organisms has not been as extensively studied as that of the more common prototypical phytochromes. Although bathy phytochromes were identified more than 20 years ago, there is still limited understanding of how signal input correlates with signal output, often manifested as autokinase activity.

The present thesis finds its root in previous research conducted in our group on the bacterial phytochrome of *P. aeruginosa*, focusing on the biochemical characterization of heterologously produced *PaBphP* (Tasler *et al.*, 2005). Recently, Mukherjee and colleagues made significant progress in this field by identifying the NtrC homolog *PaAlgB* as the related RR of the orphan sensor kinase *PaBphP* (Mukherjee *et al.*, 2019). This identification allows further elucidation of the physiological role of the phytochrome in this pathogenic organism, which is believed to have a virulence-associated role during infection and biofilm formation.

The other part of this thesis focuses on the investigation of the bacterial phytochrome *PaBphP* in the global context of bathy phytochromes. The work provides evidence that bathy phytochromes possess certain unique properties and differ functionally from prototypical phytochromes. Therefore, the *P. aeruginosa* phytochrome was compared to other bacterial bathy phytochromes, a conventional prototypical phytochrome, and an unconventional prototypical phytochrome regarding their spectral absorption behavior, their autokinase activity under different light conditions, and their dark reversion performance.

#### **Part 1 – The bacterial phytochrome *PaBphP* of the human opportunistic pathogen *Pseudomonas aeruginosa***

##### **3.1 Homologous expression and purification of the *P. aeruginosa* bacterial phytochrome was successful**

The *P. aeruginosa bphP* gene was expressed in PA14 $\Delta$ *bphP* using an *araBAD* promoter-driven C-terminal Strep-tag II expression system, which allows purification of the encoded protein from its native host bacterium (Fig. 3.1B). The SDS-PAGE gel revealed the presence of a pure protein with a relative molecular weight of ~ 83 kDa in the elution fractions, consistent with the predicted molecular mass calculated from the amino acid composition. Additionally, the



protein was immunologically detected using Rabbit  $\alpha$  BphP-Serum via western blot analysis (Fig. 3.1A). The general aim was to purify the recombinant *PaBphP* and variants in their holo-form, pairing it to the chromophore biosynthesis pathway. The heme oxygenase (HO) *PaBphO*, whose gene is located chromosomally upstream of *bphP*, provides BV IX $\alpha$  to the phytochromes. However, native *PaBphO* is not able to supply all overproduced apo-phytochromes with the chromophore (Fig. 3.1C, dark pink bar). Several methods are available to achieve saturation of the molecules. One method was to co-express an additional HO on another plasmid. An advantage of this technique is that the chromophore is produced directly within the bacterial cell and can be correctly incorporated into the binding pocket of the phytochrome during protein folding. Nevertheless, even a coexpressed HO was not able to provide enough BV IX $\alpha$  and can disrupt the heme balance within the cells (data not shown). A second approach to saturate *PaBphP* consisted in adding BV IX $\alpha$  to the purified, dialyzed, and concentrated protein. The low amount of chromophore required offers a cost-effective advantage, but during spectroscopic experiments, the residual free BV IX $\alpha$  covered the Soret and Q bands of the phytochrome absorption spectra (data not shown). A third method, although requiring the incorporation into a fully folded protein, resulted in the highest saturation (Fig. 3.1C, dark gray bar). Therefore, BV IX $\alpha$  was added to the cell-free lysate prior to protein purification. The BV IX $\alpha$  incubation led to around nine times more saturated phytochromes in the total protein amount compared to the proteins without chromophore incubation (Fig. 3.1C, D; dark gray compared to dark pink bar and spectrum). Whether complete saturation can be achieved is also not clear, as it is possible that some of the proteins always remain in their apo-form. To obtain apo-phytochrome, the *bphP* gene was expressed in a *bphOP* deletion mutant. However, *P. aeruginosa* possesses the genetic information for encoding another HO (HemO; synonym PigA). *In vitro*, this enzyme catalyzes the oxidation of heme to the unusual biliverdin isomers BV IX $\beta$  (30 %) and BV IX $\delta$  (70 %) (Caignan *et al.*, 2002). In previous work, it was even shown that BV IX $\delta$  is able to covalently bind to *PaBphP*, resulting in the formation of an photoactive holo-protein (Tasler *et al.*, 2005; Wegele *et al.*, 2004). The affinity of BV IX $\delta$  to *PaBphP* was demonstrated to be around 80 % lower than that of the natural chromophore BV IX $\alpha$  as seen from the very weak difference spectrum of apo-*PaBphP*, which is most likely due to binding of BV IX $\delta$  (Fig. 3.1C, D, inset; dark pink compared to dark blue bar and spectrum).

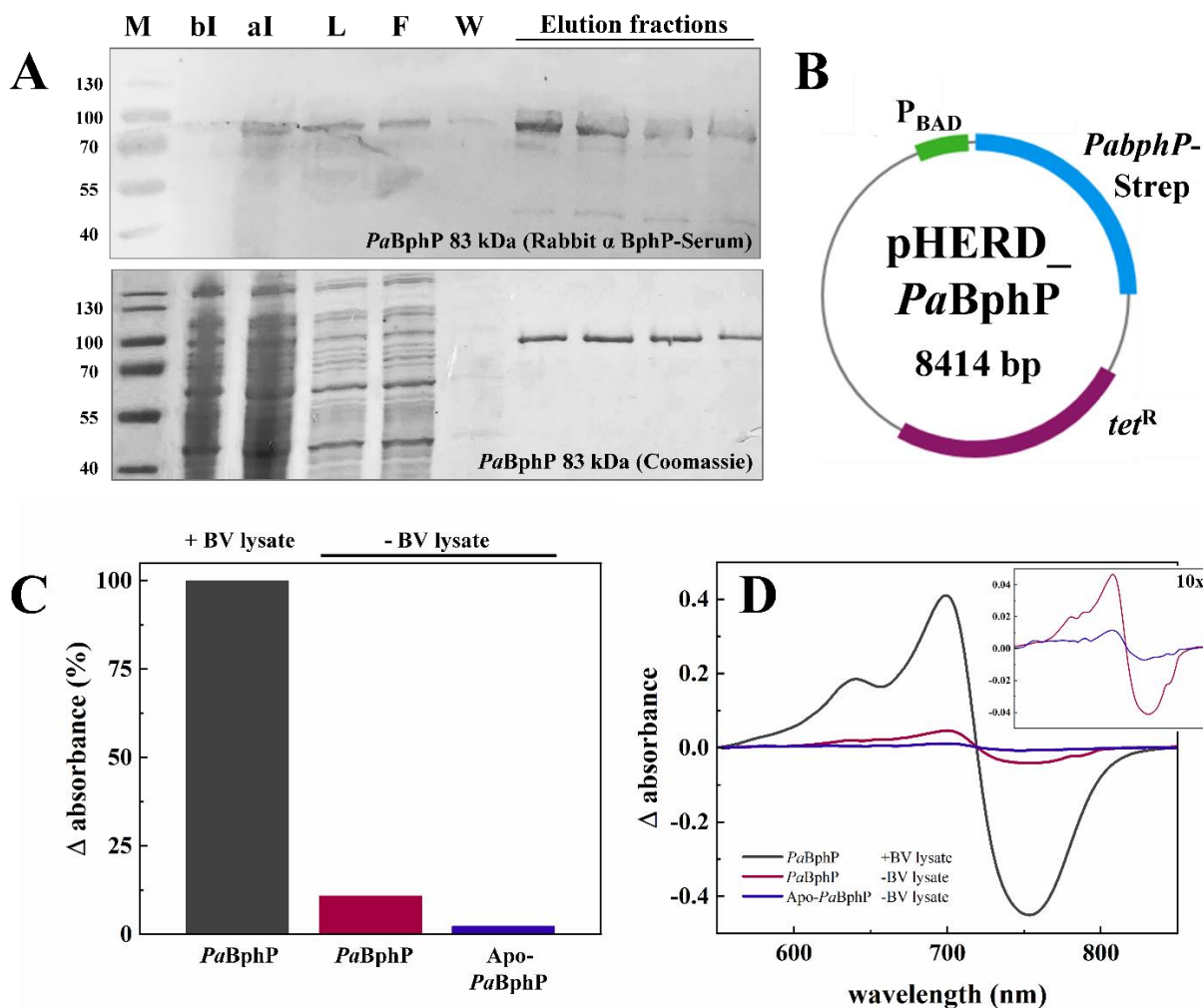


**Fig. 3.1: Homologous production of the bacterial phytochrome BphP from *Pseudomonas aeruginosa* and its saturation with the chromophore BV IX $\alpha$ .**

(A) Immunological detection with Rabbit  $\alpha$  BphP-Serum after transfer to PVDF membrane (top) and corresponding Coomassie-stained SDS-PAGE gel (10 % (w/v); bottom) after affinity chromatography purification of *PaBphP* with Strep-Tactin<sup>®</sup> Sepharose<sup>®</sup>. Sample application of the total cells before (bl) as well as after induction (al) of the gene expression, cell-free lysate (L), flow-through fraction (F), washing fraction (W) and different elution fractions containing the purified protein (elution fractions). *PaBphP* has a relative molecular weight of approximately 83 kDa (marker: Thermo Fisher Scientific PageRuler<sup>™</sup> Prestained Protein Ladder).

(B) Schematic representation of the overexpression vector pHERD\_*PaBphP* (8414 bp) bearing the phytochrome gene *bphP* of *P. aeruginosa* with a C-terminal Strep-tag II (blue) in an *araBAD* promoter-driven (green) system. The tetracycline resistance gene (purple) confers resistance to this antibiotic to bacteria carrying the plasmid.

(C) Representation of the differences ( $\Delta$  absorbance) between the Pfr-form (dark conditions,  $\lambda_{max}$  750 nm) subtracted from the Pr-form (far-red light conditions,  $\lambda_{max}$  700 nm) of purified proteins with a normalization of *PaBphP* +BV IX $\alpha$  (dark gray bar) to 100 %. The heading “+ BV lysate” or “- BV lysate” indicates if the cell-free lysate after cell disruption and before purification was incubated with an excess of BV IX $\alpha$  (+) or not (-).

(D) Manually calculated difference spectra (far-red irradiated minus dark incubated form; mathematically smoothed with Origin, Version 2022. OriginLab Corporation, Northampton, MA, USA. “Loess, Use Proportion for Span, Span 0.1”) of *PaBphP* +BV IX $\alpha$  (dark gray), *PaBphP* -BV IX $\alpha$  (dark pink) and apo-*PaBphP* -BV IX $\alpha$  (dark blue) associated with the bar chart in “C”. The inset shows the difference spectra of *PaBphP* (dark pink), and apo-*PaBphP* (dark blue) without BV IX $\alpha$  incubation at 10x magnification.

### 3.2 The conformation of the chromophore - stabilized by two amino acid residues - influences autophosphorylation behavior of *PaBphP*

Previous work from our laboratory have shown that *PaBphP* contains a C-terminal HKD, typical for autokinase activity (Tasler *et al.*, 2005). The structure of the photosensory domain with the subdomains PAS, GAF, PHY and the HKD ensures that *PaBphP* belongs to the type 1 of bacterial phytochromes (Rottwinkel *et al.*, 2010). To confirm that *PaBphP* is an active light-regulated kinase (Fig. 3.2A) and part of a TCS, its ability to autophosphorylate at the phosphorylation site His 513 was verified. In order to establish a correlation between the conformation of *PaBphP* and its histidine kinase activity, protein variants locked in the Pr- or in the Pfr-form were generated (Fig. 3.2B, C). These variants are insensitive to external light exposure and allow light-independent experiments.

In plant and most cyanobacterial phytochromes, a conserved cysteine residue in the GAF domain is involved in the attachment of the chromophore (Montgomery and Lagarias, 2002). *PaBphP* lacks this cysteine residue in the GAF domain, instead localizing it in the PAS domain (Cys 12). Nevertheless, the GAF domain has a stabilizing and coordinating function for BV IX $\alpha$ . For example, for the phytochrome of *Deinococcus radiodurans* it was shown that BV IX $\alpha$  binds in the PAS but is located in a groove in the GAF domain. The Vierstra group succeeded in generating a Pr-locked variant of the BphP in *D. radiodurans* by changing Asp 207 to a histidine (Wagner *et al.*, 2005). The corresponding amino acid residue in *P. aeruginosa* was identified in Asp 194 (Fig. 3.2D). The exchange of Asp 194 to His (*PaBphP*\_D194H; Fig. 3.3E, top) resulted in a protein that is locked in the Pr-form ( $\lambda_{\max}$  699 nm) under far-red and red light as well as under dark conditions (Fig. 3.3A). Similarly, a Pfr-locked variant was created, on already published data for *P. aeruginosa* (Yang *et al.*, 2011). The replacement of Ser 261 by alanine results in a variant (*PaBphP*\_S261A; Fig. 3.3E, bottom) present in the Pfr ground state ( $\lambda_{\max}$  750 nm) under all tested light conditions (Fig. 3.3B). These two variants are no longer capable of photoisomerization, which is also reflected by the absence a difference spectrum (Fig. 3.3C). Subtraction of the dark incubated form from the far-red light irradiated form yields almost no difference in absorption (dashed and dotted line) compared to the difference between the two forms of *PaBphP* (solid line). These locked variants were then tested in radioactive kinase assays and a clear difference in autokinase activity was observed between both (Fig. 3.3F). The results of the kinase assay demonstrate that the conformation of the chromophore influences the autophosphorylation activity. While the signal of the Pr-locked variant *PaBphP*\_D194H on the autoradiogram increased in a time-dependent manner from 2 to 20 min upon incubation with [ $\gamma$ -<sup>32</sup>P]-ATP, the Pfr-locked variant *PaBphP*\_S261A displayed no signal

after 20 min, indicating that the autokinase activity is inhibited in the Pfr-form. Contrary to a report by Yang *et al.*, 2011, this is the first time that a *PaBphP* Pr-locked protein variant is clearly correlated with high kinase activity, while in the Pfr-locked protein variant the kinase activity is absent.

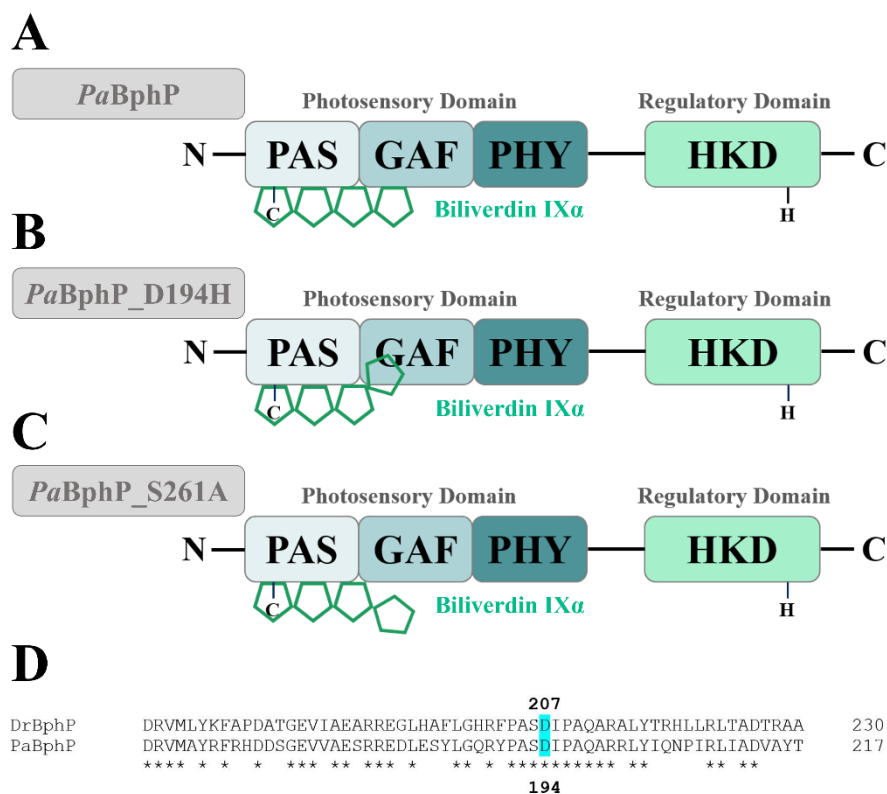


**Fig. 3.2: Schematic structure of the *PaBphP* in comparison to the two spectrally locked variants and an amino acid sequence alignment of the photosensory domain region of two bacterial phytochromes.**

The bacterial phytochrome *PaBphP* (A) and the variants (B-C) comprise a photosensory domain (PAS, GAF, PHY) on the N-terminus and a regulatory domain on the C-terminus (HKD). The chromophore, biliverdin IX $\alpha$ , which is bound to a conserved cysteine residue in the PAS domain, enables the protein to absorb light. The exchange of specific amino acids (Asp 194 or Ser 261) results in the conformational change of the chromophore-binding pocket and the immobilization of the chromophore in the pocket – depending on which amino acid is substituted – in the Pr- (B) or in the Pfr- (C) locked conformation.

(D) Section of an amino acid sequence alignment (blastp, protein-protein BLAST<sup>®</sup>) of the *D. radiodurans* phytochrome (top) and the *P. aeruginosa* phytochrome (bottom) photosensory domain region to find the amino acid residue corresponding to DrBphP\_D207 in *P. aeruginosa* (D194). The amino acid residue for generating a Pfr-locked variant in *P. aeruginosa* (S261) was already published (Yang *et al.*, 2011).

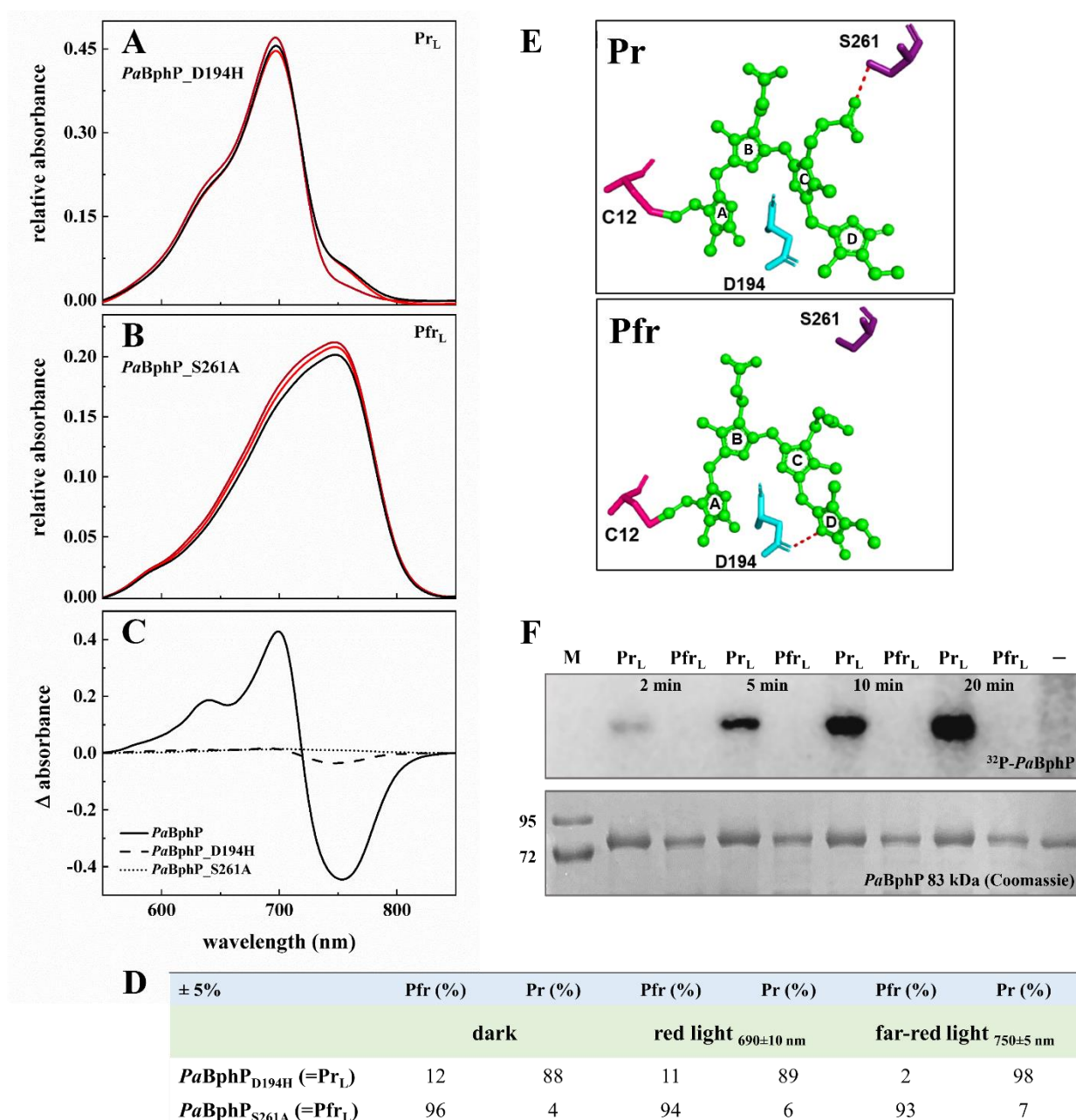


**Fig. 3.3: Spectral absorption properties and autokinase activity of recombinantly produced *PaBphP*<sub>D194H</sub> as well as *PaBphP*<sub>S261A</sub> protein variants.**

(A) Absorption spectra of *PaBphP*<sub>D194H</sub> and (B) *PaBphP*<sub>S261A</sub> (mathematically smoothed using Origin, Version 2022, OriginLab Corporation, Northampton, MA, USA. “Loess, Use Proportion for Span, Span 0.1”) after illumination with far-red light (750 nm, 5 min, dark red lines), with red light (690 nm, 5 min, red lines) and after dark incubation (60 min, black lines). All data were generated from a single set of measurements. BV IX $\alpha$  was added in excess after cell lysis prior to purification.

(C) Manually calculated difference spectra (far-red irradiated form minus dark incubated form; mathematically smoothed as in “A” and “B”) of *PaBphP*<sub>D194H</sub> (Pr<sub>L</sub>; dashed line) and *PaBphP*<sub>S261A</sub> (Pfr<sub>L</sub>; dotted line) compared to *PaBphP* wild type protein (solid line).

(D) The Pr<sub>L</sub> protein (*PaBphP*<sub>D194H</sub>) remains in its Pr-form, exhibiting a peak at 699 nm and does not undergo light-independent ground state formation. Likewise, the Pfr<sub>L</sub> protein (*PaBphP*<sub>S261A</sub>) mainly exists in its Pfr-form, with a peak at 749/750 nm (cf. Tab. 3.2). The exact fractions of Pr and Pfr for each spectrum are given in the table. A calculation error of  $\pm 5\%$  applies.

(E) Schematic structure of the BV IX $\alpha$  position in the chromophore-binding pocket and the corresponding stabilization in the Pr- or Pfr-form through Ser 261 (purple; stabilizing Pr-form) or Asp 194 (light blue; stabilizing Pfr-form). Photoconversion of the two forms is a result of a (Z)-(E) isomerization of the C15=C16 double bond between pyrrole ring C and D. Chromophore binding to the protein occurs at Cys 12 (pink) in the *P. aeruginosa* BphP (PDB accession 3NHQ and 3NOU; modified from Yang *et al.*, 2011).

(F) Autoradiogram (top) and corresponding Coomassie-stained SDS-PAGE gel (10 % (w/v); bottom) after *in vitro* radiolabeling of *PaBphP*\_D194H (= Pr<sub>L</sub>) and *PaBphP*\_S261A (= Pfr<sub>L</sub>) with [ $\gamma$ -<sup>32</sup>P]-ATP under ambient light conditions for 2, 5, 10 and 20 min. The autophosphorylation reaction was terminated at the specified times and the protein samples were separated by gel electrophoresis. The minus sign (-) indicates the negative control *PaBphP*\_H513A, which exhibits no autophosphorylation signal after 20 min incubation with radiolabeled ATP. The *PaBphP* variants have a relative molecular weight of approximately 83 kDa (marker: Color Prestained Protein Standard, Broad Range, NEB).

Having observed the significant correlation between the locked Pr-form and elevated autokinase activity, as well as the complete absence of kinase activity in the locked Pfr-form, the next objective was to further investigate the interrelation between photostate and autokinase output using wild type *PaBphP*. This requires a method to determine the Pr/Pfr-fractions in a given sample (cf. chapter 2.6.11; Tab. S2). Based on the *PaBphP* spectra of the Pr- and Pfr-forms (Fig. 3.4A; Fig. 4.3), the Pr/Pfr-fractions of the locked protein variants were calculated. Under far-red, red light and dark conditions 88-98 % of *PaBphP*\_D194H were in Pr, while at least 93 % of *PaBphP*\_S261A were in Pfr under the same conditions (Fig. 3.3D).

### **3.3 *PaBphP* is a bathy phytochrome and is inactive in its dark-adapted Pfr-ground state**

*PaBphP* is able to form a photoconvertible holo-phytochrome by autocatalytic binding of the chromophore BV IX $\alpha$ . It changes its spectral absorption properties after absorbing the typical wavelengths of light sensitive to phytochromes – far-red and red (Fig. 3.4A). Recent results have shown that the photoconversion of *PaBphP* can also be stimulated by blue light. Illumination of the protein with red (667 nm) or blue (426 nm) light resulted in the thermally equilibrated Pfr-enriched form of the phytochrome with a peak at 700 nm and an absorption shoulder at 750 nm. Based on our calculation (cf. chapter 2.6.11; Tab. S2), red light illumination led to approximately equal fractions of Pr- and Pfr-form, while blue light shifted the ratio slightly towards the Pr-form (Fig. 3.4C). As described previously (Tasler *et al.*, 2005; Yang *et al.*, 2011), these forms could be converted into a distinct Pr-form with a peak at 700 nm, lacking the 750 nm shoulder, by illumination with far-red light (791 nm). The ground state of most phytochromes – they are called prototypical or canonical phytochromes – is the Pr-form (Essen *et al.*, 2008). This form is present under far-red light conditions or after the slow dark reversion. However, the *P. aeruginosa* phytochrome does not belong to this group, but rather to the bathy phytochromes with a Pfr-form as the ground state under dark conditions (Tasler *et al.*, 2005). The conversion to the thermodynamically stable Pfr ground state is non-photochemical. Therefore, only far-red light and darkness are able to lead to fully developed Pr- and Pfr-forms,

respectively (Fig. 3.4C). The successful conversion is additionally shown in the difference spectra, which are the characteristic signature of phytochromes (Fig. 3.4B; cf. Fig. 3.3C). They were obtained by subtracting the blue-irradiated (Pfr-enriched; dotted line), the red-irradiated (Pfr-enriched; dashed line) or the dark-incubated (Pfr; solid line) form from the far-red irradiated Pr-form and they show maxima around 700 nm and minima around 750 nm.

The autophosphorylation activity of *PaBphP* at His 513 (Tasler *et al.*, 2005) was confirmed in an experiment conducted under ambient light conditions (Fig. 3.4D). The signal increased in a time-dependent manner from 1 to 10 min and could not be further enhanced (15, 20, 30 min). A protein variant, in which the phosphorylation site His 513 is replaced by alanine (*PaBphP\_H513A*), served as a negative control. For this variant, no autophosphorylation signal was detected after 30 min. The results for autokinase activity of the proteins with the locked conformations (cf. Fig. 3.3F) were confirmed for the corresponding forms of *PaBphP* under various light conditions using a new setup for radioactive kinase assays under illumination (Fig. S2). The assay revealed that the phytochrome is phosphorylated under all light conditions and is only strongly inhibited in the dark (Fig. 3.4E). Depending on the quality of the incident light and the resulting protein conformation, *PaBphP* materializes different levels of phosphorylation. The autokinase signals increased from red (667 nm;  $50 \pm 5$  % Pr) < blue (426 nm;  $67 \pm 5$  %) < far-red (791 nm;  $100 \pm 5$  %), in accordance with correspondingly increasing fractions of the Pr-form as well as decreasing fractions of Pfr-form (Fig. 3.4C). Although there is a strong correlation between the autokinase readout and the Pr-proportion in this specific case, the signal intensities observed in an autoradiogram cannot be reliably employed to quantify kinase activity as a whole. This limitation is due to their dependence on exposure time and other experimental variables. For a more accurate analysis and correlation of phytochrome activity, the Pr/Pfr-fractions calculated from the spectroscopic data can be used. In addition, the autophosphorylation behavior during the dark reversion of *PaBphP* was tested (Fig. 3.5A). Adaptation to dark conditions, started with 5 min of far-red irradiation, led to an increase in the Pfr-form (750 nm) and a decrease in the Pr-form (700 nm). During the conversion of Pr to Pfr, there was always a mixed form of the phytochrome with different Pr/Pfr-fractions (Fig. 3.5B). The longer *PaBphP* was incubated in the dark, undergoing the dark reversion progress, the lower was the autophosphorylation signal (Fig. 3.5C), indicating that the autophosphorylation activity decreased and the phytochrome is inactive in the Pfr-form. The phytochrome kinase signal was still slightly detectable after 120 min, because the dark reversion was not completed at this time point ( $13 \pm 5$  % Pr). For the negative control *PaBphP\_H513A*, no autophosphorylation signal was detected after 120 min.

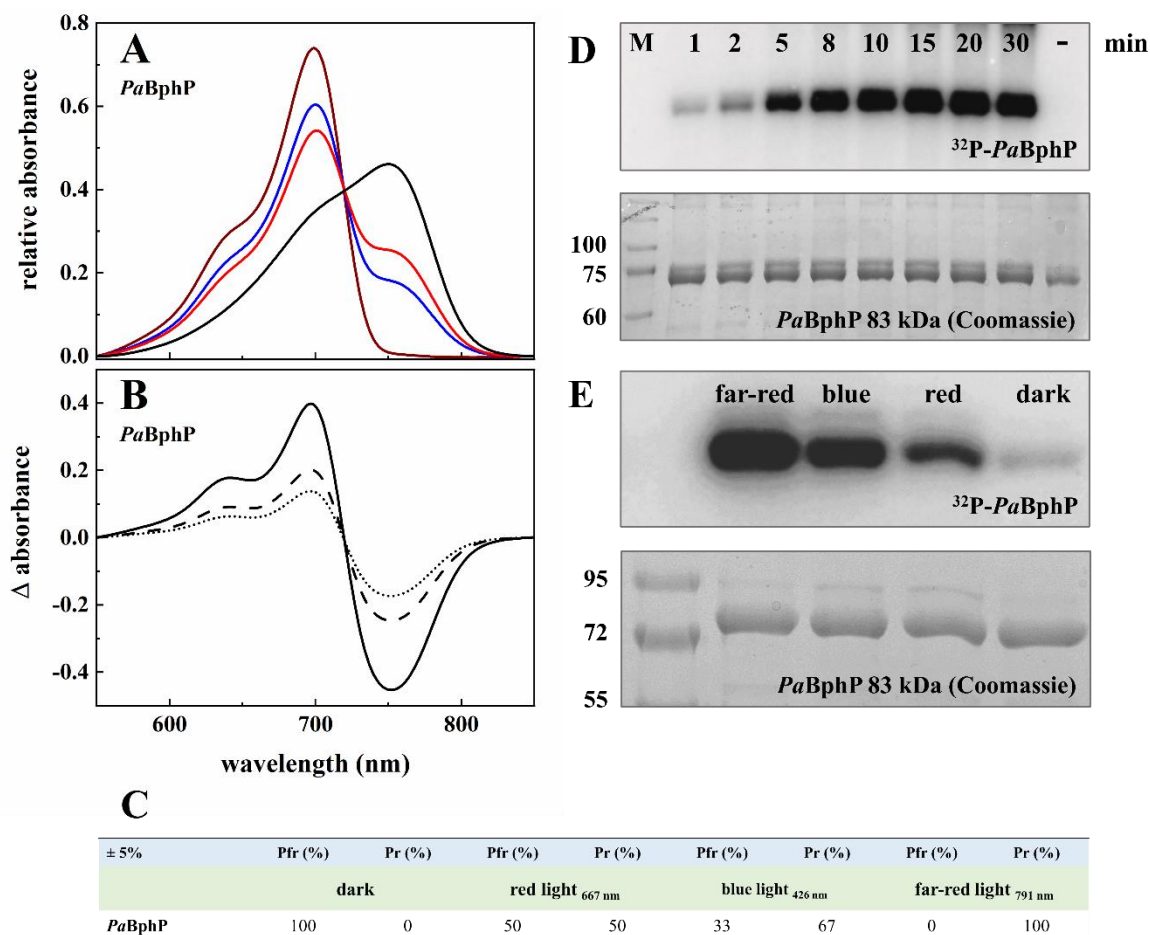


**Fig. 3.4: Spectral absorption properties and autokinase activity of recombinantly produced *PaBphP* under different light conditions.**

(A) Absorption spectra of *PaBphP* (mathematically smoothed using Origin, Version 2022. OriginLab Corporation, Northampton, MA, USA. “Loess, Use Proportion for Span, Span 0.1”) after illumination with far-red light (791 nm, 5 min, dark red line), with blue light (426 nm, 10 min, blue line), with red light (667 nm, 10 min, red line) and after dark reversion (24 h, black line). The extent of conversion cannot be improved by longer exposure times. All data were generated from a single set of measurements. BV IX $\alpha$  was added in excess after cell lysis prior to purification.

(B) Manually calculated difference spectra of *PaBphP* (far-red irradiated minus dark incubated form, solid line; far-red irradiated minus red irradiated form, dashed line; far-red irradiated minus blue irradiated form, dotted line; mathematically smoothed as in “A”).

(C) Absorption of far-red light results in a distinct Pr-form, and absorption of blue or red light results in Pfr-enriched forms. Incubation in the dark results in the non-photochemical conversion to the Pfr ground state. The exact fractions of Pr and Pfr for each spectrum are given in the table. A calculation error of  $\pm 5\%$  applies.

(D) Autoradiogram (top) and corresponding Coomassie-stained SDS-PAGE gel (10 % (w/v); bottom) after *in vitro* radiolabeling of *PaBphP* with [ $\gamma$ - $^{32}\text{P}$ ]-ATP under ambient light conditions from 1 to 30 min. The autophosphorylation reaction was terminated at the indicated times and samples were separated by gel electrophoresis. The minus sign (-) indicates the negative control *PaBphP*\_H513A, which displays no autophosphorylation signal after 30 min incubation with radiolabeled ATP. *PaBphP* has a relative molecular weight of approximately 83 kDa (marker: Prestained protein marker, proteintech). Due to issues in marker signal separation, *PaBphP* appears to be smaller than 75 kDa (Fig. S3 comparison of “Prestained protein marker, proteintech” and “Color Prestained Protein Standard, Broad Range, NEB”).

(E) Autoradiogram (top) and corresponding Coomassie-stained SDS-PAGE gel (10 % (w/v); bottom) after *in vitro* radiolabeling of *PaBphP* with [ $\gamma$ - $^{32}\text{P}$ ]-ATP under far-red (791 nm), blue (426 nm), and red (667 nm) light as well as under dark conditions. The autophosphorylation reaction was terminated after 5 min and the protein samples were separated by gel electrophoresis. Protein was pre-exposed to the appropriate light for 5 min or incubated in the dark overnight before adding the radiolabeled ATP. *PaBphP* has a relative molecular weight of approximately 83 kDa (marker: Color Prestained Protein Standard, Broad Range, NEB).



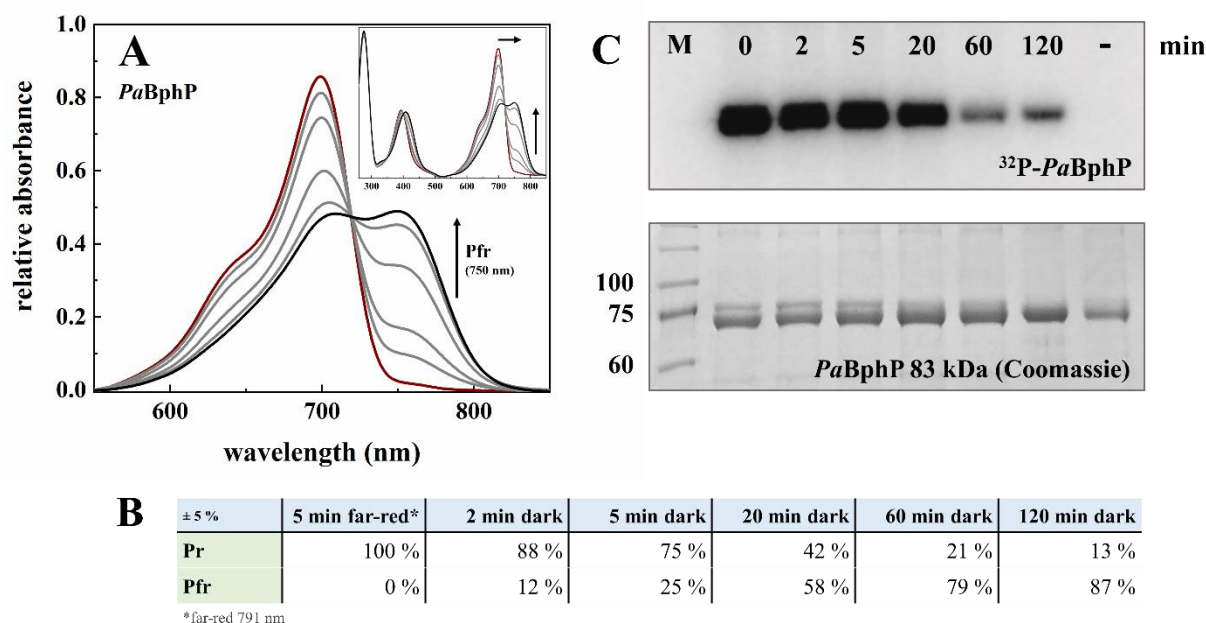


**Fig. 3.5: Spectral absorption properties and autokinase activity of recombinantly produced *PaBphP* under dark conditions.**

(A) Absorption spectra of *PaBphP* (mathematically smoothed using Origin, Version 2022. OriginLab Corporation, Northampton, MA, USA. “Loess, Use Proportion for Span, Span 0.1”) after irradiation with far-red light (791 nm, 5 min, dark red line) and different time points during dark reversion (2, 5, 20 and 60 min gray lines; 120 min black line). Course of the dark reversion (increase of Pfr-form, decrease of Pr-form) is indicated by the arrows. All data were generated from a single set of measurements. BV IX $\alpha$  was added in excess after cell lysis prior to purification. The inset shows the same spectra spanning the wavelength 260-850 nm.

(B) Absorption of far-red light results in a distinct Pr-form, and dark incubation results in increasing formation of Pfr-form. The exact fractions of Pr and Pfr for each spectrum are given in the table. A calculation error of  $\pm 5\%$  applies.

(C) Autoradiogram (top) and corresponding Coomassie-stained SDS-PAGE gel (10 % (w/v); bottom) after *in vitro* radiolabeling of *PaBphP* with [ $\gamma$ - $^{32}$ P]-ATP under far-red (791 nm) light conditions ( $t = 0$  min) and during the dark reversion after 2, 5, 20, 60 and 120 min. The minus sign (-) indicates the negative control *PaBphP*\_H513A, which displays no autophosphorylation signal after 120 min incubation with radiolabeled ATP. *PaBphP* has a relative molecular weight of approximately 83 kDa (marker: Prestained protein marker, proteintech). Due to issues in marker signal separation, *PaBphP* appears to be smaller than 75 kDa (Fig. S3 comparison of “Prestained protein marker, proteintech” and “Color Prestained Protein Standard, Broad Range, NEB”).

### 3.4 The chromophore biliverdin IX $\alpha$ and its covalent bond is not absolutely required for kinase activity of *PaBphP*

The chromophore BV IX $\alpha$  is attached via a thioether linkage to the cysteine residue 12 of the apo-protein in an autocatalytic reaction. Previous work from our group, conducted on both apo-*PaBphP* purified from *E. coli* and from a *P. aeruginosa*  $\Delta bphO$  mutant, indicated that autophosphorylation also occurs independently from an assembled chromophore (Heine, 2014; Tasler *et al.*, 2005). Contrastingly, the Basler group did not detect any autophosphorylation of the apo-phytochrome purified from *E. coli* (Mukherjee *et al.*, 2019). To investigate this discrepancy, the behavior of the apo-form and two other variants (C12A, H513A) of *PaBphP* were analyzed in more detail (Fig. 3.6; Fig. 3.7). Apo-*PaBphP* was obtained by expressing the *bphP* gene in a markerless *bphOP* deletion mutant (cf. chapter 3.1), while the genes encoding *PaBphP*\_C12A

and *PaBphP\_H513A* were expressed in a *bphP* deletion mutant (Fig. 3.6D). *PaBphP\_C12A* was initially employed under the assumption that it could also function as an apo-form of the phytochrome, since the binding site for BV IX $\alpha$  is disrupted, whereas *PaBphP\_H513A* serves as a kinase inactive variant. The variants were purified utilizing the same workflow as for *PaBphP*, along with supplementary chromophore incubation (“+BV lysate”). Apo-*PaBphP* and *PaBphP\_C12A* underwent further purification without any additional chromophore (“-BV lysate”).

The initial hypothesis that *PaBphP\_C12A* would be similar to the apo-protein was disproved as the variant is shown to undergo photoisomerization, albeit not covalently binding BV IX $\alpha$  (Fig. 3.6A left, solid lines; Tasler *et al.*, 2005). Interestingly, *PaBphP\_C12A* incorporates the chromophore in low amounts within the chromophore-binding pocket when excess BV IX $\alpha$  was added prior to purification. This Cys variant exhibits absorption spectra similar to Pr with a shift to shorter wavelengths, which is also shown in the difference spectrum (Fig. 3.6A left, gray dashed line). Moreover, complete Pfr-form development cannot be achieved, even in darkness. These observations are consistent with the calculated Pr/Pfr-fractions (Fig. 3.6E) and may be a result of a loose or misaligned BV IX $\alpha$  in the chromophore-binding pocket. Thus, the mutation of Cys 12 does not only prevent covalent binding, but also destabilizes the Pfr-form (Tasler *et al.*, 2005). If no additional BV IX $\alpha$  is provided and *PaBphP\_C12A* only retains the native chromophore, originating from BphO, the amplitude of the spectra decreases seven times (Fig. 3.6A right). Additionally, the variant is lacking a difference spectrum, meaning no photoisomerization occurs (Fig. 3.6A left, turquoise dashed line).

Incubating the cell lysate containing apo-*PaBphP* with BV IX $\alpha$  results in the assembly of holo-*PaBphP*, as demonstrated by restored absorption properties (Fig. 3.6B left, solid lines and gray dashed line; Fig. 3.6E). In absence of chromophore assembly, the purified apo-*PaBphP* exhibits the characteristic phytochrome spectra, with an amplitude over 30 times lower (Fig. 3.6B right) and is lacking a difference spectrum (Fig. 3.6B left, turquoise dashed line). The low absorption observed originates probably from the binding of BV IX $\delta$  (cf. chapter 3.1).

*PaBphP\_H513A* exhibits a pure Pr- and Pfr-form when exposed to far-red light and under dark conditions, respectively, as well as mixed forms under red and blue light irradiation (Fig. 3.6C, E). Thus, the variant displays spectra that are identical to those of wild type *PaBphP* (cf. Fig. 3.4C). This proves that the exchange of the amino acid residue does not result in loss of photoisomerization, suggesting that the PAS, GAF and PHY domains remain unaffected.

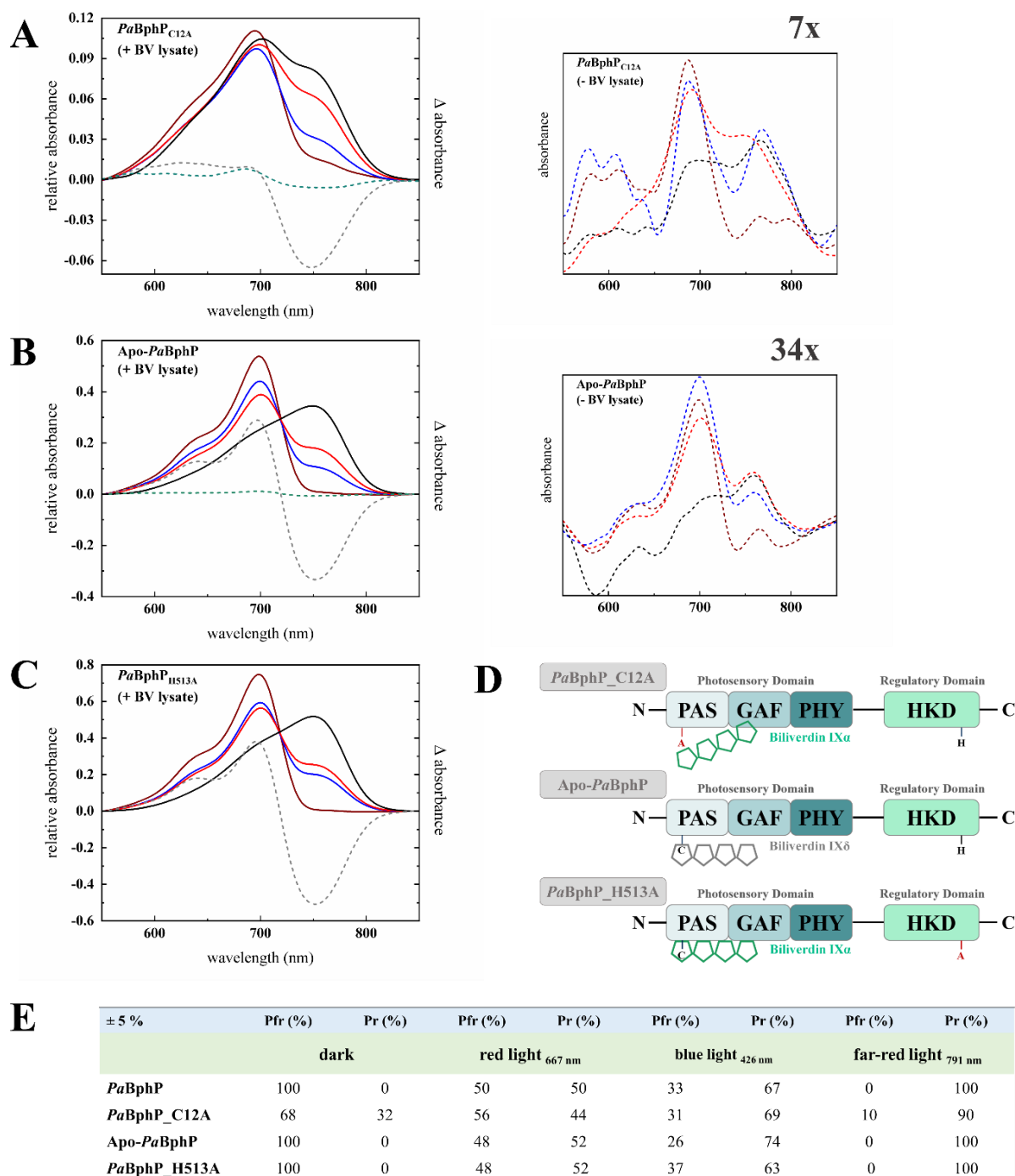


**Fig. 3.6: Spectral absorption properties under different light conditions and schematic domain structure of the apo-form and two variants of *PaBphP*.**

Absorption spectra (mathematically smoothed using Origin, Version 2022. OriginLab Corporation, Northampton, MA, USA. “Loess, Use Proportion for Span, Span 0.1”) of *PaBphP\_C12A* (A), apo-*PaBphP* (B) and *PaBphP\_H513A* (C) after irradiation with far-red light (791 nm, 5 min, dark red lines), with blue light (426 nm, 5 min, blue lines), with red light (667 nm, 5 min, red lines) and after dark reversion (24 h, black lines). BV IX $\alpha$  was added in excess after cell lysis prior to purification (left panel, “+BV lysate”). The 7x magnification (right panel in “A”) displays *PaBphP\_C12A* without chromophore incubation, while the 34x magnification (right panel in “B”) shows apo-*PaBphP* without BV IX $\alpha$  incubation (“-BV lysate”). Due to very small values on the y-axis, the labeling was omitted for clarity. The extent of conversion cannot be improved by longer exposure times. All data were generated from single sets of measurements. Manually calculated difference spectra (far-red irradiated minus dark incubated form; mathematically smoothed) were integrated into the graphs (gray dashed lines = incubation with excess BV IX $\alpha$ ; turquoise dashed lines = without BV IX $\alpha$  incubation).

(D) The *PaBphP* variants comprise a photosensory domain (PAS, GAF, PHY) on the N-terminus and a regulatory domain on the C-terminus (HKD). In *PaBphP\_C12A*, the conserved cysteine residue in the PAS domain is

substituted with alanine, thereby affecting protein photoisomerization. This substitution enables an unexpected insertion of the chromophore in the chromophore-binding pocket without covalent binding. Apo-*PaBphP* can bind the intrinsically produced BV IX $\delta$  in small quantities. In the *PaBphP\_H513A* variant, the substitution of the conserved histidine residue within the regulatory domain with an alanine, doesn't affect the photosensory domain activity.

(E) The exact fractions of Pr and Pfr for each spectrum are given in the table. A calculation error of  $\pm 5\%$  applies.

Apo-*PaBphP* as well as the two variants were additionally assayed for autophosphorylation activity by adding [ $\gamma$ - $^{32}$ P]-ATP (Fig. 3.7). The autokinase signals decrease according to the decreasing amount of bound chromophore from *PaBphP* > *PaBphP\_C12A* > apo-*PaBphP* and finally to *PaBphP\_H513A*, showing no autophosphorylation activity (Fig. 3.7A, each without BV IX $\alpha$  incubation “-BV”). The autokinase signal of *PaBphP\_C12A* (+BV), when compared to *PaBphP* (+BV) is significantly decreased and that of *PaBphP\_C12A* (-BV) and apo-*PaBphP* (-BV) are even more reduced (Fig. 3.7B, last two lanes). Based on this data, a strong correlation between chromophore saturation and its binding mode can be clearly observed.

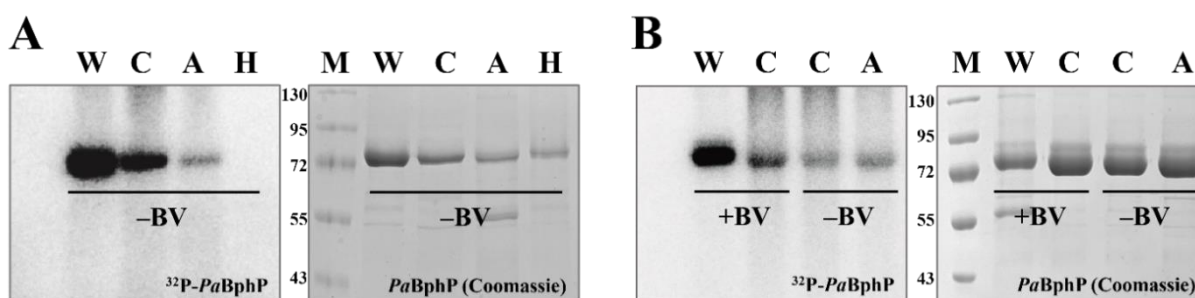


**Fig. 3.7: Autokinase activity of heterologously produced *PaBphP* wild type and variants.**

(A) Autoradiogram (left) and corresponding Coomassie-stained SDS-PAGE gel (10 % (w/v); right) after *in vitro* radiolabeling of *PaBphP* (W), *PaBphP\_C12A* (C), apo-*PaBphP* (A) and *PaBphP\_H513A* (H) with [ $\gamma$ - $^{32}$ P]-ATP under ambient light conditions. Proteins were not incubated with excess BV IX $\alpha$  (-BV).

(B) Autoradiogram (left) and corresponding Coomassie-stained SDS-PAGE gel (10 % (w/v); right) after *in vitro* radiolabeling of *PaBphP* (W), *PaBphP\_C12A* (C) and apo-*PaBphP* (A) with [ $\gamma$ - $^{32}$ P]-ATP under ambient light conditions. *PaBphP* and *PaBphP\_C12A* were incubated with excess BV IX $\alpha$  (+BV) and another sample of *PaBphP\_C12A* as well as apo-*PaBphP* were not incubated with excess BV IX $\alpha$  (-BV).

The samples *PaBphP\_C12A* (-BV) and apo-*PaBphP* (-BV) are the same in (A) and (B), but in relative comparison with other protein samples.

Autophosphorylation reactions were terminated after 10 min and samples were separated by gel electrophoresis. *PaBphP* and the variants have a relative molecular weight of approximately 83 kDa (marker: Color Prestained Protein Standard, Broad Range, NEB).

### 3.5 *PaBphP* is the histidine kinase required for activation of the response regulator *PaAlgB*

One of the major goals of this project was to analyze the physiological role and the associated downstream signaling pathway of BphP in *P. aeruginosa*. Previous research identified *PaBphP* as the histidine kinase phosphorylating *PaAlgB* at Asp 59 (Mukherjee *et al.*, 2019). The gene for *PaAlgB* is organized in an operon together with the gene for *PaKinB* and is known to

regulate the alginate synthesis in *P. aeruginosa* (Ma *et al.*, 1998; Ma *et al.*, 1997). In order to verify the role of *PaAlgB* as the postulated RR of *PaBphP*, phosphotransfer was assessed. Therefore, the *algB* gene was cloned into the *E. coli* overexpression vector pASK-IBA3 with a C-terminal Strep-tag II and the protein was purified by affinity chromatography. To yield *PaBphP* autophosphorylation, [ $\gamma$ - $^{32}\text{P}$ ]-ATP was added and the mix was incubated for 30 min under ambient light conditions. After the addition of *PaAlgB*, time-dependent phosphotransfer was monitored from 2 to 30 min. A clear decrease in the autophosphorylation signal intensity of the kinase and an increase in the signal intensity for the RR could be detected (Fig. 3.8A). The same experiment was performed for the following protein variants of *PaBphP*: the Pr-locked variant *PaBphP*\_D194H, the Pfr-locked variant *PaBphP*\_S261A and the inactive variant *PaBphP*\_H513A (Fig. 3.8B). *PaBphP* and the corresponding variants were incubated with [ $\gamma$ - $^{32}\text{P}$ ]-ATP for 20 min. After the addition of *PaAlgB*, the mixtures were incubated for further 30 min. The autoradiogram shows that *PaBphP* and the Pr-locked variant (D194H) are able to autophosphorylate and further transfer the phosphoryl group to the RR *PaAlgB* (D194H stronger than WT). Contrastingly, the Pfr-locked variant (S261A) and the variant lacking the phosphorylation site His 513 (H513A) are unable to autophosphorylate and thus incapable of transferring the phosphoryl group to *PaAlgB*. This assay showed that the autophosphorylation and transphosphorylation activities of *PaBphP* are related and that the conformation of the chromophore affects both activities. To further confirm this, *PaBphP* was employed for transphosphorylation assays under different light conditions (Fig. 3.8C). It is evident that *PaBphP* materializes different levels of autokinase activity depending on the quality of the incident light (cf. Fig. 3.4E), which is reflected in the transphosphorylation process. The transphosphorylation signal intensity of *PaAlgB* increase from red (667 nm) < blue (426 nm) < far-red (791 nm), corresponding to increasing proportions of the Pr-form of *PaBphP* (cf. Fig. 3.4C). Phosphoryl group transfer to the RR is only strongly inhibited under dark conditions. In conclusion, these assays demonstrate that the kinase *PaBphP* has the ability to phosphorylate the RR *PaAlgB* *in vitro* and that the extent of the transfer correlates with the calculated Pr/Pfr-fractions. The transferred radioactivity is indicative of phosphotransfer because the control (*PaAlgB* with [ $\gamma$ - $^{32}\text{P}$ ]-ATP) showed no signal, indicating that *PaAlgB* is incapable of autophosphorylation. Since free radiolabeled ATP was not removed prior to the additions of *PaAlgB* in the experiments, the radioactivity transferred to *PaAlgB* are typically stronger than those of the kinase.

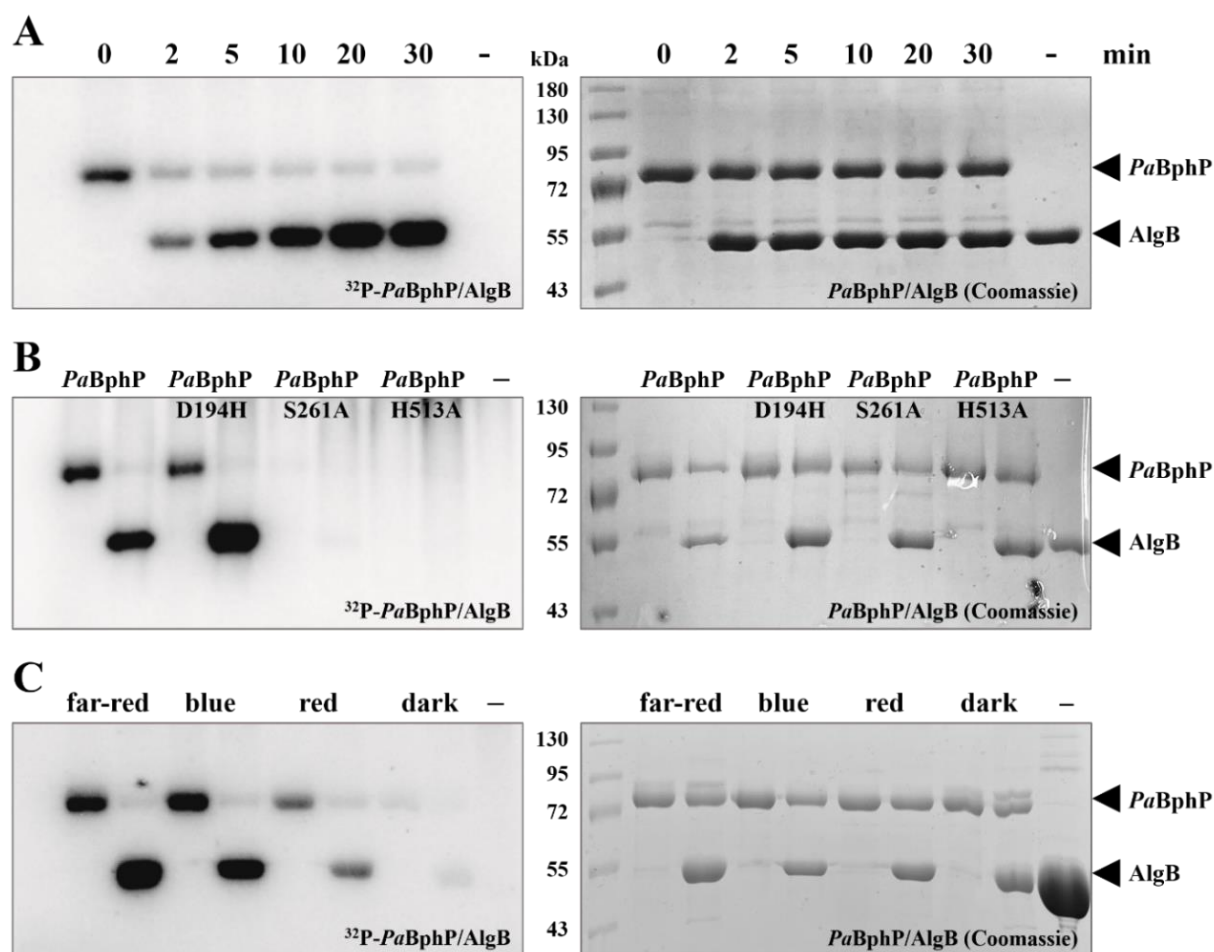


**Fig. 3.8: Phosphotransfer from the kinase *PaBphP* or variants to the response regulator *PaAlgB*.**

(A) Autoradiogram (left) and corresponding Coomassie-stained SDS-PAGE gel (10 % (w/v); right) after *in vitro* radiolabeling of *PaBphP* with  $[\gamma\text{-}^{32}\text{P}]\text{-ATP}$  for 30 min under ambient light conditions ( $t = 0$  min). Autophosphorylation of *PaBphP* was followed by addition of an equimolar amount of *PaAlgB* for additional 30 min. Samples were taken after 2, 5, 10, 20 and 30 min to detect transphosphorylation events.

(B) Autoradiogram (left) and corresponding Coomassie-stained SDS-PAGE gel (10 % (w/v); right) after *in vitro* radiolabeling of *PaBphP* and variants (D194H, S261A and H513A) with  $[\gamma\text{-}^{32}\text{P}]\text{-ATP}$  under ambient light conditions (left lane in each sample pair). Incubation time (20 min) was followed by addition of equimolar amounts of *PaAlgB* for additional 30 min (right lane in each sample pair).

(C) Autoradiogram (left) and corresponding Coomassie-stained SDS-PAGE gel (10 %, (w/v); right) after *in vitro* radiolabeling of *PaBphP* under far-red, blue, and red light as well as dark conditions (left lane in each sample pair). Pre-irradiation with the respective light (10 min) or dark incubation overnight and autophosphorylation reaction (10 min) was followed by the addition of equimolar amounts of *PaAlgB* for additional 10 min (right lane in each sample pair).

The minus sign (-) in every assay indicates the negative control (*PaAlgB* incubated with  $[\gamma\text{-}^{32}\text{P}]\text{-ATP}$ ), which displays no autophosphorylation signal. *PaBphP* and the variants have a relative molecular weight of approximately 83 kDa and *PaAlgB* of 52 kDa (marker: Color Prestained Protein Standard, Broad Range, NEB).

### 3.6 *PaKinB* is the phosphatase required for dephosphorylation of the response regulator *PaAlgB*

After identifying *PaBphP* as the kinase of *PaAlgB*, it was shown that *PaKinB* assumes an opposing function (Mukherjee *et al.*, 2019) because it has been previously known in connection with the RR *PaAlgB* (Chand *et al.*, 2012; Chand *et al.*, 2011; Ma *et al.*, 1998; Ma *et al.*, 1997). In order to confirm the role as a phosphatase, the gene for the cytosolic domain of *PaKinB*

(*kinB\_CD*) was cloned into the *E. coli* overexpression vector pASK-IBA3 with a C-terminal Strep-tag II. The soluble protein was purified via affinity chromatography and its dephosphorylation activity was tested (Fig. 3.9A). [ $\gamma$ - $^{32}$ P]-ATP was added to *PaBphP* and incubated for 20 min under ambient light conditions. After addition of an equimolar amount of *PaAlgB*, the autophosphorylation signal intensity of the kinase decreased while the signal intensity for the RR was increasing. As shown in Fig. 3.8, the transferred radioactive signal is indicative of phosphotransfer, because *PaAlgB* is not capable to autophosphorylate. Upon introduction of the phosphatase *PaKinB*, the signal intensity of *PaAlgB* decreased, indicating that *PaKinB* dephosphorylates the RR. Another control experiment was performed using a comparable setup and an additional variant of the phosphatase *PaKinB* (Fig. 3.9B). After successful autophosphorylation of the kinase *PaBphP* and phosphoryl group transfer to the RR *PaAlgB*, both *PaKinB* (lane 4-5) and *PaKinB\_P390S* (lane 9-10) were added to the mix. This conserved prolin residue (P390) was shown to be responsible for the activity of the phosphatase *PaKinB* (Chand *et al.*, 2012). The assay revealed the P390S variant is no longer capable of dephosphorylating *PaAlgB*. Therefore, these results confirm the phosphatase activity of *PaKinB* is responsible for dephosphorylating the RR *PaAlgB* of the kinase *PaBphP*.

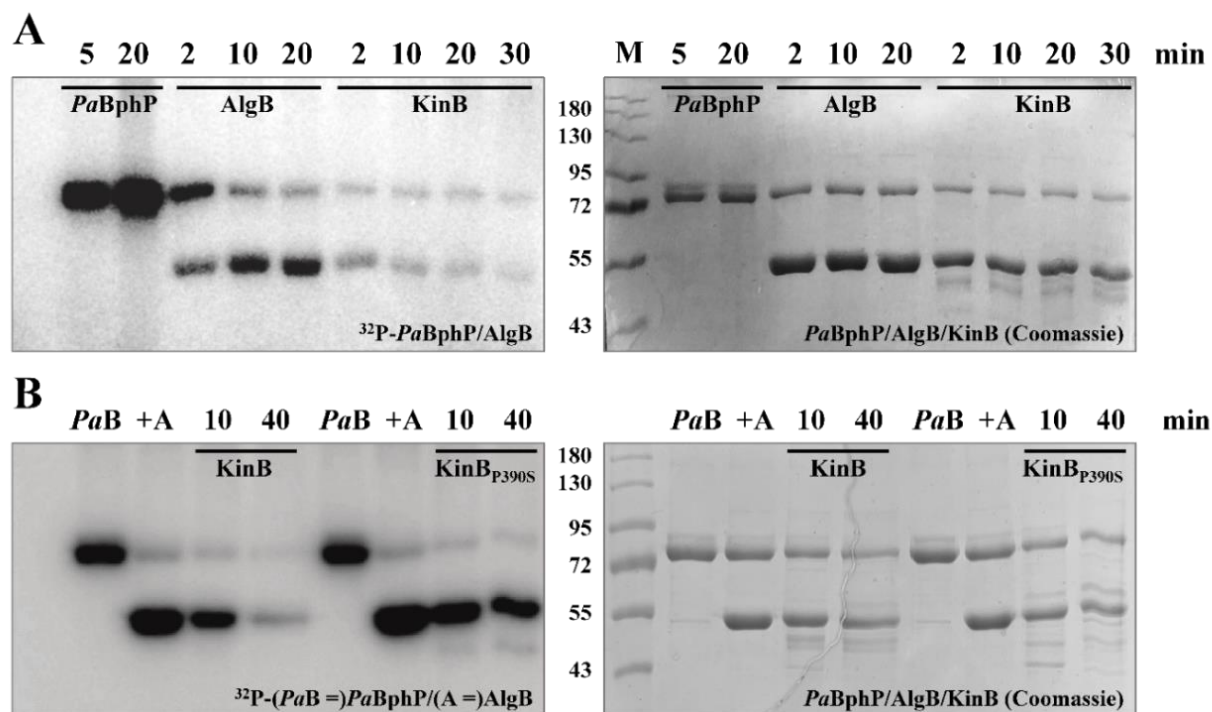


**Fig. 3.9: Phosphotransfer from the kinase *PaBphP* to *PaAlgB* and dephosphorylation of the response regulator by the phosphatase *PaKinB*.**

(A) Autoradiogram (left) and corresponding Coomassie-stained SDS-PAGE gel (10 % (w/v); right) after *in vitro* radiolabeling of *PaBphP* with [ $\gamma$ - $^{32}$ P]-ATP for 20 min under ambient light conditions (samples were taken after 5 and 20 min). Autophosphorylation of *PaBphP* was analyzed by adding *PaAlgB* for additional 20 min (samples were taken after 2, 10 and 20 min). Phosphotransfer to the RR *PaAlgB* was followed by removing [ $\gamma$ - $^{32}$ P]-ATP from the reaction and addition of *PaKinB* for additional 30 min (samples were taken after 2, 10, 20 and 30 min).

(B) Autoradiogram (left) and corresponding Coomassie-stained SDS-PAGE gel (10 % (w/v); right) after *in vitro* radiolabeling of *PaBphP* with [ $\gamma$ - $^{32}$ P]-ATP for 10 min under ambient light conditions (first and fifth lane “*PaB*”). Autophosphorylation of *PaBphP* was analyzed by adding *PaAlgB* for additional 10 min (second and sixth lane “+A”). Phosphotransfer to the response regulator *PaAlgB* was followed by removing [ $\gamma$ - $^{32}$ P]-ATP from the reaction and addition of *PaKinB* or *PaKinB*<sub>P390S</sub> for additional 40 min (samples were taken after 10 and 40 min). *PaBphP* has a relative molecular weight of approximately 83 kDa, *PaAlgB* of 52 kDa and *PaKinB* as well as *PaKinB*<sub>P390S</sub> of 47 kDa (marker: Color Prestained Protein Standard, Broad Range, NEB).

### 3.7 The deletion of *bphP*, *bphOP* and *kinB* in *P. aeruginosa* PA14 do not affect the bacterial growth

The next aim was to investigate the effect of various gene deletions in PA14. Gene knockouts (KOs) can result in growth deficits of bacteria or even in non-viable cells. It is crucial to ensure that the deletion mutants do not fail to grow under standard temperatures for subsequent phenotypic experiments. Therefore, the growth patterns of the mutants PA14 $\Delta$ *bphP*, PA14 $\Delta$ *bphOP* and PA14 $\Delta$ *kinB* were examined. Growth was monitored for 26 h under aerobic conditions at 37 °C in LB medium (Fig. 3.10A). The growth curves of the KO strains are similar to those of PA14 wild type, indicating that the gene deletions have no impact on growth under aerobic conditions. Additionally, the growth of PA14 and PA14 $\Delta$ *bphP* was monitored in LB media for 25 h under aerobic conditions and at different temperatures: 37 °C, 25 °C and 17 °C (Fig. 3.10B). The growth curves indicate slower growth at lower temperatures, but no significant difference can be observed between the two strains.

To determine at which time points native *PaBphP* is produced in *P. aeruginosa* under standard conditions (37 °C and 17 °C, LB media), culture samples were taken during the growth (Fig. 3.10B, PA14). The total protein content was separated via SDS-PAGE, and *PaBphP* was identified via immunological detection (Fig. 3.10C). Levels of native *PaBphP* were either very low or undetectable from  $t_1$ - $t_4$  (data not shown). Although quorum sensing does not directly control the induction of expression, the alternative sigma factor RpoS and the transcriptional activator LasR has been clearly demonstrated to be involved in the process (Barkovits *et al.*, 2008; Barkovits *et al.*, 2011). As previously demonstrated by Barkovits, the expression of the *bphOP* operon was also cell density-dependent and started during the early stationary phase in course of this work. The protein was detectable after 5 h at 37 °C (Fig. 3.10D). Over the next 5 hours ( $t_6$ - $t_{10}$ ) and in the overnight sample ( $t_{25}$ ), the signal intensity increased further. This pattern was consistent in all similar experiments. Unexpectedly, *PaBphP* was already detectable in cells grown at 17 °C during the exponential phase. For phenotypic experiments, several overexpression plasmids were mobilized via conjugation in PA14 and PA14 $\Delta$ *bphP*. These strains were also employed in the assays and compared to the wildtype and the deletion mutant, possessing empty vectors controls.



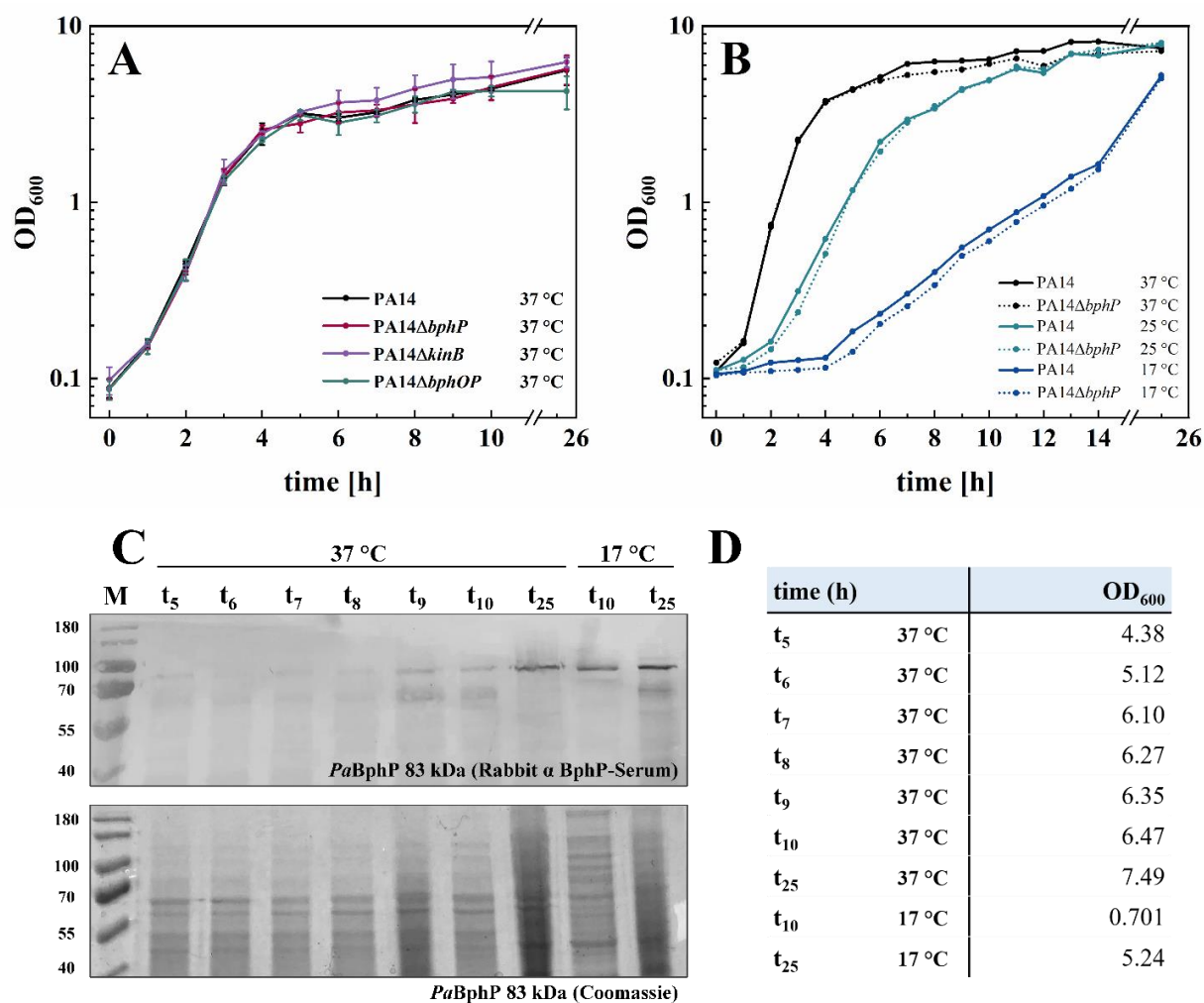


**Fig. 3.10: Effect of *bphP*-, *bphOP*- or *kinB*-deletion on bacterial growth compared to PA14 wild type at different temperatures and detection of the native phytochrome in *P. aeruginosa* cells.**

(A) LB overnight cultures of PA14 (black line), PA14Δ*bphP* (dark red line), PA14Δ*kinB* (purple line) and PA14Δ*bphOP* (green line) were set to an initial OD<sub>600</sub> of 0.1 in LB media and incubated at 37 °C. Cell density was monitored hourly for 10 h and after 25.75 h by measuring the optical density at 600 nm and plotted as the logarithm of the bacterial count in two biological replicates.

(B) LB overnight cultures of PA14 (solid lines) and PA14Δ*bphP* (dotted lines) were set to an initial OD<sub>600</sub> of 0.1 in LB media and incubated at 37 °C (black lines), 25 °C (green lines) and 17 °C (blue lines). Cell density was monitored hourly for 14 h and after 25 h by measuring the optical density at 600 nm and plotted as the logarithm of the bacterial count in one biological replicate.

(C) Immunological detection of PaBphP using Rabbit α BphP-Serum (top) and corresponding Coomassie-stained SDS-PAGE gel (10 % (w/v); bottom) of various samples from the growth curve (B). Total cells grown at 37 °C are indicated by t<sub>5</sub>-t<sub>25</sub> and cells grown at 17 °C by the following t<sub>10</sub> and t<sub>25</sub>. Equal amounts of bacterial cells were applied to each lane of the polyacrylamide gel. Native PaBphP has a relative molecular weight of approximately 83 kDa (marker: Thermo Scientific™ PageRuler™ Prestained Protein Ladder).

(D) Optical density values at 600 nm of the samples analyzed on the SDS-PAGE in “C”.

### 3.8 Phosphorylation state of the kinase *PaBphP* and of the corresponding response regulator *PaAlgB* regulates swimming motility

Swimming motility of *P. aeruginosa* is a flagellum-dependent movement and can be triggered by low agar concentration in the medium (Moradali *et al.*, 2017). To investigate the correlation between the phosphorylation state of *PaBphP/PaAlgB* and the swimming ability of PA14 strains, cells were grown on LB-agar plates (0.3 % (w/v)) for 24 h (Fig. 3.11A). After overnight incubation, the diameters of the swimming zones were manually measured (Fig. 3.11B). The diameter increased in the following order: PA14Δ*bphP* +pBphP < PA14Δ*kinB* (+EV) < PA14 (+EV) = PA14Δ*bphP* (+EV) = PA14Δ*bphP* +pBphP<sub>H513A</sub>, according to the RR phosphorylation state. Compared to PA14, the swimming zone diameter decreased by 40 % for PA14Δ*bphP* +pBphP and 22 % for PA14Δ*kinB*. This indicates that the function of the polar flagellum is affected by high levels of unphosphorylated *PaAlgB* or low levels of phosphorylated *PaAlgB* and their further downstream regulation steps.

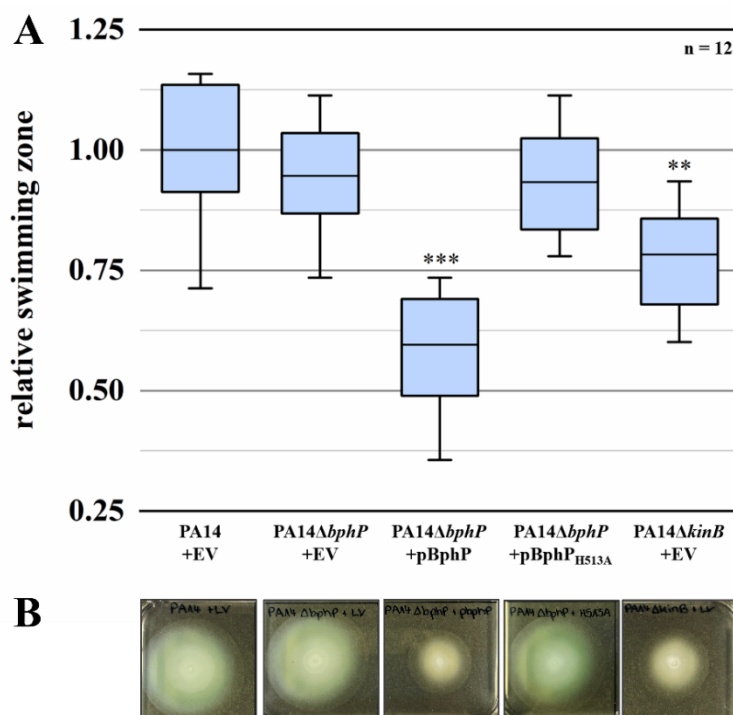


**Fig. 3.11: Swimming motility of *P. aeruginosa* mutant and overexpression strains in comparison to PA14.** (A) The boxes represent the data from 25-75 % and display the mean (solid line in the box) normalized to PA14. The whiskers show the data from the minimal to the maximal value. The asterisks mark the statistical significance. The cultures were grown 3 h at 37 °C after induction of the gene expression with 0.1 % (w/v) L(+)-arabinose under ambient light conditions (580 nm dominates). 1 μl of every culture was applied on a 0.3 % LB-agar plate and incubated 24 h at 30 °C. Swimming motility was analyzed by measuring the swimming zone of PA14 with the empty vector (= EV), PA14Δ*bphP* +EV, PA14Δ*bphP* + pBphP (= pHERD26T\_ *PaBphP*), PA14Δ*bphP* + pBphP<sub>H513A</sub> (= pHERD26T\_ *PaBphP*\_ H513A) and PA14Δ*kinB* +EV. The experiment was performed using 12 biological replicates. Statistical analysis was performed on all data sets. Samples with a Gaussian distribution (confirmed with Kolmogorov-Smirnov test) were compared with PA14+EV using unpaired two-tailed Student's *t*-test. Equality of variances in unpaired samples Student's *t*-tests was assessed with an *F*-test. This was followed

by a *post hoc* Bonferroni correction applied for multiple comparisons. Significance values were defined as follows: \* $p < 0.0125$ ; \*\* $p < 0.0025$ ; \*\*\* $p < 0.00025$ .

(B) Corresponding swimming zones of the strains showed in the box blot in “A” on swimming-agar (0.3 % (w/v)) with tetracycline and 0.1 % (w/v) L(+) arabinose (cf. Fig. S4).

The twitching motility, which is mediated by the attachment and retraction of type IV pili on solid surfaces (Moradali *et al.*, 2017) was also tested in this study. Therefore, bacterial cultures were applied to the plastic bottom under the LB-agar of the petri dish and the twitching zones were stained with crystal violet after two days. Preliminary data indicate no difference in twitching motility ability between PA14 and the *bphP* as well as *kinB* deletion mutants (data not shown). Swarming motility, which is facilitated by the flagellum, type IV pili and rhamnolipids was also investigated, but did not show clear results. The addition of tetracycline and L(+)arabinose to low-nitrogen, semisolid LB-agar plates, resulted in the inhibition of swarming motility for all tested strains.

### 3.9 Phosphorylation state of the kinase *PaBphP* and of the corresponding response regulator *PaAlgB* regulate pyocyanin secretion

As previously mentioned, the *PaBphP/PaAlgB* TCS seems to be involved in the regulation of virulence. Pyocyanin (PYO) is a blue-green colored virulence factor secreted by *P. aeruginosa*. It is synthesized from the precursor chorismate by a series of complex steps mediated by gene products of two *phzA-G* operons, *phzH*, *phzM* and *phzS* (Fig. 3.12A). PYO is classified as a phenazine and belongs to the nitrogen-containing heterocyclic compounds (Pierson and Pierson, 2010). Its redox properties allow it to easily permeate through membranes and cause oxidative cell damage (Lau *et al.*, 2004). To investigate the interrelation between the phosphorylation state of *PaBphP/PaAlgB* and the quantity of secreted PYO (Fig. 3.12B), the total amount of this compound was measured from culture supernatants (Fig. 3.12C). The amount of PYO decreased in the following order: PA14 $\Delta$ *bphP* +pBphP<sub>H513A</sub>  $\geq$  PA14 $\Delta$ *bphP* (+EV) > PA14 (+EV) > PA14 $\Delta$ *kinB* (+EV)  $\geq$  PA14 $\Delta$ *bphP* +pBphP, according to the RR phosphorylation state. Compared to PA14, the quantity increased by 50 % for PA14 $\Delta$ *bphP* and 57 % for PA14 $\Delta$ *bphP* +pBphP<sub>H513A</sub>, while it decreased by 76 % for PA14 $\Delta$ *bphP* +pBphP and 72 % for PA14 $\Delta$ *kinB*. This suggests that PYO secretion is based on high levels of unphosphorylated *PaAlgB* or low levels of phosphorylated *PaAlgB* and their further downstream regulation steps.

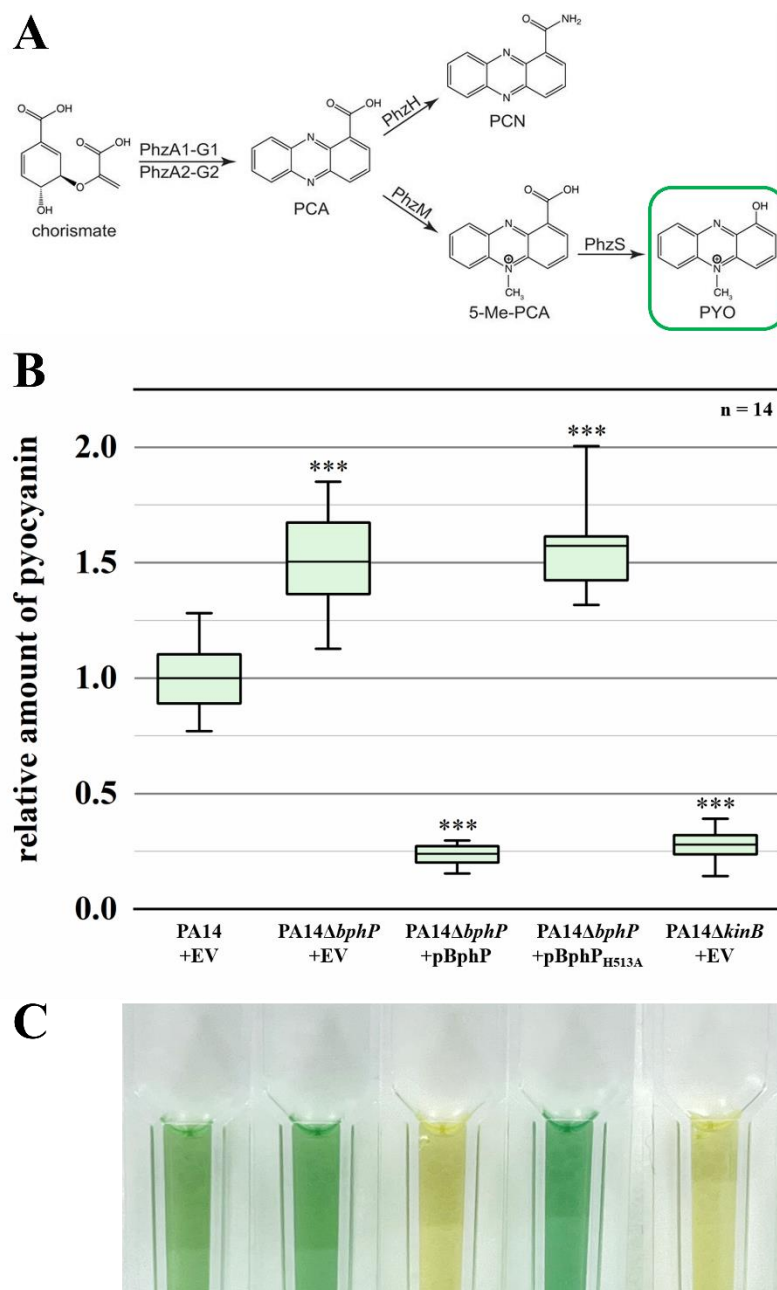


**Fig. 3.12: Pyocyanin secretion by *P. aeruginosa* mutants and overexpression strains in comparison to PA14.**

(A) Biosynthetic pathway of pyocyanin (PYO) in *P. aeruginosa*, starting from chorismate, to phenazine-1-carboxylic acid (PCA), to phenazine-1-carboxamide (PCN) by PhzH or 5-methyl-phenazine-1-carboxylic acid (5-Me-PCA) by PhzM to ultimately PYO by PhzS. Figure modified from Kahl *et al.*, 2020.

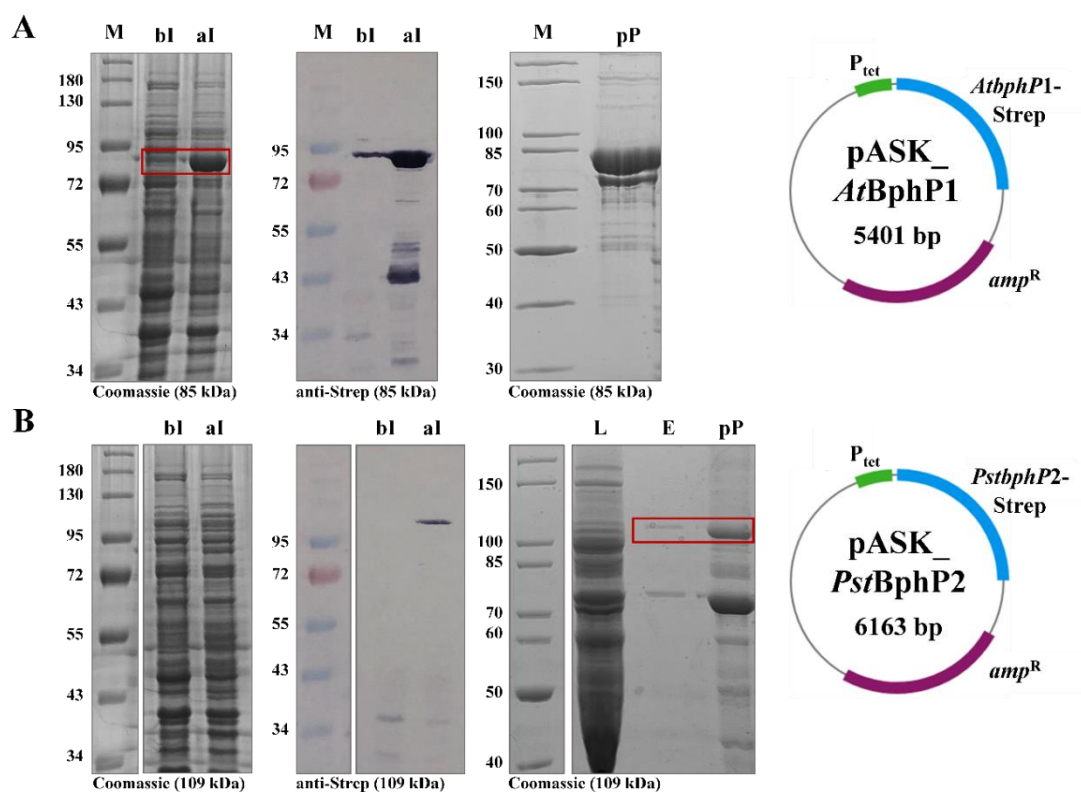
(B) The boxes represent the data from 25-75 % and display the mean (solid line in the box) normalized to PA14. The whiskers show the data from the minimal to the maximal value. The asterisks mark the statistical significance. The cultures were grown 5 h at 37 °C after induction of the gene expression with 0.1 % (w/v) L(+)-arabinose under ambient light conditions (580 nm predominant). The amount of secreted PYO was determined by measuring the OD<sub>695nm</sub> from culture supernatants: PA14 with the empty vector (= EV), PA14Δ*bphP* +EV, PA14Δ*bphP* +pBphP (= pHERD26T\_*PaBphP*), PA14Δ*bphP* +pBphP<sub>H513A</sub> (= pHERD26T\_*PaBphP*\_H513A) and PA14Δ*kinB* +EV. The measured values were normalized to an OD<sub>600</sub> = 1. The experiment was performed with 14 biological replicates. Statistical analysis was performed on all data sets. Samples with a Gaussian distribution (confirmed with Kolmogorov-Smirnov test) were compared using unpaired two-tailed Student's *t*-test. Equality of variances in unpaired samples Student's *t*-tests was assessed with a *F*-test. This was followed by a *post hoc* Bonferroni correction applied for multiple comparisons. Significance values were defined as follows: \**p* < 0.0125; \*\**p* < 0.0025; \*\*\**p* < 0.00025.

(C) Corresponding culture supernatants of the five strains showed in the box blot in "B".

## Part 2 – Bathy and prototypical phytochromes in different non-photosynthetic human and plant pathogens

### 3.10 Heterologous expression and purification of the *A. tumefaciens* and *P. syringae* prototypical phytochromes was successful

The *A. tumefaciens* and *P. syringae* prototypical phytochrome genes were expressed using a *tet* promoter-driven C-terminal Strep-tag II expression system, allowing purification and detection of the encoded proteins (Fig. 3.13). The SDS-PAGE gels revealed the presence of *AtBphP1* and *PstBphP2* with a relative molecular weight of ~ 85 kDa (Fig. 3.13A) and ~ 109 kDa (Fig. 3.13B), consistent with the predicted molecular mass calculated from the amino acid composition. The proteins were immunologically detected using Strep-Tactin® AP conjugate via western blot analysis. The gene encoding *PstBphP1* was expressed using a T7 promoter-driven C-terminal polyhistidine-tag expression system and coexpressed with the HO gene *bphO* from *P. syringae*. The SDS-PAGE gel revealed the presence of *PstBphP1* with a relative molecular weight of ~ 83 kDa (Fig. 3.13C). The protein was immunologically detected using 6x-His tag monoclonal antibody via western blot analysis. Although, the chromophore was produced together with *PstBphP1*, the protein was not sufficiently saturated (data not shown). Therefore, an excess of BV IX $\alpha$  was added to the cell lysates of all three overproductions (*AtBphP1*, *PstBphP1*, *PstBphP2*). *PstBphP2* was only obtained in low amounts and the holo-phytochrome resulted to be highly instable, preventing further experiments.



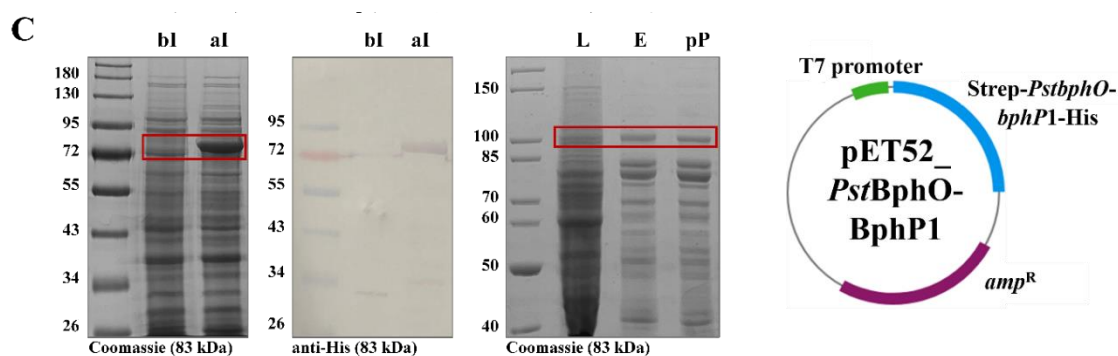


**Fig. 3.13: Homologous production of bacterial prototypical phytochromes from different organisms.**

(A) Coomassie-stained SDS-PAGE gel (10 % (w/v); left) and corresponding immunological detection against Strep-tag II (middle) of *AtBphP1* with schematic representation of the overexpression vector pASK\_*AtBphP1* [5401 bp], encoding the phytochrome with a C-terminal Strep-tag II (blue) in a *tet* promoter-driven (green) system. The ampicillin resistance gene (purple) confers resistance to the mentioned antibiotic to bacteria carrying the plasmid. Sample application of the total cells before (bl) and after induction (al) of the gene expression. The cultures were grown over night at 17 °C after induction with 200 ng/ml AHT. Coomassie-stained SDS-PAGE gel (10 % (w/v); right) of *AtBphP1* after affinity chromatography purification (pP = purified protein) with Strep-Tactin® Sepharose® resin. The protein has a relative molecular weight of approximately 85 kDa.

(B) Coomassie-stained SDS-PAGE gel (10 % (w/v); left) and corresponding immunological detection against Strep-tag II (middle) of *PstBphP2* with schematic representation of the overexpression vector pASK\_*PstBphP2* [6163 bp], encoding the phytochrome with a C-terminal Strep-tag II (blue) in a *tet* promoter-driven (green) system. The ampicillin resistance gene (purple) confers resistance to the mentioned antibiotic to bacteria carrying the plasmid. Sample application of the total cells before (bl) and after induction (al) of the gene expression. The cultures were grown over night at 17 °C after induction with 200 ng/ml AHT. Coomassie-stained SDS-PAGE gel (10 % (w/v); right) of *PstBphP2* after affinity chromatography purification (L = cell lysate, E = elution fraction, pP = purified protein) with Strep-Tactin® Sepharose® resin. The protein has a relative molecular weight of approximately 109 kDa.

(C) Coomassie-stained SDS-PAGE gel (10 % (w/v); left) and corresponding immunological detection against polyhistidine-tag (middle) of *PstBphP1* with schematic representation of the overexpression vector pET52\_*PstBphP1*-BphP1, encoding the HO *bphO* with a N-terminal Strep-tag II and the phytochrome with a C-terminal polyhistidine-tag (blue) in a T7 promoter-driven (green) system. The ampicillin resistance gene (purple) confers resistance to the mentioned antibiotic to bacteria carrying the plasmid. Sample application of the total cells before (bl) and after induction (al) of the gene expression. The cultures were grown over night at 17 °C after induction with 0.5 mM IPTG. Coomassie-stained SDS-PAGE (10 % (w/v); right) of *PstBphP1* after affinity chromatography purification (L = cell lysate, E = elution fraction, pP = purified protein) with TALON® Superflow™. The protein has a relative molecular weight of approximately 83 kDa.

Marker: Thermo Scientific™ PageRuler™ Prestained Protein Ladder

### 3.11 Heterologous expression and purification of various bacterial bathy phytochromes was successful

The bathy phytochrome genes from *A. tumefaciens*, *A. vitis* and *X. campestris* were expressed using a T7 promoter-driven C-terminal polyhistidine-tag expression system, which permits purification and detection of the encoded proteins (Fig. 3.15). In 2019, it was demonstrated that *AtBphP2*, the phytochrome of *A. tumefaciens*, lacks autokinase activity (Xue *et al.*, 2019). The main hypothesis proposed was that the C-terminally located RR (cf. Fig. 1.3B) is rapidly trans- and dephosphorylated. Therefore, the RR domain amino acid residue typically phosphorylated by the kinase was mutagenized (D783; Fig. 3.14A). As predicted, the *AtBphP2\_D783N* variant exhibited an autokinase signal. However, additional investigations contradicted the initial interpretation and revealed, through size exclusion chromatography (SEC) experiments, that

the mutation significantly impacted protein conformation. According to the hypothesis of the Lamarter laboratory, the RR module masks the conserved histidine residue in the HKD. Through the mutation, the RR domain loosens, consequently enabling access to the phosphorylation site (Xue *et al.*, 2019). To verify if this is also true for *AvBphP2*, a similar approach was conducted. Therefore, the corresponding residue was identified and exchanged: Asp 793 (Fig. 3.14C). The substitution of Asp with Asn (D793N) resulted in an unstable protein having a yellowish color, necessitating the use of an Asp-to-Ala variant (*AvBphP2\_D793A*) for further studies (Fig. 3.14A). Otero *et al.*, 2016 categorized *XccBphP* as a bathy-like phytochrome due to the absence of a pure Pfr-form under dark conditions. The construct lacking the PAS9 domain examined in their study was also employed in this research (Fig. 3.14B). The BphPs or their variants were purified via affinity chromatography and analyzed on an SDS-PAGE gel. The predominant chromatography products have a molecular weight of ~ 95 kDa (Fig. 3.15A-D; *AtBphP2*, *AvBphP2*), ~ 70 kDa (Fig. 3.15F; *XccBphP*) (Klinke *et al.*, 2014) and ~ 60 kDa (Fig. 3.15G; *XccBphP* $\Delta$ PAS9) (Otero *et al.*, 2016), consistent with the predicted molecular mass calculated from the amino acid composition. The recombinant phytochromes and the variants were purified in their holo-forms. To reach chromophore saturation, BV IX $\alpha$  was added in excess to the cell lysate after cell disruption.

The *R. tataouinensis* bathy phytochrome gene was expressed in *E. coli* Top10 using an *araBAD* promoter-driven N-terminal polyhistidine-tag expression system, enabling purification and detection of the encoded protein. The predominant chromatography product has a relative molecular weight of ~ 83 kD (Fig. 3.15 E), consistent with the predicted molecular mass calculated from the amino acid composition. The *R. tataouinensis* phytochrome was produced and purified in its holo-form by coexpressing it with the *Bradyrhizobium* sp. ORS278 HO *hmuO* encoded on the same plasmid. This HO provided the chromophore BV IX $\alpha$  in sufficient amounts.

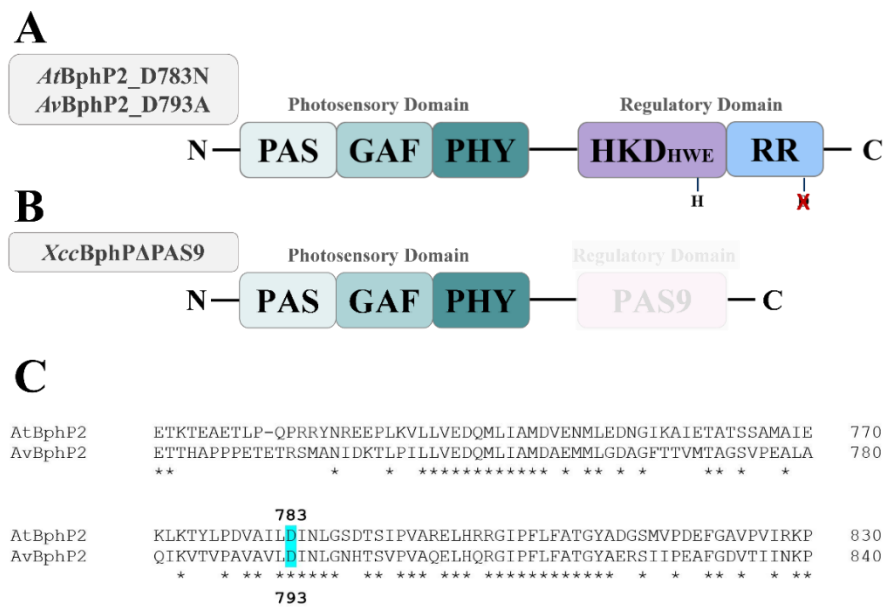


**Fig. 3.14: Domain arrangement of various bathy phytochromes and an amino acid sequence alignment of the response regulator domain region of two bacterial phytochromes.**

(A) Schematic structure of *AtBphP2* and *AvBphP2* (cf. Fig. 1.3B, C) with the substitution of the conserved Asp residue in the RR domain. This residue is typically phosphorylated by the HKD and was exchanged to generate *AtBphP2\_D783N* (Xue *et al.*, 2019) and *AvBphP2\_D793A*.

(B) Schematic structure of *XccBphP* (cf. Fig. 1.3D) without the PAS9 regulatory domain (Otero *et al.*, 2016).

(C) Section of an amino acid sequence alignment (blastp, protein-protein BLAST®) of the *A. tumefaciens* phytochrome (top) and the *A. vitis* phytochrome (bottom) response regulator domain region to find the amino acid residue corresponding to *AtBphP\_D783* in *A. vitis* (D793).



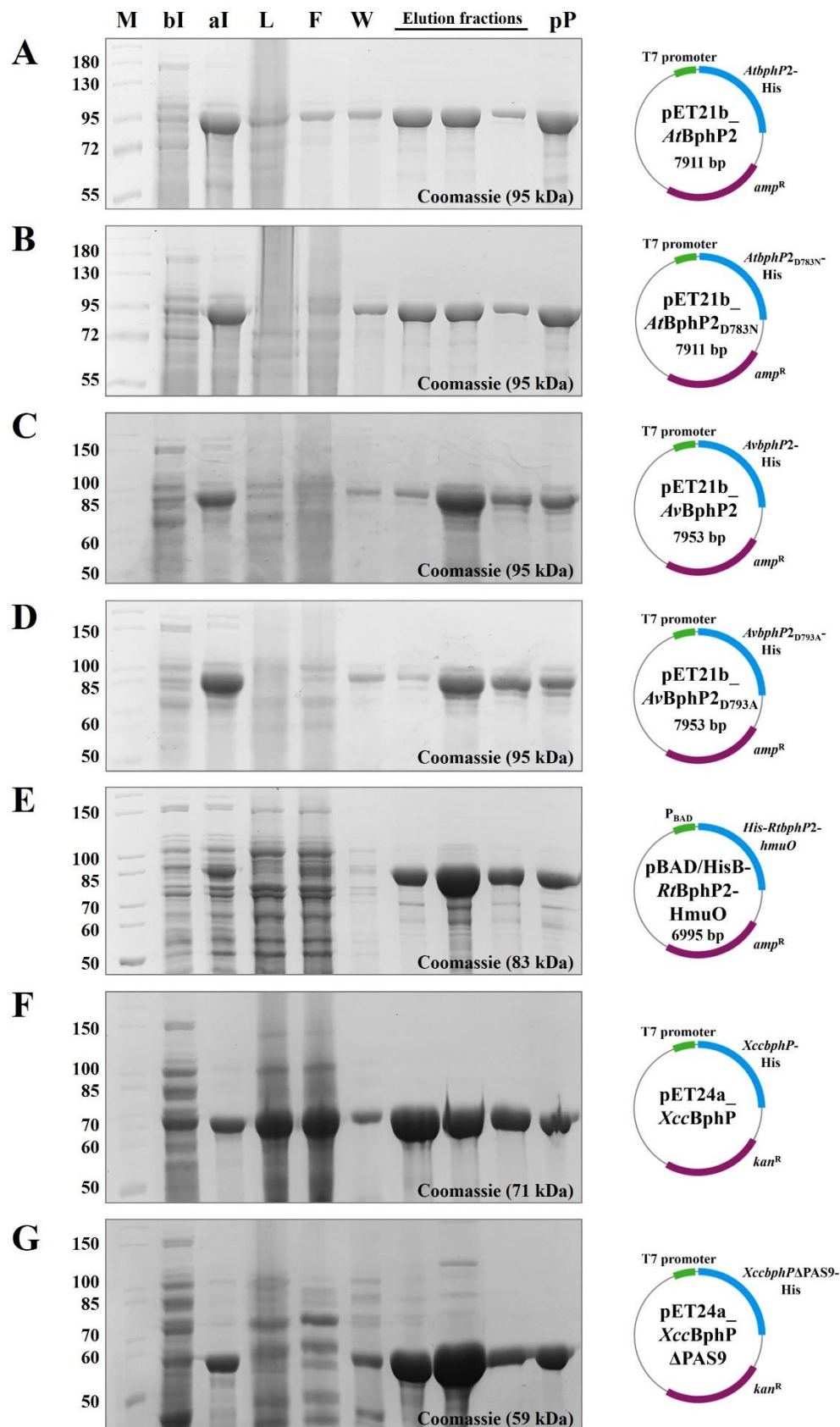


**Fig. 3.15: Homologous production of bacterial bathy phytochromes from different organisms.**

(A) Coomassie-stained SDS-PAGE gel (10% (w/v); left) of affinity chromatography purification of *AtBphP2* [95 kDa] with TALON<sup>®</sup> Superflow<sup>™</sup> (polyhistidine-tag purification) and schematic representation of the overexpression vector pET21b\_AtBphP2 [7911 bp], encoding the phytochrome with a C-terminal polyhistidine-tag (blue) in a T7 promoter-driven (green) system.

**(B)** Coomassie-stained SDS-PAGE gel (10 % (w/v); left) of affinity chromatography purification of *AtBphP2\_D783N* [95 kDa] with TALON<sup>®</sup> Superflow<sup>™</sup> (polyhistidine-tag purification) and schematic representation of the overexpression vector pET21b\_ *AtBphP2\_D783N* [7911 bp], encoding the phytochrome with a C-terminal polyhistidine-tag (blue) in a T7 promoter-driven (green) system.

**(C)** Coomassie-stained SDS-PAGE gel (10 % (w/v); left) of affinity chromatography purification of *AvBphP2* [97 kDa] with TALON<sup>®</sup> Superflow<sup>™</sup> (polyhistidine-tag purification) and schematic representation of the overexpression vector pET21b\_ *AvBphP2* [7953 bp], encoding the phytochrome with a C-terminal polyhistidine-tag (blue) in a T7 promoter-driven (green) system.

**(D)** Coomassie-stained SDS-PAGE gel (10 % (w/v); left) of affinity chromatography purification of *AvBphP2\_D793A* [97 kDa] with TALON<sup>®</sup> Superflow<sup>™</sup> (polyhistidine-tag purification) and schematic representation of the overexpression vector pET21b\_ *AvBphP2\_D793A* [7953 bp], encoding the phytochrome with a C-terminal polyhistidine-tag (blue) in a T7 promoter-driven (green) system.

**(E)** Coomassie-stained SDS-PAGE gel (10 % (w/v); left) of affinity chromatography purification of *RtBphP2* [83 kDa] with TALON<sup>®</sup> Superflow<sup>™</sup> (polyhistidine-tag purification) and schematic representation of the overexpression vector pBAD/HisB- *RtBphP2-HmuO* [6995 bp], encoding the phytochrome with a N-terminal polyhistidine-tag (blue) in an *araBAD* promoter-driven (green) system.

**(F)** Coomassie-stained SDS-PAGE gel (10 % (w/v); left) of affinity chromatography purification of *XccBphP* [71 kDa] with TALON<sup>®</sup> Superflow<sup>™</sup> (polyhistidine-tag purification) and schematic representation of the overexpression vector pET24a\_ *XccBphP*, encoding the phytochrome with a C-terminal polyhistidine-tag (blue) in a T7 promoter-driven (green) system.

**(G)** Coomassie-stained SDS-PAGE gel (10 % (w/v); left) of affinity chromatography purification of *XccBphPΔPAS9* [59 kDa] with TALON<sup>®</sup> Superflow<sup>™</sup> (polyhistidine-tag purification) and schematic representation of the overexpression vector pET24a\_ *XccBphPΔPAS9*, encoding the phytochrome with a C-terminal polyhistidine-tag (blue) in a T7 promoter-driven (green) system.

Sample application of the total cells before (bI) as well as after induction (aI) of the gene expression, cell lysate (L), flow-through fraction (F), washing fraction (W), different elution fractions, and the concentrated protein after dialysis (pP). The ampicillin or kanamycin resistance gene (purple) confers resistance to the mentioned antibiotic on bacteria carrying the plasmid.

Marker: Color Prestained Protein Standard, Broad Range, NEB (A, B); Unstained Protein Standard, Broad Range, NEB (C-G).

### 3.12 An HWE type HKD was identified in *AvBphP2*

Although all investigated BphPs share the organization of the photosensory domain, their output domains differ (cf. Fig. 1.3). BphP1 of *A. tumefaciens* as well as *P. syringae* and BphP2 of *R. tataouinensis* share their photosensory and regulatory domains entirely with *PaBphP* (De Luca *et al.*, 2019; Rottwinkel *et al.*, 2010; Shah *et al.*, 2012). *AtBphP2* and *PstBphP2* both contain a so-called HWE kinase domain. In *A. tumefaciens*, the HWE kinase domain is located downstream of the photosensory domain and precedes the attached C-terminal located RR domain. In *P. syringae*, the HWE kinase domain is arranged downstream of a typical HKD, forming the C-terminus of the phytochrome (Karniol and Vierstra, 2004). For the phytochrome of *A. vitis* it is reasonable to assume that it also has an HWE kinase domain due to its close similarity to *AtBphP2*. This hypothesis was verified by conducting multiple sequence alignment (Fig. 3.16) and using InterPro to identify the kinase domain as an HWE-like one (IPR011102; PF07536). BphP of *X. campestris* completely lacks a kinase output domain, but carries an PAS9 domain, likely involved in protein-protein interaction (Klinke *et al.*, 2014). All phytochromes with a kinase domain possess an H-box containing a conserved His residue (pink) subject to autophosphorylation, irrespective of whether they are bathy (black) or prototypic (white). The

H-box is followed by an N-box with a conserved Asn residue (pink) and up to three G-rich boxes that include conserved Gly residues (yellow). HWE kinase domains are characterized by the presence of an HWE motif (light blue) and the absence of a F-box (green). The HWE motif consists of uniquely conserved amino acid residues, including a His in the N-box and a Trp-X-Glu sequence near the G1-box (Herrou *et al.*, 2017; Karniol and Vierstra, 2004).

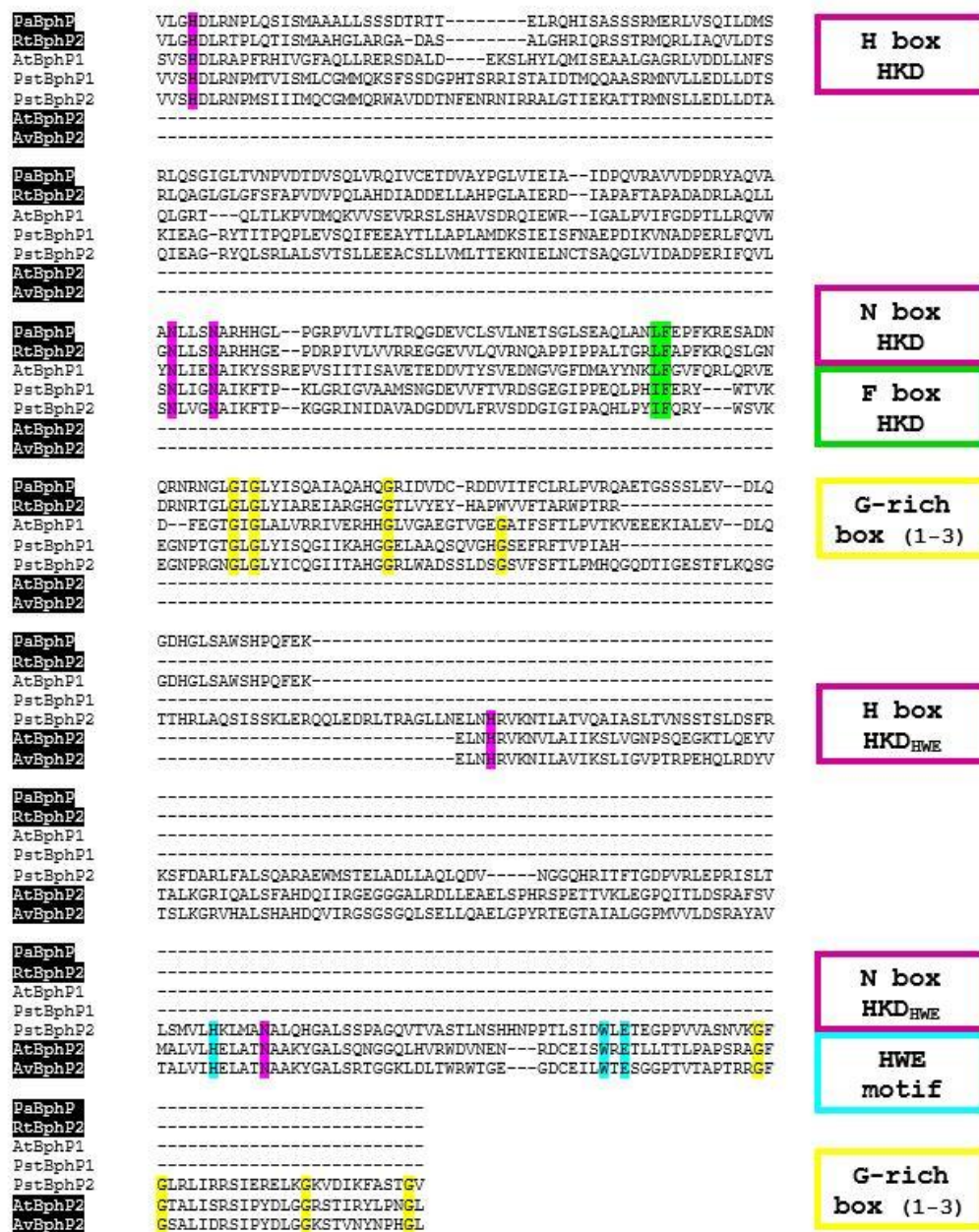


**Fig. 3.16: Amino acid sequence alignment of the kinase region of different bathy and prototypical BphPs.** Section of an amino acid sequence alignment (blastp, protein-protein BLAST®) of the kinase region of bathy phytochromes (black) *PaBphP*, *RtBphP2*, *AtBphP2* and *AvBphP2* as well as of the prototypical phytochromes (white) *AtBphP1*, *PstBphP1* and *PstBphP2*. All BphPs possess an H-box (pink; H-box HKD and HKD<sub>HWE</sub>) with a conserved His residue, an N-box (pink; N-box HKD and HKD<sub>HWE</sub>) with a conserved Asn residue and up to three G-rich boxes (yellow) with conserved Gly residues. HWE type kinase domains lack an F-box (green) with an L/I+F (Leu/Ile+Phe) motif and are characterized by an HWE (His+Trp+Glu) motif.

### 3.13 Spectral absorption properties identify *AtBphP1* as a conventional and *PstBphP1* as an unconventional prototypical phytochrome

In order to gain more insight into the role of bacterial phytochromes in these organisms, their absorption characteristics were analyzed under identical conditions and settings optimized for *PaBphP*. Regarding their absorption properties, most prototypical phytochromes adhere to the classical definition of phytochrome behavior. In particular, *AtBphP1*, the phytochrome of the plant pathogen *A. tumefaciens*, is a model for phytochrome spectral behavior (Karniol and Vierstra, 2003). Far-red light irradiation (791 nm) resulted in the photoconversion to a distinct Pr-form with  $\lambda_{\max}$  702 nm, while red light irradiation (667 nm) yielded a distinct Pfr-form with  $\lambda_{\max}$  748 nm (Fig. 3.17A; Tab. 3.2). As described for prototypical phytochromes, *AtBphP1* exhibits a pure Pr-form, without Pfr contamination in the absence of light (Tab. 3.1). In contrast to *AtBphP1*, *PstBphP1* exhibits an unusual behavior and shows no pure Pr-form (Fig. 3.17B; Tab. 3.2). It maintains residual Pfr-fractions of 27 % and 16 % under far-red light illumination or in the absence of light, respectively. Even under red light conditions *PstBphP1* failed to accumulate a pure Pfr-form. The maximum Pfr-fraction measured was set at 100 % Pfr for the calculation, despite this unconventional spectroscopic behavior. In addition to the above-described light conditions, all BphPs were investigated for their spectral behavior under exposure to blue light. The idea to study the effect of blue light arose from previous research, which showed *PaBphP* to be sensitive to it (Mukherjee *et al.*, 2019). *AtBphP1* and *PstBphP1* show mixed forms with equal Pr and Pfr fractions under blue light conditions (Tab. 3.1). The difference spectra (Fig. 3.17, gray dashed lines) demonstrate the disparities between the far-red light irradiated and red-light irradiated forms and summarize the previously mentioned findings. Since these two forms of *AtBphP1* are easily distinguishable, the difference is greater than that of *PstBphP1*, where the two forms are more similar.

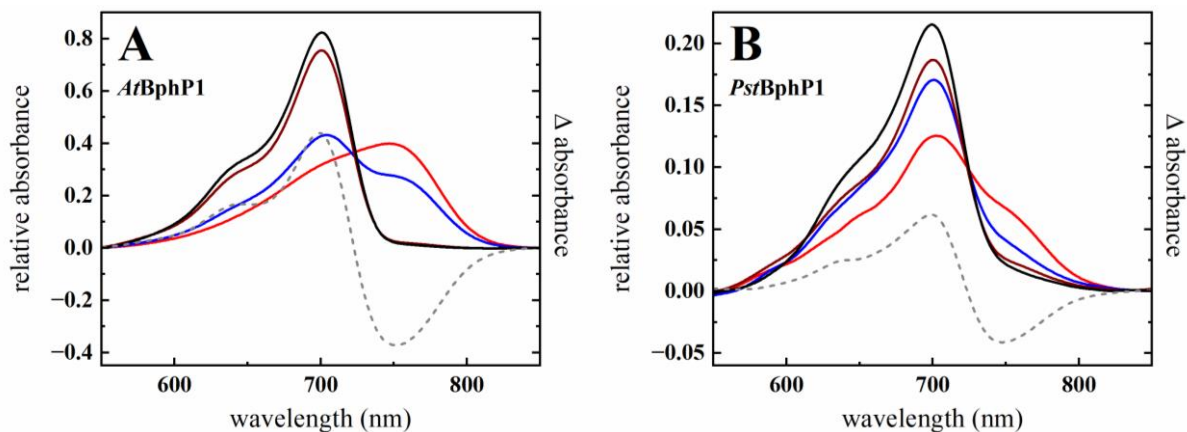


**Fig. 3.17: Spectral absorption properties of heterologously produced prototypical phytochromes from *A. tumefaciens* and *P. syringae* under different light conditions.**

Absorption spectra (mathematically smoothed with Origin, Version 2022. OriginLab Corporation, Northampton, MA, USA. “Loess, Use Proportion for Span, Span 0.1”) of *AtBphP1* (**A**) and *PstBphP1* (**B**) after illumination with far-red light (791 nm, 5 min, dark red lines), with blue light (426 nm, 5 min, blue lines), with red light (667 nm, 5 min, red lines) and after dark reversion (24 h, black lines). The extend of conversion cannot be improved by longer exposure times. All data were generated from single sets of measurements (excepted *PstBphP1* dark, black line). BV IX $\alpha$  was added in excess after cell lysis prior to purification. Manually calculated difference spectra (far-red irradiated minus red irradiated form; mathematically smoothed) were integrated into the graphs (gray dashed lines).

### 3.14 The spectral absorption properties of *PaBphP* are widespread among the bathy type phytochromes

In contrast to most prototypical phytochromes, which show a distinct Pfr-form when exposed to red light, the bathy *PaBphP* does not exhibit a pure Pfr-form, independent of the quality and intensity of incident red light (cf. Fig. 3.4A). The spectrum shows the same amount of Pr and Pfr fractions (Fig. 3.18A). A pure Pfr-form is only present in complete darkness, during the light-independent dark reversion. The study conducted by Rottwinkel *et al.*, 2010 provided initial indications that the spectral patterns of the phytochromes in the Alphaproteobacteria *A. tumefaciens* and *A. vitis* may resemble those of *PaBphP*. The investigations appeared to be valuable, prompting the inclusion and systematic examination of additional protein variants, *RtBphP2*, and *XccBphP*, to determine their prevalence among bathy type BphPs (Fig. 3.18; Tab. 3.1). Far-red irradiation (791 nm) results in the photoconversion of all tested bathy phytochromes into a pure Pr-species. The Pr-form of *RtBphP2* displays a  $\lambda_{\max}$  684 nm and very broad spectrum with an unusually low amplitude (Fig. 3.18B; Tab. 3.1). Regarding the two bathy phytochromes from *Agrobacterium* and *Allorhizobium*, the wildtype protein and variants lacking the phosphor-acceptor aspartate within the receiver domain were employed. Illumination of *AtBphP2*, *AtBphP2\_D783N*, *AvBphP2* and *AvBphP2\_D793A* with far-red light yields spectral forms that closely resemble each other, with minimal absorption at 750 nm (Fig. 3.18C-F; Tab. 3.1) and Pr  $\lambda_{\max}$  between 698 and 702 nm (Tab. 3.2). The far-red light adapted

forms of *XccBphP* and *XccBphP* $\Delta$ PAS9 are most similar to the Pr-form of *PaBphP*, in showing no absorption at 750 nm (Fig. 3.18G, H; Tab. 3.1). However, the Pr  $\lambda_{\max}$  of the *X. campestris* phytochrome is shifted to a shorter wavelength (686 nm) in comparison to *PaBphP* (Tab. 3.2). Based on the spectra of the respective pure forms of Pr and Pfr, the Pr/Pfr-fractions were determined spectroscopically for each phytochrome (cf. chapter 2.6.11; Tab. S2). Contrary to the pronounced Pr-forms, illumination with red and blue light consistently results in a mixture of Pr/Pfr-forms (Tab. 3.1). Observed differences in Pr/Pfr-fractions among various phytochromes exposed to identical illumination conditions can be attributed to changes specific to each phytochrome. The involved parameters are the  $\lambda_{\max}$  of Pr and Pfr in the Soret- and Q-band regions, their corresponding extinction coefficients and photoisomerization quantum yields as well as rates of dark reversion. Only incubation in darkness led to the highest level of Pfr-form in all bathy phytochromes, thus distinguishing them from prototypical BphPs that exhibit the highest Pfr-form quantity under red light exposure. However, *XccBphP* and *AvBphP2*, along with its protein variant *AvBphP2\_D793A*, accumulates hardly any pure Pfr-state (Fig. 3.18E-G). This is in slight contrast to the *AvBphP2* published spectra, which show a higher accumulation of the Pfr-form when incubated in the dark (Rottwinkel *et al.*, 2010). Despite this unconventional spectroscopic behavior, the maximum Pfr-fraction measured was set at 100 % Pfr for the calculation (cf. chapter 3.13, *PstBphP1*). The *XccBphP* truncated version lacking the PAS9 output domain behaves like a typical bathy phytochrome and keeps a steady state in the homogeneous Pfr-form (Fig. 3.18H). In the wildtype variant of *XccBphP*, the PAS9 domain seems to interfere with chromophore binding and the thermodynamics of dark reversion (Otero *et al.*, 2016). The difference spectra (Fig. 3.18, gray dashed lines) show the disparities between the far-red light irradiated and red-light irradiated forms and summarize the previously mentioned findings. The shifts of the Pr and Pfr  $\lambda_{\max}$  values (Tab. 3.2) are also clearly visible in the difference spectra. In summary, all five phytochromes and their variants exhibit the development of a Pr-form after exposure to far-red light, a Pfr-(enriched) form after incubation in the dark and mix forms with different Pr/Pfr-fractions in response to blue or red light.

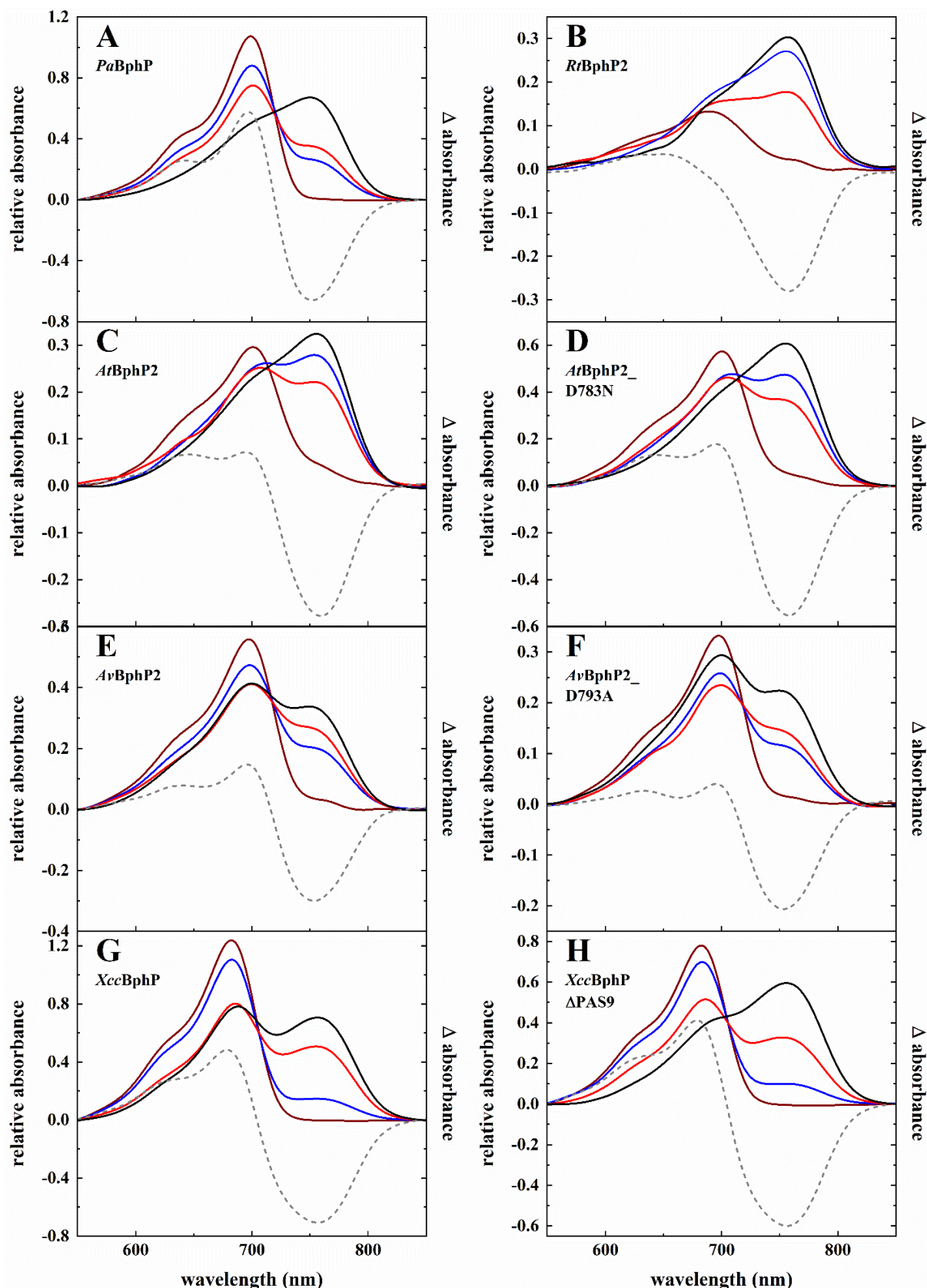


**Fig. 3.18: Spectral absorption properties of heterologously produced bathy phytochromes from *P. aeruginosa*, *R. tataouinensis*, *A. tumefaciens*, *A. vitis* and *X. campestris* under different light conditions.** Absorption spectra (mathematically smoothed with Origin, Version 2022. OriginLab Corporation, Northampton, MA, USA. “Loess, Use Proportion for Span, Span 0.1”) of *PaBphP* (A), *RtBphP2* (B), *AtBphP2* (C), *AtBphP2\_D783N* (D), *AvBphP2* (E), *AvBphP2\_D793A* (F), *XccBphP* (G) and *XccBphPΔPAS9* (H) after illumination with far-red light (791 nm, 5 min, dark red lines), with blue light (426 nm, 5 min [C-H], 10 min [A,

B], blue lines), with red light (667 nm, 5 min [B-H], 10 min [A], red lines) and after dark reversion (24 h [A, E, F], 1 h [B-D], 96 h [G-H], black lines). The extent of conversion cannot be improved by longer exposure times. The data always originate from single sets of measurements (except for *AvBphP2\_D793A* dark, black line). BV IX $\alpha$  was added in excess after cell lysis prior to purification (except for *RtBphP2*, coexpression with HO *hmuO*). Manually calculated difference spectra (far-red irradiated minus dark incubated form; mathematically smoothed) were integrated into the graphs (gray dashed lines).

**Tab. 3.1:** Pr/Pfr-fractions of recombinant purified bacterial phytochromes from *P. aeruginosa*, *R. tataouinensis*, *A. tumefaciens*, *A. vitis*, *X. campestris*, *P. syringae* and various variants of the proteins under dark, red light, blue light, or far-red light conditions. The dashed line separates the bathy (top) and the prototypical (bottom) BphPs. A calculation error of  $\pm 5\%$  (for *AtBphP2* and the variant  $\pm 8\%$ ) applies.

$\pm 5/8\%$	Pfr (%)	Pr (%)	Pfr (%)	Pr (%)	Pfr (%)	Pr (%)	Pfr (%)	Pr (%)
	dark		red light (667 nm)		blue light (426 nm)		far-red light (791 nm)	
<i>PaBphP</i>	100	0	50	50	33	67	0	100
<i>PaBphP_D194H*</i>	12	88	11	89	n.d.	n.d.	2	98
<i>PaBphP_S261A*</i>	96	4	94	6	n.d.	n.d.	93	7
<i>RtBphP2</i>	100	0	53	47	83	17	2	98
<i>AtBphP2</i>	100	0	66	34	81	19	4	96
<i>AtBphP2_D783N</i>	97	3	57	43	72	28	0	100
<i>AvBphP2</i>	97	3	81	19	56	44	1	99
<i>AvBphP2_D793A</i>	92	8	78	22	60	40	0	100
<i>XccBphP</i>	72	28	56	44	13	87	0	100
<i>XccBphP<math>\Delta</math>PAS9</i>	96	4	57	43	16	84	0	100
<i>AtBphP1</i>	0	100	98	2	69	31	1	99
<i>PstBphP1</i>	16	84	92	8	47	53	27	73

\*irradiation with interference filters (red 690 $\pm$ 10 nm, far-red 750 $\pm$ 5 nm); n.d. = not determined

$\Delta\alpha = \alpha * 0.01 + (1-\alpha) * 0.05$  or  $\Delta\alpha = \alpha * 0.01 + (1-\alpha) * 0.08$  for *AtBphP2* and *AtBphP2\_D783N*

**Tab. 3.2:** Summary of the maximum absorption wavelength of the respective Pr- as well as Pfr-forms (Soret and Q bands) and the approximate time points when half of the molecules of a bathy phytochrome population (= DR  $t_{1/2}$ ) of *P. aeruginosa*, *R. tataouinensis*, *A. tumefaciens*, *A. vitis*, *X. campestris* and various variants of the proteins are in their inactive Pfr-form or half of the molecules of a prototypical phytochrome population (= DR  $t_{1/2}$ ) of *A. tumefaciens* and *P. syringae* are in their inactive Pr-form. The dashed line separates the bathy (top) and the prototypical (bottom) BphPs.

Phytochrome	Pfr $\lambda_{max}$ (Soret / Q band)	Pr $\lambda_{max}$ (Soret / Q band)	DR $t_{1/2}$
<i>PaBphP</i>	410 / 752 nm	398 / 702 nm	15 min
<i>PaBphP_D194H</i>	394 / 699 nm	394 / 699 nm	n.d.
<i>PaBphP_S261A</i>	400 / 750 nm	400 / 749 nm	n.d.
<i>RtBphP2</i>	405 / 757 nm	390 / 684 nm	1-2 min
<i>AtBphP2</i>	407 / 753 nm	394 / 702 nm	< 5 s
<i>AtBphP2_D783N</i>	413 / 756 nm	394 / 701 nm	< 5 s
<i>AvBphP2</i>	395 / 748 nm	388 / 698 nm	5 min
<i>AvBphP_D793A</i>	388 / 751 nm	387 / 698 nm	n.d.
<i>XccBphP</i>	407 / 754 nm	392 / 686 nm	3-4 h*
<i>XccBphP<math>\Delta</math>PAS9</i>	414 / 754 nm	392 / 686 nm	50 min
<i>AtBphP1</i>	406 / 748 nm	394 / 702 nm	20-30 min
<i>PstBphP1</i>	396 nm / n.d.	394 / 700 nm	5 min**

\**XccBphP* reached a maximum of 78 % Pfr; \*\**PstBphP1* reached a maximum of 84 % Pr; n.d. = not determined



### 3.15 The autokinase activity of bathy and prototypical BphPs differs – but still shares similarities

All bathy phytochromes examined in this study share the formation of a well-defined Pr-form in response to far-red light and accumulation of a pure Pfr- or Pfr-enriched form in the absence of light. To assess whether the correlation between the absorbing form and autokinase activity in *Pa*BphP remains consistent among bathy phytochromes, the autophosphorylation activity of *At*BphP2\_D783N, *Av*BphP2\_D793A and *Rt*BphP2 was evaluated (Fig. 3.19). All of them show a consistent decrease in autokinase activity when light is absent. Although these proteins display comparable autophosphorylation signals under far-red, blue, and red light, their calculated Pr/Pfr-fractions differ. Therefore, establishing a direct correlation between autokinase and Pr-fraction is not as straightforward as for *Pa*BphP (cf. Fig. 3.4E). However, it is proposed that the level of active kinase in a particular phytochrome can be determined from the spectrally derived Pr/Pfr-fraction, given that the Pr-form alone has autokinase activity (Tab. 3.1).

Moreover, the autokinase activity of the protein variants lacking their phosphor-accepting aspartate (*At*BphP2\_D783N, *Av*BphP2\_D793A) was compared to that of their respective wild type versions. *At*BphP2 does not undergo autophosphorylation (Fig. 3.20A), consistent with the findings of Xue *et al.*, 2019 (cf. chapter 3.11). In comparison to *At*BphP2, the impact of the amino acid exchange in *Av*BphP2 is less evident. *Av*BphP2 exhibits a clear signal under far-red light conditions, a weaker one when exposed to blue light and almost no signal in red light or darkness (Fig. 3.20B). These data are consistent with the measured UV/Vis spectra (Fig. 3.18E) and Pr/Pfr-fractions calculation (Tab. 3.1). Nevertheless, it is worth noting that the signal observed is most likely the result of transphosphorylation rather than pure autokinase activity. Since the phosphor-accepting amino acid residue in the response regulator domain is not substituted, a rapid transfer of the phosphoryl group from the His residue in the HKD to the Asp residue in the RR domain is facilitated.

All of the prototypical phytochromes analyzed in this study exhibit a distinct Pr-form under far-red light conditions and accumulate a pure Pfr- or Pfr-enriched form in response to red light. To gain further understanding into phytochrome activity in general, the prototypical phytochromes *At*BphP1 and *Pst*BphP1 were assessed for their autokinase activity. For *At*BphP1 it was not possible to identify a protein conformation (Pr or Pfr) lacking autokinase activity (Fig. 3.21A). In the absence of light, the signal on the radiogram was strongest. However, clear signals were also detected under far-red, blue and red light conditions, albeit with lower intensity. Despite the unusual absorption spectra, clearer results for the kinase activity of *Pst*BphP1 can be identified (Fig. 3.21B). *Pst*BphP1 materialize different levels of

phosphorylation depending on the incoming light and the resulting protein conformation. The protein exhibits the highest level of phosphorylation in the Pfr-enriched form when exposed to red light. Although weaker phosphorylation signals were detected under blue light conditions, the phytochrome remains partially active. The Pr-form, as the dark-adapted state and existing in far-red light, does not undergo autophosphorylation, thus being inactive.

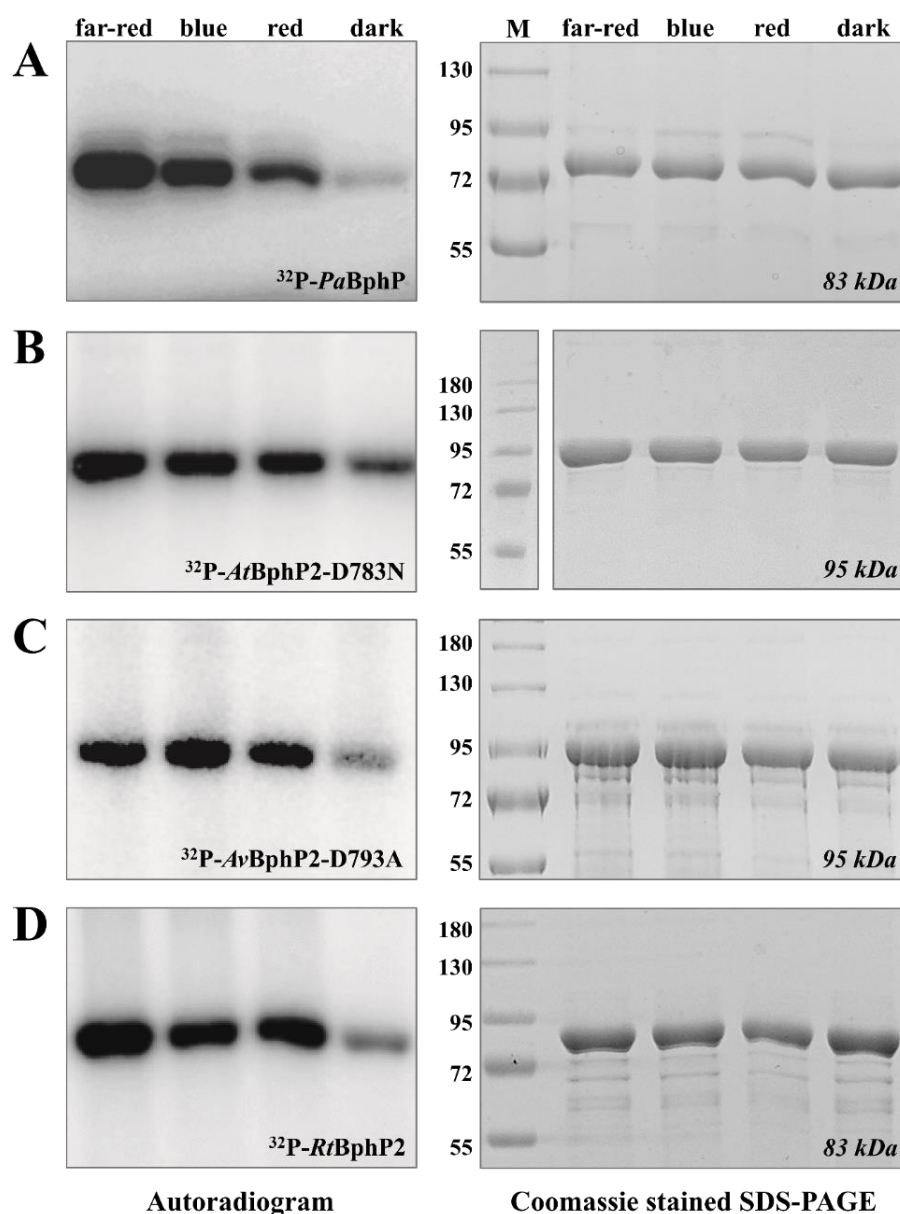


**Fig. 3.19: Autokinase activity of heterologously produced *PaBphP*, *AtBphP2\_D783N*, *AvBphP2\_D793A* and *RtbphP2* under different light conditions.**

Autoradiogram (left) and corresponding Coomassie-stained SDS-PAGE gel (10 % (w/v), right) after *in vitro* radiolabeling of *PaBphP* (A), *AtBphP2\_D783N* (B), *AvBphP2\_D793A* (C) and *RtbphP2* (D) with [ $\gamma$ -<sup>32</sup>P]-ATP under far-red (791 nm), blue (426 nm) and red (667 nm) light as well as dark conditions. The autophosphorylation reaction was terminated after 5 min and samples were separated by gel electrophoresis. Proteins were pre-irradiated with the respective light for 5 min or incubated dark overnight before adding the radiolabeled ATP. *PaBphP* has a relative molecular weight of approximately 83 kDa, *AtBphP2\_D783N* and *AvBphP2\_D793A* of 95 kDa and *RtbphP2* of 83 kDa (marker: Color Prestained Protein Standard, Broad Range, NEB).

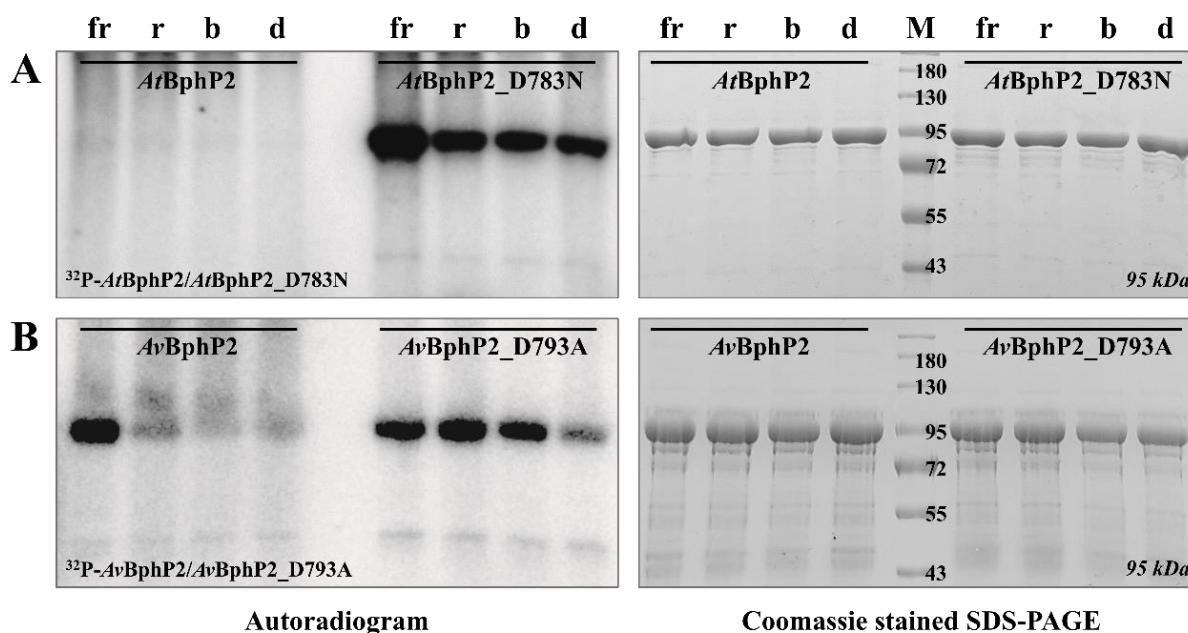


**Fig. 3.20: Autokinase activity of heterologously produced *AtBphP2*, *AtBphP2\_D783N*, *AvBphP2* and *AvBphP2\_D793A* under different light conditions.**

Autoradiogram (left) and corresponding Coomassie-stained SDS-PAGE gel (10 % (w/v), right) after *in vitro* radiolabeling of *AtBphP2* and *AtBphP2\_D783N* (A) as well as *AvBphP2* and *AvBphP2\_D793A* (B) with [ $\gamma$ - $^{32}$ P]-ATP under far-red (791 nm), blue (426 nm) and red (667 nm) light as well as dark conditions. The autophosphorylation reaction was terminated after 5 min and samples were separated by gel electrophoresis. Proteins were pre-irradiated with the respective light for 5 min or incubated dark overnight before adding the radiolabeled ATP. The proteins have a relative molecular weight of approximately 95 kDa (marker: Color Prestained Protein Standard, Broad Range, NEB).

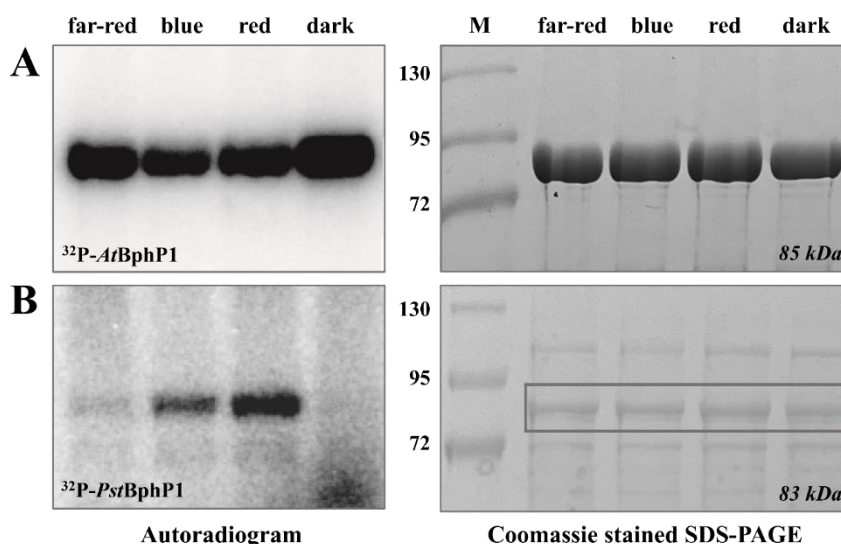


**Fig. 3.21: Autokinase activity of heterologously produced *AtBphP1* and *PstBphP1* under different light conditions.**

Autoradiogram (left) and corresponding Coomassie-stained SDS-PAGE gel (10 % (w/v), right) after *in vitro* radiolabeling of *AtBphP1* (A) and *PstBphP1* (B) with [ $\gamma$ - $^{32}$ P]-ATP under far-red (791 nm), blue (426 nm) and red (667 nm) light as well as dark conditions. The autophosphorylation reaction was terminated after 5 min (A) or 10 min (B) and samples were separated by gel electrophoresis. Proteins were pre-irradiated with the respective light for 5 min or incubated dark overnight before adding the radiolabeled ATP. *AtBphP1* has a relative molecular weight of approximately 85 kDa and *PstBphP1* of 83 kDa (marker: Color Prestained Protein Standard, Broad Range, NEB).

### 3.16 Dark reversion rates of various bathy and prototypical BphPs differ

In addition to light-induced photoconversion, phytochromes also undergo a light-independent dark reversion process (Taylor, 1968). This process affects the level of physiologically active or inactive phytochromes within the bacterial cell and results in the accumulation of the Pfr-form in bathy phytochromes and the Pr-form in prototypical phytochromes. To compare the DR rates of different phytochromes, pure Pr-forms were generated by irradiating all bathy BphPs with far-red light and pure Pfr-forms were generated by exposing all prototypical BphP to red light. Absorption spectroscopy was used to track the subsequent dark adaptation for 24 h (*PaBphP*, *AtBphP2*, *AtBphP2\_D793N*, *AvBphP2*, *RtBphP2*, *AtBphP1*, *PstBphP1*) or for 96 h (*XccBphP* and *XccBphPΔPAS9*). The Pr/Pfr-fractions were calculated for every time point (Fig. 3.22). *AtBphP2* (turquoise line) and the corresponding *AtBphP2\_D793N* variant (orange line) exhibits the fastest DR with a half-life of less than 5 s, supporting the findings of Piatkevich *et al.*, 2013. This proves that the altered amino acid residue has no impact on DR processing (Tab. 3.2). Moreover, the Pr-states of *RtBphP2* (green line) and *AvBphP2* (pink line) are also highly unstable and promptly adopt the Pfr-form in the absence of light, achieving 50 % Pfr in about 1-2 min or 5 min, respectively. In comparison, the relaxation rate of *PaBphP* (black line), with DR  $t_{1/2}$  of approximately 15 min, is slower than that of the other phytochromes. The DR rate of *XccBphP* (burgundy line) and its truncated version *XccBphPΔPAS9* (gray line) is very slow, albeit the formation of the Pfr-state is accelerated for the truncated version. According to Otero *et al.*, 2016, the PAS9 output domain modulates the chromophore during its dark adaptation kinetics. *XccBphPΔPAS9* has a ground state formation half-life of approximately 50 min, whereas the DR process of *XccBphP* requires 3-4 h to reach 50 % Pfr and attains a maximum of 78 % after 96 h dark incubation. The DR dynamics of the prototypical *PstBphP1* (purple line) closely resembles those of *AvBphP2*, with DR  $t_{1/2}$  of about 5 min. However, it can only achieve a maximum of 84 % Pfr. The second phytochrome in *A. tumefaciens*, the prototypical *AtBphP1* (light blue line), displays a slower DR rate compared to its bathy BphP counterpart. Its half-life is around 20-30 min, which is slower than the most phytochromes from both types.

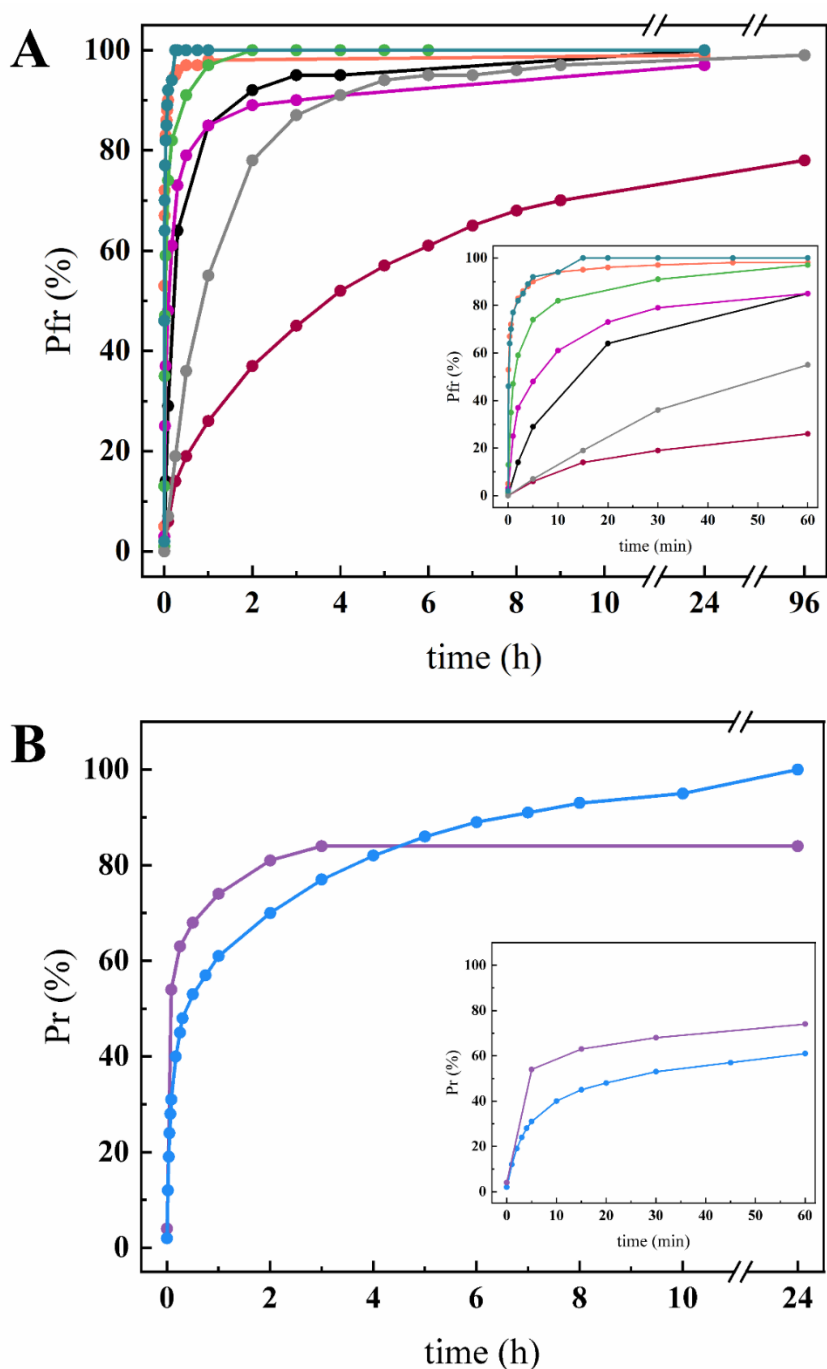


**Fig. 3.22: Kinetics of dark reversion of different bathy and prototypical phytochromes.**

(A) Sufficient far-red irradiation to allow formation of Pr-form preceded the incubation in darkness. Pr-to-Pfr conversion was monitored for a period of 24 h (*AtBphP2*, turquoise line; *AtBphP2\_D793N*, orange line; *RtBphP2*, green line; *AvBphP2*, pink line; *PaBphP*, black line) or 96 h (*XccBphP*, burgundy line; *XccBphPΔPAS9*, gray line) and the kinetics were plotted in a line chart.

(B) Sufficient red irradiation in sufficient time to allow formation of Pfr-form preceded the incubation in darkness. Pfr-to-Pr conversion was monitored for a period of 24 h (*PstBphP1*, purple line; *AtBphP1*, light blue line) and the kinetics were plotted in a line chart.

Insets: dark reversion up to 60 min; calculated half-life times (50 % BphPs in Pfr- or Pr-form) in Tab. 3.2

## 4 Discussion

### **Part 1 – Understanding the function of the phytochrome in the heterotrophic bacterium *Pseudomonas aeruginosa***

Light plays a multifaceted and crucial role for countless living organisms across all kingdoms. Heterotrophic bacteria, such as *P. aeruginosa*, do not require light as a source of energy, but rather prioritize estimating the wavelength of incoming light and converting it into cellular signals (Kottke *et al.*, 2018). Genome analysis has identified the bacterial phytochrome *PaBphP* as the only light receptor currently found in the human opportunistic pathogen *P. aeruginosa*. Since the function of the far-red/red light sensor in this nosocomial bacterium remains largely unknown, the present study aims to clarify its physiological role. Therefore, the results need to be placed into the complex network of biofilm formation, virulence factor secretion, and motility. Consistent with the mechanism of most other bacterial phytochromes, *PaBphP* acts as a light-triggered histidine kinase within a TCS (Bhoo *et al.*, 2001). This study offers insights into the biochemical and spectroscopic behavior, as well as into the autokinase activity of *PaBphP*, along with its recently identified RR *PaAlgB* (Mukherjee *et al.*, 2019).

#### **4.1 The bacterial phytochrome *PaBphP* – An unorthodox far-red/red light sensor or the reevaluation of a traditional pattern?**

Conducting research on *P. aeruginosa* is of immense importance due to its high clinical relevance as a human pathogen (Botelho *et al.*, 2019; Diggle and Whiteley, 2020). Furthermore, this pathogenic organism is one of the first heterotrophic bacteria that has been identified to possess a phytochrome (Bhoo *et al.*, 2001; Davis *et al.*, 1999). As previously hinted, the present study reinforces the conception that *PaBphP* functions as a light sensor, exhibiting light-dependent kinase activity. However, the earlier work has not demonstrated a significant difference in autokinase activity between far-red and red light conditions (Tasler *et al.*, 2005). Later, it was discovered that at least under dark conditions the autophosphorylation activity of the bathy *PaBphP* is remarkably decreased (Mukherjee *et al.*, 2019; Yang *et al.*, 2011). Additionally, only insufficient research has been hitherto conducted on the autokinase activity of bathy BphPs, and, thus, no protein conformation has been conclusively identified as inactive. In contrast, many prototypical phytochromes have a well-defined active or inactive state based on the exposure to far-red or red light, respectively (Giraud *et al.*, 2005; Multamäki *et al.*, 2021; Scheerer *et al.*, 2010; Xue *et al.*, 2019). To identify the triggers of autokinase activity in bathy BphPs, it is imperative to analyze the spectral behavior of *PaBphP* thoroughly. Employing UV-

Vis spectroscopy, it becomes evident that the *P. aeruginosa* phytochrome behaves atypically. While most prototypical phytochromes behave consistently to the classical taxonomy, displaying a Pr-form ( $\lambda_{\max}$  700 nm) under far-red light and a Pfr-form ( $\lambda_{\max}$  750 nm) under red light conditions, this pattern is not observed for *PaBphP* (Fig. 4.1) (Bhoo *et al.*, 2001; Scheerer *et al.*, 2010; Tasler *et al.*, 2005). Although this bathy BphP also exhibits a distinct Pr-form in response to far-red light, exposure to red light, regardless of the intensity or quality, exclusively produces a Pfr-enriched form with equal fractions of Pr and Pfr. Finally, a pure Pfr-form can only be achieved under complete dark conditions.

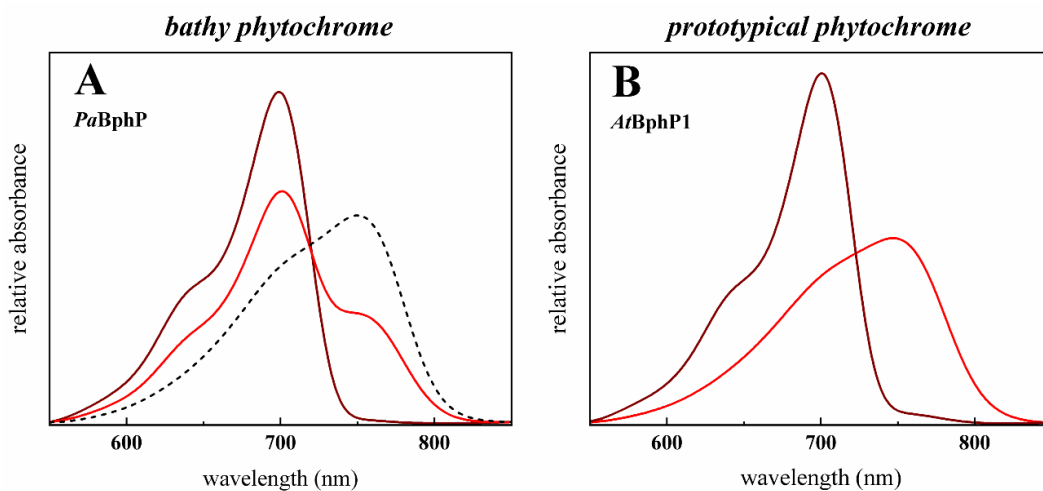


**Fig. 4.1: Comparative overview of spectral behavior of the bathy phytochrome *PaBphP* and *AtBphP1*, representative of most prototypical phytochromes.**

(A) Bathy *PaBphP* under far-red light (dark red line), red light (red line) and dark conditions (black dashed line) in its Pr-, Pfr-enriched and pure Pfr-form, respectively.

(B) Prototypical *AtBphP1* under far-red light (dark red line) and red light (red line) conditions, in its pure Pr- and Pfr-form, respectively.

This study provides proof of a direct correlation between *PaBphP* Pr-form, dominating under far-red light, and the highest level of kinase activity. Contrary to Mukherjee's results, which indicate constant activity under all light conditions, this work reveals a variation in the autophosphorylation levels. With decreasing Pr-fractions of *PaBphP* exposed to blue or red light, the level of kinase activity decreases equally. Only darkness leads to the pure Pfr-form, interrelated with the lowest autokinase activity. The identical autophosphorylation behavior was demonstrated for locked variants of the phytochrome that are insensitive to external light exposure. The Pr-locked variant, with a clearly blocked dark reversion, exhibited kinase activity, whereas the Pfr-locked variant, with inhibited photoconversion, was kinase inactive. Based on these findings, a model was established which defines *PaBphP* as a molecular regulator. Rather than acting as a typical on/off switch, it gives *P. aeruginosa* the ability to fine-

tune its cellular response in relation to the incoming light wavelength and the resulting Pr/Pfr-fractions (Fig. 4.2).

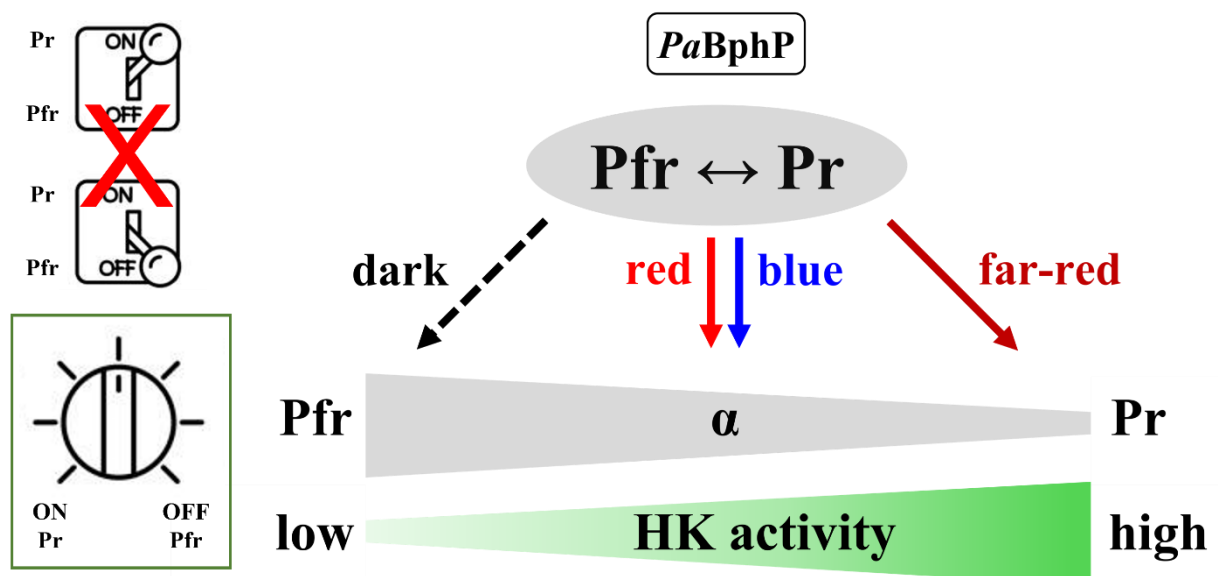


**Fig. 4.2: *PaBphP* acts as a molecular light switch to adjust its histidine kinase (HK) activity.**

The phytochrome *PaBphP* functions as a switch that regulates the autokinase output in the bacterial cells. It is not a simple on/off system, but rather adjusts HK activity as Pr-fractions increase (=  $\alpha$  decreases) and Pfr-fractions decrease (=  $\alpha$  increases). Far-red light is associated with the highest Pr-fractions, lowest  $\alpha$ , and highest HK activity. Dark conditions are associated with the lowest Pfr-fractions, highest  $\alpha$ , and lowest HK activity. Blue and red light exhibit a mix of Pr/Pfr-fractions and reduced HK activity when compared to far-red light conditions or enhanced HK activity when compared to dark conditions. In a *PaBphP* population, exposure to blue light generally yields higher Pr-fractions than exposure to red light. The  $\alpha$  value defines the fraction of Pfr available in a phytochrome population ( $\alpha = [P_{fr}]/([P_{fr}] + [P_r])$ ).

#### 4.2 The reaction of the far-red/red light sensor *PaBphP* to blue light – A special feature or biophysically explainable?

What seems peculiar at first can be comprehensively elucidated with the absorption bands of the phytochrome chromophores (Fig. 4.3). In addition to the typical Q band defining Pr ( $\lambda_{\max}$  700 nm) and Pfr ( $\lambda_{\max}$  750 nm), phytochromes exhibit a protein band and a Soret band (Eilfeld and Rüdiger, 1985; Gouterman, 1961). The Soret band characterizes molecules with a conjugated  $\pi$ -system, such as the phytochrome chromophores, being tetrapyrrole molecules. Due to the position of this Soret band at around 400 nm, blue light is able to stimulate *PaBphP*, thereby triggering a spectroscopic response and causing a modification in the Pr/Pfr fractions. Thus, blue light is also implicated in regulating the autokinase output (Fig. 4.2). This principle also applies to other (bacterial) phytochromes. Therefore, spectral, and phenotypical behavior of various bacteria under blue light is occasionally reviewed in the literature (Hatfield *et al.*, 2023; Mukherjee *et al.*, 2019; Wu *et al.*, 2013).



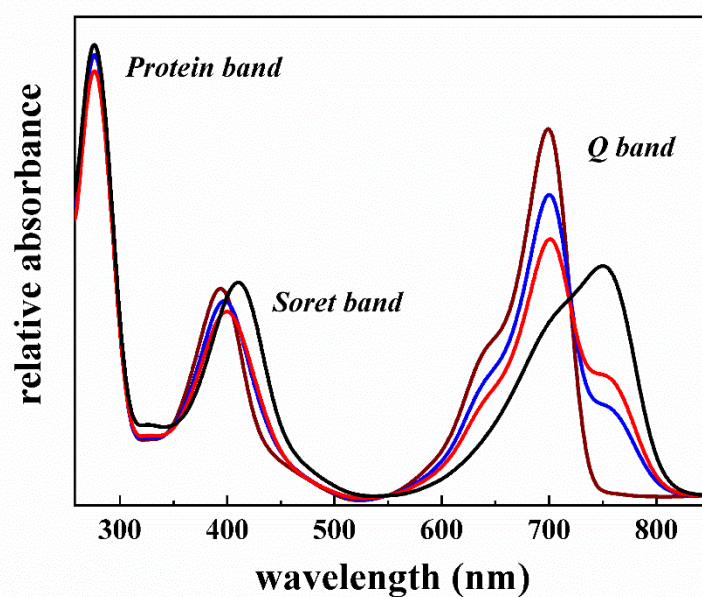


**Fig. 4.3: Three prominent absorption bands of phytochromes shown by the example of *PaBphP*.**

Three distinct bands are visible in the conformations of *PaBphP* under far-red (dark red line), blue (blue line), red (red line) light and dark conditions. The absorption of aromatic amino acids results in the protein band (~ 280 nm). The Soret band (~ 400 nm) and the Q band (~ 700 nm) are characteristic of tetrapyrroles. Compared to the Pr-form, the Pfr-form is red-shifted in the Soret and Q band (~ 50 nm).

#### 4.3 The phytochrome has the ability to form a photoconvertible holo-protein with different BV isomers – *PaBphP* a promiscuous light receptor?

*P. aeruginosa* was the first organism discovered to possess the genetic information for two active HOs, each able of cleaving heme with different regiospecificity yielding different BV isomers. Although both HOs are responsible for the oxidation of heme, they have distinct functions within the opportunistic pathogen. First discovered was HemO (synonym PigA), a HO that produces the unusual BV isomers BV IX $\beta$  and BVIX $\delta$  (Ratliff *et al.*, 2001; Wegele *et al.*, 2004). Since pathogenic organisms require iron to successfully infect host cells and the bioavailability in the environment is exceedingly limited, they develop several effective iron scavenging strategies (Josts *et al.*, 2019; Vasil and Ochsner, 1999). Therefore, the gene for HemO is expressed under iron-limiting conditions for mining the heme-iron by targeting the  $\beta$ - and  $\delta$ -meso carbons of heme (Ratliff *et al.*, 2001). Compared to  $\alpha$ -hydroxylating HOs found in other pathogenic organisms with the major function of extracting the heme-iron, the  $\beta/\delta$ -target site of HemO is atypical (Ratliff *et al.*, 2001; Rivera and Zeng, 2005; Wegele *et al.*, 2004). The production of BV IX $\alpha$  in *P. aeruginosa* is primarily assigned to its second HO BphO, commonly known as the “classical” pathway (Tasler *et al.*, 2005; Wegele *et al.*, 2004). The specific biological reason for the BV IX $\beta/\delta$  production is not completely clear. It is possible that BV IX $\beta$  and/or BV IX $\delta$  transcriptionally or post-transcriptionally regulates the hemophore HasA because its extracellular level is decreased when both BV isomers are absent. HasA is

usually secreted by *P. aeruginosa* to scavenge heme from their host and bring it back to the bacteria (Mouriño *et al.*, 2016). An additional hypothesis posits for a functional separation in heme oxidation pathways: the production of HemO is increased to regulate iron homeostasis whereas BphO is produced in the early stationary phase to provide the chromophore for *PaBphP* (Barkovits *et al.*, 2008; Ratliff *et al.*, 2001; Tasler *et al.*, 2005; Wegele *et al.*, 2004). Nevertheless, in addition to BV IX $\alpha$ , at least one of the HemO products (BV IX $\delta$ ) is a possible chromophore for *PaBphP*, allowing the formation of a photoconvertible holo-phytochrome (cf. Fig. 3.1) (Tasler *et al.*, 2005; Wegele *et al.*, 2004). In agreement with existing literature (Wegele *et al.*, 2004), the data of this study demonstrate that the affinity of BV IX $\delta$  to *PaBphP* is lower than the one of the natural chromophore, resulting in a holo-phytochrome complex of *PaBphP*:BVIX $\delta$  only one-fifth of the *PaBphP*:BV IX $\alpha$  complex. Covalent binding to the conserved cysteine residue located in the PAS domain necessitates a C 3 vinyl side chain on the bilin A-ring (Karniol *et al.*, 2005; Lamparter *et al.*, 2003). Since BV IX $\delta$  possess this same A-ring side chain as the natural chromophore BV IX $\alpha$ , formation of a photoconvertible holo-phytochrome is possible. The incubation with BV IX $\delta$  leads to the formation of a covalent bond, proved by zinc-induced red fluorescence. Additionally, BV XIII $\alpha$  has the same side chain, enabling to form a covalent bond with Cys 12 of *PaBphP*. BV III $\alpha$ , 3,3'DHBV, as well as meso BV share a similar A-ring with BV IX $\alpha$  (cf. Fig. S5), allowing the insertion into the binding pocket without a covalent bond (similar as BV IX $\alpha$  to *PaBphP*\_C12A). All these *in vitro* formed photoconvertible holo-*PaBphP*s exhibit blue- or red-shifted Pr and Pfr  $\lambda_{\max}$  (Tasler *et al.*, 2005). Most of these BV isomers do not occur naturally or in *P. aeruginosa*, indicating that their *in vitro*-binding is without any biological function. It is possible that the covalent bond between BV IX $\delta$  and Cys 12 is solely due to its chemical similarity to BV IX $\alpha$  and has no biological role.

#### **4.4 The BphP/AlgB/KinB regulation system of *P. aeruginosa* – Part of a complex network?**

##### ***– The prolonged quest for the response regulator of the kinase PaBphP –***

The phytochrome *PaBphP* was long believed to be an orphan histidine kinase since the identity of the corresponding RR was unknown. The genomes of *Deinococcus radiodurans*, *Pseudomonas putida*, and *Rhizobium leguminosarum* comprise a tricistronic phytochrome operon (Bhoo *et al.*, 2001), whereas only the bicistronic form is found in *P. aeruginosa* (Barkovits *et al.*, 2008). Consequently, the gene for the associated RR (*bphR*) is not placed with the gene for the HO (*bphO*) and the gene for the apo-phytochrome (*bphP*), resulting in

difficulties trying to identify BphR in the opportunistic pathogen. Furthermore, the significant number of genes encoding elements of one- or two-component regulatory systems in *P. aeruginosa* hindered the elucidation of the RR. About 20 years ago, around 60-70 RRs were identified in the genome of these Gammaproteobacteria (Gooderham and Hancock, 2009; Rodrigue *et al.*, 2000; Stover *et al.*, 2000). However, almost 10 years ago, the number of putative RR had already exceeded 100 (Heine, 2014). Meanwhile, the *Pseudomonas* database (pseudomonas.com), which is constantly updated, lists more than 180 described and postulated “signal transduction response regulator (receiver domain)”. Despite these challenges, *PaAlgB* was identified as the RR of *PaBphP* around four years ago (Mukherjee *et al.*, 2019). *PaAlgB* itself has been extensively studied for years, particularly in relation to *PaKinB*. Over two decades ago, *kinB* was identified downstream of *algB* in *P. aeruginosa* and proven to encode the corresponding histidine kinase phosphorylating the RR *PaAlgB* (Ma *et al.*, 1997). Almost 13 years later, it was demonstrated that *PaKinB* is critical for numerous virulence-associated phenotypes, including quorum sensing, biofilm formation, and motility. However, this regulation was found to be unrelated to the kinase activity of *PaKinB* and the resulting phosphorylation state of *PaAlgB*, suggesting that their coupled activity does not match the one of a conventional TCS model (Chand *et al.*, 2011). Mukherjee and colleagues hypothesized that activation of *PaAlgB* requires phosphorylation by an unknown kinase. In their experimental approach, the *kinB* knockout mutant exhibited a smooth colony biofilm phenotype, which would revert upon defects in the upstream element, necessary for *PaBphP* phosphorylation. These spontaneously arising suppressor mutants were isolated and whole genome sequencing revealed deletions or mutations in the *algB* as well as in the *bphP* gene. After further verification, *PaBphP* was finally confirmed as the phosphorylating kinase and *PaKinB* as the antagonistic phosphatase (Mukherjee *et al.*, 2019).

– Long believed as a kinase: the special phosphatase *PaKinB* –

Whether proteins containing a histidine kinase domain function as a kinase or phosphatase can typically be determined by analyzing their H-box. The region surrounding the phosphor-accepting histidine residue (*PaBphP*, H513; *PaKinB*, H385) is critical for the identification. An aspartate (D) or a glutamate (E) residue in the H+1 position is considered crucial for histidine kinases (Casino *et al.*, 2014; Multamäki *et al.*, 2021; Willett and Kirby, 2012). For phosphatase activity it is deemed important to have a threonine (T) or an asparagine (N) residue in the H+4 position (Willett and Kirby, 2012). The presence of D514 at the H+1 site of *PaBphP* confirms its function as a kinase. Similarly, the presence of E386 at the H+1 position in *PaKinB* also

indicates its kinase activity, as proven 25 years ago (Ma *et al.*, 1997). *PaKinB* has the ability to phosphorylate itself and even transfer the phosphoryl group to the RR *PaAlgB*. However, during *in vitro* experiments this transphosphorylation is of short duration and, after approximately 5 min, the phosphatase activity of *PaKinB* takes over, causing dephosphorylation of *PaAlgB*. Furthermore, no autophosphatase activity was observed for *PaKinB* (Chand *et al.*, 2012). The presence of T389 in the H+4 position confirms that *PaKinB* acts as a phosphatase, as described in current literature (Mukherjee *et al.*, 2019) and demonstrated in course of this study. *PaBphP* possesses an asparagine residue located at the H+4 position (N517), indicating potential phosphatase activity. However, no supporting evidence has been found yet. Additionally, this hypothesis was not verified in preliminary experiments conducted in this work (data not shown).

– The phytochrome *PaBphP* is part of a truly complex regulation system –

The confirmed *PaBphP/PaAlgB/PaKinB* network and the results of the phenotypical assays are summarized in a light-dependent regulation model (Fig. 4.4). Phenotypic experiments under ambient light conditions demonstrate decreased PYO secretion and swimming motility for the *bphP* overexpression strain and the *kinB* knockout mutant, when compared to PA14. It is assumed that these two strains behave similarly to PA14 under far-red light conditions or other light conditions, generating high Pr-fractions in the phytochrome population. In such instances, the kinase *PaBphP* and its corresponding RR *PaAlgB* are phosphorylated, causing changes in cellular responses. Conversely, the *bphP* deletion mutant and the strain overproducing the inactive *PaBphP* variant (H513A) exhibit increased PYO secretion and swimming motility, when compared to PA14. It can be inferred that these two strains demonstrate behavior similar to PA14 under light exclusion with the phytochrome population in Pfr. Under these conditions, the kinase and its RR are in their unphosphorylated state. The signal and the precise involvement of the phosphatase *PaKinB* in ongoing processes remains unclear at this time. Since previous research conducted by our group has focused on biofilm regulation related to *PaBphP* and the existing literature has also established a correlation, biofilm formation will be discussed below and integrated into the regulation models. Quorum sensing (QS) activates the expression of *algB*, while photosensing activates its function. The model currently disregards the QS input through RhlR since the presence or absence of light can potentially override the effect (Mukherjee *et al.*, 2019).

Moreover, the BphP/AlgB/KinB system is highly conserved in the *Pseudomonas* genus. The *algB/kinB* bicistronic operon, with AlgB as the cognate RR of BphP, is conserved across all

sequenced species (*P. aeruginosa*, *P. fluorescens*, *P. protegens*, *P. stutzeri*, *P. entomophila*, *P. syringae*, *P. putida*). The phytochrome gene *bphP*, is the direct downstream genetic neighbor of *bphO* in the genomes of *P. aeruginosa*, *P. fluorescens*, *P. syringae* and *P. protegens*. In *P. stutzeri*, *P. entomophila*, and *P. putida* the gene for the HO (*bphO*) is separated by two or more genes from *bphP*. Notably, *P. syringae* and *P. putida* possess two phytochromes (*bphP1*, *bphP2*). None of the *Pseudomonas* genomes include a tricistronic operon with the gene for the RR (*bphR*) (pseudomonas.com; Mukherjee *et al.*, 2019).

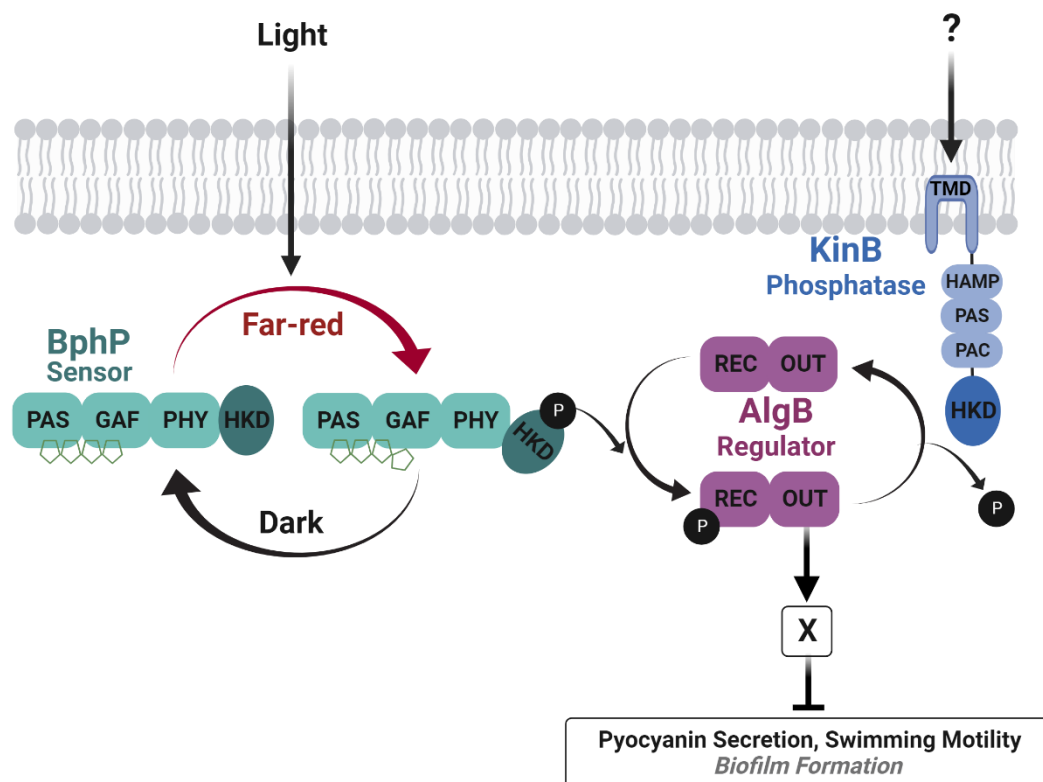


**Fig. 4.4: *PaBphP* is the histidine kinase required for activation of *PaAlgB*, and the phosphatase *PaKinB* is able to dephosphorylate the response regulator.**

The sensor histidine kinase *PaBphP* is in its inactive Pfr-form and is not phosphorylated in the absence of light. Under (far-red) light conditions the chromophore BV IX $\alpha$  undergoes a conformational change that alters the protein interactions. Consequently, *PaBphP* converts into its active Pr-form and autophosphorylates on the conserved histidine residue 513 on the HKD. This enables the transfer of the phosphoryl group to the receiver domain of the corresponding RR *PaAlgB*. The consequence of this phosphotransfer is the activation of *PaAlgB*, which acts as a transcriptional regulator. *PaAlgB* indirectly triggers the expression of inhibitors of the signaling pathway for the pyocyanin operon, swimming motility and biofilm formation. *PaKinB*, the membrane-bound phosphatase, is also a crucial player in the TCS as the antagonist of the kinase *PaBphP*. The phosphatase is able to dephosphorylate and inactivate the RR *PaAlgB* by a so far unknown signal and exert influence on phenotypic behavior. The model only includes far-red and dark conditions for simplicity. Proportional regulation occurs for all other light conditions, according to the Pr/Pfr-fractions based on the “molecular switch” presented in Fig. 4.2. “Biofilm formation” is shown in light gray and italicized, as it was not a direct focus of this study. (Created with BioRender.com)

The signaling pathway beyond *PaAlgB* activation remains intricate and requires further elucidation. The results of this work and existing literature have aided in establishing a detailed

*PaBphP*-dependent regulation scheme (Fig. 4.5). Mainly, research indicates that the “Alg-system” of *P. aeruginosa* has a significant impact on the regulation of the PYO biosynthesis, the swimming motility, and the biofilm formation. Light-dependent phosphorylation of *PaAlgB* via *PaBphP* promotes activation of the protease AlgW (Borges *et al.*, 2020; Chand *et al.*, 2012). MucA is an anti-sigma factor, which normally binds and inhibits the sigma factor AlgU (also known as AlgT). The activated protease AlgW degrades MucA, triggering the release of AlgU (Damron *et al.*, 2009; Intile *et al.*, 2014; Vakulskas *et al.*, 2015; Wu *et al.*, 2004). Free AlgU can positively regulate its own expression and increases the expression of *algD*, encoding a key regulator of alginate biosynthesis and resulting in an overproduction of this polysaccharide (Cross and Goldberg, 2019; Damron *et al.*, 2009; Kimbara and Chakrabarty, 1989; Martin *et al.*, 1993; Wozniak and Ohman, 1991). However, increased amounts of alginate do not necessarily indicate enhancements in biofilm formation but might rather impact colony structure and architecture (Boyd and Chakrabarty, 1995; Franklin *et al.*, 2011). This is also explaining the smooth mucous colonies lacking wrinkles observed in the *kinB* deletion mutant strain, wherein *PaAlgB* is phosphorylated (Mukherjee *et al.*, 2019). In addition, released AlgU positively regulates the expression of *algR* and *amrZ*. Both encoded proteins are transcriptional regulators that additionally activate the *alg* operon and *algD* expression, enhancing the alginate overproduction (Borges *et al.*, 2020; Cross and Goldberg, 2019; Damron *et al.*, 2009). There are also reports that *PaAlgB* directly influences the expression of *algD*, thereby amplifying the alginate effect again (Hershberger *et al.*, 1995; Leech *et al.*, 2008). AlgR is part of a classic TCS as a RR and has demonstrated the capability to regulate some genes independent of its activation by the kinase (Deretic *et al.*, 1992; Yu *et al.*, 1997). One of these independent regulations involves the binding of the *rsmA* promoter, resulting in overexpression of the gene. The abundance of RsmA cause partially released proteins that do not bind to the non-coding sRNAs *rsmY/Z*, leading to inhibition of biofilm formation (Franklin *et al.*, 2011; Intile *et al.*, 2014; Irie *et al.*, 2010; Stacey and Pritchett, 2016). The post-transcriptional regulator RsmA is additionally regulated by the GacS/GacA TCS. When the kinase GacS undergoes autophosphorylation, it leads to the transphosphorylation of the RR GacA. Activated GacA triggers the expression of *rsmY/Z*, which consequently binds to RsmA, promoting biofilm formation (Vakulskas *et al.*, 2015). Furthermore, free RsmA has the ability to inhibit Vfr (virulence factor regulator), thus inhibiting the *fleQ* gene, encoding the flagellar master regulator FleQ that downregulates their biosynthesis (Dasgupta *et al.*, 2002; Tart *et al.*, 2006; Tart *et al.*, 2005). As the swimming motility of the bacteria is based on flagellar movement, it is diminished in strains with phosphorylated *PaAlgB*. However, AlgR can also directly inhibit

Vfr (Jones *et al.*, 2014; Vakulskas *et al.*, 2015), while the transcriptional regulator AmrZ can inhibit *fleQ* expression. This results in a double negative effect on flagella biosynthesis (Jones *et al.*, 2014; Tart *et al.*, 2006). Finally, the regulation of the PYO synthesis is controlled by the transcription regulator AlgR, depending on its phosphorylation state. Phosphorylated AlgR activates the expression of the negative transcriptional regulator *czcR*. CzcR is capable of inhibiting the *phzA1-G1* operon, necessary for the first step of the PYO synthesis (cf. Fig. 3.12A), resulting in low PYO levels (Little *et al.*, 2018).

Upon closer examination of the various regulatory pathways in *P. aeruginosa*, it is apparent that an interrelation has to exist among maturation of biofilms, flagella synthesis and PYO production and its secretion. It is often necessary to equally up- or downregulate the expression of the relevant factors to achieve successful infections. For instance, decreased flagella production may imply reduce biofilm maturation or formation due to their essential role in the initial adherence to surfaces (Haiko and Westerlund-Wikström, 2013; O'Toole and Kolter, 1998; Yamamoto *et al.*, 2012). Contrary, abundantly flagellated bacteria may promote surface attachment and thus biofilm maturation. In addition, it is beneficial for the organisms to avoid regulation PYO secretion and biofilm formation in opposite ways (Costa *et al.*, 2017). The blue-green virulence factor has been demonstrated to be toxic not only to other bacteria, but also to eukaryotes (Price-Whelan *et al.*, 2007). During *P. aeruginosa* infections, PYO can harm the lung cells of cystic fibrosis patients, by reducing oxygen to ROS, thereby promoting biofilm formation (Costa *et al.*, 2017; Lu *et al.*, 2014). Furthermore, PYO acts as an oxidant to contribute to redox balancing of bacteria in anoxic biofilm zones, potentially promoting survival (Jo *et al.*, 2022). PYO production or its secretion assists in regulating the redox status of the cells across different layers of the multicellular bacterial communities (Friedheim, 1931; Price-Whelan *et al.*, 2007). By participating in the electron transport chain, PYO can facilitate the reoxidation of NADH through its own reduction (Jo *et al.*, 2022). Under conditions of limited resources and nutrients or poor energy balance, there is often an excess of electrons, but PYO can serve as an electron sink (Okegbe *et al.*, 2017). The generated NAD<sup>+</sup> can act as an electron acceptor to absorb the excess electrons (Dietrich *et al.*, 2013; Price-Whelan *et al.*, 2007). The reduced PYO can be reoxidized in the oxic zones of the biofilm. In summary, it is hypothesized that the coordination of biofilm formation, flagella biosynthesis, and PYO secretion allows bacteria to establish harsh infections and increase the virulence of *P. aeruginosa*. Whether this infection strategy is suitable for a light/dark-adapted regulation will be discussed in “Part 2” in comparison with other phytochromes.

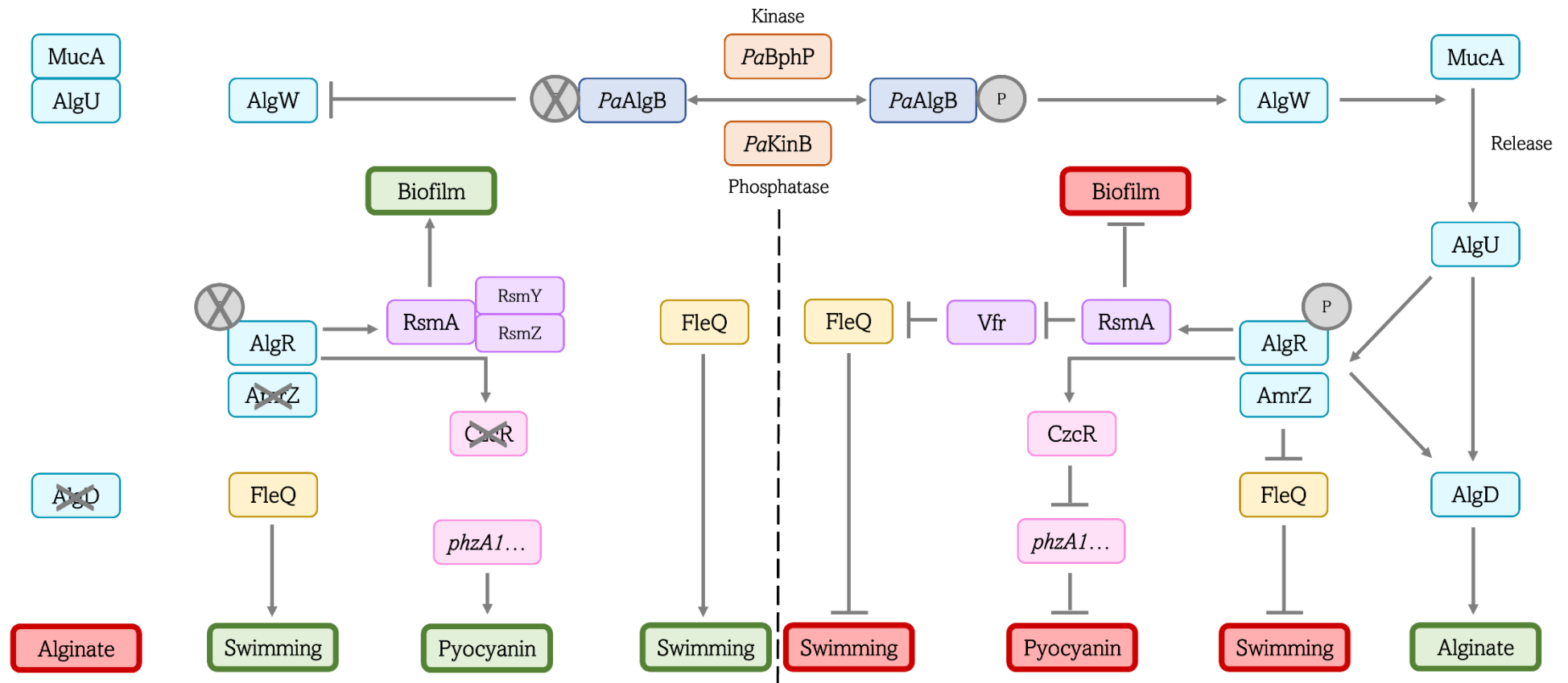


**Fig. 4.5: The regulation of biofilm formation, alginate production, pyocyanin synthesis and flagellar biosynthesis (reflected in swimming motility) in *P. aeruginosa* is attained via a complex network involving the light dependent kinase *PaBphP* and the phosphatase *PaKinB* acting as antagonistic players.**

The preceding paragraph comprehensively describes the detailed regulation steps. The model omits the level of regulation in the individual steps (transcriptional regulation, post-transcriptional regulation, phosphorylation, protein-protein interaction, protease activity, non-coding sRNAs, ...), unless explicitly stated. For simplicity, the model solely presents regulatory steps relevant to the subjects of this study. Further intermediary steps containing more precise information are not included.



## **Part 2 – Comprehensive systematic analysis of various BphPs provides new insights into light-triggered signaling processes**

“Das Licht überliefert das Sichtbare dem Auge; das Auge überliefert’s dem ganzen Menschen. [...] Die Totalität des Inneren und Äußeren wird durchs Auge vollendet.“ (Goethe, Farbenlehre). What Johann Wolfgang von Goethe said in his lifetime remains highly relevant to our current understanding of phytochromes. If we see the phytochromes as the eye of the cell, the light transduction processes align with Goethe’s concepts: Light transmits the visible to the eye, completing the combination of the inner and outer world for the individual (Übers. d. Verf.). Figuratively, this means that light transmits an environmental signal to the phytochrome, which then converts it into an intracellular process, ultimately triggering a cellular response. A comparative analysis was conducted, to verify if the hypothesis that *PaBphP* does not act as a typical on/off-far-red/red switch is also valid for other bathy phytochromes. This is the first study, which examines various BphPs found in Proteobacteria under identical conditions. It allows to create a global statement about the potential function of these light receptors. Thus, this work focused on analyzing spectroscopical properties and autokinase outputs under well-defined circumstances. A direct quantitative correlation of both was achieved by calculating the Pr/Pfr-fractions of each spectrum by a novel application. The detailed investigation of the kinase activity offers a substantial contribution, addressing a gap in the existing literature. Based on the results of phenotypical assays on *P. aeruginosa* and the function of other BphPs postulated in the literature, conclusions could be drawn regarding the general function of bathy phytochromes. The study analyzes not only the two defined pure states (Pr and Pfr), but also the naturally occurring forms with different Pr/Pfr-fractions and their significance for the organisms.

### **4.5 The presence of HWE type histidine kinases - Extending the diversity within the histidine kinase subfamilies?**

While the phytochromes *PaBphP*, *AtBphP1*, *RtBphP2* and *PstBphP1* adhere to the classical PAS-GAF-PHY-HKD sequence, the composition of the other phytochromes deviates from this common domain structure (cf. Fig. 1.3). *XccBphP* lacks an HKD with autokinase activity entirely, whereas *AtBphP2*, *AvBphP2* and *PstBphP2* possess HWE-type kinase domains. Their classification as a histidine kinase (HK) superfamily, together with HisKA2, is based on unique sequence motifs in both the catalytic as well as non-catalytic region (Herrou *et al.*, 2017; Karniol and Vierstra, 2004). The subfamily is named after the conserved HWE motif (cf. Fig. 3.16), which includes a histidine (H) in the N-box and a tryptophan-X-glutamate (WxE) residue

sequence near the G1-box (Karniol and Vierstra, 2004). In addition, HWE kinase domains are characterized by the absence of an F-box and the replacement of the first asparagine (N) in the N-box with a glutamate (E) residue (Herrou *et al.*, 2017; Karniol and Vierstra, 2004). The function typically fulfilled by the F-box in classical HKs is executed through hydrophobic residue within the G2-box in HWE kinase domains (Herrou *et al.*, 2017). The fundamental chemistry necessary for transferring the  $\gamma$ -phosphoryl group from ATP to the histidine in the H-box is undoubtedly comparable between classical HKs and HWE kinases. In typical HKs, there is a glutamate or an aspartate (E/D) residue at position H+1 serving as a catalytic base by deprotonating the histidine. The deprotonation enhances its nucleophilicity, promoting the attack of the  $\gamma$ -phosphoryl group. The first asparagine (N) within the N-box also interacts with the acidic H+1 residue, amplifying the effect (Casino *et al.*, 2014; Dago *et al.*, 2012; Herrou *et al.*, 2017). In HWE kinase domains, an arginine (R) is located at position H+1. There is no indication that this residue is involved in the deprotonation of the histidine in the H-box. Instead, the glutamate (E) at the H minus 3 position or in the N-box is probably responsible (Herrou *et al.*, 2017).

Typical HKs are widely distributed among all domains of life, while the majority of HWE kinases are exclusively present in the family of Rhizobiaceae within the class of Alphaproteobacteria (Herrou *et al.*, 2017; Karniol and Vierstra, 2004; Rinaldi *et al.*, 2016). Investigation on the HWE kinase superfamily, motivated by the interest in bacterial photobiology and protein photosensors, has revealed a distinct correlation between these kinases and bacterial photoreception, involving phytochromes and blue-sensing LOV domains (Correa *et al.*, 2013; Herrou *et al.*, 2017; Karniol and Vierstra, 2003; Karniol and Vierstra, 2004; Kim *et al.*, 2014; Rinaldi *et al.*, 2016). Classical HKs and HWE kinases are composed of a DHp and a CA domain (cf. Fig. 1.4) allowing for autophosphorylation (Karniol and Vierstra, 2004). The critical differentiation between the two is predominantly not within the domain itself but rather in the downstream two-component phosphoryltransfer pathway that they participate in. The cognate RR of HWE kinases is mainly associated directly with the protein, and typically does not signal via classical DNA-binding. It consists of a REC domain that either lacks an output domain or possesses an atypical one. There is evidence indicating that HWE kinases and their associated RRs act in signaling pathways with numerous sensory kinase inputs. In these systems, the RRs can modulate gene expression through protein-protein interactions or by controlling transcription termination regulating proteins (Herrou *et al.*, 2017). Using InterPro and SMART, the associated RRs of *AtBphP2* and *AvBphP2* were identified as CheY-like RRs (IPR011006) or CheY-homologous REC domains (SM000448). Thus, the RRs of these two

phytochromes seem to perform solely phosphoaccepting REC domain functions. They are merely intermediate elements, with the phosphoryl group being further transferred to generate a cellular response (Galperin, 2010). In *PstBphP2*, there is no RR downstream, but a typical HKD is located upstream of the HWE kinase domain. The importance of autophosphorylation in the HKD, the HWE kinase domain, or both domains for subsequent processes remains unclear (Shah *et al.*, 2016).

In summary, categorizing the HWE kinases as a subfamily of HKs is a logical decision based on their unique motifs and their associated uncommon RR signaling without DNA-binding. However, their fundamental mode of autokinase activity does not substantially differ from that of typical HKs, as demonstrated in the autophosphorylation assays in this work.

#### **4.6 The paradox of bathy and prototypical phytochromes – Do they end up sharing more similarities or more differences?**

##### *– The spectral behavior of bathy and prototypical phytochromes in comparison –*

While the spectral behavior of the bathy phytochromes *RtBphP2* and *XccBphP* was largely similar to that described in the existing literature, differences were observed for *AtBphP2* and *AvBphP2*. *RtBphP2* has only been studied under dark and far-red light conditions so far (De Luca *et al.*, 2019), with the results of this work in agreement. Under red and blue light conditions, *RtBphP2* exhibits mixed Pr/Pfr-forms like *PaBphP*, but those of *RtBphP2* have a significant red-shift to Pfr (750 nm). In present results *XccBphP* showed a distinct Pr-form under far-red light conditions, a nearly balanced Pr/Pfr-form under red light conditions and a Pfr-enriched form under dark conditions. A clear Pfr-form could only be generated in a protein variant lacking the PAS9 output domain (Otero *et al.*, 2016). In the course of this study, identical observations were made, and, in addition, a mixed form was measured under blue light conditions, which shifts to Pr (700 nm) identically to the *PaBphP* spectrum. Otero and colleagues attribute the lack of a clear Pfr-form in the absence of light to differences in the quaternary structure. Unlike *XccBphP*, which is present as a dimer, *XccBphP* $\Delta$ PAS9 exists as a monomer, leading to structural disparities that impact the chromophore binding to the photosensory domain and the thermodynamics of the dark reversion (DR) (Otero *et al.*, 2016). The bathy phytochrome *XooBphP* of the related organism *X. oryzae* exhibits a similar spectral behavior to *XccBphP*. However, this BphP is able to produce a distinct Pfr-form, even though its PAS4 output domain is still attached (Verma *et al.*, 2020). Contrary to prior research, which asserted that a clear Pr-form is unattainable for the bathy phytochrome *AtBphP2* (Karniol and Vierstra, 2003; Lamparter *et al.*, 2017), the present study proves that a distinct Pr-form can

actually be achieved under far-red light conditions. The spectra obtained under red light conditions as well as in darkness are consistent with those in the literature, while under blue light conditions, a Pfr-shifted mixed form is observed. There are only minimal differences in the spectral behavior between *AtBphP2* and the variant with the substituted phosphoaccepting aspartate in the REC domain (D783N). Only a Pfr-enriched form was measurable during this study for the bathy phytochrome *AvBphP2* in the absence of light. Nevertheless, there is already evidence indicating that the protein is capable of forming a distinct Pfr-form (Rottwinkel *et al.*, 2010). Furthermore, there were no significant differences in the spectral behavior observed between *AvBphP2* and *AvBphP2\_D793A*.

The measured spectra of the prototypical phytochrome *AtBphP1* also align with the existing literature (Karniol and Vierstra, 2003; Scheerer *et al.*, 2010). As previously indicated in chapter 4.1, *AtBphP1* exhibits a clear Pr-form under far-red light and dark conditions, a clear Pfr-form under red light conditions and a mixed form is only observed under blue light conditions. The same observations hold true for the prototypical phytochrome *DrBphP*, found in *D. radiodurans*. The Pr- and the Pfr-form are strictly distinguishable under far-red and red light conditions, without any Pr/Pfr-mixed or enriched-forms present (Multamäki *et al.*, 2021). In contrast, *PstBphP1* of *P. syringae*, which was also investigated in this study, deviates from this pattern, and exhibits characteristics of an unconventional prototypical phytochrome. According to the existing literature, it is incapable of producing a Pfr-form under any light condition. Each spectrum of *PstBphP1* displays high Pr-fractions (Hatfield *et al.*, 2023; Shah *et al.*, 2012). With *RpBphP2*, the phytochrome of *R. palustris*, another example is added to the series of unconventional prototypical phytochromes. It has been observed that *RpBphP2* cannot undergo a pure Pfr-form when exposed to red light (Giraud *et al.*, 2005).

In summary, the spectral behavior pattern of *PaBphP* is adhered to all examined bathy phytochromes. None of the bathy BphPs is capable of generating a clear Pfr-form upon exposure to red light. Only darkness initiates the formation of a pure or a highly enriched Pfr-form. The location of the Soret band, as explained in chapter 4.2, is responsible for the variations in the Pr/Pfr-fractions under blue light conditions between the different BphPs. Even in prototypical phytochromes, the differentiation between the Pr- and Pfr-forms is not always entirely strict. In certain examples, red light can generate solely a Pfr-enriched form.

#### – The autokinase output of bathy and prototypical phytochromes in comparison –

The autokinase activity of bathy phytochromes has not been adequately studied thus far. There are only initial studies investigating the trigger for autophosphorylation of *PaBphP* and

*AtBphP2*. The research on *PaBphP* solely utilized a locked variant (Yang *et al.*, 2011) or yielded less clear results than those presented in this work (Mukherjee *et al.*, 2019). Additionally, this study conclusively disproved previous findings that the Pfr-form of *AtBphP2* autophosphorylates significantly stronger than the Pr-form (Karniol and Vierstra, 2003) or as strong as the Pr-form (Xue *et al.*, 2019). In return, the existing literature provides some more research on the autokinase activity of prototypical phytochromes (Tab. 4.1). The results generated in the course of this study on *AtBphP1* and *PstBphP1* substantiate prior findings (Bhoo *et al.*, 2001; McGrane and Beattie, 2017; Njimona and Lamparter, 2011; Xue *et al.*, 2019).

**Tab. 4.1: Summary of the active forms (= highest level of autophosphorylation in kinase assay) of bathy and prototypical phytochromes from various organisms. The BphPs of *X. campestris* and *X. oryzae* do not have an HKD (instead PAS9 or PAS4 output domain). The BphP of *D. radiodurans* possess an HKD but it has only phosphatase activity. The phytochrome of the cyanobacterium *F. diplosiphon* is included in the list because it bears remarkable similarities to bacterial phytochromes.**

Organism	BphP	Active form	Reference
<b>Bathy Phytochromes</b>			
<i>Pseudomonas aeruginosa</i>	<i>PaBphP</i>	Pr	This study, 1, 2
<i>Agrobacterium tumefaciens</i>	<i>AtBphP2</i>	Pr	This study
<i>Allorhizobium vitis</i>	<i>AvBphP2</i>	Pr	This study
<i>Ramlibacter tataouinensis</i>	<i>RtBphP2</i>	Pr	This study
<i>Xanthomonas campestris</i>	<i>XccBphP</i>	no HKD	3
<i>Xanthomonas oryzae</i>	<i>XooBphP</i>	no HKD	4
<b>Prototypical Phytochromes</b>			
<i>Agrobacterium tumefaciens</i>	<i>AtBphP1</i>	Pr	This study, 5-9
<i>Pseudomonas syringae</i>	<i>PstBphP1</i>	Pfr	This study, 10, 11
<i>Ramlibacter tataouinensis</i>	<i>RtBphP1</i>	Pr	12
<i>Rhodospseudomonas palustris</i>	<i>RpBphP2</i>	Pr	13
	<i>RpBphP3</i>	Pr	13
<i>Deinococcus radiodurans</i>	<i>DrBphP</i>	no autokinase	6
<i>Fremyella diplosiphon</i>	<i>FdCphB</i>	Pr	14

(1) Mukherjee *et al.*, 2019; (2) Yang *et al.*, 2011; (3) Otero *et al.*, 2016; (4) Verma *et al.*, 2020; (5) Karniol and Vierstra, 2003; (6) Multamäki *et al.*, 2021; (7) Njimona and Lamparter, 2011; (8) Scheerer *et al.*, 2010; (9) Xue *et al.*, 2019; (10) Bhoo *et al.*, 2001; (11) McGrane and Beattie, 2017; (12) Baker *et al.*, 2016; (13) Giraud *et al.*, 2005; (14) Quest *et al.*, 2007

The autokinase readout and the Pr-fractions of *PaBphP* have a strong interrelation, as explained in chapter 3.3. However, utilizing signal intensities observed in an autoradiogram cannot provide a reliable quantification of the kinase activity as a whole. To address this issue, a collaboration with the department of Biophysics (RPTU) allowed the development of a precise method employed in this study to calculate the Pr/Pfr-fractions in each spectrum of *PaBphP*,

*AtBphP1/2*, *AvBphP2*, *RtBphP*, and *PstBphP1*. The Pr-fractions (for *PstBphP1* the Pfr-fraction), which indicate the active proportion of the phytochrome population, can be correlated with their autophosphorylation activity using this novel method. Furthermore, it enables the quantification of His-kinase activity with all naturally occurring intermediate states.

In summary, the autokinase output of all investigated bathy phytochromes aligns with the pattern of the *P. aeruginosa* BphP. Each phytochrome exhibited a substantial decline in its kinase activity when a highly enriched or pure Pfr-form accumulated in the absence of light. Thus, the Pr-form is the active form of *PaBphP*, *AtBphP2*, *AvBphP2* and *RtBphP2*. The Pr-form of *AtBphP1* and the Pfr-form of *PstBphP1* could be confirmed as the active ones. Based on these results, the *PaBphP* model of the “molecular light switch” (cf. Fig. 4.2) can be accordingly expanded. Furthermore, the literature advocates for incorporating preliminary data of prototypical phytochromes in the expanded model (Fig. 4.6).

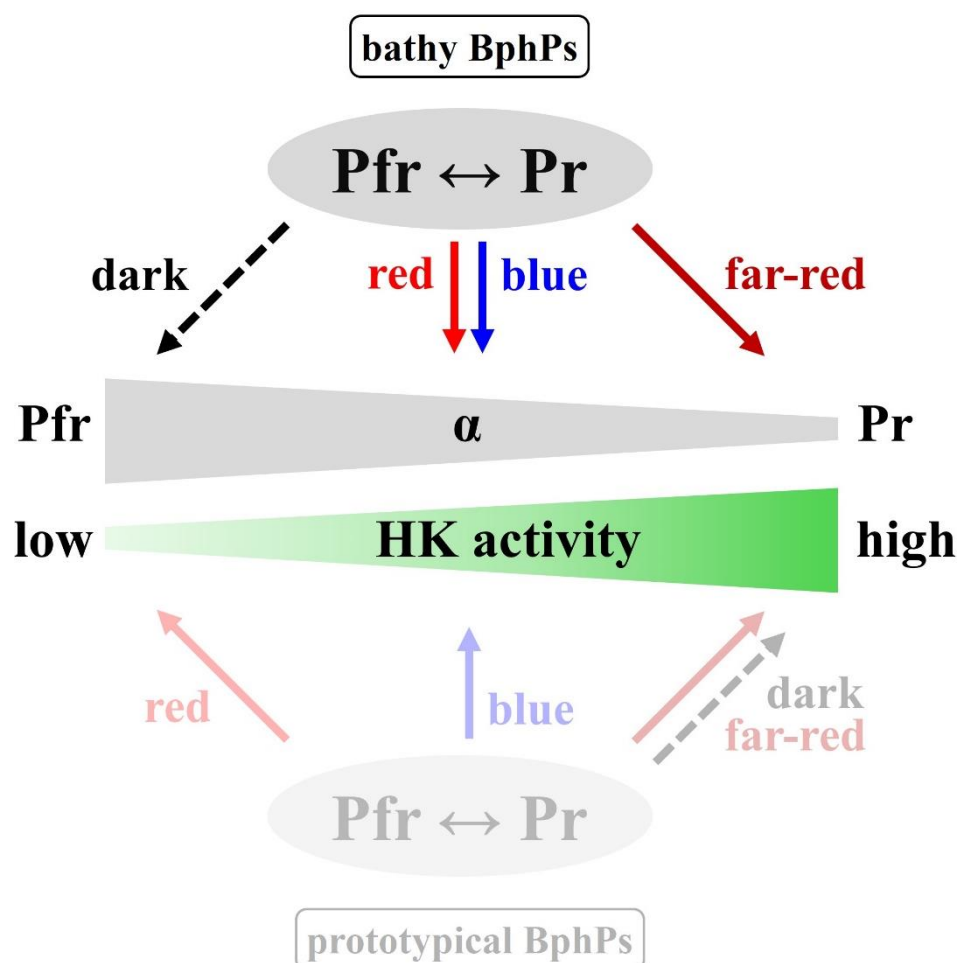


**Fig. 4.6: Bathy and prototypical phytochromes act as molecular light switches to adjust their histidine kinase (HK) activity.**

Bathy and prototypical phytochromes function as switches that regulate the autokinase output in the bacterial cells. It is not a simple on/off system, but rather adjusts HK activity as Pr-fractions increase (=  $\alpha$  decreases) and Pfr-fractions decrease (=  $\alpha$  increases). Far-red light (for bathy BphPs) and darkness (for prototypical BphPs) are

associated with the highest Pr-fractions, lowest  $\alpha$ , and highest HK activity. Darkness (for bathy BphPs) and red light conditions (for prototypical BphPs) are associated with the highest Pfr-fractions, highest  $\alpha$ , and lowest HK activity. Blue and red light exhibit mixed forms with different Pr/Pfr-fractions and kinase activity based on the Pfr-fraction. The  $\alpha$  value defines the fraction of Pfr available in a phytochrome population ( $\alpha = [P_{fr}]/([P_{fr}]+[P_r])$ ). The model for the prototypical BphPs is only preliminary (transparent background) because comprehensive investigations on their spectral and autokinase behavior were not conducted in this study. The behavior of *Pst*BphP1 deviates completely from the model due to its contradictions.

In the context of autokinase activity, further questions can be asked: What is the role of the apo-form of a phytochrome? Does the phosphotransfer to the RR also rely on light stimulation? Do the investigated bathy phytochromes possess a light-regulated phosphatase activity similar to that of the BphP in *D. radiodurans* (Multamäki *et al.*, 2021)? For *Pa*BphP, it was demonstrated that the apo-phytochrome exhibits a low autokinase activity, and only the addition of the chromophore BV IX $\alpha$  and the pure Pfr-form can fully inhibit the signal. Additional research is necessary to determine the behavioral patterns of other bathy BphPs in their apo-forms, but it is plausible that they function as a type of BV-sensor in the absence of light (J. C. Lagarias, personal communication). Currently, it remains unclear if and to what extent an apo-phytochrome has any physiological impact on these organisms.

To capture solely the autophosphorylation activity of *At*BphP2 and *Av*BphP2, protein variants were employed lacking the phosphoaccepting aspartate in the HWE kinase associated RR. In order to observe a further transfer to the RR domain, the respective wildtype variants of both phytochromes were utilized. No phosphotransfer was detected between *At*BphP2 and its RR domain, potentially due to an *in vitro* protein conformational effect, as described by Xue *et al.*, 2019. In contrast, *Av*BphP2 exhibited phosphotransfer to its RR domain under far-red light conditions, resulting in a significant stronger signal than that observed under blue light, red light, or dark conditions. Only *Pa*BphP exhibits a strict transfer pattern to its separate RR *Pa*AlgB. The transfer was possible under all light conditions (far-red > blue > red), while no transfer was detected in the absence of light. However, it is assumed that the transfer is not triggered by light, but instead, reliant on the quantity of phosphorylated kinase, which is itself light-dependent. Evidence for light-regulated phosphatase activity of bathy BphPs was neither discovered during this study, nor were any reports of it found in the existing literature.

#### – The structural signal transduction of bathy and prototypical phytochromes in comparison –

When analyzing the model, it is noteworthy that there is usually no difference in the conformation in which bathy and prototypical BphPs are active. Both types of phytochromes exhibit the highest kinase output in their Pr-form (except *Pst*BphP1). The Pr-form is present in

bathy BphPs under far-red light conditions, whereas in prototypical BphPs, the form exists under far-red light conditions and as the ground state in the absence of light. However, in darkness bathy BphPs are in their inactive Pfr-form, indicating that autophosphorylation in bathy and prototypical phytochromes occurs in the same protein conformation but is not stimulated by identical light/dark conditions. At this point, an additional contradiction arises: while plant prototypical phytochromes demonstrate Pfr activity upon exposure to red light, this is not consistently observed with prototypical bacterial phytochromes. Plant phytochromes photoregulate various physiological processes, including seed germination, floral initiation, and development, specifically responding to red light (Borthwick *et al.*, 1952a; Butler *et al.*, 1959; Mathews, 2006). Therefore, it is hypothesized that prototypical BphPs share more similarities with bathy BphPs rather than with plant phytochromes. To further investigate the complex interplay between the active conformation of bathy and prototypical phytochromes, examinations of the protein structures and the signal transduction are required.

The exact mechanism of structural signal transduction in phytochromes, which involves a conformational change of the photosensory domain after stimulus detection, remains largely unclear. Light absorption initiates a sequence of intermediate states and structural alternations that are transmitted from the bilin chromophore, which is located in the N-terminal photosensory domain, to the C-terminal HKD, resulting in its autophosphorylation. The changes are based on three structural levels, namely the chromophore-binding pocket, the photosensory module, and the output domain (Fig. 4.7A). Furthermore, it is improbable that the modifications transpire in a linear cascade; instead, the regulation involves a multifaceted interplay among these three hierarchical tiers (Takala *et al.*, 2020). Most of the phytochromes have been crystallized in their dark-adapted state because solving the crystal structure of their light-activated forms has proven to be challenging (Lee *et al.*, 2022). The phytochrome *DrBphP* from *D. radiodurans*, exhibits unique crystal structure clarification in both its Pr and Pfr state of the full-length protein (Burgie *et al.*, 2016; Takala *et al.*, 2014). While extensive research has been conducted on the signal transduction of this prototypical BphP (Björling *et al.*, 2016; Burgie *et al.*, 2016; Isaksson *et al.*, 2021; Macaluso *et al.*, 2021; Takala *et al.*, 2015; Takala *et al.*, 2020; Wahlgren *et al.*, 2022), there are only initial reports on bathy *PaBphP* and *AtBphP2* as well as bathy-like *XccBphP* (Lee *et al.*, 2022; Otero *et al.*, 2021; Otero *et al.*, 2016; Schmidt *et al.*, 2018). However, a change in the so-called “PHY-tongue” is potentially crucial and plays a key role in the signal transduction process (Burgie *et al.*, 2014; Isaksson *et al.*, 2021; Takala *et al.*, 2014). This tongue serves as a structural component that connects the PHY domain to the chromophore-binding pocket in the GAF domain, forming a hairpin structure. Through studies



on *DrBphP*, it was observed that the (*Z*)/(*E*) isomerization of the chromophore (cf. chapter 1.3) within the binding pocket is relayed to the PHY domain (Fig. 4.7A). The tongue transforms from a  $\beta$ -sheet structure in the Pr-form to an  $\alpha$ -helical configuration in the Pfr-form (Isaksson *et al.*, 2021; Takala *et al.*, 2014; Takala *et al.*, 2020; Wahlgren *et al.*, 2022). Therefore, the PHY tongue functions as a switch, controlling the placement of the GAF and PHY domain. These structural adjustments cause the reorientation of the HKD, resulting in alternations in the dimer interface that facilitate autophosphorylation (Lee *et al.*, 2022; Takala *et al.*, 2014; Takala *et al.*, 2020). Recent studies have identified a figure-eight knot in the PAS/GAF domain and a long helix extending across the entire photosensory module (“spine”) as significant structural elements in addition to the PHY tongue (Fig. 4.7B). A distinct contrast in the knot region and the lower section of the helical spine of *DrBphP* between the Pr- and the Pfr-form describe an additional signaling pathway (Isaksson *et al.*, 2021). It is unclear whether the signal transduction to the output domain relies on the synchronous function or redundancy of both pathways – PHY tongue as well as knot/helical spine alternation (Isaksson *et al.*, 2021; Takala *et al.*, 2014). A molecular dynamics simulation, based on the resolved crystal structure of the photosensory domain of *PaBphP* (Yang *et al.*, 2008), marked a significant milestone in comprehending the bathy phytochrome signaling. The change in the PHY tongue also contributes to the photocycle and signal transduction of this bathy BphP, however, the detailed structural alternations involved in the phototransitions differ from those of prototypical phytochromes (Fig. 4.7C). The helical backbones (red and blue helices), which transition from an II-framed close form (Pfr) to an O-framed open form (Pr) in bathy BphPs, exhibit dissimilarities in prototypical phytochromes. In bathy BphPs the O-form permits accessibility to the phosphorylation site within the DHP domain of the HDK in the Pr-conformation (Lee *et al.*, 2022). Although, the *X. campestris* phytochrome lacks an HKD, light-induced alternations in its crystal structure can potentially facilitate the elucidation of the signal transduction pathway. In *XccBphP*, the D-ring isomerization of the chromophore triggers the light-induced transition of the PHY tongue to a  $\beta$ -sheet structure. This structural change causes the dissociation of the dimer and the reorientation of the PAS9 output domain (Otero *et al.*, 2021). In summary, there is currently inadequate research to ascertain a clear structural comparison between bathy and prototypical BphPs. Although the PHY tongue alternation from  $\beta$ -sheet to  $\alpha$ -helix (Pr/Pfr) is fundamental in both types, numerous distinctions in the transduction process remain. Technological advancements can facilitate further understanding of crystal structure in light- and dark-adapted states, as well as provide stronger comparisons between bathy and prototypical phytochromes.

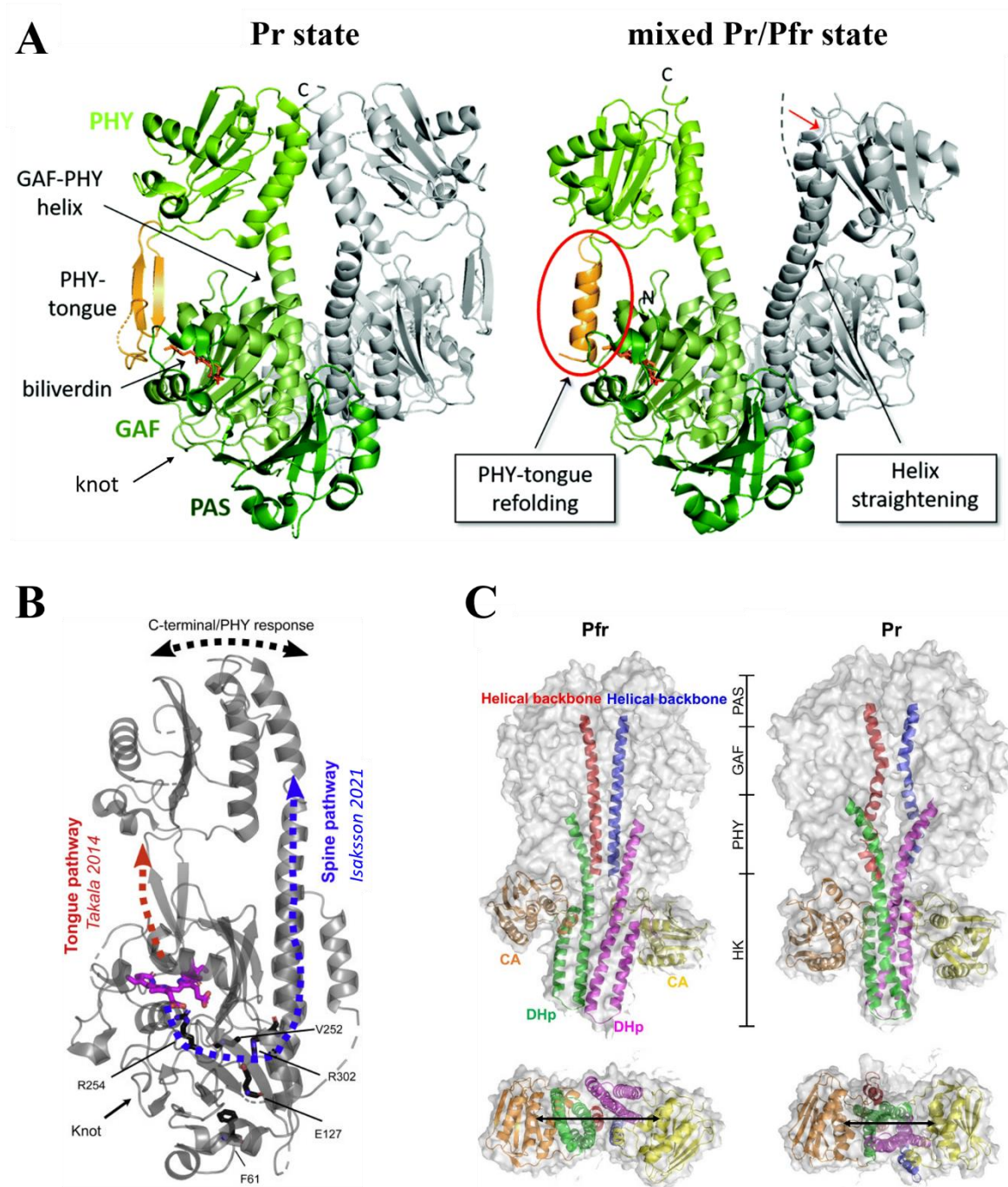


**Fig. 4.7: Overview of structural signal transduction in the prototypical *DrBphP* and the bathy *PaBphP*.**

(A) Structure of the photosensory domain of the *D. radiodurans* prototypical phytochrome *DrBphP* in the Pr-state (left) and in the Pr/Pfr-mixed state under red light conditions (right). Monomer 1 is highlighted with its PAS, GAF, and PHY domain in various shades of green, while the sister-monomer 2 is colored in gray. The chromophore biliverdin IX $\alpha$  (orange), the PHY-tongue (yellow), the knot, and the GAF-PHY helix are indicated by arrows in monomer 1. The light-induced structural changes (PHY-tongue refolding and Helix straightening) are indicated in boxes. Figure modified from Takala *et al.*, 2020 (PDB Pr: 4O0P; PDB Pr/Pfr mix: 4O01 from Takala *et al.*, 2014).

(B) Structure of *DrBphP* includes the “tongue pathway” (Takala *et al.*, 2014) as well as the “spine pathway” (Isaksson *et al.*, 2021), which relayed the signal to the PHY and further to the output domains. Crucial amino acids, involved in the “spine pathway” are indicated. Figure adapted from Isaksson *et al.*, 2021 (PDB: 4O0P).

(C) Simulated structure of full-length *PaBphP*, based on the crystal structure of the photosensory domain (Yang *et al.*, 2008) in the Pfr- (left) as well as Pr-state (right). Alternating structures of the sister-monomers are highlighted in different colors (CA domains in orange and yellow; DHp domains in green and purple; helical backbones, which are extended through the PAS, GAF, and PHY domains in red and blue). The black arrows in the bottom view display the distances between the CA domains of the sister-monomers, which is shorter in the Pr-state compared to the distance in the Pfr-state. Figure adapted from Lee *et al.*, 2022.

– The rate of dark reversion varies significantly among diverse phytochromes –

Dark reversion is the Pr-to-Pfr conversion in bathy phytochromes and the Pfr-to-Pr conversion in prototypical phytochromes in a light-independent thermal process (Borthwick *et al.*, 1952b; Rockwell *et al.*, 2006; Taylor, 1968). The time frame for the development of a pure Pr- or Pfr-form after the onset of darkness can fluctuate greatly, ranging from mere seconds to several hours, or even days (Chen *et al.*, 2004; Rockwell *et al.*, 2006). The DR time can be affected by various cellular conditions such as temperature or pH (Jung *et al.*, 2016; Legris *et al.*, 2017; Rockwell *et al.*, 2006; Velazquez Escobar *et al.*, 2015). For *AtBphP2*, it was demonstrated that the same proton translocations which are responsible for the formation of the photoactivated state, activating the output module, are also involved in the thermal back-isomerization of the chromophore. Thus, the identical re-arrangement of protons also stimulates the deactivation of the output module, similar to a negative feedback mechanism (Velazquez Escobar *et al.*, 2015). UV-Vis spectroscopy was utilized to determine the approximate half-life, indicating the point where 50 % of the bathy BphP population is present in its Pr-form (prototypical BphPs in its Pfr-form). Compared to the 15 min half-life DR of *PaBphP*, the other examined bathy BphPs exhibit notably shorter DR times. However, *XccBphP* is an outlier, requiring 1-4 h to develop 50 % of its Pfr-form. The two prototypical phytochromes (*AtBphP1*, *PstBphP1*) have similar DR times to *PaBphP*. Currently, it is completely unclear if there is a physiological reason behind the time needed to develop the ground state. It can only be speculated whether the combination of DR and temperature sensing has a biological impact, or whether a rapid DR compensate for phosphatase activity. Phytochrome TCSs lacking a phosphatase or BphPs without an autophosphatase activity may rely on rapid DR to efficiently return to their inactive and unphosphorylated state. While *PaKinB* is described as a phosphatase in the regulatory system with *PaBphP* and *PaAlgB* (Mukherjee *et al.*, 2019), there is no literature supporting the existence of phosphatases in the other studied phytochrome organisms.

#### **4.7 Bathy phytochromes in different Proteobacteria – Model systems for a new classification of their light sensing function?**

Based on all described results, it can be postulated that bathy phytochromes function as light/dark sensors rather than classical far-red/red light sensors. The hypothesis is that changing Pr/Pfr-fractions, which modify the proportion of the autokinase active Pr-form, enables bacteria to precisely adjust their kinase output in response to specific light qualities and environments. Only darkness and the associated pure or highly enriched Pfr-form is able to turn the system off. The precise evolutionary history of phytochromes having a Pr- or Pfr-ground state across

all domains of life, and their potential independent or interconnected evolution cannot be addressed in this study. However, the biological significance of having a sensor for darkness and the ability to respond to diverse light qualities is explainable. All investigated organisms that possess a bathy phytochrome are either plant pathogens or soil bacteria. The ubiquitous human opportunistic pathogen *P. aeruginosa*, and the other bacteria (*A. tumefaciens*, *A. vitis*, *X. campestris*, *R. tataouinensis*) are required to acclimate to the distinct ecological niche of living in the soil or in association with plants. Having a bathy phytochrome could offer an evolutionary advantage in specific environments with unique conditions. Based on the results of this study and a comprehensive literature review, a model aiming to elucidate the function of bathy phytochromes was developed (Fig. 4.8).

*A. tumefaciens* and *A. vitis* are Gram-negative, rod-shaped plant pathogenic soil bacteria, which belong to the class of Alphaproteobacteria and to the family of Rhizobiaceae (Mousavi *et al.*, 2014; Mousavi *et al.*, 2015; Ophel and Kerr, 1990; Tindall, 2014). They are closely related to each other and have many homologous characteristics. Due to their ability to transfer tumor-inducing (Ti) plasmids into host plant cells, *A. tumefaciens* and *A. vitis* are the best-known agents of crown gall disease. The expression of the T-DNA within the plant leads to tumor formation, resulting in the production of opines. *A. tumefaciens* and *A. vitis* can utilize these opines as a food source (Burr and Otten, 1999; Chilton *et al.*, 1977; Gelvin, 2010). The soil-borne bacteria carry two genes which encode BV-binding phytochromes – the prototypical *AtBphP1/AvBphP1* whose photoproduct is the Pfr-form and the bathy *AtBphP2/AvBphP2* with Pfr being thermally stable state (Lamparter *et al.*, 2002; Rottwinkel *et al.*, 2010). Thus, both BphPs have possibly opposing functions and the respective organism is therefore able to adapt even better to red light-rich and far-red light-rich habitats (Karniol and Vierstra, 2003; Rottwinkel *et al.*, 2010). The gene for the HO, which synthesizes and supplies the BphPs with chromophore, is located outside the phytochrome operons (Karniol and Vierstra, 2003). Proteome analysis for both species confirmed a light-dependent regulation of the flagellar proteins FlaA and FlaB. The presence of light reduces flagellar biosynthesis, negatively impacting bacterial virulence by inhibiting motility, and disrupting the bacteria-plant interaction. Under light conditions, infection assays demonstrate reduced adhesion of the bacteria to tomato roots and decreased cucumber infection. The tumor formation increased in the absence of light, indicating higher virulence in darkness (Oberpichler *et al.*, 2008). The induction of tumor formation is directly related to the conjugation of the Ti plasmid into the plant. Different research has demonstrated that the DNA-transfer is inhibited by light, which is

potentially associated with the suppression of the type IV secretion system (T4SS) (Bai *et al.*, 2016; Lamparter *et al.*, 2021; Rottwinkel *et al.*, 2010; Xue *et al.*, 2021).

*X. campestris* pv. *campestris* is one of over 140 pathovars of *X. campestris*. The plant pathogen is a Gram-negative bacterium which is assigned to the class of Gammaproteobacteria (Chan and Goodwin, 1999). It can cause different plant diseases like black rot in cruciferous vegetables, for example cabbage and cauliflower or in mustard plants (Williams, 1980). The bacterium only encodes one bacterial phytochrome, the bathy-like *XccBphP*. In a bicistronic operon, the gene for the HO BphO is arranged upstream from the phytochrome-coding gene. The phytochrome is a confirmed light-dependent virulence repressor. In the presence of light, *XccBphP* inhibits various secretion systems and the flagellar operon (especially *flg* and *fli*), resulting in reduced swimming motility. Moreover, light inhibits xanthan production, which has an enormous detrimental effect on biofilm formation (Bonomi *et al.*, 2016). The phytochrome *XooBphP* from *X. oryzae* regulates the transition from a sessile to a free-swimming motile lifestyle and virulence-associated functions. It seems to act as a light-sensing phosphodiesterase that modulates the intracellular secondary messenger cyclic di-GMP (c-di-GMP), affecting biofilm development (Verma *et al.*, 2020). Otero *et al.*, 2021 proposed that *XccBphP* from *X. campestris* has no recognizable biochemical activity and regulates the c-di-GMP levels through its PAS9 domain and downstream signaling partners. The domain may interact with a partner possessing either phosphodiesterase- or diguanylate cyclase activity. The second messenger is degraded in response to light, triggered by activation of the PAS9 domain and enzyme interaction, resulting in inhibited biofilm formation (An *et al.*, 2020).

*R. tataouinensis* is a Gram-negative bacterium that can exist in either spherical cysts or rod-shaped cells, depending on its environment. The Betaproteobacterium was discovered within the novel genus of *Ramlibacter* and was identified as a new species after being isolated from a semi-arid region of Tunisia (Heulin *et al.*, 2003). *R. tataouinensis* possesses two genes that encode phytochromes: the prototypical *RtBphP1* and the bathy type *RtBphP2*, both able to bind BV IX $\alpha$ . The gene for the HO *hmuO* is located in an operon along with *RtbphP1*. Nonetheless, the heme-cleaving protein supplies the chromophore BV IX $\alpha$  for both phytochromes, *RtBphP1* and *RtBphP2* (De Luca *et al.*, 2019). It is reported that the light sensors allow *R. tataouinensis* to adapt to the day-night rhythm in their natural desert environment. The bacterium is forced to cope with extreme conditions due to cold nights and hot days with varying water availability. During the nighttime in dark conditions, the bacteria are characterized by cyst division and a cyst-rod-cyst (CRC) cycle. The rods divide when exposed to red or far-red light. At sunrise, associated with dew formation, red light induces this rapid division for effective use of available

water and facilitates motility, dissemination, and colonization of new environments. Before the midday, bacteria embed themselves again in cyst matrices consisting of EPS to avoid intense sunlight, high temperatures, and desiccation. This process is potentially triggered by blue or white light-sensing (De Luca *et al.*, 2011; Heulin *et al.*, 2003). A plausible scenario involves the light-triggered phosphorylation of a RR by *RtBphP2*, which activates downstream signaling pathways and inhibits EPS and cyst formation. Although De Luca *et al.*, 2019 reported the inhibition of rod formation due to autophosphorylation in the dark, they only mention the autokinase activity of *RtBphP1* (Baker *et al.*, 2016).

The light-dependent behavior of the human pathogen *P. aeruginosa* is explained in chapter 4.4 in great detail. As all investigated bathy BphPs downregulate the virulence of their organism in a light-dependent manner, the hypothesis proposed above, indicating that they act as light/dark sensors rather than far-red/red light sensors can be further expanded. It is postulated that the bacteria utilize phytochromes to synchronize their infection strategies with the circadian clock and the day/night rhythm of their hosts. In living organisms physiological processes occur with a periodicity of around 24 h (Bell-Pedersen *et al.*, 2005). The circadian light/dark cycle regulates sleep and wake periods, changes in body temperature, as well as hormone production in humans (Curtis *et al.*, 2014; Más and Yanovsky, 2009; Scheiermann *et al.*, 2013). Similarly, this periodicity affects hormone release, certain development processes, as well as the loss of substrates from seeds and roots in plants (Más and Yanovsky, 2009). Additionally, gene expression for defending against pathogens is decreased during the night (Bhardwaj *et al.*, 2011; Roden and Ingle, 2009). In summary, the circadian clock constitutes a complex network of metabolic, and immunological pathways across all living beings. The circadian system has a large impact on the regulation of infections and host-pathogen interactions (Barik, 2019). Therefore, it appears that the Pfr-form of the BphPs associated with darkness triggers the derepression of virulence gene expression in both plant as well as human pathogens. Essentially, it is reasonable for *P. aeruginosa* not to inhibit biofilm formation and production of virulence factors in the absence of light. The lack of light inside the human body can drive infections of the lung and other parts or tissues. Additionally, the bacteria have the ability to utilize light as an indication for detecting the highest efficacy of the host immune system. Therefore, it is advantageous for the pathogen to infect during the night to circumvent the host defenses (Mukherjee *et al.*, 2019). Effective infections of the plant pathogens *X. campestris*, *A. tumefaciens*, and *A. vitis* are also facilitated by maintaining virulence and flagella synthesis in the absence of light. The defense mechanism does not need to be evaded during the night since it is regulated by light and reaches its peak functionality during the day (Bonomi *et al.*,

2016). Nevertheless, it remains a fine-tuning system dependent on the incident light rather than an on/off system.

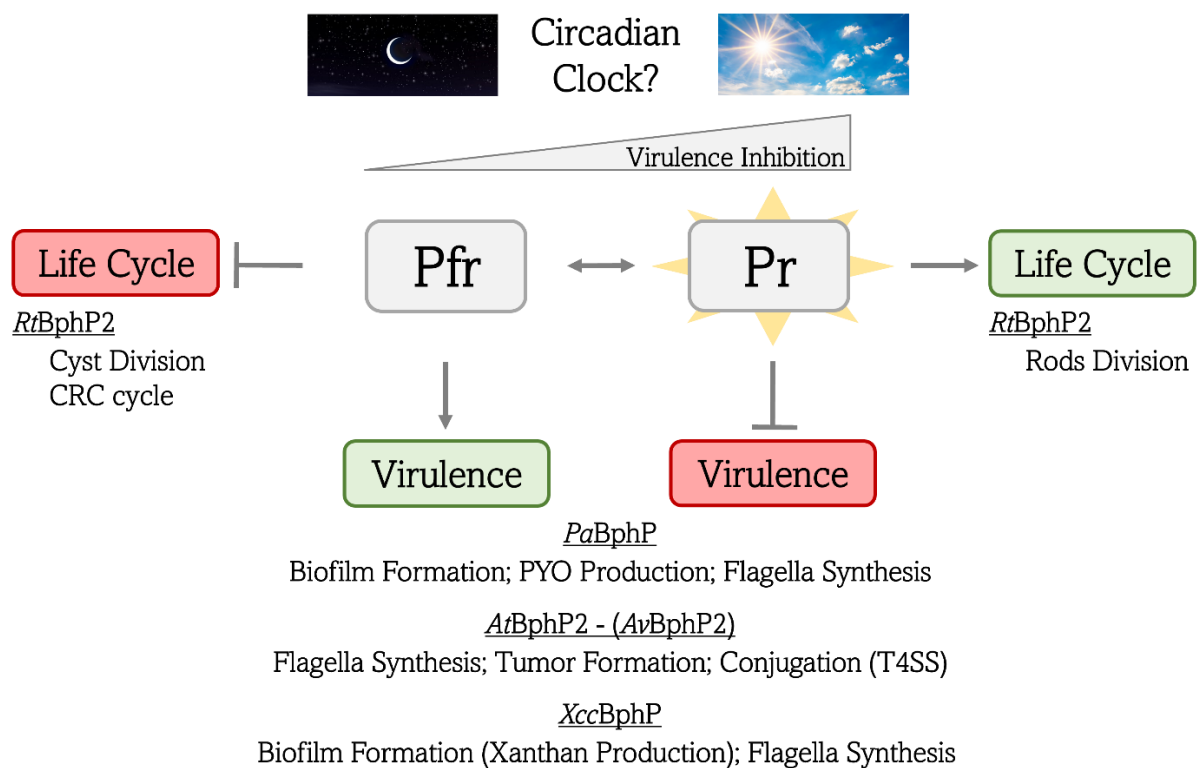


**Fig. 4.8: Bathy phytochromes negatively regulates *P. aeruginosa*, *A. tumefaciens*, *A. vitis* and *X. campestris* virulence in a light-dependent manner.**

Bathy BphPs inhibit bacterial virulence depending on the Pr/Pfr-fractions (represented by the gray virulence inhibition triangle) of the phytochrome population in the cells, with the Pr-form as the active form (demonstrated by the yellow star) and the Pfr- form as the inactive form. While the precise mechanism of regulatory pathways and detailed signaling are not completely comprehended, it is hypothesized that the Pr-form suppresses virulence (red box), whereas the Pfr-form halts inhibition, leading to increased virulence (green box). In *P. aeruginosa* a part of the regulation system is shown in Fig. 4.5 and for *X. campestris* some candidate genes involved in the regulation are derived from RNA-seq analysis (An *et al.*, 2020; Bonomi *et al.*, 2016). The light-triggered virulence downregulation in *P. aeruginosa* results in reduced biofilm formation, reduced PYO production and reduced flagellar synthesis, which is important for swimming motility; in *A. tumefaciens* and *A. vitis* it results in enhanced flagellar synthesis, which is important for host attachment, and reduced tumor formation, triggered by Ti plasmid conjugation; in *X. campestris* it results in decreased xanthan production and therefore lower rates of biofilm formation as well as enhanced flagella synthesis. In *R. tataouinensis* light seems to trigger the inhibition of cyst division and the cyst-rod-cyst (CRC) cycle, resulting in a life cycle with rods division (green box). The virulence of the bacteria is not inhibited over night to achieve optimal infection efficiency by avoiding the human or plant defense mechanisms, regulated by the circadian day/night cycle. If the bacteria possess an additional prototypical phytochrome (*AtBphP1*, *AvBphP1*, *RtBphP1*) or blue light sensors (*X. campestris*, *R. tataouinensis*) with potentially opposite functions, those are not incorporated in the model.

---

– A short excursion into the world of prototypical phytochromes –

Prototypical BphPs also regulate significant processes within their respective organisms. The phytochromes of the plant pathogen *P. syringae* demonstrate a light-triggered negative effect on swarming motility (Wu *et al.*, 2013). Additionally, both BphPs are associated with virulence inhibition and initiation, as they participate in lesion formation and colonization of plant tissues (McGrane and Beattie, 2017). The phytochrome of *D. radiodurans* contributes to the synthesis of the carotenoid deinoxanthin, which provides protection against UV radiation for the bacteria. The amount of the carotenoid is increased under red light exposure compared to far-red light or dark conditions (Davis *et al.*, 1999). The phytochromes *RpBphP2*, *RpBphP3* and *RpBphP4* from *Rhodospseudomonas palustris* as well as *BrBphP3* from *Bradyrhizobium* are involved in the regulation of their photosynthetic antenna complexes (Giraud and Verméglio, 2008). *BphG1* from *Rhodobacter sphaeroides* possesses a GGDEF- and EAL-output domain. Therefore, the phytochrome modulates c-di-GMP levels via its phosphodiesterase- and diguanylate cyclase activity, possibly also linked to virulence association (Tarutina *et al.*, 2006).

Intensive research is necessary to enhance comprehension of the signal transduction networks of bathy and prototypical phytochromes in various Proteobacteria. Although information on downstream elements, including RRs, additional kinases, or potential phosphatases, remains incomplete, further structural elucidation would reveal more about the signal transduction processes. If an organism possesses multiple phytochromes or other light-sensing proteins, its physiology necessitates an in-depth analysis from multiple perspectives while contextualizing the transduction mechanisms.



## 5 Summary

The ability to sense and respond to different environmental conditions allows living organisms to adapt quickly to their surroundings. In order to use light as a source of information, plants, fungi, and bacteria employ phytochromes. With their ability to detect far-red and red light, phytochromes constitute a major photoreceptor family. Bacterial phytochromes (BphPs) are composed of an apo-phytochrome and an open-chain tetrapyrrole, the chromophore biliverdin IX $\alpha$ , which mediates the photosensory properties. Depending on the photoexcitation and the quality of the incident light, phytochromes interconvert between two photoconvertible parental states: the red light-absorbing Pr-form and the far-red light-absorbing Pfr-form. In contrast to prototypical phytochromes, with a thermal stable Pr ground state, there is a group of bacterial phytochromes that exhibit dark reversion from the Pr- to the Pfr-form. These special proteins are classified as bathy phytochromes and range across different classes of bacteria. Moreover, the majority of BphPs act as sensor histidine kinases in two-component regulatory systems. The light-triggered conformational change results in the autophosphorylation of the histidine kinase domain and the transphosphorylation of an associated response regulator, inducing a cellular response. Spectroscopic analysis utilizing homologously produced protein identified *PaBphP*, the histidine kinase of the human opportunistic pathogen *Pseudomonas aeruginosa*, as a bathy phytochrome. Intensive research on *PaBphP* revealed evidence that the interconversion between its physiological active and inactive states is influenced by light and darkness rather than far-red and red light. In order to conduct a comprehensive systematic analysis, further bacterial phytochromes were investigated regarding their biochemical and spectroscopic behavior, as well as their autokinase activity. In addition to *PaBphP*, this work employs the bathy phytochromes *AtBphP2*, *AvBphP2*, *XccBphP* from the non-photosynthetic plant pathogens *Agrobacterium tumefaciens*, *Allorhizobium vitis*, *Xanthomonas campestris*, as well as *RtBphP2* from the soil bacterium *Ramlibacter tataouinensis*. All investigated BphPs displayed a bathy-typical behavior by developing a distinct Pr-form under far-red light conditions and undergoing dark reversion to their Pfr-form. Different Pr/Pfr-fractions can be identified among the BphP populations in varying natural light conditions, including red or blue light. The Pr-form is considered as the active form due to autophosphorylation activity in the heterologously produced phytochromes when exposed to light. In the absence of light, associated with the development of the Pfr-form, the phytochromes exhibited disabled or strongly reduced autokinase activity. Additionally, light-triggered phosphorylation was observed for the response regulator *PaAlgB*, which is linked to the phytochrome of

*P. aeruginosa*. This study presents the first comparative investigation of numerous bathy phytochromes under identical conditions. The work addressed a gap in the literature by providing quantitative correlation between kinase activity and calculated Pr/Pfr-fractions obtained from spectroscopic measurements. The biological role of *PaBphP* was partially elucidated through phenotypic characterization employing *P. aeruginosa* mutant and overexpression strains. The generation of a functional model was possible by considering the postulated functions of the other phytochromes found in the literature. In summary, bathy BphPs are hypothesized to modulate bacterial virulence according to the circadian day/night rhythm of their hosts. The pathogens are believed to reduce their virulence during daylight hours to evade immune and defense reactions, while increasing their virulence during the evening and night, enabling more effective infections.

## 6 Zusammenfassung

Die Fähigkeit zur Wahrnehmung und Reaktion auf verschiedenste Umweltbedingungen ermöglicht Lebewesen eine schnelle Anpassung an ihre Umgebung. Um Licht als Informationsquelle nutzen zu können, besitzen Pflanze, Pilze und Bakterien Phytochrome. Diese Proteine bilden eine wichtige Photorezeptorfamilie, da sie in der Lage sind rotes wie auch dunkelrotes Licht wahrzunehmen. Bakterielle Phytochrome (BphPs) bestehen aus einem Apo-Phytochrom, sowie einem offenkettigen Tetrapyrrol, dem Chromophor Biliverdin IX $\alpha$ , welches die photosensorischen Eigenschaften vermittelt. Phytochrome wandeln, je nach Photoanregung und Qualität des einfallendes Lichtes, zwischen zwei photokonvertierbaren Zuständen um: der Pr-Form, die in der Lage ist, rotes Licht zu absorbieren und der Pfr-Form, die zur Absorption von dunkelrotem Licht befähigt ist. Im Gegensatz zu prototypischen BphPs, die einen thermisch stabilen Pr-Grundzustand aufweisen, gibt es eine Gruppe von Bakteriophytochromen, welche im Dunkeln eine Reversion von der Pr- zur Pfr-Form zeigen. Diese speziellen BphP-Typen werden als *bathy* Phytochrome bezeichnet und sind in verschiedenen Bakterienklassen vorzufinden. Die meisten BphPs fungieren zudem als Sensorhistidinkinasen in regulatorischen Zweikomponentensystemen. Eine, durch Licht ausgelöste, Konformationsänderung führt sowohl zu einer Autophosphorylierung der Histidinkinase-Domäne als auch zur Transphosphorylierung eines zugehörigen Antwortregulators, wodurch eine zelluläre Antwort generiert wird. Spektroskopische Untersuchungen, mit homolog produziertem Protein, identifizierten die Histidinkinase *PaBphP* des humanen opportunistischen Pathogens *Pseudomonas aeruginosa* als *bathy* Phytochrome. Ausführliche Studien an *PaBphP* ergaben Hinweise darauf, dass der Wechsel zwischen dem physiologisch aktiven und inaktiven Zustand eher durch Licht und Dunkelheit, als durch rotes und dunkelrotes Licht beeinflusst wird. Um eine umfassende systematische Analyse durchzuführen, wurden weitere bakterielle Phytochrome auf ihr biochemisches und spektroskopisches Verhalten, sowie auf ihre Autokinase-Aktivität hin untersucht. In dieser Arbeit wurden, zusätzlich zu *PaBphP*, auch die *bathy* Phytochrome *AtBphP2*, *AvBphP2*, *XccBphP* aus den nicht-photosynthetischen Pflanzenpathogenen *Agrobacterium tumefaciens*, *Allorhizobium vitis*, *Xanthomonas campestris* und *RtBphP2* aus dem Bodenbakterium *Ramlibacter tataouinensis* betrachtet. Diese Phytochrome zeigten *bathy*-typisches Verhalten, durch die Ausbildung einer ausgeprägten Pr-Form unter dunkelroten Lichtbedingungen und ihrer Dunkelreversion zur Pfr-Form. Darüber hinaus sind unter natürlicherweise vorkommenden verschiedensten Lichtbedingungen, wie beispielsweise rotem oder blauem Licht, unterschiedlichste Pr/Pfr-Fractionen in den

BphP-Populationen festzustellen. Die Pr-Form kann als aktive Form definiert werden, da unter Lichteinfluss Autophosphorylierung für die heterolog produzierten Phytochrome beobachtet wurde. Unter Ausschluss von Licht, was mit der Ausbildung der Pfr-Form einhergeht, zeigten die Phytochrome keine oder stark reduzierte Autokinase-Aktivität. Außerdem wurde beim Antwortregulator *PaAlgB*, der mit dem Phytochrome aus *P. aeruginosa* im Zusammenhang steht, eine lichtabhängige Phosphorylierung festgestellt. Die vorliegende Arbeit präsentiert die erste Studie, die eine derart hohe Anzahl an *bathy* Phytochromen unter identischen definierten Bedingungen vergleicht. Die quantitative Korrelation der Kinase-Aktivität mit den kalkulierten Pr/Pfr-Fractionen, aus spektroskopischen Messungen, erlaubt neue Einblicke in die Funktionsweise dieses Phytochrom-Typ. Basierend auf den Ergebnissen von phänotypischen Charakterisierungen mittels *P. aeruginosa*-Mutanten und Überexpressionsstämmen lässt sich ein Teil der biologischen Rolle von *PaBphP* aufklären. Unter Berücksichtigung, der in der Literatur postulierten Bedeutung, der anderen Phytochromen wurde ein Funktionsmodell generiert. Zusammenfassend wird die Hypothese aufgestellt, dass *bathy* BphPs ihre Virulenz abhängig vom zirkadianen Tag-Nacht-Rhythmus ihres Wirts regulieren. Um im Laufe des Tages auftretende Immun- und Abwehrreaktionen zu umgehen, wird angenommen, dass die Pathogene ihre Virulenz entsprechend reduzieren. Erst im Verlauf des Abends und der Nacht werden die Bakterien wieder virulenter, um die effektivsten Infektionen zu ermöglichen.

---

## References

- Aaij, C. and Borst, P. (1972).** The gel electrophoresis of DNA. *Biochim. Biophys. Acta*, 269, 192-200.
- An, S. Q., Potnis, N., Dow, M., Vorhölter, F. J., He, Y. Q., Becker, A., Teper, D., Li, Y., Wang, N., Bleris, L. and Tang, J. L. (2020).** Mechanistic insights into host adaptation, virulence and epidemiology of the phytopathogen *Xanthomonas*. *FEMS Microbiol. Rev.*, 44, 1-32.
- Aravind, L. and Ponting, C. P. (1997).** The GAF domain: an evolutionary link between diverse phototransducing proteins. *Trends Biochem. Sci.*, 22, 458-9.
- Auldridge, M. E. and Forest, K. T. (2011).** Bacterial phytochromes: more than meets the light. *Crit. Rev. Biochem. Mol. Biol.*, 46, 67-88.
- Bai, Y., Rottwinkel, G., Feng, J., Liu, Y. and Lamparter, T. (2016).** Bacteriophytochromes control conjugation in *Agrobacterium fabrum*. *J. Photochem. Photobiol. B: Biol.*, 161, 192-9.
- Baker, A. W., Satyshur, K. A., Moreno Morales, N. and Forest, K. T. (2016).** Arm-in-arm response regulator dimers promote intermolecular signal transduction. *J. Bacteriol.*, 198, 1218-29.
- Barik, S. (2019).** Molecular interactions between pathogens and the circadian clock. *Int. J. Mol. Med.*, 20.
- Barkovits, K., Harms, A., Benkartek, C., Smart, J. L. and Frankenberg-Dinkel, N. (2008).** Expression of the phytochrome operon in *Pseudomonas aeruginosa* is dependent on the alternative sigma factor RpoS. *FEMS Microbiol. Lett.*, 280, 160-8.
- Barkovits, K., Schubert, B., Heine, S., Scheer, M. and Frankenberg-Dinkel, N. (2011).** Function of the bacteriophytochrome BphP in the RpoS/Las quorum-sensing network of *Pseudomonas aeruginosa*. *Microbiology (Reading)*, 157, 1651-1664.
- Baron, S. S. and Rowe, J. J. (1981).** Antibiotic action of pyocyanin. *Antimicrob. Agents Chemother.*, 20, 814-820.
- Bell-Pedersen, D., Cassone, V. M., Earnest, D. J., Golden, S. S., Hardin, P. E., Thomas, T. L. and Zoran, M. J. (2005).** Circadian rhythms from multiple oscillators: lessons from diverse organisms. *Nat. Rev. Genet.*, 6, 544-56.
- Bhardwaj, V., Meier, S., Petersen, L. N., Ingle, R. A. and Roden, L. C. (2011).** Defence responses of *Arabidopsis thaliana* to infection by *Pseudomonas syringae* are regulated by the circadian clock. *PLoS One*, 6, e26968.
- Bhoo, S. H., Davis, S. J., Walker, J., Karniol, B. and Vierstra, R. D. (2001).** Bacteriophytochromes are photochromic histidine kinases using a biliverdin chromophore. *Nature*, 414, 776-9.

- Bilici, K. (2020).** Phänotypische Analysen zur Funktion des Bakteriophytochroms *PaBphP* in *Pseudomonas aeruginosa* PA14. *TU Kaiserslautern: Masterarbeit*.
- Björling, A., Berntsson, O., Lehtivuori, H., Takala, H., Hughes, A. J., Panman, M., Hoernke, M., Niebling, S., Henry, L., Henning, R., Kosheleva, I., Chukharev, V., Tkachenko, N. V., Menzel, A., Newby, G., Khakhulin, D., Wulff, M., Ihalainen, J. A. and Westenhoff, S. (2016).** Structural photoactivation of a full-length bacterial phytochrome. *Sci, Adv.*, 2, e1600920.
- Blumenstein, A., Vienken, K., Tasler, R., Purschwitz, J., Veith, D., Frankenberg-Dinkel, N. and Fischer, R. (2005).** The *Aspergillus nidulans* phytochrome FphA represses sexual development in red light. *Curr. Biol.*, 15, 1833-8.
- Bonomi, H. R., Toum, L., Sycz, G., Sieira, R., Toscani, A. M., Gudesblat, G. E., Leskow, F. C., Goldbaum, F. A., Vojnov, A. A. and Malamud, F. (2016).** *Xanthomonas campestris* attenuates virulence by sensing light through a bacteriophytochrome photoreceptor. *EMBO Rep.*, 17, 1565-1577.
- Borges, A. L., Castro, B., Govindarajan, S., Solvik, T., Escalante, V. and Bondy-Denomy, J. (2020).** Bacterial alginate regulators and phage homologs repress CRISPR-Cas immunity. *Nat. Microbiol.*, 5, 679-687.
- Borthwick, H. A., Hendricks, S. B. and Parker, M. W. (1952a).** The reaction controlling floral initiation. *Proc. Natl. Acad. Sci. USA*, 38, 929-34.
- Borthwick, H. A., Hendricks, S. B., Parker, M. W., Toole, E. H. and Toole, V. K. (1952b).** A reversible photoreaction controlling seed germination. *Proc. Natl. Acad. Sci. USA*, 38, 662-6.
- Botelho, J., Grosso, F. and Peixe, L. (2019).** Antibiotic resistance in *Pseudomonas aeruginosa* - Mechanisms, epidemiology and evolution. *Drug Resist. Updat.*, 44, 100640.
- Boyd, A. and Chakrabarty, A. M. (1995).** *Pseudomonas aeruginosa* biofilms: role of the alginate exopolysaccharide. *J. Ind. Microbiol. Biotechnol.*, 15, 162-8.
- Bradley, D. E. (1980).** A function of *Pseudomonas aeruginosa* PAO polar pili: twitching motility. *Can. J. Microbiol.*, 26, 146-54.
- Braslavsky, S. E., Gärtner, W. and Schaffner, K. (1997).** Phytochrome photoconversion. *Plant Cell Environ.*, 20, 700-706.
- Burgie, E. S., Bussell, A. N., Walker, J. M., Dubiel, K. and Vierstra, R. D. (2014).** Crystal structure of the photosensing module from a red/far-red light-absorbing plant phytochrome. *Proc. Natl. Acad. Sci. USA*, 111, 10179-84.
- Burgie, E. S., Zhang, J. and Vierstra, R. D. (2016).** Crystal structure of *Deinococcus* phytochrome in the photoactivated state reveals a cascade of structural rearrangements during photoconversion. *Structure*, 24, 448-57.
- Burr, T. J. and Otten, L. (1999).** Crown gall of grape: biology and disease management. *Annu. Rev. Phytopathol.*, 37, 53-80.

- Butler, W. L., Norris, K. H., Siegelman, H. W. and Hendricks, S. B. (1959).** Detection, assay, and preliminary purification of the pigment controlling photoresponsive development of plants. *Proc. Natl. Acad. Sci. USA*, 45, 1703-8.
- Caignan, G. A., Deshmukh, R., Wilks, A., Zeng, Y., Huang, H. W., Moënné-Loccoz, P., Bunce, R. A., Eastman, M. A. and Rivera, M. (2002).** Oxidation of heme to  $\beta$ - and  $\delta$ -biliverdin by *Pseudomonas aeruginosa* heme oxygenase as a consequence of an unusual seating of the heme. *J. Am. Chem. Soc.*, 124, 14879-92.
- Casino, P., Miguel-Romero, L. and Marina, A. (2014).** Visualizing autophosphorylation in histidine kinases. *Nat. Commun.*, 5, 3258.
- Chan, J. W. Y. F. and Goodwin, P. H. (1999).** The molecular genetics of virulence of *Xanthomonas campestris*. *Biotechnol. Adv.*, 17, 489-508.
- Chand, N. S., Clatworthy, A. E. and Hung, D. T. (2012).** The two-component sensor KinB acts as a phosphatase to regulate *Pseudomonas aeruginosa* virulence. *J. Bacteriol.*, 194, 6537-47.
- Chand, N. S., Lee, J. S., Clatworthy, A. E., Golas, A. J., Smith, R. S. and Hung, D. T. (2011).** The sensor kinase KinB regulates virulence in acute *Pseudomonas aeruginosa* infection. *J. Bacteriol.*, 193, 2989-99.
- Chen, M., Chory, J. and Fankhauser, C. (2004).** Light signal transduction in higher plants. *Annu. Rev. Genet.*, 38, 87-117.
- Chernov, K. G., Redchuk, T. A., Omelina, E. S. and Verkhusha, V. V. (2017).** Near-infrared fluorescent proteins, biosensors, and optogenetic tools engineered from phytochromes. *Chem. Rev.*, 117, 6423-6446.
- Chilton, M. D., Drummond, M. H., Merio, D. J., Sciaky, D., Montoya, A. L., Gordon, M. P. and Nester, E. W. (1977).** Stable incorporation of plasmid DNA into higher plant cells: the molecular basis of crown gall tumorigenesis. *Cell*, 11, 263-71.
- Corral, J., Pérez-Varela, M., Barbé, J. and Aranda, J. (2020).** Direct interaction between RecA and a CheW-like protein is required for surface-associated motility, chemotaxis and the full virulence of *Acinetobacter baumannii* strain ATCC 17978. *Virulence*, 11, 315-326.
- Correa, F., Ko, W.-H., Ocasio, V., Bogomolni, R. A. and Gardner, K. H. (2013).** Blue light regulated two-component systems: enzymatic and functional analyses of light-oxygen-voltage (LOV)-histidine kinases and downstream response regulators. *Biochemistry*, 52, 4656-4666.
- Costa, K. C., Glasser, N. R., Conway, S. J. and Newman, D. K. (2017).** Pyocyanin degradation by a tautomerizing demethylase inhibits *Pseudomonas aeruginosa* biofilms. *Science*, 355, 170-173.

- Courtney, J. M., Bradley, J., Mccaughan, J., O'connor, T. M., Shortt, C., Bredin, C. P., Bradbury, I. and Elborn, J. S. (2007). Predictors of mortality in adults with cystic fibrosis. *Pediatr. Pulmonol.*, 42, 525-32.
- Cross, A. R. and Goldberg, J. B. (2019). Remodeling of O antigen in mucoid *Pseudomonas aeruginosa* via transcriptional repression of *wzz2*. *MBio*, 202, e00445-20.
- Curtis, A. M., Bellet, M. M., Sassone-Corsi, P. and O'Neill, L. A. (2014). Circadian clock proteins and immunity. *Immunity*, 40, 178-86.
- Dago, A. E., Schug, A., Procaccini, A., Hoch, J. A., Weigt, M. and Szurmant, H. (2012). Structural basis of histidine kinase autophosphorylation deduced by integrating genomics, molecular dynamics, and mutagenesis. *Proc. Natl. Acad. Sci. USA*, 109, E1733-42.
- Damron, F. H., Qiu, D. and Yu, H. D. (2009). The *Pseudomonas aeruginosa* sensor kinase KinB negatively controls alginate production through AlgW-dependent MucA proteolysis. *J. Bacteriol.*, 191, 2285-95.
- Dasgupta, N., Ferrell, E. P., Kanack, K. J., West, S. E. and Ramphal, R. (2002). *fleQ*, the gene encoding the major flagellar regulator of *Pseudomonas aeruginosa*, is  $\sigma^{70}$  dependent and is downregulated by Vfr, a homolog of *Escherichia coli* cyclic AMP receptor protein. *J. Bacteriol.*, 184, 5240-50.
- Davis, S. J., Vener, A. V. and Vierstra, R. D. (1999). Bacteriophytochromes: phytochrome-like photoreceptors from nonphotosynthetic eubacteria. *Science*, 286, 2517-20.
- De Lorenzo, V. and Timmis, K. N. (1994). Analysis and construction of stable phenotypes in gram-negative bacteria with Tn5- and Tn10-derived minitransposons. *Methods Enzymol.*, 235, 386-405.
- De Luca, G., Barakat, M., Ortet, P., Fochesato, S., Jourlin-Castelli, C., Ansaldi, M., Py, B., Fichant, G., Coutinho, P. M., Voulhoux, R., Bastien, O., Maréchal, E., Henrissat, B., Quentin, Y., Noirot, P., Filloux, A., Méjean, V., Dubow, M. S., Barras, F., Barbe, V., Weissenbach, J., Mihalcescu, I., Verméglio, A., Achouak, W. and Heulin, T. (2011). The cyst-dividing bacterium *Ramlibacter tataouinensis* TTB310 genome reveals a well-stocked toolbox for adaptation to a desert environment. *PLoS One*, 6, e23784.
- De Luca, G., Fochesato, S., Lavergne, J., Forest, K. T., Barakat, M., Ortet, P., Achouak, W., Heulin, T. and Verméglio, A. (2019). Light on the cell cycle of the non-photosynthetic bacterium *Ramlibacter tataouinensis*. *Sci. Rep.*, 9, 16505.
- Denig, L. M. (2020). Untersuchungen zum Einfluss der Temperatur auf das Phytochrom PaBpP von *Pseudomonas aeruginosa*. Rheinische Friedrichs-Wilhelms-Universität Bonn: Masterarbeit.
- Deretic, V., Leveau, J. H., Mohr, C. D. and Hibler, N. S. (1992). *In vitro* phosphorylation of AlgR, a regulator of mucoidy in *Pseudomonas aeruginosa*, by a histidine protein kinase and effects of small phospho-donor molecules. *Mol. Microbiol.*, 6, 2761-7.



- Dietrich, L. E., Okegbe, C., Price-Whelan, A., Sakhtah, H., Hunter, R. C. and Newman, D. K. (2013).** Bacterial community morphogenesis is intimately linked to the intracellular redox state. *J. Bacteriol.*, 195, 1371-80.
- Diggle, S. P. and Whiteley, M. (2020).** Microbe profile: *Pseudomonas aeruginosa*: opportunistic pathogen and lab rat. *Microbiology (Reading)*, 166, 30-33.
- Eilfeld, P. and Rüdiger, W. (1985).** Absorption spectra of phytochrome intermediates. *Z. Naturforsch.*, 40, 109-114.
- Essen, L. O., Mailliet, J. and Hughes, J. (2008).** The structure of a complete phytochrome sensory module in the Pr ground state. *Proc. Natl. Acad. Sci. USA*, 105, 14709-14.
- Fauvart, M., Phillips, P., Bachaspatimayum, D., Verstraeten, N., Fransaeer, J., Michiels, J. and Vermant, J. (2012).** Surface tension gradient control of bacterial swarming in colonies of *Pseudomonas aeruginosa*. *Soft Matter*, 8, 70-76.
- Fiedler, B., Börner, T. and Wilde, A. (2005).** Phototaxis in the cyanobacterium *Synechocystis* sp. PCC 6803: role of different photoreceptors. *Photochem. Photobiol.*, 81, 1481-8.
- Fiedler, B., Broc, D., Schubert, H., Rediger, A., Börner, T. and Wilde, A. (2004).** Involvement of cyanobacterial phytochromes in growth under different light qualities and quantities. *Photochem. Photobiol.*, 79, 551-5.
- Fitzsimmons, S. C. (1993).** The changing epidemiology of cystic fibrosis. *J. Pediatr.*, 122, 1-9.
- Frankenberg-Dinkel, N. (2004).** Bacterial heme oxygenases. *Antioxid. Redox Signal.*, 6, 825-34.
- Frankenberg, N., Mukougawa, K., Kohchi, T. and Lagarias, J. C. (2001).** Functional genomic analysis of the HY2 family of ferredoxin-dependent bilin reductases from oxygenic photosynthetic organisms. *Plant Cell*, 13, 965-978.
- Franklin, M. J., Nivens, D. E., Weadge, J. T. and Howell, P. L. (2011).** Biosynthesis of the *Pseudomonas aeruginosa* extracellular polysaccharides, alginate, Pel, and Psl. *Front Microbiol*, 2, 167.
- Fraser, G. M. and Hughes, C. (1999).** Swarming motility. *Curr. Opin. Microbiol.*, 2, 630-5.
- Friedheim, E. A. (1931).** Pyocyanine, an accessory respiratory enzyme. *J. Exp. Med.*, 54, 207-21.
- Fuller, K. K., Ringelberg, C. S., Loros, J. J. and Dunlap, J. C. (2013).** The fungal pathogen *Aspergillus fumigatus* regulates growth, metabolism, and stress resistance in response to light. *MBio*, 4, e00142-13.
- Furuya, M. (1993).** Phytochromes: their molecular species, gene families, and functions. *Annu. Rev. Plant Physiol. Plant Mol. Biol.*, 44, 617-645.

- Galperin, M. Y. (2006).** Structural classification of bacterial response regulators: diversity of output domains and domain combinations. *J. Bacteriol.*, 188, 4169-4182.
- Galperin, M. Y. (2010).** Diversity of structure and function of response regulator output domains. *Curr. Opin. Microbiol.*, 13, 150-159.
- Gao, R. and Stock, A. M. (2009).** Biological insights from structures of two-component proteins. *Annu. Rev. Microbiol.*, 63, 133-54.
- García-Domínguez, M., Muro-Pastor, M. I., Reyes, J. C. and Florencio, F. J. (2000).** Light-dependent regulation of cyanobacterial phytochrome expression. *J. Bacteriol.*, 182, 38-44.
- Gelvin, S. B. (2010).** Plant proteins involved in *Agrobacterium*-mediated genetic transformation. *Annu. Rev. Phytopathol.*, 48, 45-68.
- Gill, S. C. and Von Hippel, P. H. (1989).** Calculation of protein extinction coefficients from amino acid sequence data. *Anal. Biochem.*, 182, 319-26.
- Giraud, E., Fardoux, J., Fourrier, N., Hannibal, L., Genty, B., Bouyer, P., Dreyfus, B. and Verméglio, A. (2002).** Bacteriophytochrome controls photosystem synthesis in anoxygenic bacteria. *Nature*, 417, 202-205.
- Giraud, E. and Verméglio, A. (2008).** Bacteriophytochromes in anoxygenic photosynthetic bacteria. *Photosynth. Res.*, 97, 141-53.
- Giraud, E., Zappa, S., Vuillet, L., Adriano, J. M., Hannibal, L., Fardoux, J., Berthomieu, C., Bouyer, P., Pignol, D. and Verméglio, A. (2005).** A new type of bacteriophytochrome acts in tandem with a classical bacteriophytochrome to control the antennae synthesis in *Rhodospseudomonas palustris*. *J. Biol. Chem.*, 280, 32389-97.
- Goethe, J. W. (Farbenlehre).** 1950-55 Stuttgart (Kohlhammer), *Erstausgabe 1810*.
- Gooderham, W. J. and Hancock, R. E. (2009).** Regulation of virulence and antibiotic resistance by two-component regulatory systems in *Pseudomonas aeruginosa*. *FEMS Microbiol. Rev.*, 33, 279-94.
- Goodman, A. L., Kulasekara, B., Rietsch, A., Boyd, D., Smith, R. S. and Lory, S. (2004).** A signaling network reciprocally regulates genes associated with acute infection and chronic persistence in *Pseudomonas aeruginosa*. *Dev. Cell*, 7, 745-54.
- Gouterman, M. (1961).** Spectra of porphyrins. *J. Mol. Spectrosc.*, 6, 138-163.
- Govan, J. R. and Deretic, V. (1996).** Microbial pathogenesis in cystic fibrosis: mucoid *Pseudomonas aeruginosa* and *Burkholderia cepacia*. *Microbiol. Rev.*, 60, 539-74.
- Hahn, H. P. (1997).** The type-4 pilus is the major virulence-associated adhesin of *Pseudomonas aeruginosa*--a review. *Gene*, 192, 99-108.
- Haiko, J. and Westerlund-Wikström, B. (2013).** The role of the bacterial flagellum in adhesion and virulence. *Biology (Basel)*, 2, 1242-67.

- Hanahan, D. (1983).** Studies on transformation of *Escherichia coli* with plasmids. *J. Mol. Biol.*, 166, 557-80.
- Hancock, R. E. and Speert, D. P. (2000).** Antibiotic resistance in *Pseudomonas aeruginosa*: mechanisms and impact on treatment. *Drug Resist. Updat.*, 3, 247-255.
- Harshey, R. M. (1994).** Bees aren't the only ones: swarming in Gram-negative bacteria. *Mol. Microbiol.*, 13, 389-94.
- Hatfield, B. M., Lasarre, B., Liu, M., Dong, H., Nettleton, D. and Beattie, G. A. (2023).** Light cues induce protective anticipation of environmental water loss in terrestrial bacteria. *Proc. Natl. Acad. Sci. USA*, 120, e2309632120.
- He, J., Baldini, R. L., Déziel, E., Saucier, M., Zhang, Q., Liberati, N. T., Lee, D., Urbach, J., Goodman, H. M. and Rahme, L. G. (2004).** The broad host range pathogen *Pseudomonas aeruginosa* strain PA14 carries two pathogenicity islands harboring plant and animal virulence genes. *Proc. Natl. Acad. Sci. USA*, 101, 2530-5.
- Heine, S. (2014).** Das Phytochrom-Regulon und eine Phosphodiesterase als Beispiel zur Wahrnehmung von Umweltsignalen in *Pseudomonas aeruginosa*. *Ruhr-Universität Bochum: Dissertation*.
- Heirwegh, K. P., Blanckaert, N. and Van Hees, G. (1991).** Synthesis, chromatographic purification, and analysis of isomers of biliverdin IX and bilirubin IX. *Anal. Biochem.*, 195, 273-8.
- Hellingwerf, K. J. (2000).** Key issues in the photochemistry and signalling-state formation of photosensor proteins. *J. Photochem. Photobiol. B: Biol.*, 54, 94-102.
- Herrou, J., Crosson, S. and Fiebig, A. (2017).** Structure and function of HWE/HisKA2-family sensor histidine kinases. *Curr. Opin. Microbiol.*, 36, 47-54.
- Hershberger, C. D., Ye, R. W., Parsek, M. R., Xie, Z. D. and Chakrabarty, A. M. (1995).** The *algT* (*algU*) gene of *Pseudomonas aeruginosa*, a key regulator involved in alginate biosynthesis, encodes an alternative  $\sigma$  factor ( $\sigma^E$ ). *Proc. Natl. Acad. Sci. USA*, 92, 7941-5.
- Heulin, T., Barakat, M., Christen, R., Lesourd, M., Sutra, L., De Luca, G. and Achouak, W. (2003).** *Ramlibacter tataouinensis* gen. nov., sp. nov., and *Ramlibacter henchirensis* sp. nov., cyst-producing bacteria isolated from subdesert soil in Tunisia. *Int. J. Syst. Evol. Microbiol.*, 53, 589-594.
- Hmelo, L. R., Borlee, B. R., Almblad, H., Love, M. E., Randall, T. E., Tseng, B. S., Lin, C., Irie, Y., Storek, K. M., Yang, J. J., Siehnel, R. J., Howell, P. L., Singh, P. K., Tolker-Nielsen, T., Parsek, M. R., Schweizer, H. P. and Harrison, J. J. (2015).** Precision-engineering the *Pseudomonas aeruginosa* genome with two-step allelic exchange. *Nat. Protoc.*, 10, 1820-1841.
- Ho, Y. S., Burden, L. M. and Hurley, J. H. (2000).** Structure of the GAF domain, a ubiquitous signaling motif and a new class of cyclic GMP receptor. *EMBO J.*, 19, 5288-99.

- Idnurm, A. (2013).** Light sensing in *Aspergillus fumigatus* highlights the case for establishing new models for fungal photobiology. *MBio*, 4, e00260-13.
- Ikeuchi, M. and Ishizuka, T. (2008).** Cyanobacteriochromes: a new superfamily of tetrapyrrole-binding photoreceptors in cyanobacteria. *Photochem. Photobiol. Sci.*, 7, 1159-1167.
- Intile, P. J., Diaz, M. R., Urbanowski, M. L., Wolfgang, M. C. and Yahr, T. L. (2014).** The AlgZR two-component system recalibrates the RsmAYZ posttranscriptional regulatory system to inhibit expression of the *Pseudomonas aeruginosa* type III secretion system. *J. Bacteriol.*, 196, 357-66.
- Irie, Y., Starkey, M., Edwards, A. N., Wozniak, D. J., Romeo, T. and Parsek, M. R. (2010).** *Pseudomonas aeruginosa* biofilm matrix polysaccharide Psl is regulated transcriptionally by RpoS and post-transcriptionally by RsmA. *Mol. Microbiol.*, 78, 158-72.
- Isaksson, L., Gustavsson, E., Persson, C., Brath, U., Vrhovac, L., Karlsson, G., Orekhov, V. and Westenhoff, S. (2021).** Signaling mechanism of phytochromes in solution. *Structure*, 29, 151-160.e3.
- Jacob-Dubuisson, F., Mechaly, A., Betton, J.-M. and Antoine, R. (2018).** Structural insights into the signalling mechanisms of two-component systems. *Nat. Rev. Microbiol.*, 16, 585-593.
- Jo, J., Price-Whelan, A. and Dietrich, L. E. P. (2022).** Gradients and consequences of heterogeneity in biofilms. *Nat. Rev. Microbiol.*, 20, 593-607.
- Jones, C. J., Newsom, D., Kelly, B., Irie, Y., Jennings, L. K., Xu, B., Limoli, D. H., Harrison, J. J., Parsek, M. R., White, P. and Wozniak, D. J. (2014).** ChIP-Seq and RNA-Seq reveal an AmrZ-mediated mechanism for cyclic di-GMP synthesis and biofilm development by *Pseudomonas aeruginosa*. *PLoS Pathog.*, 10, e1003984.
- Josts, I., Veith, K. and Tidow, H. (2019).** Ternary structure of the outer membrane transporter FoxA with resolved signalling domain provides insights into TonB-mediated siderophore uptake. *eLife*, 8, e48528.
- Jung, J. H., Domijan, M., Klose, C., Biswas, S., Ezer, D., Gao, M., Khattak, A. K., Box, M. S., Charoensawan, V., Cortijo, S., Kumar, M., Grant, A., Locke, J. C., Schäfer, E., Jaeger, K. E. and Wigge, P. A. (2016).** Phytochromes function as thermosensors in *Arabidopsis*. *Science*, 354, 886-889.
- Kahl, L. J., Price-Whelan, A. and Dietrich, L. E. P. (2020).** Light-mediated decreases in cyclic di-GMP levels inhibit structure formation in *Pseudomonas aeruginosa* biofilms. *J. Bacteriol.*, 202.
- Kamlet, M. J. and Taft, R. W. (1976).** The solvatochromic comparison method. I. The  $\beta$ -scale of solvent hydrogen-bond acceptor (HBA) basicities. *J. Am. Chem. Soc.*, 98, 377-383.

- Karniol, B. and Vierstra, R. D. (2003).** The pair of bacteriophytochromes from *Agrobacterium tumefaciens* are histidine kinases with opposing photobiological properties. *Proc. Natl. Acad. Sci. USA*, 100, 2807-12.
- Karniol, B. and Vierstra, R. D. (2004).** The HWE histidine kinases, a new family of bacterial two-component sensor kinases with potentially diverse roles in environmental signaling. *J. Bacteriol.*, 186, 445-53.
- Karniol, B., Wagner, J. R., Walker, J. M. and Vierstra, R. D. (2005).** Phylogenetic analysis of the phytochrome superfamily reveals distinct microbial subfamilies of photoreceptors. *Biochem. J.*, 392, 103-16.
- Khoury, A. E., Lam, K., Ellis, B. and Costerton, J. W. (1992).** Prevention and control of bacterial infections associated with medical devices. *ASAIO J.*, 38, M174-8.
- Kim, H. S., Willett, J. W., Jain-Gupta, N., Fiebig, A. and Crosson, S. (2014).** The *Brucella abortus* virulence regulator, LovhK, is a sensor kinase in the general stress response signalling pathway. *Mol. Microbiol.*, 94, 913-25.
- Kimbara, K. and Chakrabarty, A. M. (1989).** Control of alginate synthesis in *Pseudomonas aeruginosa*: regulation of the *algR1* gene. *Biochem. Biophys. Res. Commun.*, 164, 601-8.
- Klinke, S., Otero, L. H., Rinaldi, J., Sosa, S., Guimarães, B. G., Shepard, W. E., Goldbaum, F. A. and Bonomi, H. R. (2014).** Crystallization and preliminary X-ray characterization of the full-length bacteriophytochrome from the plant pathogen *Xanthomonas campestris* pv. *campestris*. *Acta Crystallogr. F Struct. Biol.*, 70, 1636-9.
- Klockgether, J., Cramer, N., Wiehlmann, L., Davenport, C. F. and Tümmler, B. (2011).** *Pseudomonas aeruginosa* genomic structure and diversity. *Front. Microbiol.*, 2, 150.
- Köhler, T., Curty, L. K., Barja, F., Van Delden, C. and Pechère, J. C. (2000).** Swarming of *Pseudomonas aeruginosa* is dependent on cell-to-cell signaling and requires flagella and pili. *J. Bacteriol.*, 182, 5990-6.
- Kolukisaoglu, H. Ü., Marx, S., Wiegmann, C., Hanelt, S. and Schneider-Poetsch, H. a. W. (1995).** Divergence of the phytochrome gene family predates angiosperm evolution and suggests that *Selaginella* and *Equisetum* arose prior to *Psilotum*. *J. Mol. Evol.*, 41, 329-337.
- Kottke, T., Xie, A., Larsen, D. S. and Hoff, W. D. (2018).** Photoreceptors take charge: emerging principles for light sensing. *Annu Rev Biophys.*, 47, 291-313.
- Laemmli, U. K. (1970).** Cleavage of structural proteins during the assembly of the head of bacteriophage T4. *Nature*, 227, 680-685.
- Lagarias, D. M., Wu, S.-H. and Lagarias, J. C. (1995).** Atypical phytochrome gene structure in the green alga *Mesotaenium caldariorum*. *Plant Mol. Biol.*, 29, 1127-1142.
- Lagarias, J. C. and Lagarias, D. M. (1989).** Self-assembly of synthetic phytochrome holoprotein *in vitro*. *Proc. Natl. Acad. Sci. USA*, 86, 5778-80.

- Lamparter, T., Krauß, N. and Scheerer, P. (2017).** Phytochromes from *Agrobacterium fabrum*. *Photochem. Photobiol.*, 93, 642-655.
- Lamparter, T. and Michael, N. (2005).** *Agrobacterium* phytochrome as an enzyme for the production of ZZE bilins. *Biochemistry*, 44, 8461-9.
- Lamparter, T., Michael, N., Caspani, O., Miyata, T., Shirai, K. and Inomata, K. (2003).** Biliverdin binds covalently to *Agrobacterium phytochrome* Agp1 via its ring A vinyl side chain. *J. Biol. Chem.*, 278, 33786-92.
- Lamparter, T., Michael, N., Mittmann, F. and Esteban, B. (2002).** Phytochrome from *Agrobacterium tumefaciens* has unusual spectral properties and reveals an N-terminal chromophore attachment site. *Proc. Natl. Acad. Sci. USA*, 99, 11628-11633.
- Lamparter, T., Xue, P., Elkurdi, A., Kaeser, G., Sauthof, L., Scheerer, P. and Krauß, N. (2021).** Phytochromes in *Agrobacterium fabrum*. *Front. Plant Sci.*, 12, 642801.
- Lau, G. W., Hassett, D. J., Ran, H. and Kong, F. (2004).** The role of pyocyanin in *Pseudomonas aeruginosa* infection. *Trends Mol. Med.*, 10, 599-606.
- Lee, S. J., Kim, T. W., Kim, J. G., Yang, C., Yun, S. R., Kim, C., Ren, Z., Kumarapperuma, I., Kuk, J., Moffat, K., Yang, X. and Ihee, H. (2022).** Light-induced protein structural dynamics in bacteriophytochrome revealed by time-resolved X-ray solution scattering. *Sci. Adv.*, 8, eabm6278.
- Leech, A. J., Sprinkle, A., Wood, L., Wozniak, D. J. and Ohman, D. E. (2008).** The NtrC family regulator AlgB, which controls alginate biosynthesis in mucoid *Pseudomonas aeruginosa*, binds directly to the *algD* promoter. *J. Bacteriol.*, 190, 581-9.
- Legris, M., Nieto, C., Sellaro, R., Prat, S. and Casal, J. J. (2017).** Perception and signalling of light and temperature cues in plants. *Plant J.*, 90, 683-697.
- Li, L. and Lagarias, J. C. (1992).** Phytochrome assembly. Defining chromophore structural requirements for covalent attachment and photoreversibility. *J. Biol. Chem.*, 267, 19204-19210.
- Little, A. S., Okkotsu, Y., Reinhart, A. A., Damron, F. H., Barbier, M., Barrett, B., Oglesby-Sherrouse, A. G., Goldberg, J. B., Cody, W. L., Schurr, M. J., Vasil, M. L. and Schurr, M. J. (2018).** *Pseudomonas aeruginosa* AlgR phosphorylation status differentially regulates pyocyanin and pyoverdine production. *MBio*, 9, e02318-17.
- Liu, S., Gunawan, C., Barraud, N., Rice, S. A., Harry, E. J. and Amal, R. (2016).** Understanding, monitoring, and controlling biofilm growth in drinking water distribution systems. *Environ. Sci. Technol.*, 50, 8954-76.
- Lu, C., Maurer, C. K., Kirsch, B., Steinbach, A. and Hartmann, R. W. (2014).** Overcoming the unexpected functional inversion of a PqsR antagonist in *Pseudomonas aeruginosa*: an *in vivo* potent antivirulence agent targeting *pqs* quorum sensing. *Angew. Chem., Int. Ed.*, 53, 1109-1112.

- Lyczak, J. B., Cannon, C. L. and Pier, G. B. (2000).** Establishment of *Pseudomonas aeruginosa* infection: lessons from a versatile opportunist. *Microbes Infect.*, 2, 1051-60.
- Ma, S., Selvaraj, U., Ohman, D. E., Quarless, R., Hassett, D. J. and Wozniak, D. J. (1998).** Phosphorylation-independent activity of the response regulators AlgB and AlgR in promoting alginate biosynthesis in mucoid *Pseudomonas aeruginosa*. *J. Bacteriol.*, 180, 956-68.
- Ma, S., Wozniak, D. J. and Ohman, D. E. (1997).** Identification of the histidine protein kinase KinB in *Pseudomonas aeruginosa* and its phosphorylation of the alginate regulator AlgB. *J. Biol. Chem.*, 272, 17952-60.
- Macaluso, V., Salvadori, G., Cupellini, L. and Mennucci, B. (2021).** The structural changes in the signaling mechanism of bacteriophytochromes in solution revealed by a multiscale computational investigation. *Chem. Sci.*, 12, 5555-5565.
- Martin, D. W., Schurr, M. J., Mudd, M. H., Govan, J. R., Holloway, B. W. and Deretic, V. (1993).** Mechanism of conversion to mucoidy in *Pseudomonas aeruginosa* infecting cystic fibrosis patients. *Proc. Natl. Acad. Sci. USA*, 90, 8377-81.
- Más, P. and Yanovsky, M. J. (2009).** Time for circadian rhythms: plants get synchronized. *Curr. Opin. Plant Biol.*, 12, 574-9.
- Mascher, T., Helmann, J. D. and Uden, G. (2006).** Stimulus perception in bacterial signal-transducing histidine kinases. *Microbiol. Mol. Biol. Rev.*, 70, 910-38.
- Mathews, S. (2006).** Phytochrome-mediated development in land plants: red light sensing evolves to meet the challenges of changing light environments. *Mol. Ecol.*, 15, 3483-503.
- McGrane, R. and Beattie, G. A. (2017).** *Pseudomonas syringae* pv. *syringae* B728a regulates multiple stages of plant colonization via the bacteriophytochrome BphP1. *MBio*, 8, e01178-17.
- Miyata, M., Robinson, R. C., Uyeda, T. Q. P., Fukumori, Y., Fukushima, S. I., Haruta, S., Homma, M., Inaba, K., Ito, M., Kaito, C., Kato, K., Kenri, T., Kinoshita, Y., Kojima, S., Minamino, T., Mori, H., Nakamura, S., Nakane, D., Nakayama, K., Nishiyama, M., Shibata, S., Shimabukuro, K., Tamakoshi, M., Taoka, A., Tashiro, Y., Tulum, I., Wada, H. and Wakabayashi, K. I. (2020).** Tree of motility - A proposed history of motility systems in the tree of life. *Genes Cells*, 25, 6-21.
- Möglich, A. (2019).** Signal transduction in photoreceptor histidine kinases. *Protein Sci.*, 28, 1923-1946.
- Montgomery, B. L. and Lagarias, J. C. (2002).** Phytochrome ancestry: sensors of bilins and light. *Trends Plant Sci.*, 7, 357-66.
- Mooney, J. L. and Yager, L. N. (1990).** Light is required for conidiation in *Aspergillus nidulans*. *Genes Dev.*, 4, 1473-82.

- Moradali, M. F., Ghods, S. and Rehm, B. H. (2017).** *Pseudomonas aeruginosa* lifestyle: a paradigm for adaptation, survival, and persistence. *Front. Cell. Infect. Microbiol.*, 7, 39.
- Mouriño, S., Giardina, B. J., Reyes-Caballero, H. and Wilks, A. (2016).** Metabolite-driven regulation of heme uptake by the biliverdin IX $\beta$ / $\delta$ -selective heme oxygenase (HemO) of *Pseudomonas aeruginosa*. *J. Biol. Chem.*, 291, 20503-15.
- Mousavi, S. A., Österman, J., Wahlberg, N., Nesme, X., Lavire, C., Vial, L., Paulin, L., De Lajudie, P. and Lindström, K. (2014).** Phylogeny of the *Rhizobium*–*Allorhizobium*–*Agrobacterium* clade supports the delineation of *Neorhizobium* gen. nov. *Syst. Appl. Microbiol.*, 37, 208-215.
- Mousavi, S. A., Willems, A., Nesme, X., De Lajudie, P. and Lindström, K. (2015).** Revised phylogeny of *Rhizobiaceae*: proposal of the delineation of *Pararhizobium* gen. nov., and 13 new species combinations. *Syst. Appl. Microbiol.*, 38, 84-90.
- Mukherjee, S., Jemielita, M., Stergioula, V., Tikhonov, M. and Bassler, B. L. (2019).** Photosensing and quorum sensing are integrated to control *Pseudomonas aeruginosa* collective behaviors. *PLoS Biol.*, 17, e3000579.
- Mullis, K. B. and Faloona, F. A. (1987).** Specific synthesis of DNA *in vitro* via a polymerase-catalyzed chain reaction. *Meth. Enzymol.*, 155, 335-350.
- Multamäki, E., Nanekar, R., Morozov, D., Lievonen, T., Golonka, D., Wahlgren, W. Y., Stucki-Buchli, B., Rossi, J., Hytönen, V. P., Westenhoff, S., Ihalainen, J. A., Möglich, A. and Takala, H. (2021).** Comparative analysis of two paradigm bacteriophytochromes reveals opposite functionalities in two-component signaling. *Nat. Commun.*, 12, 4394.
- Murray, T. S., Egan, M. and Kazmierczak, B. I. (2007).** *Pseudomonas aeruginosa* chronic colonization in cystic fibrosis patients. *Curr. Opin. Pediatr.*, 19, 83-8.
- Njimon, I. and Lamparter, T. (2011).** Temperature effects on *Agrobacterium* phytochrome Agp1. *PLoS One*, 6, e25977.
- O'Toole, G. A. and Kolter, R. (1998).** Flagellar and twitching motility are necessary for *Pseudomonas aeruginosa* biofilm development. *Mol. Microbiol.*, 30, 295-304.
- Oberpichler, I., Rosen, R., Rasouly, A., Vugman, M., Ron, E. Z. and Lamparter, T. (2008).** Light affects motility and infectivity of *Agrobacterium tumefaciens*. *Environ. Microbiol.*, 10, 2020-9.
- Okegbe, C., Fields, B. L., Cole, S. J., Beierschmitt, C., Morgan, C. J., Price-Whelan, A., Stewart, R. C., Lee, V. T. and Dietrich, L. E. P. (2017).** Electron-shuttling antibiotics structure bacterial communities by modulating cellular levels of c-di-GMP. *Proc. Natl. Acad. Sci. USA*, 114, E5236-e5245.
- Ophel, K. and Kerr, A. (1990).** *Agrobacterium vitis* sp. nov. for strains of *Agrobacterium* biovar 3 from grapevines. *Int. J. Syst. Evol. Microbiol.*, 40, 236-241.



- Otero, L. H., Foscaldi, S., Antelo, G. T., Rosano, G. L., Sirigu, S., Klinke, S., Defelipe, L. A., Sánchez-Lamas, M., Battocchio, G., Conforte, V., Vojnov, A. A., Chavas, L. M. G., Goldbaum, F. A., Mroginski, M. A., Rinaldi, J. and Bonomi, H. R. (2021). Structural basis for the Pr-Pfr long-range signaling mechanism of a full-length bacterial phytochrome at the atomic level. *Sci. Adv.*, 7, eabh1097.
- Otero, L. H., Klinke, S., Rinaldi, J., Velázquez-Escobar, F., Mroginski, M. A., Fernández López, M., Malamud, F., Vojnov, A. A., Hildebrandt, P., Goldbaum, F. A. and Bonomi, H. R. (2016). Structure of the full-length bacteriophytochrome from the plant pathogen *Xanthomonas campestris* provides clues to its long-range signaling mechanism. *J. Mol. Biol.*, 428, 3702-20.
- Overhage, J., Campisano, A., Bains, M., Torfs, E. C., Rehm, B. H. and Hancock, R. E. (2008). Human host defense peptide LL-37 prevents bacterial biofilm formation. *Infect. Immun.*, 76, 4176-82.
- Papiz, M. Z., Bellini, D., Evans, K., Grossmann, J. G. and Fordham-Skelton, T. (2019). Light-induced complex formation of bacteriophytochrome RpBphP1 and gene repressor RpPpsR2 probed by SAXS. *FEBS J.*, 286, 4261-4277.
- Parkinson, J. S. (1993). Signal transduction schemes of bacteria. *Cell*, 73, 857-71.
- Parkinson, J. S. (2010). Signaling mechanisms of HAMP domains in chemoreceptors and sensor kinases. *Annu. Rev. Microbiol.*, 64, 101-122.
- Pepe, I. M. (1999). Rhodopsin and phototransduction. *J. Photochem. Photobiol. B: Biol.*, 48, 1-10.
- Perry, J., Koteva, K. and Wright, G. (2011). Receptor domains of two-component signal transduction systems. *Mol. Biosyst.*, 7, 1388-98.
- Piatkevich, K. D., Subach, F. V. and Verkhusha, V. V. (2013). Far-red light photoactivatable near-infrared fluorescent proteins engineered from a bacterial phytochrome. *Nat. Commun.*, 4, 2153.
- Pierson, L. S. and Pierson, E. A. (2010). Metabolism and function of phenazines in bacteria: impacts on the behavior of bacteria in the environment and biotechnological processes. *Appl. Microbiol. Biotechnol.*, 86, 1659-1670.
- Price-Whelan, A., Dietrich, L. E. and Newman, D. K. (2007). Pyocyanin alters redox homeostasis and carbon flux through central metabolic pathways in *Pseudomonas aeruginosa* PA14. *J. Bacteriol.*, 189, 6372-81.
- Qian, C., Wong, C. C., Swarup, S. and Chiam, K. H. (2013). Bacterial tethering analysis reveals a "run-reverse-turn" mechanism for *Pseudomonas* species motility. *Appl. Environ. Microbiol.*, 79, 4734-43.
- Qiu, D., Damron, F. H., Mima, T., Schweizer, H. P. and Yu, H. D. (2008). P<sub>BAD</sub>-based shuttle vectors for functional analysis of toxic and highly regulated genes in *Pseudomonas* and *Burkholderia* spp. and other bacteria. *Appl. Environ. Microbiol.*, 74, 7422-6.

- Quest, B., Hübschmann, T., Sharda, S., Tandeau De Marsac, N. and Gärtner, W. (2007).** Homologous expression of a bacterial phytochrome. The cyanobacterium *Fremyella diplosiphon* incorporates biliverdin as a genuine, functional chromophore. *FEBS J.*, 274, 2088-98.
- Rahme, L. G., Stevens, E. J., Wolfort, S. F., Shao, J., Tompkins, R. G. and Ausubel, F. M. (1995).** Common virulence factors for bacterial pathogenicity in plants and animals. *Science*, 268, 1899-902.
- Ratliff, M., Zhu, W., Deshmukh, R., Wilks, A. and Stojiljkovic, I. (2001).** Homologues of neisserial heme oxygenase in Gram-negative bacteria: degradation of heme by the product of the *pigA* gene of *Pseudomonas aeruginosa*. *J. Bacteriol.*, 183, 6394-403.
- Rietsch, A., Vallet-Gely, I., Dove, S. L. and Mekalanos, J. J. (2005).** ExsE, a secreted regulator of type III secretion genes in *Pseudomonas aeruginosa*. *Proc. Natl. Acad. Sci. USA*, 102, 8006-11.
- Rinaldi, J., Arrar, M., Sycz, G., Cerutti, M. L., Berguer, P. M., Paris, G., Estrín, D. A., Martí, M. A., Klinke, S. and Goldbaum, F. A. (2016).** Structural insights into the HWE histidine kinase family: the *Brucella* blue light-activated histidine kinase domain. *J. Mol. Biol.*, 428, 1165-1179.
- Rivera, M. and Zeng, Y. (2005).** Heme oxygenase, steering dioxygen activation toward heme hydroxylation. *J. Inorg. Biochem.*, 99, 337-54.
- Rockwell, N. C. and Lagarias, J. C. (2010).** A brief history of phytochromes. *Chemphyschem*, 11, 1172-80.
- Rockwell, N. C., Su, Y. S. and Lagarias, J. C. (2006).** Phytochrome structure and signaling mechanisms. *Annu. Rev. Plant Biol.*, 57, 837-58.
- Roden, L. C. and Ingle, R. A. (2009).** Lights, rhythms, infection: the role of light and the circadian clock in determining the outcome of plant-pathogen interactions. *Plant Cell*, 21, 2546-52.
- Rodrigue, A., Quentin, Y., Lazdunski, A., Méjean, V. and Foglino, M. (2000).** Two-component systems in *Pseudomonas aeruginosa*: why so many? *Trends Microbiol.*, 8, 498-504.
- Röhrig, J., Kastner, C. and Fischer, R. (2013).** Light inhibits spore germination through phytochrome in *Aspergillus nidulans*. *Curr. Genet.*, 59, 55-62.
- Rottwinkel, G., Oberpichler, I. and Lamparter, T. (2010).** Bathy phytochromes in rhizobial soil bacteria. *J. Bacteriol.*, 192, 5124-5133.
- Russo, F. D. and Silhavy, T. J. (1993).** The essential tension: opposed reactions in bacterial two-component regulatory systems. *Trends Microbiol.*, 1, 306-10.

- Sánchez-Arreguin, J. A., Cabrera-Ponce, J. L., León-Ramírez, C. G., Camargo-Escalante, M. O. and Ruiz-Herrera, J. (2020).** Analysis of the photoreceptors involved in the light-depending basidiocarp formation in *Ustilago maydis*. *Arch. Microbiol.*, 202, 93-103.
- Sanger, F., Air, G. M., Barrell, B. G., Brown, N. L., Coulson, A. R., Fiddes, C. A., Hutchison, C. A., Slocombe, P. M. and Smith, M. (1977a).** Nucleotide sequence of bacteriophage  $\phi$  X174 DNA. *Nature*, 265, 687-95.
- Sanger, F., Nicklen, S. and Coulson, A. R. (1977b).** DNA sequencing with chain-terminating inhibitors. *Proc. Natl. Acad. Sci. USA*, 74, 5463-7.
- Scheerer, P., Michael, N., Park, J. H., Nagano, S., Choe, H. W., Inomata, K., Borucki, B., Krauss, N. and Lamparter, T. (2010).** Light-induced conformational changes of the chromophore and the protein in phytochromes: bacterial phytochromes as model systems. *Chemphyschem*, 11, 1090-105.
- Scheiermann, C., Kunisaki, Y. and Frenette, P. S. (2013).** Circadian control of the immune system. *Nat. Rev. Immunol.*, 13, 190-8.
- Schmidt, A., Sauthof, L., Szczepek, M., Lopez, M. F., Escobar, F. V., Qureshi, B. M., Michael, N., Buhrke, D., Stevens, T., Kwiatkowski, D., Von Stetten, D., Mroginski, M. A., Krauß, N., Lamparter, T., Hildebrandt, P. and Scheerer, P. (2018).** Structural snapshot of a bacterial phytochrome in its functional intermediate state. *Nat. Commun.*, 9, 4912.
- Schneckmann, T. (2021).** Untersuchungen zu Bestandteilen des Zweikomponentensystems um die Sensor kinase BphP in *Pseudomonas aeruginosa*. *TU Kaiserslautern: Bachelorarbeit*.
- Schultheiß, I. (2023).** Untersuchung zur Photobiologie verschiedener bathy Phytochrome. *RPTU Kaiserslautern-Landau: Masterarbeit*.
- Schumacher, J. (2017).** How light affects the life of *Botrytis*. *Fungal Genet. Biol.*, 106, 26-41.
- Shah, R., Pathak, G., Drepper, T. and Gärtner, W. (2016).** Selective photoreceptor gene knock-out reveals a regulatory role for the growth behavior of *Pseudomonas syringae*. *Photochem. Photobiol.*, 92, 571-8.
- Shah, R., Schwach, J., Frankenberg-Dinkel, N. and Gärtner, W. (2012).** Complex formation between heme oxygenase and phytochrome during biosynthesis in *Pseudomonas syringae* pv. *tomato*. *Photochem. Photobiol. Sci.*, 11, 1026-31.
- Sharrock, R. A. and Quail, P. H. (1989).** Novel phytochrome sequences in *Arabidopsis thaliana*: structure, evolution, and differential expression of a plant regulatory photoreceptor family. *Genes Dev.*, 3, 1745-57.
- Siegelman, H. W. and Firer, E. M. (1964).** Purification of phytochrome from oat seedlings. *Biochemistry*, 3, 418-423.

- Spiers, A. J., Buckling, A. and Rainey, P. B. (2000).** The causes of *Pseudomonas* diversity. *Microbiology (Reading)*, 146 ( Pt 10), 2345-2350.
- Stacey, S. D. and Pritchett, C. L. (2016).** *Pseudomonas aeruginosa* AlgU contributes to posttranscriptional activity by increasing *rsmA* expression in a *mucA22* strain. *J. Bacteriol.*, 198, 1812-1826.
- Stewart, R. C. (2010).** Protein histidine kinases: assembly of active sites and their regulation in signaling pathways. *Curr. Opin. Microbiol.*, 13, 133-141.
- Stock, A. M., Robinson, V. L. and Goudreau, P. N. (2000).** Two-component signal transduction. *Annu. Rev. Biochem.*, 69, 183-215.
- Stover, C. K., Pham, X. Q., Erwin, A. L., Mizoguchi, S. D., Warrenner, P., Hickey, M. J., Brinkman, F. S. L., Hufnagle, W. O., Kowalik, D. J., Lagrou, M., Garber, R. L., Goltry, L., Tolentino, E., Westbrook-Wadman, S., Yuan, Y., Brody, L. L., Coulter, S. N., Folger, K. R., Kas, A., Larbig, K., Lim, R., Smith, K., Spencer, D., Wong, G. K. S., Wu, Z., Paulsen, I. T., Reizer, J., Saier, M. H., Hancock, R. E. W., Lory, S. and Olson, M. V. (2000).** Complete genome sequence of *Pseudomonas aeruginosa* PAO1, an opportunistic pathogen. *Nature*, 406, 959-964.
- Studier, F. W. and Moffatt, B. A. (1986).** Use of bacteriophage T7 RNA polymerase to direct selective high-level expression of cloned genes. *J. Mol. Biol.*, 189, 113-30.
- Takala, H., Björling, A., Berntsson, O., Lehtivuori, H., Niebling, S., Hoernke, M., Kosheleva, I., Henning, R., Menzel, A., Ihalainen, J. A. and Westenhoff, S. (2014).** Signal amplification and transduction in phytochrome photosensors. *Nature*, 509, 245-248.
- Takala, H., Björling, A., Linna, M., Westenhoff, S. and Ihalainen, J. A. (2015).** Light-induced changes in the dimerization interface of bacteriophytochromes. *J. Biol. Chem.*, 290, 16383-92.
- Takala, H., Edlund, P., Ihalainen, J. A. and Westenhoff, S. (2020).** Tips and turns of bacteriophytochrome photoactivation. *Photochem. Photobiol. Sci.*, 19, 1488-1510.
- Talà, L., Fineberg, A., Kukura, P. and Persat, A. (2019).** *Pseudomonas aeruginosa* orchestrates twitching motility by sequential control of type IV pili movements. *Nat. Microbiol.*, 4, 774-780.
- Tart, A. H., Blanks, M. J. and Wozniak, D. J. (2006).** The AlgT-dependent transcriptional regulator AmrZ (AlgZ) inhibits flagellum biosynthesis in mucoid, nonmotile *Pseudomonas aeruginosa* cystic fibrosis isolates. *J. Bacteriol.*, 188, 6483-9.
- Tart, A. H., Wolfgang, M. C. and Wozniak, D. J. (2005).** The alternative sigma factor AlgT represses *Pseudomonas aeruginosa* flagellum biosynthesis by inhibiting expression of *fleQ*. *J. Bacteriol.*, 187, 7955-62.
- Tarutina, M., Ryjenkov, D. A. and Gomelsky, M. (2006).** An unorthodox bacteriophytochrome from *Rhodobacter sphaeroides* involved in turnover of the second messenger c-di-GMP. *J. Biol. Chem.*, 281, 34751-8.

- Tasler, R., Moises, T. and Frankenberg-Dinkel, N. (2005).** Biochemical and spectroscopic characterization of the bacterial phytochrome of *Pseudomonas aeruginosa*. *FEBS J.*, 272, 1927-36.
- Taylor, A. O. (1968).** *In vitro* phytochrome dark reversion process. *Plant Physiol.*, 43, 767-74.
- Taylor, B. L. and Koshland, D. E., Jr. (1974).** Reversal of flagellar rotation in monotrichous and peritrichous bacteria: generation of changes in direction. *J. Bacteriol.*, 119, 640-2.
- Taylor, B. L. and Zhulin, I. B. (1999).** PAS domains: internal sensors of oxygen, redox potential, and light. *Microbiol. Mol. Biol. Rev.*, 63, 479-506.
- Tindall, B. J. (2014).** *Agrobacterium radiobacter* (Beijerinck and van Delden 1902) Conn 1942 has priority over *Agrobacterium tumefaciens* (Smith and Townsend 1907) Conn 1942 when the two are treated as members of the same species based on the principle of priority and Rule 23a, Note 1 as applied to the corresponding specific epithets. Opinion 94. *Int. J. Syst. Evol. Microbiol.*, 64, 3590-3592.
- Vakulskas, C. A., Potts, A. H., Babitzke, P., Ahmer, B. M. and Romeo, T. (2015).** Regulation of bacterial virulence by Csr (Rsm) systems. *Microbiol. Mol. Biol. Rev.*, 79, 193-224.
- Van Der Horst, M. A. and Hellingwerf, K. J. (2004).** Photoreceptor proteins, "star actors of modern times": a review of the functional dynamics in the structure of representative members of six different photoreceptor families. *Acc. Chem. Res.*, 37, 13-20.
- Vasil, M. L. and Ochsner, U. A. (1999).** The response of *Pseudomonas aeruginosa* to iron: genetics, biochemistry and virulence. *Mol. Microbiol.*, 34, 399-413.
- Velazquez Escobar, F., Piwowarski, P., Salewski, J., Michael, N., Fernandez Lopez, M., Rupp, A., Qureshi, B. M., Scheerer, P., Bartl, F., Frankenberg-Dinkel, N., Siebert, F., Andrea Mroginski, M. and Hildebrandt, P. (2015).** A protonation-coupled feedback mechanism controls the signalling process in bathy phytochromes. *Nat. Chem.*, 7, 423-430.
- Verma, R. K., Biswas, A., Kakkar, A., Lomada, S. K., Pradhan, B. B. and Chatterjee, S. (2020).** A bacteriophytochrome mediates interplay between light sensing and the second messenger cyclic Di-GMP to control social behavior and virulence. *Cell Rep.*, 32, 108202.
- Wadhwa, N. and Berg, H. C. (2022).** Bacterial motility: machinery and mechanisms. *Nat. Rev. Microbiol.*, 20, 161-173.
- Wagner, J. R., Brunzelle, J. S., Forest, K. T. and Vierstra, R. D. (2005).** A light-sensing knot revealed by the structure of the chromophore-binding domain of phytochrome. *Nature*, 438, 325-31.
- Wahlgren, W. Y., Claesson, E., Tuure, I., Trillo-Muyo, S., Bódizs, S., Ihalainen, J. A., Takala, H. and Westenhoff, S. (2022).** Structural mechanism of signal transduction in a phytochrome histidine kinase. *Nat Commun*, 13, 7673.

- Wegele, R., Tasler, R., Zeng, Y., Rivera, M. and Frankenberg-Dinkel, N. (2004).** The heme oxygenase(s)-phytochrome system of *Pseudomonas aeruginosa*. *J. Biol. Chem.*, 279, 45791-802.
- Wilks, A. (2002).** Heme oxygenase: evolution, structure, and mechanism. *Antioxid. Redox Signal.*, 4, 603-14.
- Wilks, A. and Schmitt, M. P. (1998).** Expression and characterization of a heme oxygenase (HmuO) from *Corynebacterium diphtheriae*: iron acquisition requires oxidative cleavage of the heme macrocycle. *J. Biol. Chem.*, 273, 837-841.
- Willett, J. W. and Kirby, J. R. (2012).** Genetic and biochemical dissection of a HisKA domain identifies residues required exclusively for kinase and phosphatase activities. *PLoS Genet.*, 8, e1003084.
- Williams, P. H. (1980).** Black rot: a continuing threat to world crucifers. *Plant Dis.*, 64, 736-742.
- Wozniak, D. J. and Ohman, D. E. (1991).** *Pseudomonas aeruginosa* AlgB, a two-component response regulator of the NtrC family, is required for *algD* transcription. *J. Bacteriol.*, 173, 1406-13.
- Wu, L., Mcgrane, R. S. and Beattie, G. A. (2013).** Light regulation of swarming motility in *Pseudomonas syringae* integrates signaling pathways mediated by a bacteriophytochrome and a LOV protein. *MBio*, 4, e00334-13.
- Wu, W., Badrane, H., Arora, S., Baker, H. V. and Jin, S. (2004).** MucA-mediated coordination of type III secretion and alginate synthesis in *Pseudomonas aeruginosa*. *J. Bacteriol.*, 186, 7575-85.
- Xue, P., Bai, Y., Rottwinkel, G., Averbukh, E., Ma, Y., Roeder, T., Scheerer, P., Krauß, N. and Lamparter, T. (2021).** Phytochrome mediated responses in *Agrobacterium fabrum*: growth, motility and plant infection. *Curr. Microbiol.*, 78, 2708-2719.
- Xue, P., El Kurdi, A., Kohler, A., Ma, H., Kaeser, G., Ali, A., Fischer, R., Krauß, N. and Lamparter, T. (2019).** Evidence for weak interaction between phytochromes Agp1 and Agp2 from *Agrobacterium fabrum*. *FEBS Lett.*, 593, 926-941.
- Yamamoto, K., Arai, H., Ishii, M. and Igarashi, Y. (2012).** Involvement of flagella-driven motility and pili in *Pseudomonas aeruginosa* colonization at the air-liquid interface. *Microbes Environ.*, 27, 320-3.
- Yang, X., Kuk, J. and Moffat, K. (2008).** Crystal structure of *Pseudomonas aeruginosa* bacteriophytochrome: photoconversion and signal transduction. *Proc. Natl. Acad. Sci. USA*, 105, 14715-14720.
- Yang, X., Ren, Z., Kuk, J. and Moffat, K. (2011).** Temperature-scan cryocrystallography reveals reaction intermediates in bacteriophytochrome. *Nature*, 479, 428-432.

- Yu, H., Mudd, M., Boucher, J. C., Schurr, M. J. and Deretic, V. (1997).** Identification of the *algZ* gene upstream of the response regulator *algR* and its participation in control of alginate production in *Pseudomonas aeruginosa*. *J. Bacteriol.*, 179, 187-93.
- Zegadło, K., Gieroń, M., Żarnowiec, P., Durlik-Popińska, K., Kręcisz, B., Kaca, W. and Czerwonka, G. (2023).** Bacterial motility and its role in skin and wound infections. *Int. J. Mol. Sci.*, 24, 1707.

## Appendix

**Tab. S1: Name of the bacterial strains, plasmids, and oligonucleotides used in this thesis in comparison to the name in the collections of the department of Microbiology, RPTU “Gefrierkulturen\_Gordon-85°C 3.0”, “Plasmide 3.1; Plasmidsammlung” and “Primer aktuell” with the assigned numbers. (EV = empty vectors from “Plasmide 3.1; Leerplasmid-Sammlung”)**

No.	Name in Thesis	Name in Collection
<i>Pseudomonas aeruginosa</i> strains		
603	PA14	PA14
598	PA14 $\Delta$ <i>bphP</i>	PA14::JFP01 <i>new</i>
563	PA14 $\Delta$ <i>bphP</i> *	PA14::JFP01 <i>old</i>
602	PA14 $\Delta$ <i>bphP</i> pHERD26T	PA14::JFP01 <i>new</i> pHERD26T
599	PA14 $\Delta$ <i>bphP</i> pHERD26T_ <i>PaBphP</i>	PA14::JFP01 <i>new</i> pSH14P46
601	PA14 $\Delta$ <i>bphP</i> pHERD26T_ <i>PaBphP</i> _H513A	PA14::JFP01 <i>new</i> pLMD02
566	PA14 $\Delta$ <i>bphP</i> * pHERD26T_ <i>PaBphP</i> _D194H	PA14::JFP01 <i>old</i> pKEB01
567	PA14 $\Delta$ <i>bphP</i> * pHERD26T_ <i>PaBphP</i> _S261A	PA14::JFP01 <i>old</i> pKEB02
568	PA14 $\Delta$ <i>bphP</i> * pHERD26T_ <i>PaBphP</i> _C12A	PA14::JFP01 <i>old</i> pLMD01
576	PA14 $\Delta$ <i>kinB</i>	PA14::CHP02
570	PA14 $\Delta$ <i>bphOP</i>	PA14::CHP01
571	PA14 $\Delta$ <i>bphOP</i> pHERD26T_ <i>PaBphP</i>	PA14::CHP01 pSH14P46
Plasmids used in <i>Escherichia coli</i>		
43 EV	pASK-IBA3	pASK-IBA3
46	pASK_ <i>PaBphP</i>	pASK-IBA3- <i>BphP</i>
1392	pASK_ <i>PaAlgB</i>	pASK-IBA3- <i>algB</i>
1393	pASK_ <i>PaKinBCD</i>	pASK-IBA3- <i>kinBCD</i>
1406	pASK_ <i>PaKinBCD</i> _P390S	pCHP03
61	pASK_ <i>AtBphP</i> 1	pASK-IBA3- <i>agp1</i> Midi
1407	pET21b_ <i>AtBphP</i> 2	pET21b- <i>Agp2</i>
1426	pET21b_ <i>AtBphP</i> 2_D783N	pCHP06
1427	pET21b_ <i>AvBphP</i> 2	pETavi3496#2
1468	pET21b_ <i>AvBphP</i> 2_D793A	pETavi3496#2- <i>avp2</i> -D793A
427	pET52_ <i>PstBphO</i> _BphP1	pET52 <i>bphOPhy</i> 1
424	pASK_ <i>PstBphP</i> 2	pAH6
1429	pBAD/HisB_ <i>RtBphP</i> 2HmuO	pBAD/HisB- <i>RtBphP</i> 2-HmuO



1435	pET24a_XccBphP	pET24a-XccBphP
1436	pET24a_XccBphPΔPAS9	pET24a-XccBphPΔPAS9
Plasmids used in <i>Pseudomonas aeruginosa</i>		
143 EV	pHERD26T	pHERD26T
609	pHERD26T_PaBphP	pSH14P46
1279	pHERD26T_PaBphP_H513A	pSH14P46_H513A
1280	pHERD26T_PaBphP_D194H	pSH14P46_D194H
1283	pHERD26T_PaBphP_S261A	pSH14P46_S261A
1284	pHERD26T_PaBphP_C12A	pSH14P46_C12A
168 EV	pEXG2	pEXG2
1391	pEXG2_ΔbphP	pEXG2ΔbphP
1384	pEXG2_ΔbphOP	pCHP01
1385	pEXG2_ΔkinB	pCHP02
Oligonucleotides		
3309	pEXG2ΔbphOP_upF	PA14bphOP_upF
3310	pEXG2ΔbphOP_upR	PA14bphOP_upR
3311	pEXG2ΔbphOP_downF	PA14bphOP_downF
3312	pEXG2ΔbphOP_downR	PA14bphOP_downR
3512	pEXG2ΔkinB_upF	PA14_72390_UpF
3513	pEXG2ΔkinB_upR	PA14_72390_UpR
3313	pEXG2ΔkinB_downF	PA14_72390_DownF_CH
3515	pEXG2ΔkinB_downR	PA14_72390_DownR
3518	pASK-PaAlgB_fwd	algB_Xba_RBS_fwd
3519	pASK-PaAlgB_rev	algB_xho_noSTOP_rev
3520	pASK-PaKinBCD_fwd	kinB_CD_pASK_for
3521	pASK-PaKinBCD_rev	kinB_CD_pASK_rev
3529	pASK-PaKinBCDP390S_fwd	kinB_CD_P390S_fw
3530	pASK-PaKinBCDP390S_rev	kinB_CD_P390S_rev
3595	pET21b-AtBphP2D783N_fwd	pET21b-agp2D783N_fwd
3596	pET21b-AtBphP2D783N_rev	pET21b-agp2D783N_rev
3173	pEXG2_seqF	pEXG2-seqF
3174	pEXG2_seqR	pEXG2-seqR
3315	ΔbphOP_seqF	shortbphOP_seqF
3316	ΔbphOP_seqR	shortbphOP_seqR
3317	ΔkinB_seqF	shortkinB_seqF

3318	$\Delta kinB\_seqR$	shortkinB_seqR
1255	pET_seqF	T7_fwd
1497	pET_seqR	T7Term/Duet Down 2

\* The plasmids pHERD26T\_PaBphP\_D194H, pHERD26T\_PaBphP\_S261A, and pHERD26T\_PaBphP\_C12A were used in an incorrect *bphP* deletion mutant (gene is correctly deleted, but strain is Gm<sup>R</sup>) from J. Pielage, 2017.

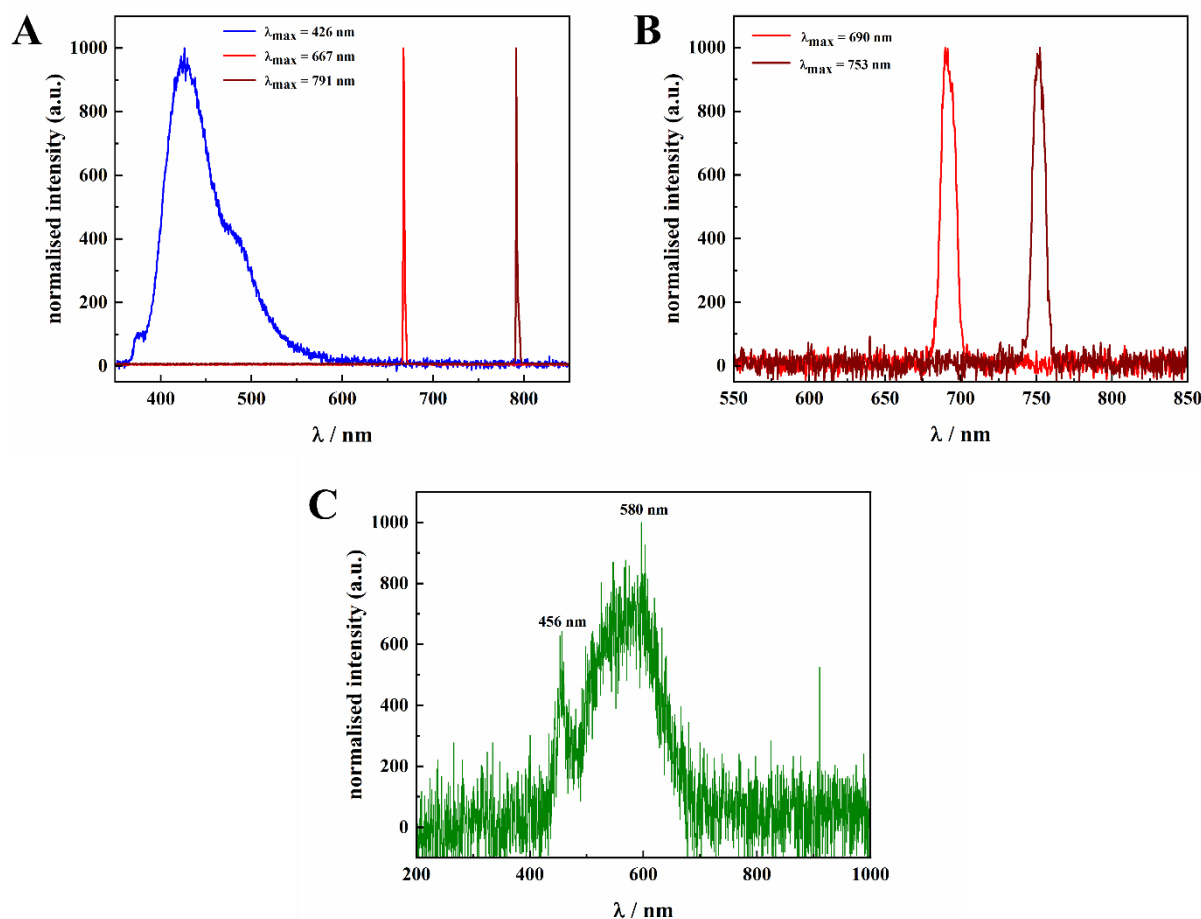


**Fig. S1:** Peak wavelengths of the light sources used to establish the photostationary states of the BphPs for UV/Vis spectroscopy and kinase assays, as well as the peak wavelength of the light sources in the 37 °C incubation room determined by an optical multichannel analyzer (*Ocean Optics OMA, USB2000+UV/Vis*). (A) Normalized emission spectra of the blue LED (DLE-038-046 from Everlight Electronics) with 426 (70) nm, the red with 667 (2) nm and the far-red laser diode with 791 (2) nm (both LNCT28PS01WW from Panasonic). (B) Normalized emission spectra of the red (690 nm; LOT-Oriel) and far-red (753 nm; Kodak) interference filters. (C) Normalized emission spectra of the light sources in the 37 °C incubation room.

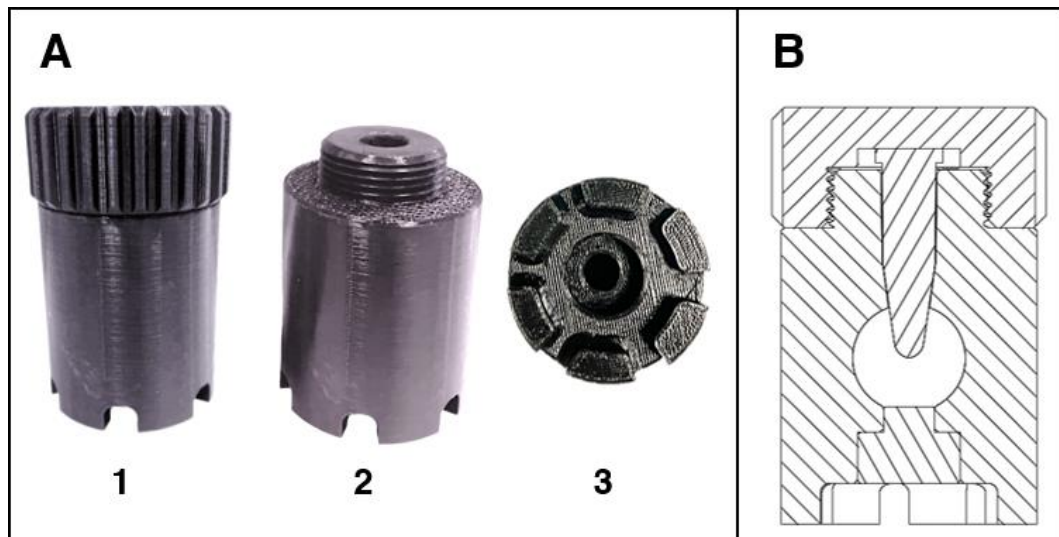


**Fig. S2: Photograph (A) and technical drawing (B) of the new illumination set-up used for the radioactive kinase assays.**

It consists of a main pod (A2) with a screw cap (A1), both made of black polylactide to protect the sample from unwanted ambient light. A diode can be inserted from the bottom (A3, B). The phytochrome sample itself is in an Eppendorf tube (B). Figure and description from Merle Strack.

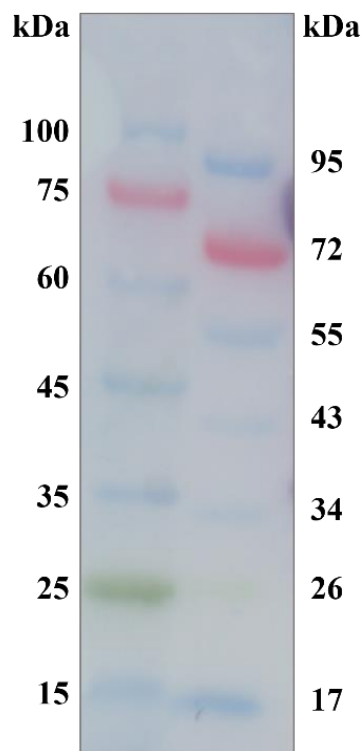


**Fig. S3: Comparison of „Prestained protein marker, proteintech” (left) and “Color Prestained Protein Standard, Broad Range; NEB” (right) on a PVDF membrane after western-blot transfer from an SDS-PAGE gel.**

The marker on the left side from “proteintech” is not running properly, so it is possible that actually larger proteins may be misinterpreted compared to the relative molecular mass of the marker proteins.

- 1: Prestained protein marker;  
proteintech  
2: Color Prestained Protein Standard,  
Broad Range; NEB

**Tab. S2: Fit parameters for the pure form spectra  $P_{fr}^0(\tilde{\nu})$  and  $P_r^0(\tilde{\nu})$  of the simulated bathy-phytochromes.**  
 1: *PaBphP*, 2: *AtBphP2*, 3: *AtBphP2\_D783N*, 4: *AvBphP2*, 5: *AvBphP2\_D793A*, 6: *RtBphP2*, 7: *XccBphP*,  
 8: *XccBphP* $\Delta$ PAS9. Table from Merle Strack.

		$P_{fr}^0(\tilde{\nu})$				$P_r^0(\tilde{\nu})$			
		$G_1$	$G_2$	$G_3$	$G_4$	$G_1$	$G_2$	$G_3$	$G_4$
<b>1</b>	$\tilde{\nu}^c$	13165 $\pm$ 3	13926 $\pm$ 16	14946 $\pm$ 108	-	14172 $\pm$ 4	14572 $\pm$ 29	15208 $\pm$ 4	15572 $\pm$ 13
	$w$	721 $\pm$ 9	1216 $\pm$ 54	1879 $\pm$ 75	-	503 $\pm$ 8	704 $\pm$ 30	2001 $\pm$ 13	812 $\pm$ 21
	$a$	375 $\pm$ 21	594 $\pm$ 78	499 $\pm$ 60	-	351 $\pm$ 35	392 $\pm$ 40	687 $\pm$ 12	121 $\pm$ 8
<b>2</b>	$\tilde{\nu}^c$	12956 $\pm$ 7	13196 $\pm$ 18	13936 $\pm$ 20	15195 $\pm$ 71	14059 $\pm$ 30	14422 $\pm$ 85	14859 $\pm$ 19	15771 $\pm$ 193
	$w$	534 $\pm$ 17	786 $\pm$ 14	1389 $\pm$ 21	1700 $\pm$ 52	492 $\pm$ 23	606 $\pm$ 65	1825 $\pm$ 44	2690 $\pm$ 89
	$a$	177 $\pm$ 28	492 $\pm$ 38	1215 $\pm$ 49	529 $\pm$ 47	234 $\pm$ 82	254 $\pm$ 85	1046 $\pm$ 88	428 $\pm$ 90
<b>3</b>	$\tilde{\nu}^c$	12988 $\pm$ 2	13297 $\pm$ 4	14056 $\pm$ 22	15027 $\pm$ 75	14164 $\pm$ 4	17289 $\pm$ 34	14659 $\pm$ 11	15037 $\pm$ 6
	$w$	565 $\pm$ 4	883 $\pm$ 10	1411 $\pm$ 37	2156 $\pm$ 42	523 $\pm$ 5	1237 $\pm$ 55	481 $\pm$ 13	1968 $\pm$ 8
	$a$	204 $\pm$ 6	598 $\pm$ 31	837 $\pm$ 68	513 $\pm$ 42	407 $\pm$ 7	56 $\pm$ 4	124 $\pm$ 8	1229 $\pm$ 3
<b>4, 5</b>	$\tilde{\nu}^c$	13133 $\pm$ 2	14194 $\pm$ 2	15155 $\pm$ 21	-	14139 $\pm$ 3	14490 $\pm$ 20	15226 $\pm$ 5	-
	$w$	756 $\pm$ 2	1090 $\pm$ 7	1963 $\pm$ 18	-	487 $\pm$ 10	737 $\pm$ 16	1872 $\pm$ 4	-
	$a$	421 $\pm$ 3	660 $\pm$ 14	741 $\pm$ 15	-	245 $\pm$ 24	411 $\pm$ 27	1098 $\pm$ 5	-
<b>6</b>	$\tilde{\nu}^c$	13009 $\pm$ 2	13396 $\pm$ 14	14300 $\pm$ 22	14677 $\pm$ 18	14398 $\pm$ 2	15498 $\pm$ 11	-	-
	$w$	538 $\pm$ 6	890 $\pm$ 8	908 $\pm$ 25	1936 $\pm$ 13	971 $\pm$ 7	2453 $\pm$ 12	-	-
	$a$	677 $\pm$ 34	2059 $\pm$ 41	735 $\pm$ 56	2021 $\pm$ 43	744 $\pm$ 11	1720 $\pm$ 14	-	-
<b>7</b>	$\tilde{\nu}^c$					14551 $\pm$ 4	15082 $\pm$ 9	15783 $\pm$ 2	15783 $\pm$ 11
	$w$	from $\Delta$ PAS9 scaled with 1.01				642 $\pm$ 3	633 $\pm$ 12	2493 $\pm$ 6	1023 $\pm$ 14
	$a$					592 $\pm$ 10	232 $\pm$ 14	774 $\pm$ 4	290 $\pm$ 9
<b>8</b>	$\tilde{\nu}^c$	13049 $\pm$ 1	13616 $\pm$ 3	14049 $\pm$ 4	15080 $\pm$ 36	14574 $\pm$ 1	15130 $\pm$ 3	15692 $\pm$ 8	15897 $\pm$ 3
	$w$	739 $\pm$ 2	553 $\pm$ 4	1419 $\pm$ 13	2161 $\pm$ 22	660 $\pm$ 2	539 $\pm$ 6	1124 $\pm$ 12	2453 $\pm$ 6
	$a$	484 $\pm$ 4	82 $\pm$ 2	713 $\pm$ 21	424 $\pm$ 16	661 $\pm$ 3	137 $\pm$ 6	378 $\pm$ 8	690 $\pm$ 4

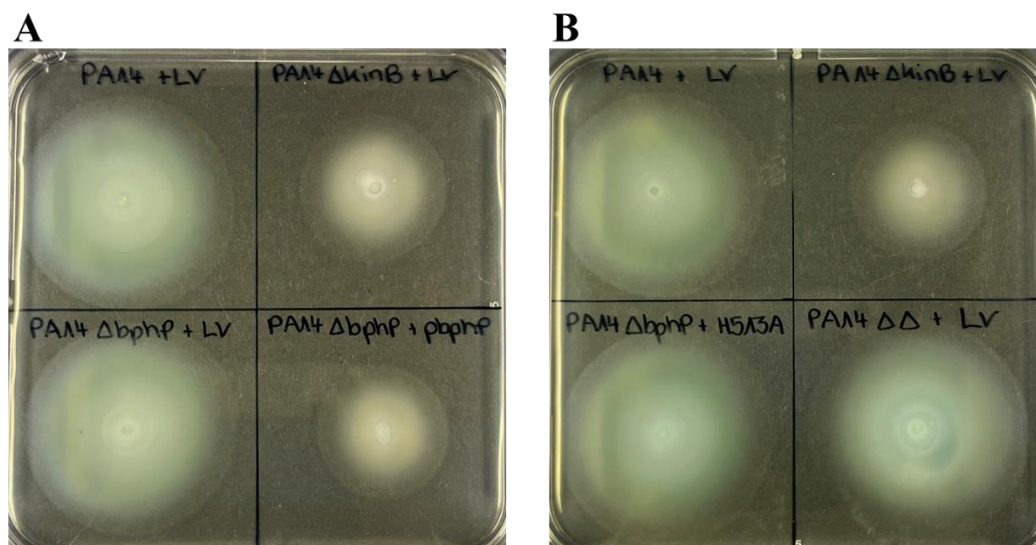


**Fig. S4: Original proportioned, uncut photo of the swimming zones of *P. aeruginosa* from Fig. 3.11.** In Fig. 3.11 PA14 +EV, PA14Δ*bphP* +EV, PA14Δ*kinB* +EV and PA14Δ*bphP* +p*BphP* are derived from “A” and PA14Δ*bphP* +p*BphP*<sub>H513A</sub> is derived from “B”.

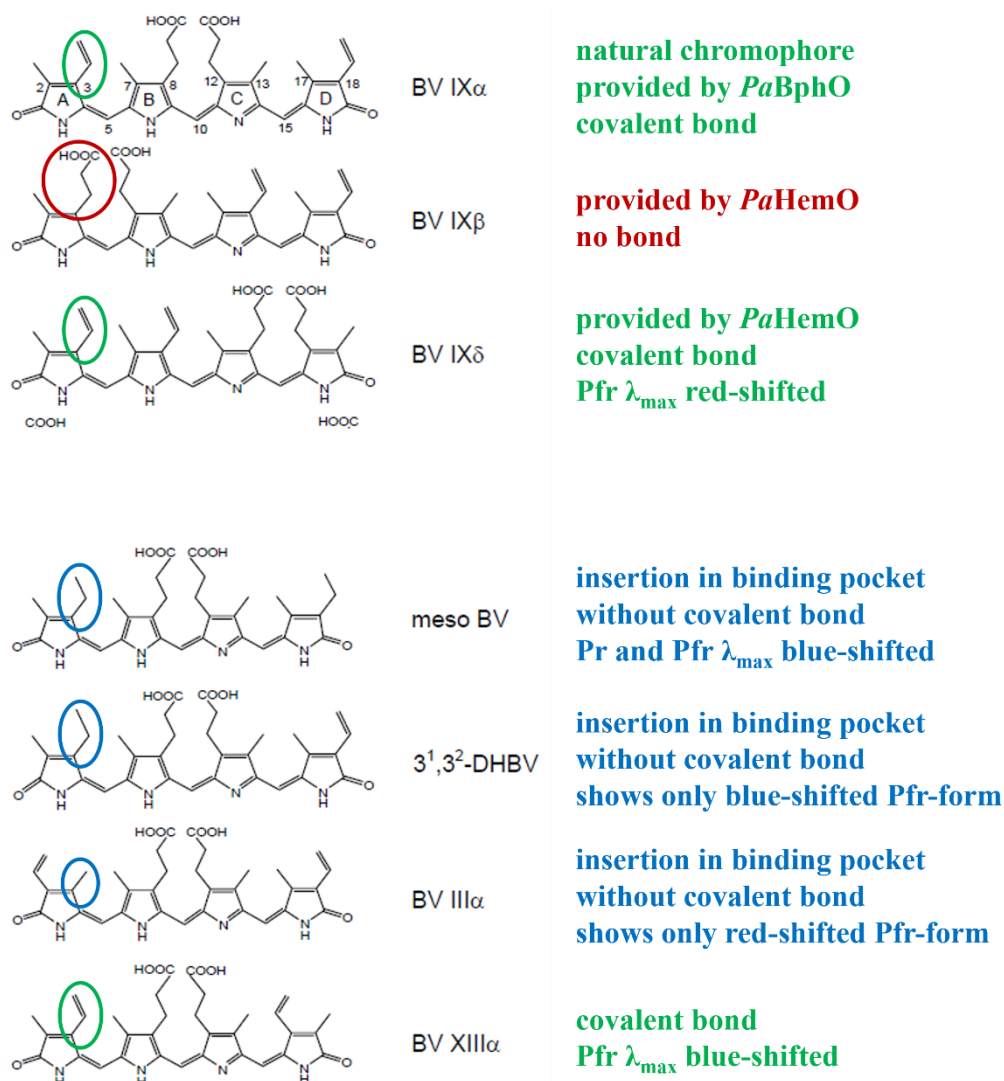


**Fig. S5: Chemical structures of biliverdin isomers (modified from Tasler *et al.*, 2005).**

# Curriculum Vitae

## PERSÖNLICHE DATEN

---

**Christina Huber**

## STUDIUM UND SCHULISCHE LAUFBAHN

---

10/2019	07/2023	<b>Rheinland-Pfälzische Technische Universität Kaiserslautern-Landau</b> Wissenschaftliche Mitarbeiterin / Promotion in der Abteilung für Mikrobiologie von Prof. Dr. Nicole Frankenberg-Dinkel
10/2017	08/2019	<b>Technische Universität Kaiserslautern</b> Studium der Biologie (Master of Science)
10/2013	02/2017	<b>Technische Universität Kaiserslautern</b> Studium der Biologie (Bachelor of Science)
08/2006	03/2013	<b>Hofenfels-Gymnasium Zweibrücken</b> Allgemeine Hochschulreife

## CONFERENCE CONTRIBUTIONS

---

### Talks

**Christina Huber, Julia Pielage, Merle Strack, Rolf Diller and Nicole Frankenberg-Dinkel** (2021). “Phenotypical and functional characterization of the bacterial phytochrome *PaBphP* of *Pseudomonas aeruginosa*” VAAM Herbstschule zur Regulation und Signaltransduktion in Prokaryoten (RSTiP), Germany.

**Christina Huber, Julia Pielage and Nicole Frankenberg-Dinkel** (2020). “Functional characterization of the *Pseudomonas aeruginosa* bacteriophytochrome BphP” Faculty Seminar Biology TU Kaiserslautern, Germany.

**Christina Huber, Julia Pielage, Kevser Bilici, Lisa-Marie Denig and Nicole Frankenberg-Dinkel** (2020). “Phenotypical and functional characterization of the bacterial phytochrome *PaBphP* of *Pseudomonas aeruginosa*” VAAM Annual Meeting, Leipzig, Germany.

**Christina Huber, Julia Pielage and Nicole Frankenberg-Dinkel** (2019). “Functional characterization of the *Pseudomonas aeruginosa* bacteriophytochrome BphP” Rheinland-Pfalz Microbiology Symposium, Kaiserslautern, Germany.

## Posters

**Christina Huber, Merle Strack, Julia Pielage, Rolf Diller and Nicole Frankenberg-Dinkel** (2022). “Phenotypical and functional characterization of the bacterial phytochrome *PaBphP* of *Pseudomonas aeruginosa*” Gordon Research Conference and Seminar: Photosensory Receptors and Signal Transduction, Ventura, California, United States.

**Christina Huber, Julia Pielage and Nicole Frankenberg-Dinkel** (2019). “Biochemical and functional characterization of the bacterial phytochrome *PaBphP* of *Pseudomonas aeruginosa*” VAAM Annual Meeting, Mainz, Germany.

## Erklärung

### **Erklärungen lt. § 6 (4) der Promotionsordnung des Fachbereichs Biologie vom 27.11.2018:**

Ich erkläre wahrheitsgemäß, dass ich die eingereichte Dissertation selbst angefertigt und alle für die Arbeit benutzten Hilfsmittel und Hilfestellungen in der Arbeit angegeben habe.

Die Dissertation oder Teile hiervon habe ich bisher nicht als Prüfungsarbeit für eine staatliche oder andere wissenschaftliche Prüfung eingereicht.

Ebenso habe ich die gleiche oder eine andere Abhandlung nicht bei einem anderen Fachbereich oder einer anderen Universität als Dissertation eingereicht.

Kaiserslautern, 15.11.2023

Christina Huber



## Darlegung des Eigenanteil

Christina Huber

The bathy phytochrome *PaBphP* of the human pathogen *Pseudomonas aeruginosa*: Introducing a novel perspective on light sensing in Proteobacteria

Die Konzeption, die Planung, das Versuchsdesign und die Methodenentwicklung der vorliegenden Arbeit wurde in Teilen von Prof. Nicole Frankenberg-Dinkel und von Dr. Julia Pielage (bis Frühsommer 2022) unterstützt.

Die Literaturrecherche, die Datenerhebung, die Datenanalyse, die Interpretation und Diskussion der Ergebnisse wurden, sofern im Folgenden nicht anders dargelegt, nicht von Dritten unterstützt.

Bakterienstämme sowie Plasmide, die von dritter Seite generiert wurden, sind, in Tab. 2.3 und Tab. 2.4, mit der entsprechenden Quelle, aufgeführt.

Die Datenerhebung für Abbildung 3.10 wurde von Kevser Bilici (ehemalige Masterstudentin, RPTU, Mikrobiologie) unterstützt. Die Datenanalyse und -auswertung für diese Abbildung wurde nicht von Dritten unterstützt. Des Weiteren sind diese Ergebnisse nicht Teil der Master-Arbeit von Frau Bilici.

Die Daten für die Abbildungen 3.15, 3.18B-H, 3.19C+D und 3.20B wurden von Isabel Schultheiß (ehemalige Masterstudentin, RPTU, Mikrobiologie) erhoben. Die Datenanalyse und -auswertung aller genannten Abbildungen wurde nicht durch Dritte unterstützt. Mittels der, von Frau Schultheiß übermittelten und zur Verfügung gestellten Daten, wurden die jeweiligen Abbildungen durch eigene Daten und Ergebnissen vervollständigt. Des Weiteren finden sich diese Ergebnisse teilweise oder vollständig, jedoch in modifizierter Form, in der Master-Arbeit von Frau Schultheiß wieder. Die Daten in Abbildung 3.22 sind ebenfalls in der Master-Arbeit von Frau Schultheiß zu finden, wurden allerdings von mir generiert und Frau Schultheiß zur Verfügung gestellt. Jegliche Experimente und Datenerhebungen, die von Frau Schultheiß übernommen wurden, erfolgten unter meiner Anleitung mit gemeinsamer Konzeption, Planung und Entwicklung der Methoden.

Die Methode, wie sie in Kapitel 2.6.11 beschrieben ist, dient dazu, die Pr/Pfr-Fractionen für jedes Spektrum zu kalkulieren. Diese Methode und der entsprechende Versuchsaufbau (Fig. S2, Tab. S2) wurde in Zusammenarbeit mit Prof. Rolf Diller (RPTU, Biophysik), Merle Strack (Masterstudentin, RPTU, Biophysik) und ihrem Team entwickelt. Die Datenerhebung erfolgte eigenständig und ohne Unterstützung Dritter. Jedoch wurde zur Analyse der Daten, das, von Merle Strack entwickelte Programm für „MATLAB (R2022a, academic use), Natick, Massachusetts: The MathWorks Inc.“, verwendet. Die Auswertung findet sich in den Abbildungen 3.3D, Fig. 3.4C, Fig. 3.5B, Fig. 3.6E und Tab. 3.1 wieder.

Die LEDs und Laserdioden, wie sie im Material und Methoden-Teil ausführlich beschrieben sind, und für UV-Vis Spektroskopie sowie Kinase-Assays verwendet wurden, wurden ebenfalls von der Abteilung Biophysik, RPTU zur Verfügung gestellt. Die Bestimmung der *Peak*-Wellenlänge dieser Dioden, unserer eigenen Interferenzfilter sowie der Beleuchtungsapparatur im 37 °C-Inkubationsraum (Fig. S1) wurde von Merle Strack, mit einem dafür geeigneten Gerät der Abteilung Biophysik, RPTU durchgeführt.

Die vorliegende Einschätzung über die erbrachte Leistung von Dritten wurde mit den genannten Personen einvernehmlich abgestimmt.

Kaiserslautern, 15.11.2023

Prof. Nicole Frankenberg-Dinkel

Christina Huber

## **Darlegung aller benutzten Hilfestellungen und Hilfsmitteln**

Christina Huber

The bathy phytochrome *PaBphP* of the human pathogen *Pseudomonas aeruginosa*: Introducing a novel perspective on light sensing in Proteobacteria

Die Analyse der Daten erfolgte mit Hilfe von Microsoft Excel; Origin, Version 2022. OriginLab Corporation, Northampton, MA, USA. und Corel DRAW Graphics Suite. Weitere verwendete Programme und Webseiten waren Microsoft Word sowie PowerPoint; SnapGene – Software for everyday molecular biology; ImageJ; ApE – A plasmid Editor; BioRender; Clustal Omega; BLAST®; pseudomonas.com; InterPro 97.0 – Classification of protein families und Protein Calculator v3.4. Details zu Verwendung sind dem Material und Methoden- sowie Ergebnis-Teil zu entnehmen.

MATLAB (R2022a, academic use), Natick, Massachusetts: The MathWorks Inc. wurde gemäß der Beschreibung zur „Darlegung des Eigenanteils“ verwendet.

Handelt es sich nicht um frei nutzbare Programme oder Webseiten wurden sie von der RPTU oder der Abteilung Mikrobiologie zur Verfügung gestellt.

Die Arbeit wurde von Federica Frascogna (Doktorandin, RPTU, Mikrobiologie), Thomas Schmidt (Doktorand, RPTU, Mikrobiologie) sowie Anna Scherhag (ehemalige Doktorandin, RPTU, Mikrobiologie) jeweils in Teilen Korrektur gelesen.

Die Übersetzungsprogramme Google Übersetzer und DeepL sowie DeepL Write wurden genutzt, um manche Textpassagen im Hinblick auf ihre akademische Sprachqualität zu verbessern oder Synonyme zu finden. Dabei wurden keinerlei inhaltlichen Änderungen vorgenommen.

Kaiserslautern, 15.11.2023

Christina Huber

## Danksagung

Allen voran ergeht ein herzlicher Dank an meine Doktormutter Prof. Dr. Nicole Frankenberg-Dinkel für die Möglichkeit zur Promotion in ihrer Arbeitsgruppe. Ich durfte an einem Thema arbeiten, welches mich bereits während meiner Master-Arbeit vollständig begeisterte. Vielen Dank für das beständige Vertrauen in allen Belangen und die jahrelange Motivation sowie wissenschaftliche Unterstützung.

Für die freundliche Übernahme des Zweitgutachtens möchte ich mich bei Prof. Dr. Matthias Hahn bedanken. Außerdem danke ich Prof. Dr. Stefan Kins für die Bereitschaft der Übernahme des Vorsitzes der Prüfungskommission. Ein zusätzlicher Dank gilt Prof. Dr. Matthias Hahn und Prof. Dr. Rolf Diller für das Mitwirken in meinem Thesis Advisory Committee.

Weiterhin gilt mein besonderer Dank Prof. Dr. Rolf Diller und Merle Strack der Abteilung Biophysik, RPTU für die hervorragende Zusammenarbeit. Unter der Anleitung von Prof. Rolf Diller und der tatkräftigen Unterstützung seines Teams, allen voran Merle, haben wir eine innovative Methode mit einer einzigartigen Versuchskonstruktion entwickelt. Neben diversen LEDs, Dioden und Messgeräten, die sie zur Verfügung stellten, standen mir aber beide auch immer mit Rat und Tat bei physikalischen Fragestellungen oder Problemen bei der Spektroskopie zur Seite.

Bei Tilman Lamparter (Karlsruher Institut für Technologie, Deutschland), Gilles De Luca (Aix-Marseille Université, Frankreich) und Hernán Bonomi (Fundación Instituto Leloir, Argentinien) bedanke ich mich für die Bereitstellung von benötigten Plasmiden.

Bei Dr. Ilka Haferkamp der Abteilung Pflanzenphysiologie, RPTU bedanke ich mich für die regelmäßige Bestellung der Radioaktivität und die Hilfestellung bei jeglichen Fragen rund ums Isotopen-Labor.

Ganz herzlich möchte ich mich aber auch bei Dr. Julia Pielage bedanken, die schon während meines Master-Studiums meine bessere Hälfte im „Team BphP“ war und mir immer treu zur Seite stand. Liebe Julia, ich habe die letzten 1,5 Jahre ohne dich, immer versucht unser Projekt nach bestem Wissen und Gewissen weiterzuführen, genauso wie du es auch getan hättest. Ich habe, trotz aller Spektren, biochemischer Experimente und Kalkulationen nie vergessen meinen Blick auch auf die Physiologie von *P. aeruginosa* zu richten, da ich weiß, wie sehr dir das am Herzen lag.

In diesem Zusammenhang danke ich noch ganz besonders allen ehemaligen und jetzigen Mitgliedern des Mibi-Teams für eine unvergessliche Zeit im, aber auch außerhalb des Labors und im Lager. Danke an Änna, Fedi, Nori und Thomäs, dass ich in euch nicht nur Arbeitskollegen, sondern auch wahre Freunde gefunden habe. Danke für alles, was wir erlebt haben, danke für eure immerwährende Unterstützung, aber auch danke für viele fachliche Diskussionen. Hier möchte ich auch unsere liebe Uti erwähnen, die dem Begriff „gute Seele“ nochmal einen ganz neuen Ausdruck verleiht und die wirklich immer und in jeder Situation für mich da war. Wir haben uns gegenseitig die ein oder andere Träne getrocknet. Außerdem danke ich meinen Studenten Jacqueline Hackh, Tim Schneckmann (Tom), Tim Krier (Tam) sowie Laura Esch und hoffe, dass ihr viel von mir lernen konntet. Ich bin mir jedenfalls sicher, dass ihr mich unterstützt habt, viel über mich selbst zu lernen. An dieser Stelle möchte ich natürlich Isabel Schultheiß, meine liebe Ilse, nicht vergessen. Den Fortschritt meiner Doktorarbeit im letzten halben Jahr habe ich zu großen Stücken dem Fleiß und der unermesslichen Unterstützung von Isabel zu verdanken. Kein Experiment war ihr zu viel oder zu komplex, keine Literaturrecherche zu aufwendig und keine Stunde, die sie mit mir länger im Labor oder im Büro geblieben ist zu schade.

Den letzten, aber auch größten Dank richte ich an meine Familie und meine Freunde. Es ist selbstverständlich, dass das alles ohne EUCH niemals möglich gewesen wäre. Dazu muss ich gar nicht viele Wort verlieren, denn ihr wisst alle, wie dankbar ich euch bin. Ihr habt unaufhörlich an mich geglaubt.